THE EFFECTS OF LOW DOSES OF IONISING RADIATION ON THE VIABILITY OF MAMMALIAN CELLS

The response of mammalian cells to low doses of ionising radiation

by

Brian Marples, MSc.

A thesis submitted to the University of London
for the degree of Doctor of Philosophy
in the faculty of Science

1991

Gray Laboratory of the Cancer Research Campaign,
Mount Vernon Hospital, Northwood, Middlesex.

ProQuest LLC.
789 East Eisenhower Parkway
P.O. Box 1346
Ann Arbor, MI 48106 – 1346

Abstract

The clonogenic response of V79-379A cells to single doses of X-rays (0.01-10 Gy) and neutrons (0.02-3 Gy) was determined using a computerised microscope (DMIPS) for locating and identifying cells. Survival estimates over the X-ray dose range 1 Gy to 10 Gy showed a good fit to a Linear-Quadratic (LQ) model. For X-ray doses below 0.6 Gy, an *increased* X-ray sensitivity was observed, with survival below the LQ prediction. This phenomenon was not seen with neutrons, and cell survival decreased exponentially with dose. The increased X-ray effectiveness was reflected by a decrease in the RBE from ≈4.1 to ≈1.7 as the X-ray dose decreased from 1 Gy to below 0.05 Gy.

Comparing the survival measurements from a DMIPS recognition assay with those obtained from a conventional assay suggest that this phenomenon cannot be attributed to the use of the recognition assay for measuring cell survival. Experiments performed on synchronised populations of cells indicate that the low-dose X-ray hypersensitivity is unlikely to be due to either cell cycle effects or a static subpopulation of X-ray sensitive cells.

The X-ray dose response over the range 0.04-1 Gy was altered by repair modifiers in three ways. 3-aminobenzamide reduced the increase in radioresistance that occurred in non drug-treated cells as the X-ray dose was increased over the range 0.2-0.6 Gy, but did not affect the response below 0.2 Gy. Exposure to β-ara-A sensitised the cells to X-rays over the whole dose range (0.04-1 Gy) but did not prevent an increase in radioresistance with increasing X-ray dose. Hydrogen peroxide increased the radioresistance of cells to subsequent doses of X-rays below 0.6 Gy. The dose response was also modified by X-rays; a 0.05 Gy, 0.2 Gy or 1 Gy X-ray 'priming' treatment, given 4-6 hours before the 'test' doses of X-rays, *eliminated* the low-dose X-ray hypersensitivity that was seen in cells not given the priming treatment. This was *not* seen when the priming dose was administered 24 hours before the subsequent 'test' X-ray doses.

These data are consistent with a hypothesis that the increase in radioresistance as the X-ray dose increases from 0.2-0.6 Gy is due to the manifestation of "induced repair" or a stress response: low doses (<0.2 Gy) are more effective, per gray, at killing cells than higher doses because only at higher doses (>>0.2 Gy) is there sufficient damage to trigger the protective mechanism. An induced-repair model fitted to the X-ray data predicts that repair is activated in the dose range 0.2-0.6 Gy with a 2 fold decrease in the sensitivity between the very low-dose response (< 0.2 Gy) and the normal high-dose response (>>0.6 Gy). Treatment with the protein synthesis inhibitor, cycloheximide, following a single dose of radiation reduced the increase in radioresistance that is seen normally over the X-ray dose range 0.2-0.6 Gy. Similarly, cycloheximide present during the interval between a priming dose and a subsequent X-ray dose eliminated the effect of the priming treatment. These data suggest that *de novo* protein synthesis is required to express the protective mechanism, possibly for the production of repair enzymes. A novel protein was detected in an irradiated sample of cells (1 Gy of X-rays) using 2D gel electrophoresis that was *not* present in unirradiated cells.

These data appear to indicate that an inducible radioprotective mechanism exists in V79-379A cells that is triggered by H_2O_2 or small radiation doses and requires the synthesis of new proteins to induce radioresistance, possibly through a biochemical pathway affected by 3AB. The mechanism is induced within 4 hours of being triggered but is absent after 24 hours.

Acknowledgements

It is with great pleasure that I thank Dr. Michael Joiner for his help, encouragement and excellent supervision throughout this work. I am also indebted to Dr. Neil Gillies for his guidance, interest and constructive criticisms. It was a pleasure to work with both these people as colleagues and as friends.

I have also benefitted from the help of many colleagues at the Gray Laboratory. I would like to express my thanks to Dr. George Wilson and Mrs Christine Martindale for their assistance with the cell cycle studies, Mr Mick Woodcock for guidance in tissue culture techniques, Ms Tracy Robson for her patience and encouragement with the electrophoresis studies and finally to Mr Brian Hall and Mr Keith Allen for their continued patience with my low dose work on the Van de Graaff accelerator. I wish to thank Dr. Pat Lawton and Ms Helen Johns for their help and encouragement. I am grateful to Mrs Sue Malcolm and Miss Paula Reynolds for help in the typing of this thesis.

I wish to thank the Cancer Research Campaign for the studentship which has enabled this work to be carried out. I particularly wish to thank my adopted "CRC parents", the Luton and District Committee of the Cancer Research Campaign for providing me with additional encouragement and resolution.

Finally, I wish to thank my wife, Helen, without whose patience, time and encouragement this work could not have been completed.

Abbreviations used in this thesis

3-AB	3-aminobenzamide
adprt	adenine di-phosphate-ribosyltransferase
β-ara-A	β-arabinofuranosyladenine
AE	attachment efficiency
AP	apurinic/apyrimidinic site
BrdUrd	bromodeoxyuridine
CELREC	cell recognition program
CSCAN	cell location and classification program
CV	coefficient of variation
DMIPS	dynamic microscope image processing system
DNA	deoxyribonucleic acid
DSB	double strand break
ELU	elutriation experiment code
EPG	effect per gray
FCM	flow cytometry
GSCAN	general cell scanning program
HU	hydroxyurea
LET	linear energy transfer
LMDS	locally multiply damaged site
α-MEM	minimum essential medium-alpha modified
MEM	minimum essential medium
MEM-S	minimum essential medium-suspension modified
MNNG	N-methyl-N-1-nitro-N-nitrosoguanidine
MNUA	N-methyl-N-nitrourea
NAD	nicotinamide adenine dinucleotide
PAGE	polyacrylamide gel electrophoresis
PBS	phosphate buffered saline
PE	plating efficiency
PLD	potentially lethal damage
PLDR	potentially lethal damage repair
RBE	relative biological effectiveness
RSCAN	revisiting cell program
SDS	Sodium-dodecyl-sulphate
SF	surviving fraction
SLD	sublethal damage
SLDR	sublethal damage repair
SSCAN	survival scan program
SSB	single strand break
SSP	standard plating procedure
XIP	X-ray induced protein

Contents

Chapter 1 Introduction

1.1 Radiobiological definition of low-dose radiation

The biological and physical interpretation of the phrase, 'low-dose radiation' varies by several orders of magnitude. Physically, it is possible to measure doses of radiation down to fractions of a centigray, far lower than the resolution of any biological system, such as a cell survival assay whereas, the biological use of the phrase 'low dose' often reflects the experimental situation in which it is quoted. In the field of radiation protection, 'low dose' usually refers to doses equivalent to environmental levels of radiation, whereas in radiation biology the term 'low dose' usually refers to the lowest dose at which a biological effect can be measured reliably by the assay being used. This may cover a dose range from several centigray (e.g. some clonogenic survival assays) to several gray (e.g. measurement of double strand breaks). In this study the definition of 'low dose' is used when refering to doses of radiation less than 1 Gy.

1.2 The relevance of the study of low-dose radiation

The radiobiological effect of high doses of radiation (>1 Gy) are well documented (Hall, 1978). However, the biological effects that result following exposure to much smaller doses (<<1 Gy) are less well understood. There is general agreement that the principal late effect of exposure to small doses of ionising radiation is carcinogenesis (Breimar, 1988), and this is understood to be a result of non-lethal alterations to the DNA, possibly resulting from the mis-repair of radiation induced lesions. At high radiation doses, the level of damage that is received by the DNA may be sufficient to cause cell death, therefore masking possible mutagenic or carcinogenic lesions. Therefore, the mutagenic and carcinogenic risk increases as the radiation dose is gradually increased, but it then *decreases* as the mutated cells are killed. The underlying damage in the processes of mutagenesis, carcinogenesis and cell killing are probably similar and result from the deposition of energy in the DNA of the cell but the biological consequences of the three processes are different.

At low doses (<1 Gy) the precise relationship between radiation dose, carcinogenesis and cell killing has yet to be fully established because *in vivo* carcinogenic experiments are imprecise and *in vitro* models of carcinogenesis do not provide consistent data. Therefore, at present, the estimates for assessing carcinogenesis and mutagenesis following exposure to small doses of radiation have been calculated by back extrapolating the risk derived from higher radiation doses. These have involved *in vivo* and *in vitro* experiments (Ullrich, 1980; Hall and Miller, 1981), employing moderate to high radiation doses and retrospective statistical analysis of human populations exposed to radiation during the treatment of non-malignant conditions (Mole, 1989) and the analysis of the data from the survivors of the atomic bombs dropped at Hiroshima and Nagasaki (Pierce and Vaeth, 1989).

However, while the assays for determining the risk of carcinogenesis have not improved significantly to generate precise data at low doses the clonogenic assay which measures the cytotoxicity of radiation *has* developed to a point where very accurate assessments of the lethal effects of small doses of radiation can be measured. As carcinogenesis is modified by cell killing improved assays which measure the cytotoxic effect of radiation might provide data to improve the estimates for low-dose carcinogenic risk.

Precisely determining the relationship between low-dose radiation and cell lethality might also provide a clearer understanding of the initial shape of the survival curve. The majority of studies to delineate the shape of the cell survival curve have involved large single doses of radiation. These data have then been used to predict the response of cells to low doses of radiation. There are doubts about the validity of extrapolating the survival curve obtained at high doses to the low-dose region of the survival curve (Palcic and Skarsgard, 1984). The correlation that has been reported between the initial slope of the survival curve and the clinical radioresponsiveness of some tumour lines (Fertil and Malaise, 1981; Deacon *et al.*, 1984) has provided further stimulus to precisly determine low-dose cell lethality and consequently the shape of the cell survival curve.

1.3 The cell survival curve

The cell survival curve describes the viability of a population of cells exposed to a lethal agent, e.g. radiation, in the form of a dose-response relationship. The loss of viability in an irradiated population of cells is assessed usually by determining the number of surviving cells, rather than scoring those that are killed, as this is an easier parameter to score. The most direct method for assessing the survival of a cell is to measure its ability to proliferate indefinitely to form a macroscopic colony (see section 1.8.1). The dose-response relationship is therefore described in terms of cell survival as a function of radiation dose. Cell survival curves are plotted traditionally with the fraction of surviving cells on a logarithmic scale against dose on a linear scale. This method of presenting survival data developed from the early studies on the radiosensitivity of bacteria as many bacteria exhibit an exponential reduction in survival with increasing radiation dose. Therefore, plotting the fraction of surviving cells on a logarithmic scale produced a straight line which enabled the numerical value that described the slope of this survival curve to be used for quantification.

The shape of the dose-response curve for mammalian cells is dependent on the energy of the radiation and the irradiation conditions. Cells exposed to densely-ionising high linear energy transfer (LET) radiation, e.g. 4 MeV neutrons, have survival curves that approximate to a straight line, whereas the dose-response of mammalian cells exposed to sparsely-ionising low LET radiation commonly has an initial region where a smaller proportion of cells are killed per unit of dose than at higher doses, producing a curved or shouldered dose-response when survival is plotted on a logarithmic scale. Most cell lines exhibit these two basic characteristic survival-curve shapes (see section 1.4 for exemptions) after exposure to low or high LET radiation. As the LET of the radiation to which the cells are exposed is gradually increased, the survival curve progressively straightens and it loses the initial curved region (Fig. 1.1)(Barendsen, 1968). However, some repair-deficient cell lines and cells of patients suffering from *xeroderma pigmentosum* or *ataxia telangiectasia* have linear survival responses with little or no shoulder following exposure to low LET irradiation (Fig. 1.2).

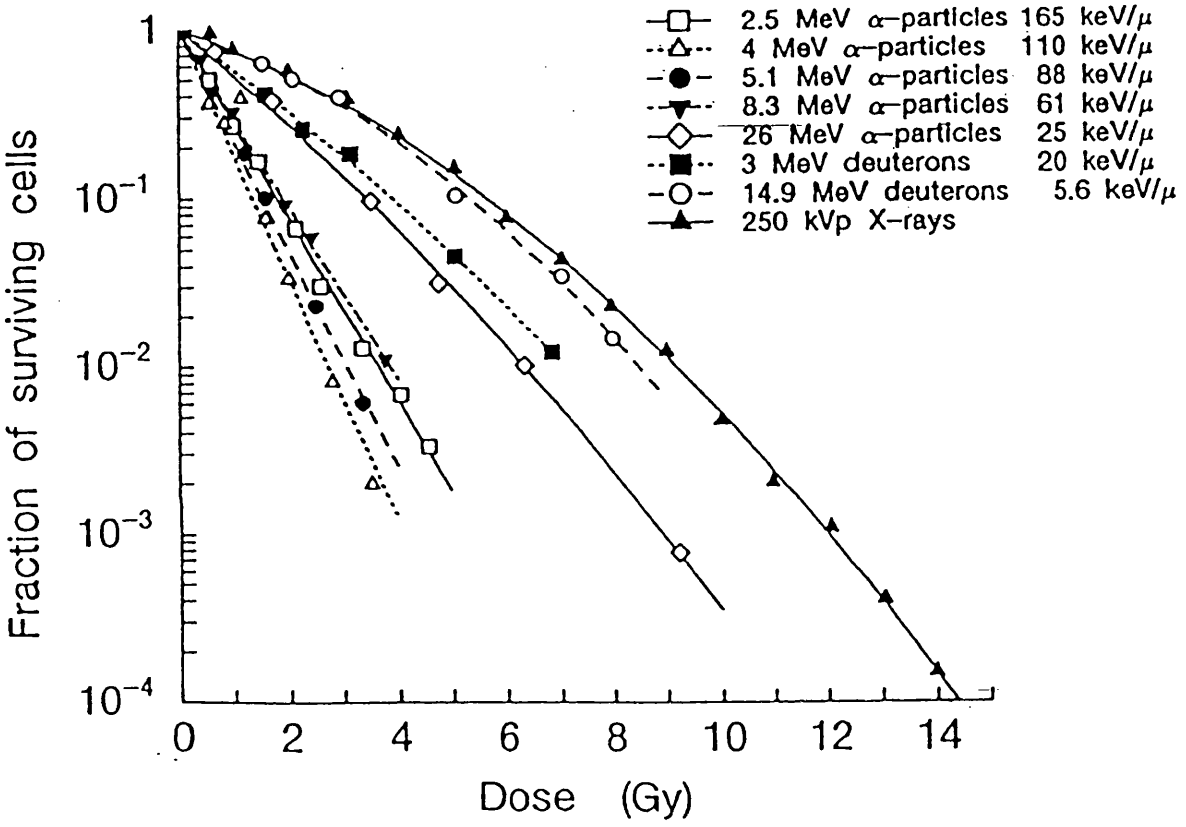

Fig. 1.1

Survival of mammalian cells plotted against radiation dose for eight different radiations with LET varying from 2 keV μm^{-1} (250 kVp X-rays) to 165 keV μm^{-1} (2.5 MeV α-particles). As the LET increases over the range 2-110 keV μm^{-1} the slope of the survival curve increases and the shoulder disappears (from Barendsen, 1968).

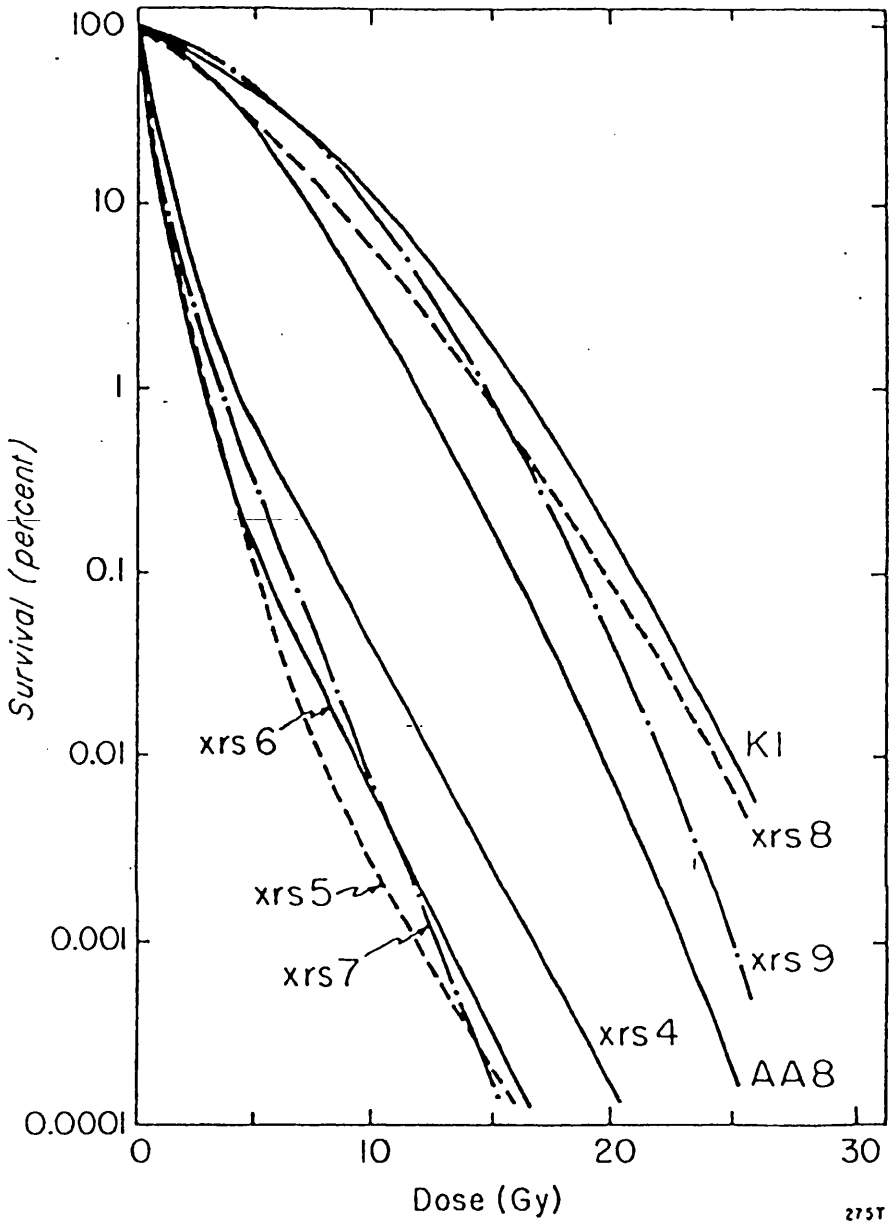

Fig. 1.2

The survival curves of different repair-deficient cell lines. The wild type parental cell lines, CHO-K1 and CHO-AA8 have typical mammalian cell survival curves with an initial curved region followed by a more linear region at higher doses. The radiosensitive repair-deficient cell lines (xrs 4, xrs 5, xrs 6, xrs 7) have atypical survival curves without an initial 'shouldered' region (reproduced from Denekamp et al., 1989).

The presence of a shoulder on the survival curve suggests that the additional damage incurred by a cell from a unit amount of radiation given following a low doseof radiation is less effective than the damage from the same amount of radiation given after a high dose of radiation. This has prompted the suggestion that some of the damage incurred by the cell over the dose range covered by the shoulder of the survival curve is sub-effective and therefore, it is often referred to as sublethal damage (Elkind *et al.*, 1967). This term was used in a purely descriptive sense to explain the presence of the shoulder of the survival curve. The term sublethal damage is also used in radiobiology to describe a type of lesion in some theoretical models which have been developed to explain the mechanism of action of radiation (Chadwick and Leenhouts, 1973). This dual usage causes confusion when discussing and interpreting the effectof radiation. A distinction in the terminology should be made between the description of the shape of the survival curve in terms of the recovery from radiation damage and the theoretical lesions postulated to exist in models of radiation action. Describing the actual shape of the dose-response curve for most cell lines maybe relatively simple but determining the biophysical mechanisms which account for this shape is however, more difficult (see section 1.5).

1.4 Multi-component cell survival curves

Multiphasic survival curves with an inflexion point have been observed in yeast (Calkins and Todd, 1968) and insect cells (Koval, 1984 see Fig. 1.3). These biphasic survival curves were interpreted as resulting from the induction of repair systems which do not function in unirradiated or low-dose irradiated cells. Other examples of biphasic survival curves which appear in the literature, e.g. in yeast (Beam *et al.*, 1954) and algae (Horsley & Pujara, 1969), were shown to be due to a small radiosensitive subpopulation of cells within the whole cell population.

1.5 Interpretation of the cell survival curve: historical overview

1.5.1 Biophysical models

The early models of radiation action were based on the target theory developed by Lea in 1946 and attributed cell killing to the inactivation of targets by ionisation

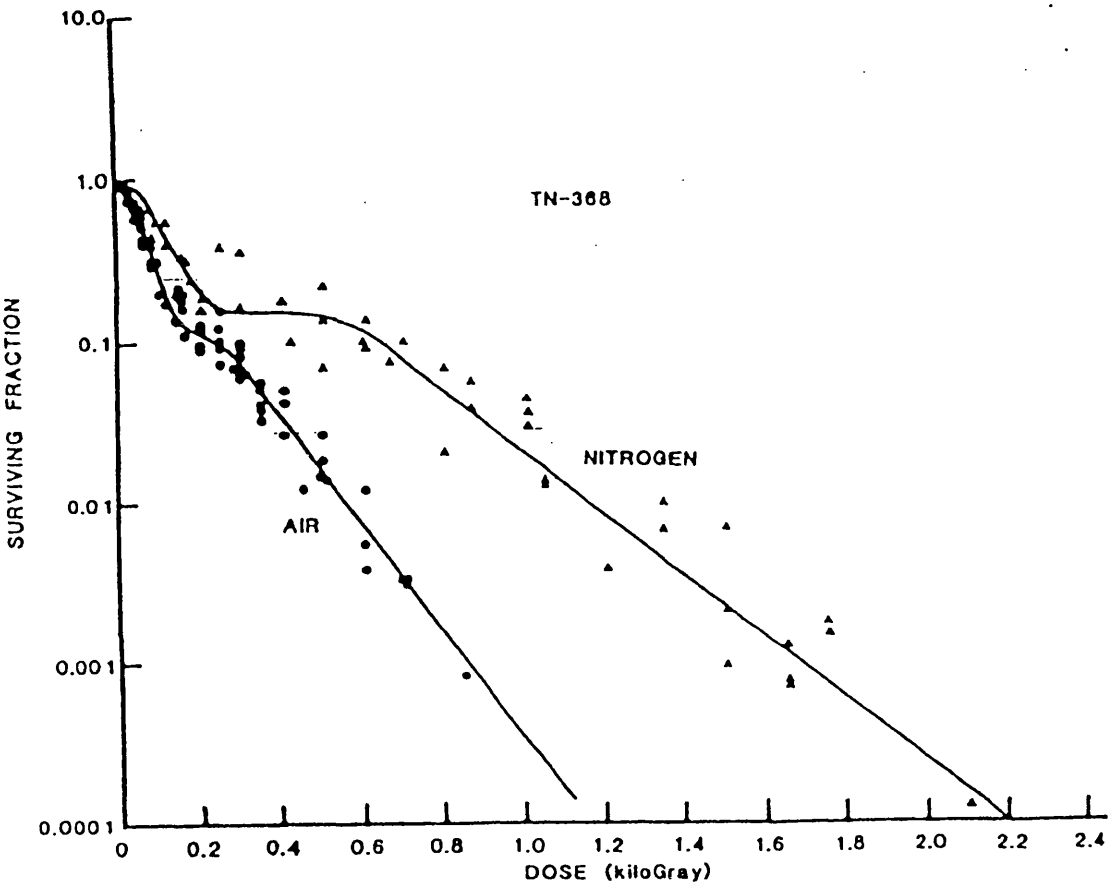

Fig. 1.3
Survival curves for TN-368 insect cells irradiated under oxic and anoxic conditions with 260 kVp X-rays. Both survival curves are characterised by an initial small component having a steep slope followed by a broad-shouldered region near the 0.1 survival level, and finally a shallower sloped component (from Koval, 1984).

events, referred to as hits. Before the development of the clonogenic assay for mammalian cells, radiobiologists measured the radiation response of bacteria and fungi. The dose response of these prokaryote cells was frequently a single exponential function and survival was therefore described by the slope of the linear survival curve (Alper, 1979). Owing to the exponential survival response it was postulated that the cell contained a single target requiring just one hit for inactivation, the probability of inactivation being proportional to dose.

In this situation Poisson statistics apply as there are a large number of 'hits' on non-target sites and the probability of the next hit occurring on the target is small. The probability of survival is therefore represented by the equation:

$$\text{surviving fraction (SF)} = e^{-D/D_o} \qquad (1.1)$$

where D = dose

D_o = is the reciprocal of the slope of the survival curve, i.e. the dose required to reduce the surviving fraction by the factor e^{-1} which is also referred to as the inactivation constant.

The first *in vitro* mammalian cell survival curve produced by Puck and Marcus (1956) did not fit this single target - single hit model: the survival curve had a small shoulder and could not be fitted by a single exponential function. The survival curve was better described by the expression:

$$\text{surviving fraction} = 1 - (1 - e^{-D/D_o})^n \qquad (1.2)$$

where D = dose

D_o = reciprocal of terminal slope (inactivation constant)

n = extrapolation number

The term n in Eqn. 1.2 became known as the extrapolation number, and represented the intercept of the terminal slope of the survival curve extrapolated back to the zero dose level (Alper, 1979). The HeLa cell survival curve produced by Puck and Marcus (1956) had an extrapolation number of 2 and this was interpreted as indicating two targets in the cell. It was thought that a single hit was required on each of the two targets for the cell to be killed. Subsequent mammalian survival curves had higher extrapolation numbers and cells were therefore thought to contain multiple targets or possibly a single target that required multiple hits. The shoulder of

the survival curve was interpreted as representing the accumulation of either single hits in the multiple targets or multiple hits in the single target. In the multi-target hypothesis, all of the n targets had to be inactivated for cell death to occur; one or more unaffected targets would rescue the cell. Alternatively the cell would survive n-1 hits in a single target but succumb to the n^{th} hit. At a mechanistic level the concept of an accumulation of damage implied the existence of sublethal lesions which were capable of complete repair providing additional damage was not accumulated. This concept was developed and used to explain the split-dose recovery that was seen when the radiation dose was fractionated (Elkind and Sutton, 1960) and consequently therefore the experimental observation of split-dose recovery became synonymous with the concept of a mechanistic sublethal lesion.

The multi-target model (Eqn. 1.2) describes the mammalian cell survival response adequately at high doses of radiation but not at lower clinically-relevant doses. At very low doses the model predicts an initial zero slope whereas the majority of the published experimental data are not consistent with this. Bender and Gooch (1962) therefore proposed a modification to the multi-target model to eliminate the non-zero slope by incorporating an additional exponential term to describe cell survival at very low radiation doses. This became known as the two component model and was represented by the equation.

$$\text{surviving fraction} = e^{-D/D_1}\,[1 - (1 - e^{-D(1/D_0 - 1/D_1)})^n] \qquad (1.3)$$

D_1	=	slope of initial linear region of the survival curve
D_0	=	slope of the final exponential region
$e^{-D/D1}$	=	This parameter describes the sensitivity at very low doses and indicates a non-zero initial slope, it is sometimes postulated as the 'one-hit' component. It is thought that the initial non-zero slope may account for the action of high LET radiation within the low LET spectrum, or the densely ionising track ends of secondary and tertiary electrons produced by the interactions of low LET radiation.

Using the two component model the survival curve can be characterised by the initial slope D_1, the final slope D_0 and n, the extrapolation number. A large n value ($n \geq 10$) signifies a survival curve with a broad shoulder whereas smaller values of n

(1-2) imply narrower shoulders. Although the survival curves generated by this model fit experimental data with reasonable accuracy the model predicts that the change in cell survival that occurs over the dose range 0-D_q Gy is almost linear and this contradicts some experimental data. D_q is defined as the intercept of the back-extrapolated terminal straight line on the 100% survival axis (Alper, 1979).

1.5.2 Lesion interaction models

The concept that the shoulder of the survival curve demonstrates the requirement for more than one hit in the target volume was also suggested by Kellerer and Rossi (1972) in the 'theory of dual radiation action'. This model proposes that cell inactivation is through the formation of lesions in critical sites. A biological lesion is formed through the interaction of two sublesions. The production of sublesions in the cell and the number of such sublesions is directly proportional to dose. It is possible that sublesions interact at significant distances on a subcellular scale. All pairs of sublesions within a specific distance of one another have equal probability of interacting. The initial term in the dose response equation (αD) reflects the formation of lethal lesions which are produced as a result of sublethal lesions via intratrack ionisation events, whereas the dose squared parameter (βD^2) which generates the shoulder of the survival curve is due to sublesions interacting from intertrack ionisation events. The dual theory of radiation action proposes that the survival response should be fitted with a linear quadratic (LQ) equation (see Figs. 1.4 and 1.5):

$$SF = \exp(-\alpha D - \beta D^2) \qquad (1.4)$$

where D = dose
α, β = constants

The molecular theory of Chadwick and Leenhouts (1973) also describes the dose response by a linear quadratic equation. The molecular theory postulates that the primary target in the cell is DNA and that the double strand break (DSB) is the critical lesion in cell killing. The model assumes that DSBs produced by low LET radiations are responsible for the curvature of the dose-response curve and arise from the interaction of lesions produced from independent ionisation tracks in the DNA. The LQ model predicts a continuously bending survival curve with no final exponential region. The α term describes the shape of the survival at low doses and

(A)

Single-target/Single-hit model

$$SF = e^{-D/Do}$$

These straight survival curves are commonly found for viral inactivation and bacterial killing.

(B)

Multi-target single-hit model

$$SF = 1 - (1 - e^{-D/Do})^{n}$$

These survival curves have a shoulder with an initial zero slope and are useful for describing mammalian cell radiation responses at high doses, but not at low or clinically-relevant doses.

(C)

Two component model

$$SF = e^{-D/D1} [1 - (1 - e^{-D(1/Do-1/D1)})^{n}]$$

The multi-target model can be multiplied by an exponential function to give an initial non-zero slope which better accounts for the radiation response in the 'shoulder region' and is called the two component model.

(D)

Linear Quadratic Model

$$SF = \exp(-\alpha D - \beta D^2)$$

This model produces a continuously-bending survival curve which is characterised by the α/β ratio, which is the dose at which the 'linear' contribution to damage (αD) equals the quadratic contribution (βD^2). This model describes the radiation response in the low dose region better than the two component model which predicts an almost linear response.

Fig. 1.4
Equations describing the shape of the survival curves represented in Fig. 1.5

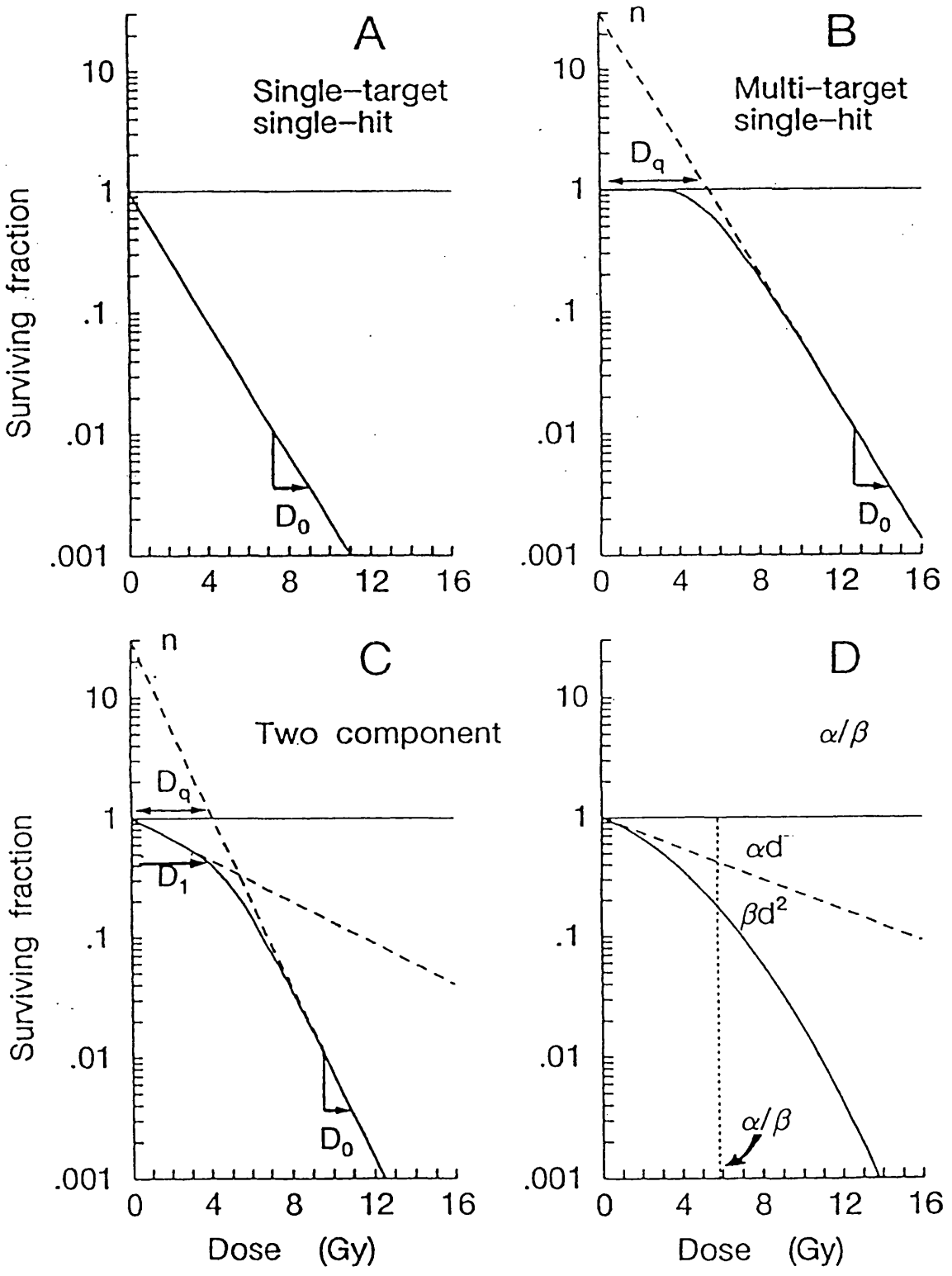

Fig. 1.5
Parameters used to describe the shape of the cell survival curve in the single-target, single-hit, multi target single-hit, two component and linear quadratic survival models.

is similar to the $e^{-D/D1}$ term in the two-component model whereas the β term reflects the high dose response. The dose at which the linear (α term) and quadratic (β term) components are equal is the α/β ratio and this can be used to describe the curvaturesurvival function and therefore the 'recovery capacity' of the experimental system.

The LQ models and the two-component model both describe experimental data reasonably well; the two component model gives the better fit at very high doses where survival curves seem experimentally to straighten out whereas the LQ model provides a better fit at lower doses. The LQ model is increasingly being adopted to describe the cell-survival response because it is the easier of the two types of model to use and it gives a better fit to the experimental data in the clinically relevant dose range.

Although the biophysical and biological basis of the molecular theory (Chadwick and Leenhouts, 1973) and theory of dual radiation action (Kellerer and Rossi, 1972) are no longer thought to be valid the LQ equation is still used extensively and effectively to describe the survival data of a wide variety of cell lines. Some subsequent models of radiation action have therefore attempted to explain the biophysical basis for the LQ model.

1.5.3 Models combining lesion interaction and repair

The interest in explaining the shape of the radiation dose-response curve for mammalian cells as a consequence of the repair of radiation-induced damage, evolved from studies in the field of microbiology and the investigations of the repair mechanisms of UV-induced radiation damage. Setlow and Carrier (1964) reported that radiation-induced thymine dimers were removed from bacteria by an excision mechanism specific for that type of damage. In the same year Rasmussen and Painter (1964) reported that mammalian cells were able to repair damage which had been introduced experimentally into the cells DNA. Subsequently, it was shown that the cells from patients with *xeroderma pigmentosum* were defective in repairing UV-induced thymine dimers (Cleaver, 1968) and that cells from people suffering from *ataxia telangiectasia* were deficient in DNA repair after X-irradiation (Paterson, 1978),

implying that the extreme radiosensitivity of cells associated with these diseases was due to defective DNA repair systems. Other studies also suggested that DNA was the critical target in radiation induced cell death (see section 7.1.1). These observations lead to the development of models of radiation action which included components to account for the repair of radiation induced lesions.

The repair-misrepair (RMR) model proposed by Tobias *et al.* (1978) suggested four distinct phases of the response of cells to radiation. The initial phase was the transfer of ionisation energy to the cell, followed secondly by the migration of the deposited energy and the establishment of molecular lesions, followed thirdly by biochemical events including repair and followed finally by processes that have a genetic impact on the cell. The model is divided into dose-dependent and time-dependent phases, both of which effect the survival curve. Initial lesions produced from physical and chemical interactions are regarded by the model as uncommitted because they are still subject to enzymatic repair or modification some time after formation. The uncommitted lesion, via enzymatic repair processes, can either be repaired or misrepaired. Cell survival is a consequence of competition between the correct repair of the damage (eu-repair) and misrepair which gives rise to viable mutants or genetic alterations that are lethal.

The lethal-potentially lethal (LPL) model of Curtis (1986) is a unifying model incorporating several concepts from different models of radiation action (see Fig. 1.6). The model incorporates the concept of the competition between the correct repair and misrepair of radiation induced lesions seen in the RMR model, with the interaction of lesions seen in the theory of dual radiation action, the molecular theory of radiation action and the RMR model. The potentially lethal lesion in the LPL model is regarded as a DNA DSB. Cells may either be lethally damaged or potentially lethally damaged by radiation. Potentially lethal lesions can either be repaired correctly (eu-repair), misrepaired and become lethal, or the original damage can be fixed, which is also lethal to the cell. Misrepair occurs via the interaction of two potentially lethal lesions.

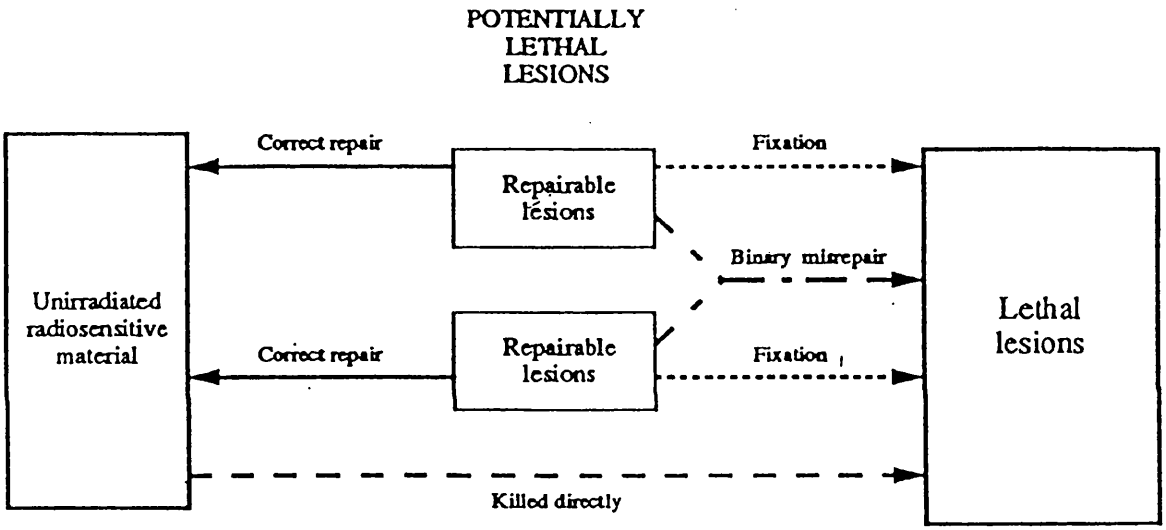

Fig. 1.6

The Curtis Lethal Potentially-Lethal (LPL) model of cell inactivation. Undamaged cells may be killed directly (dashed line) by a lethal lesion. Potentially lethal lesions may be produced which are correctly repaired (eu-repair, solid line), or fixed to become lethal (dotted line) or combined with another potentially lethal lesion to form a lethal lesion (mis-repair, dot-dashed line) which is referred to as a binary misrepair.

Other models of radiation action postulate an initial linear induction of potentially lethal lesions with increasing radiation dose with a subsequent process of repair that becomes less effective as the dose increases because of 'repair saturation'. A repair process which was equally effective at all doses would produce another survival curve of much shallower slope whereas a repair process that becomes saturated with increasing dose results in a shouldered survival curve. To distinguish the repair of potentially lethal lesions proposed in saturable repair models from the recovery response referred to as 'PLD' repair by Phillips & Tolmach (1966), Alper (1979) termed the saturable repair of potentially lethal lesions Q repair. This operates through a specific 'Q' factor. The concept of a Q factor was developed from work of Sinclair (1973) who proposed that the different radiosensitivities of the individual phases of the cell cycle were due to a factor, designated Q, which varied in amount through the cell cycle repairing damage before it could be expressed.

Powers (1962), who first postulated a saturable repair process, proposed that a 'pool of intracellular constituents or states' existed to repair lesions and this became depleted owing to repair and required replenishment for further repair to continue. The pool concept of Powers (1962) was developed by Orr *et al.* (1966), who proposed that repair saturation was achieved when the substrate sites of the enzyme molecules were saturated as part of a process where damage fixation competed with the repair of lesions carried out by a limited reserve of enzymes. Other mechanisms of achieving repair saturation have also been proposed to account for the curvature of the dose response curve. A dose dependent decrease in efficiency of repair due to the radiation-induced inactivation of the repair enzymes alone (Hayes, 1966), and coupled with a dose dependent increase in initial damage due to the depletion of molecules which compete with the repair process to fix damage (Payne & Garret, 1975) have been proposed to explain the shoulder of the survival curve. A model incorporating the concept of 'competing molecules' was also suggested by Kappos & Pohlit (1972). These authors suggested that the final level of lethal damage was dependent on the concentration of organic "scavenger" molecules present in the cell. These organic "scavenger" molecules competed with the target molecules in the cell to combine with damaging radiolytic radicals produced from the interactions of radiation with matter.

The depletion of these competing "scavenger" molecules as they combine with increasing level of the radical species would lead to a dose dependent increase in radiosensitivity and therefore provide an explanation for the curvature of the survival curve.

Calculations performed by Goodhead (1980) demonstrated that the shoulder of the survival curve is unlikely to be due to the interaction of radiation-induced lesions as proposed by Kellerer & Rossi (1972) in the dual theory of radiation action because the probability of lesions interacting over the distances proposed in the model (up to 1 mm) is negligible, over the dose range covering the shoulder. These observations coupled with the data of Wheeler and Wierowski (1983) and Wierowski *et al.* (1984) which showed that the repair of strand breaks *in vivo* followed biphasic repair kinetics and that the rate of repair of the initial component is characteristic of saturable repair also lead Goodhead (1985) to propose that a saturable repair phenomenon can account for the survival curve shoulder (see Fig. 1.7).

1.6 Recovery from radiation damage

Two types of recovery phenomena have been described which modify the shape of the cell survival curve following X-irradiation. Both are measured in terms of increased cell survival and each have been defined by experimentally descriptive phrases.

1.6.1 Sublethal Damage (SLD) recovery

The first recovery phenomenon was reported by Elkind and Sutton (1956) and relates to the restoration of the shoulder of the survival curve. They noted that a sparing effect on cell survival was achieved when a dose of radiation was fractionated rather than administered as a single dose, providing a sufficient interval was left between the fractions to allow recovery. The sparing effect became maximal as the inter-fraction period was increased to 2 hours. The increase in survival that was observed was interpreted as being due to the repair of sub-effective damage received from the first radiation dose before the second radiation dose was given. The sub-effective damage that was thought to accumulate during the first radiation dose was

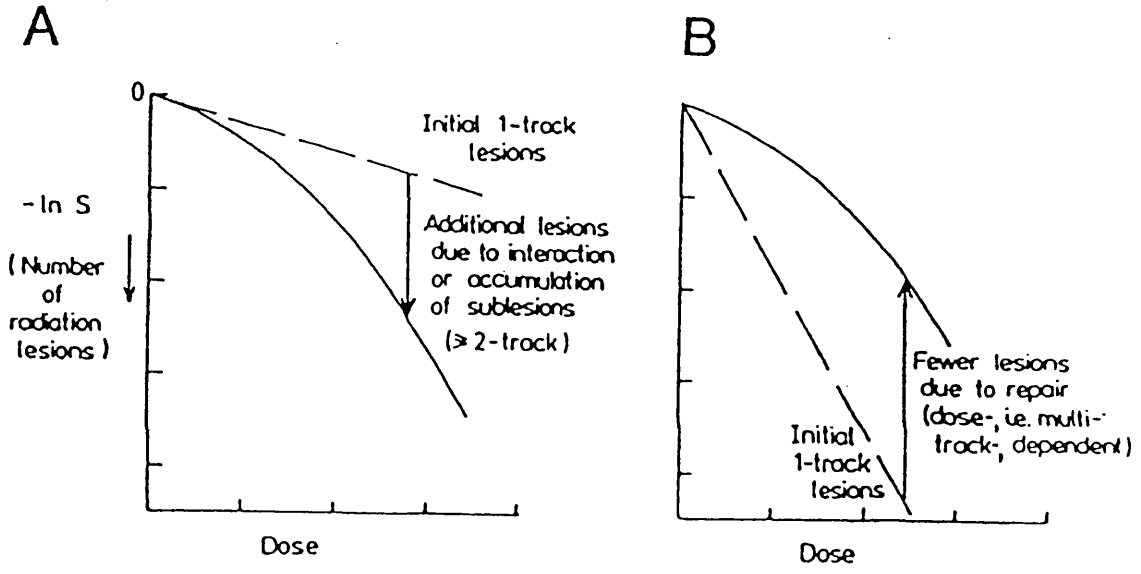

Fig. 1.7

Repair saturation models. An illustration of the basic conceptual difference between the interpretation of shouldered survival curves

A: lesion accumulation/interaction models

B: dose dependent repair models

In A the survival curve bends down due to the interaction of lesions whereas in B the downwards bending occurs because enzymatic repair of DNA damage becomes saturated (i.e. less effective) at higher doses.

designated sublethal damage (SLD) by the authors and the recovery that restored the shoulder was therefore called 'sublethal damage repair' (SLDR). The molecular basis of split dose recovery is not yet fully understood. However, the extent of recovery is a reflection of the survival curve shoulder; broad-shouldered survival curves exhibit greater sparing due to fractionation than do narrow-shouldered survival curves (see Fig. 1.8).

1.6.2 Potentially Lethal Damage (PLD) recovery

The second recovery phenomenon was first described by Phillips and Tolmach (1966). They observed an increase in cell survival following radiation treatment of G_1 phase HeLa cells incubated in culture medium containing the protein synthesis inhibitor cycloheximide, compared with G_1 cells irradiated in standard culture medium. An unexpected increase in the level of cell survival was also reported when exponentially growing cells were held at 20°C (Whitmore and Gulyas, 1967) or overlaid with a balanced salt solution (Belli and Shelton, 1969) following radiation treatment. Little (1973) reported that the survival of density-inhibited cultures of stationary phase cells was enhanced by a factor of 1.95 for cells subcultured 6 hours after receiving 5 Gy of X-rays compared with cells receiving the same dose but plated immediately after radiation treatment. The authors postulated that the increased level of survival seen in these studies was due to the repair of potentially lethal damage (PLDR). This damage was designated potentially lethal (PLD) because under normal growth conditions it would prove lethal. However, altering the post-irradiation culture conditions delayed mitosis therefore allowing the cells a period of time for the recovery of radiation damage to occur before cell division (see Fig. 1.9).

1.6.3 SLDR and PLDR: are they the same phenomena?

Sublethal and potentially lethal damage repair are operational terms to describe experimental observations. However, they have also been used to explain the effect of radiation at a mechanistic level implying a 'cause' and 'effect' relationship. These descriptive terms have caused considerable controversy. Many authors, notably Alper (1979) have questioned the existence of sublethal lesions altogether, suggesting that all radiation-induced lesions are potentially lethal. Others have proposed that SLDR

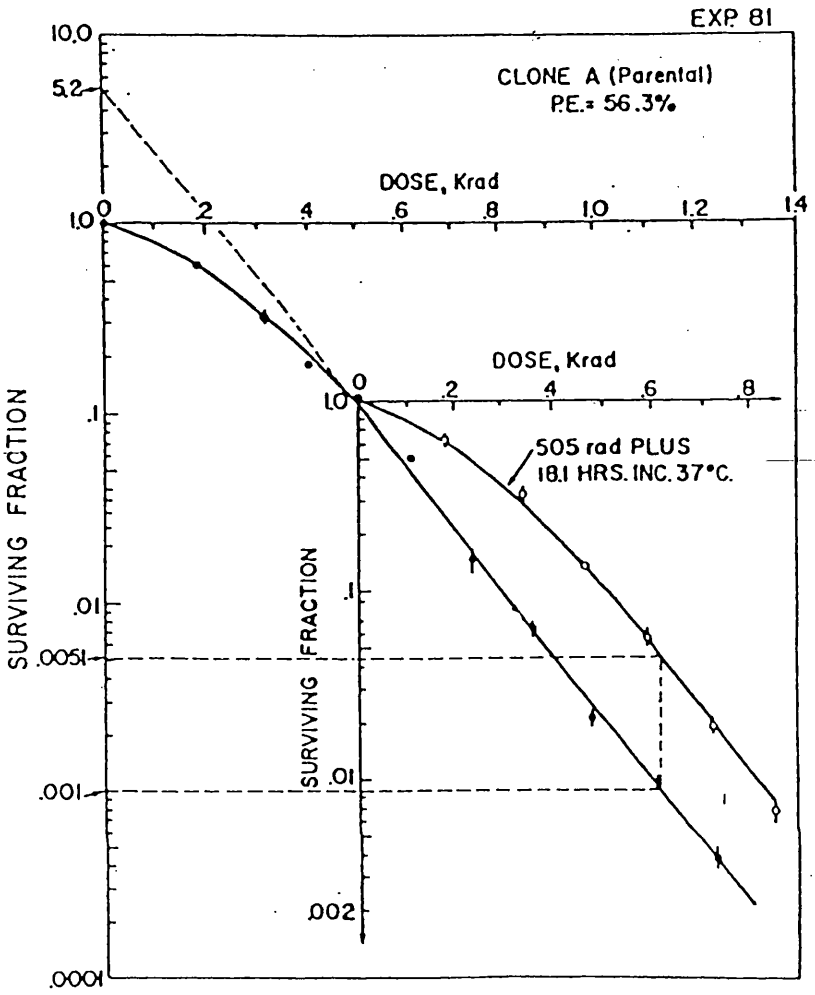

Fig. 1.8

A demonstration of split dose recovery.

The solid circles are the survival obtained after a single radiation exposure. The open circles represent the survival obtained following irradiation given as two fractions separated by 18.1 h. The first fraction was 5.05 Gy and the size of the second fraction is indicated on the diagram. Less cell killing was achieved in the fractionated regime (SF = 0.0051) compared with the single dose treatment (SF = 0.001) (dashed lines) after the same total dose. The increase in cell survival seen when the radiation dose was fractionated was postulated to reflect the repair of subeffective damage during the interval between the two fractions (reproduced from Elkind and Sutton, 1960).

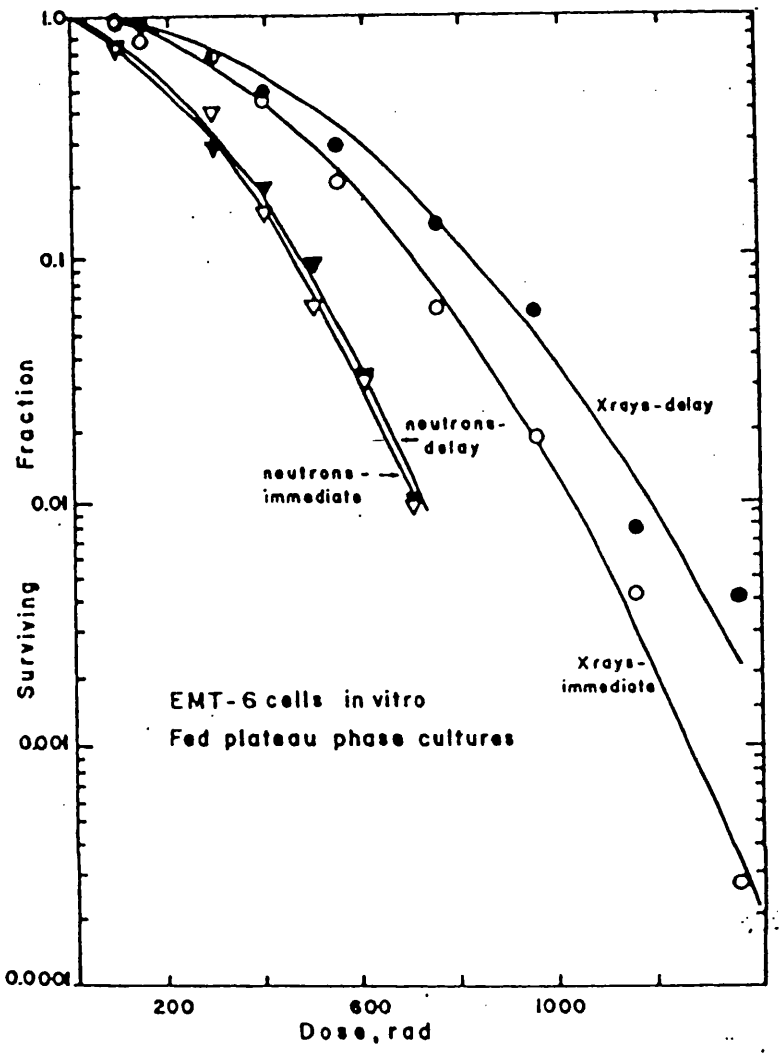

Fig. 1.9

Cell survival curves for EMT-6 cells irradiated with X-rays and neutrons. Delaying the replating of the cells by 5 h increased the level of cell survival (closed symbols) compared with the same cell population plated immediately following irradiation (open symbols). The increase in cell survival was postulated as the repair of PLD which occurred during the interval between irradiation and plating of the cells. A much greater increase in survival was seen following delayed plating after X-irradiation than was observed following neutron irradiation (from Rasey and Nelson, 1981).

and PLDR are manifestations of the same phenomenon illustrated as two separate effects by differing experimental procedures.

Elkind *et al.* (1967), noted that treating S-phase Chinese hamster cells with actinomycin D during the interval between radiation fractions (split dose experiment) or following a single dose of radiation (alteration of post-irradiation conditions), produced a similar change to the shape of the survival curve and that both experimental systems produced similar half times of repair. Elkind *et al.* (1967), therefore proposed that the experimental observations of sublethal and potentially lethal damage recovery may be the result of the same phenomenon. Dewey *et al.* (1972) also reported that the repair kinetics for SLD were similar to those of PLD, implying a common phenomenon. Other workers however have illustrated a difference between the two phenomena. Hahn *et al.* (1973) working with monolayers of plateau phase Chinese hamster cells (HA-1) proposed that the repair of PLD and SLD were independent processes noting that the repair of PLD mainly effected the slope of the survival curve whereas the repair of SLD involved the shoulder. Evans *et al.* (1974) also suggested differences between the phenomena of SLD and PLD reporting that actinomycin D inhibited SLD repair from occurring in plateau phase Chinese hamster HA-1 cells but did not inhibit PLD repair. Iliakis (1988) suggests that the confusion between SLDR and PLDR can be resolved if two categories of PLD are defined. The categories are those defined by 1), post-irradiation incubation conditions that *induce* the fixation of damage which would otherwise have been repaired e.g. treatment with caffeine, anisotonic media or DNA synthesis inhibitors and 2), those conditions that *prevent* the fixation of damage allowing repair to take place e.g. incubation of cells in sub-optimal growth conditions or in density inhibited cultures. The first category was designated α-PLD and this mainly affected the width of the curved region of the survival curve, whereas the second class of PLD was termed β-PLD as this effected the survival curve slope. The two types of PLD are characterised by different repair times, the repair of β-PLD is generally completed within 1 hour whereas α-PLD requires commonly 2-4 hours for full repair to occur. Iliakis (1988) reports a similarity between the repair of SLD and α-PLD both in terms of repair kinetics and in a change

to the survival curve parameters and therefore suggests they may be the same phenomenon. No similarity was found between SLDR and β-PLDR.

1.7 Induced repair systems

There is widespread acceptance of the existence of inducible repair pathways in prokaryotes (Peters & Jagger, 1981) and lower eukaryotes (Ruby & Szostak, 1985) following exposure to a wide variety of cytotoxic insults. Although, the induction of DNA repair mechanisms has been demonstrated in eukaryotic cells following exposure to cytotoxic chemicals 'induced repair' has not been fully substantiated following X-radiation. Mammalian cells exposed to low levels of alkylating agents are more resistant to further damage by subsequent exposure to a higher concentration of the same chemical owing to the induction of a repair process in the interval between the two exposures (Samson and Schwartz, 1980). This adaption response was thought to be due to the induction of an alkyltransferase enzyme (Olsson & Lindahl, 1980). This enzyme was postulated to repair the damage from the first exposure and then remain *in situ,* thereby reducing the extent of the damage from the second exposure. Recently, many reports have appeared in the literature proposing the existence of inducible repair systems in mammalian cells following the exposure to ionising radiation. Olivieri *et al.* (1984) reported that exposing human lymphocytes to tritiated thymidine or low doses of X-rays resulted in the induction of an adaptive response which made the cells less susceptible to the formation of chromosome aberrations from subsequent high doses of X-rays. This phenomenon was also reported by Shadley and Wolff (1987). They reported a reduced number of chromosome aberrations in human lymphocytes following an exposure to an X-ray dose of 1.5 Gy in cells previously irradiated with X-ray doses of 0.5-1 cGy, compared with cells not receiving a small pretreatment dose. It was postulated that the small pretreatment dose of radiation induced a repair mechanism that remained *in situ* and if still present at the time of the second exposure caused the primary breaks resulting from the second exposure to be repaired more efficiently. This hypothesis is supported by data of Wiencke *et al.* (1986), who reported that the adaptive response that resulted from the pretreatment could be reduced by 3-aminobenzamide (3-AB), an inhibitor of poly (ADP-ribose)

polymerase. This enzyme is thought to be manufactured by the cell in response to the production of strand breaks (Benjamin and Gill, 1980), and its presence in the cell may aid the repair of those strand breaks. The inhibition of the adaption phenomenon by 3-AB implies that the damage from the first exposure stimulates the production of enzymes which repair damage from any subsequent exposure.

The exact mechanisms or repair pathway responsible for the adaptive response following X-irradiation are as yet unknown. The production of new proteins has been shown to occur in human lymphocytes as a response to a radiation insult following X-ray doses as low as 1 cGy (Wolff *et al.*, 1989). It was reported in the same study that incubating the cells with cycloheximide, an enzyme which inhibits protein synthesis, suppresses the induction response, indicating that newly synthesised proteins are necessary for the adaptive response. It was postulated that these proteins may be repair enzymes.

The existence of inducible repair systems has also been postulated to occur *in vivo* (Joiner and Johns, 1988). The effect of low doses of radiation on normal tissues was assessed using an approach where the sub-threshold damage from small doses of radiation was topped up by a single dose of high LET radiation to a level that was sufficient to give a measurable effect. An increased radiosensitivity below X-ray doses of 1 Gy per fraction was observed in mouse skin using this top-up technique (Joiner and Denekamp, 1986). Experiments designed to explore the limitations of an LQ model for describing the effects of very low doses per fraction also observed an unexpected increased X-ray sensitivity below 1 Gy per fraction (Joiner and Johns, 1988). The LQ model described adequately murine kidney data down to X-ray doses per fraction of 1 Gy but lower X-ray doses per fraction were more effective per gray than predicted by the model (Joiner and Johns, 1988). This was not thought to reflect incomplete repair of radiation damage in the kidney between fractions as the smallest fractions (0.2 Gy) would require a half-time of repair of up to 200 hours to be consistent with the data. The low labelling index of the kidney also made it unlikely that the increased radiosensitivity was due to a redistribution of cells into radioresistant phases resulting from fractionation. The authors suggested that the phenomenon may be explained by an induction of repair causing an increase in

radioresistance of the whole cell population as the dose per fraction increased from 0 to 1 Gy.

1.8 The measurement of cell survival *in vitro*

1.8.1 Conventional clonogenic assay

The lethal effect of radiation on cells *in vitro* is assessed usually using a clonogenic assay which determines the ability of a single cell to proliferate into a macroscopic colony. Following irradiation, a surviving cell is defined as one which achieves at least 5 to 6 doublings, producing a colony of at least 50 cells. Cells which retain the ability to produce a colony of this size are regarded as having the potential to proliferate indefinitely and accordingly are classified as having survived the radiation treatment. Cells which undergo only a few divisions producing abortive colonies of less than 50 cells are classified as non-survivors as their proliferative ability is limited.

In the conventional method of measuring clonogenicity devised by Puck and Marcus (1956), a known number of cells is inoculated into a series of culture dishes and irradiated. The number of cells seeded per dish is adjusted by serial dilution in order that the same number of colonies are produced on each dish from previous estimates of surviving fraction. Too few colonies on a plate reduce the statistical significance in the survival estimate, while too many colonies can not be counted accurately since the colonies would merge into one another. The cells are then incubated and allowed to grow until the cells which have survived the treatment produce macroscopic colonies. The surviving fraction is then calculated as being the ratio of colonies produced to the number of cells plated with a correction factor to account for plating efficiency. Plating efficiency indicates the percentage of cells seeded that grow into colonies on the unirradiated control plate (Fig. 1.10). The accurate assessment of cell survival following low-dose irradiation in the dose range 0.01-2 Gy is difficult to achieve using this procedure owing to experimental and statistical uncertainties associated with the assay. Three significant errors exist which make this assay imprecise at low doses:

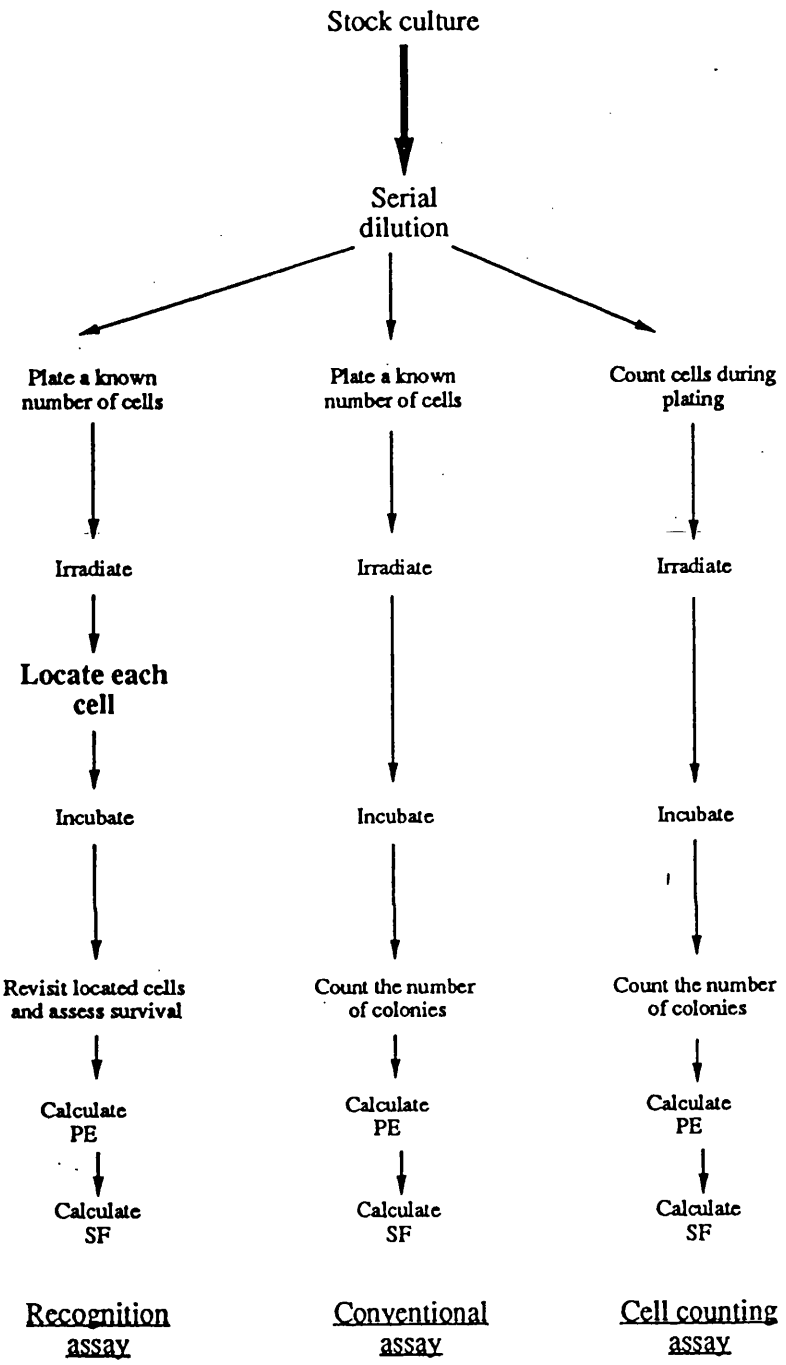

Fig. 1.10

Flow diagram showing some of the procedures in the recognition, conventional and cell counting assay to measure the clonogenicity of cells. In both the recognition assay and cell-counting assay the number of cells plated is determined. In the conventional assay the number of cells plated is calculated from the serial dilution of the stock culture of cells.

1) Counting error: uncertainty of the precise number of cells in the cell sample

2) Dilution error: inaccuracy in the volume of suspension transferred during the serial dilution.

3) Sampling error: uncertainty in the exact number of cells transferred onto the growth surface.

Additionally, uncontrolled variables which operate day to day and week to week, e.g. such as slight variation in the composition of the medium and irradiation temperature, result in procedural errors. These are reduced by good experimental techniques and by increasing the number of measurements of surviving fraction. The largest difficulty in assessing survival following exposure to low doses of radiation arises primarily from the uncertainty in the precise number of cells *actually* plated. A consistent counting, dilution or sampling error would be more important at low radiation doses (i.e. at high levels of surviving fraction) than at higher doses (i.e. low levels of surviving fraction) because the error in the number of cells plated may be larger than the fraction of cells that are killed at the very lowest doses. At higher doses the error in the number of cells plated will be masked by the greater level of cell kill that is seen at these doses.

1.8.2 Modified clonogenic assays

Watts *et al.* (1986) demonstrated that the conventional clonogenic assay can be used to produce reliable assessments of cell survival down to X-ray doses of 0.25 Gy by employing extensive replication of each dose point along with strict pipetting procedures whereby all samples were inoculated from the same cell suspension with the same pipette. Although these procedural modifications improved slightly the precision of the assay, they are too costly in manpower and resources for routine usage.

To overcome the uncertainty in the number of cells plated in the conventional assay, cell counting and cell recognition assays were developed to assess the radiation response of an *exact* number of cells, thereby, eliminating a large part of the error associated normally with measuring cell survival over the low dose range. Counting

assays determine the precise number of cells actually plated by observing them during the plating procedure, whereas, in a recognition assay cells which have attached to the growth surface are individually located and their positional co-ordinates are recorded. No direct measure of cell attachment is scored in the counting assays; this is considered in the calculation of plating efficiency. The cell counting approach was shown to reduce the uncertainty in the actual number of cells plated to half of that seen using the conventional plating assay in two studies investigating the radiation response of protozoa (Calkins, 1967) and Chinese hamster lung fibroblasts (Bedford and Griggs, 1975). The recognition assay can be even more precise than the cell counting method because by recording the position of each cell the number of killed cells, as well as the number of clonogenic cells, can be scored. This facility improves the statistical accuracy of the assay because all the cells in the sample are accounted for, whereas cells which fail to attach in the cell counting assay and therefore do not produce colonies are incorrectly classified as radiation killed adding to the statistical uncertainty of the survival measurement. In addition, the recognition system also permits the life history of individual cells to be followed from the time of plating until the assessment of survival so that the growth of the logged cell can be investigated.

One of the earliest recognition assays was the automated low dose assay system (ALDAS) (Palcic *et al.*, 1983) which combined the manual location and recognition of the cells by an operator with an automatic logging of the positions of each cell. This semi-automated system was subsequently fully mechanised, to automatically locate and recognise individually plated mammalian cells without interfering with their ability to proliferate or perform other cellular functions. The complete automated system was named the Dynamic Microscope Image Processing Scanner (DMIPS) cell analyser (Palcic and Jaggi, 1986) (see section 2.1 for a fuller description). This system allows very accurate low dose survival measurements to be made with much greater statistical confidence than the conventional assay as a precise number of cells are assayed.

1.9 Aims of the investigation.

Previous work performed at the Gray laboratory optimised the plating procedure necessary for a recognition assay to be performed using the DMIPS cell analyser for one of the laboratory's cell lines, Chinese hamster V79-379A cells (Marples, 1987). Two cell survival experiments carried out previously using these procedures, measured the radiation response of this cell line down to an X-ray dose of 1.0 Gy. A primary aim of this study was to develop the DMIPS recognition assay in order to produce measurements of clonogenic cell survival that were consistent with values obtained using the conventional clonogenic assay in a region of dose assessable to both assays (e.g. 2-7 Gy) and then to go on and measure cell survival in the dose region not assessable to the conventional Puck and Marcus clonogenic assay. This would provide accurate measurements of low-dose cell killing, with an improved statistical precision than seen in the other studies, and therefore help to elucidate the precise shape of a mammalian cell survival curve at doses not previously accessible using a clonogenic assay. The effects of chemical repair modifiers and the radiation response of synchronised populations of cells can also be studied using this experimental system to determine the contribution of DNA repair and cell cycle phase in cell killing at these low doses. Recent software upgradings have also provided the potential to investigate other cell lines.

2.1 The DMIPS cell analyser

2.1.1 The hardware system (see Figs. 2.1, 2.2, 2.3)

2.1.1.1 The host computer (IBM-PC AT)

The computer acts as the system controller, initialising and co-ordinating the cell analyser. The majority of programs are menu driven and executed mainly by dedicated processors. The computer possesses the facilities to perform the image analysis, compute recognition algorithms and perform data analysis.

2.1.1.2 Inverted microscope

The microscope is the Nikon TMD model used in the brightfield mode. No condenser lens is used, to ensure the object is illuminated with parallel light rays. Sufficient information can be collected for the recognition of cells at 10× magnification (4× objective magnification coupled with 2.5× projection lens magnification). Using higher magnifications would generate more optical information which would reduce the speed at which a flask could be scanned. Low magnification also provides a greater range of focus than would be possible at higher magnification.

2.1.1.3 Microscope stage plate

An indented template on the microscope stage ensures that each culture flask is positioned precisely and reproducibly. The stage is equipped with X and Y plane stepping motors and can be controlled automatically by the host computer or manually via a joystick. Under computer control the stage is configured routinely to move in 1 μm steps (0.1 μm minimum - 10 μm maximum) with a maximum speed of 2 cm per second. The stage can return to any previously logged position with an accuracy of, ≤ 1.5 μm.

2.1.1.4 Solid state image sensor

The sensor is mounted in the microscope camera port and detects the bright field microscope image. It contains a line of 1724 pixels (picture elements) each with an area of 1.3 μm × 1.3 μm spaced 1.3 μm apart. Cells are located by moving the

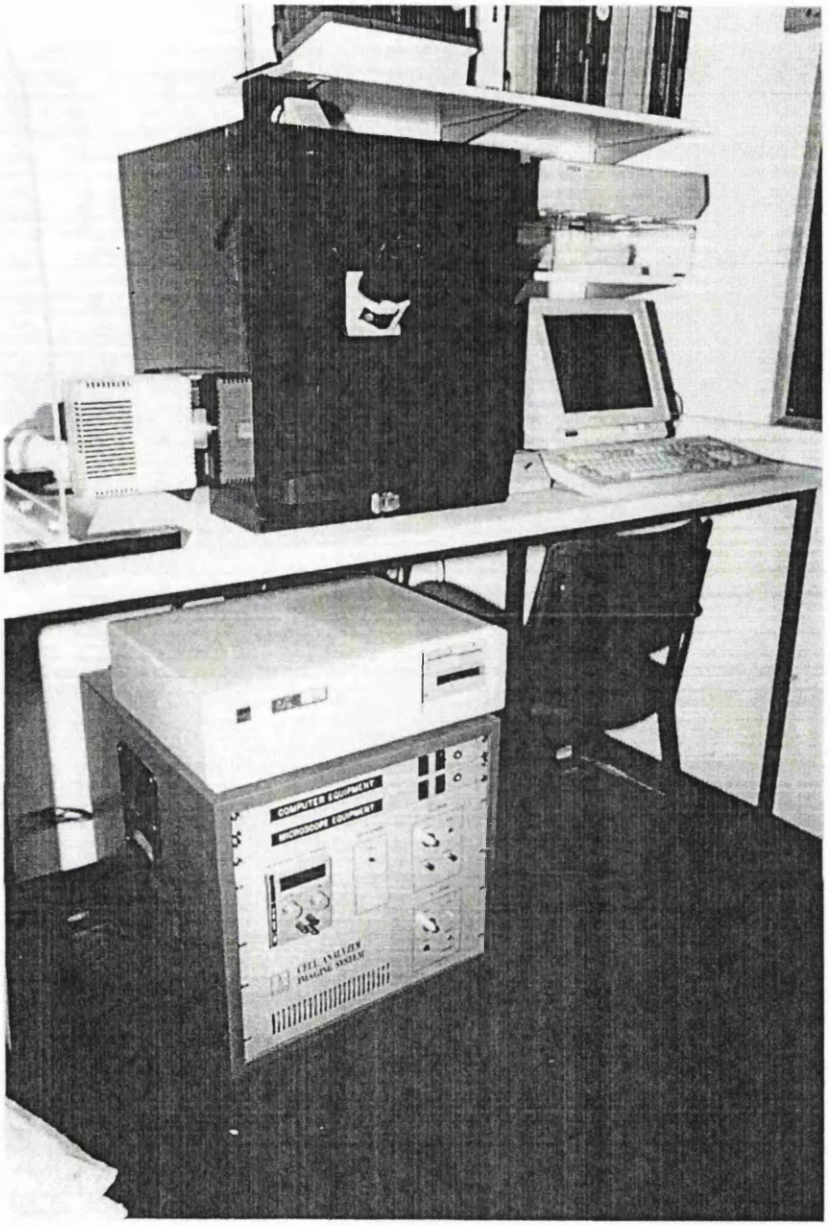

Fig. 2.1
The Dynamic Microscope Image Processing Scanner (DMIPS) cell analyser. The inverted microscope is surrounded by a darkened perspex incubator. A thermostatically controlled hot air blower maintains the temperature around the microscope stage. The computer and hardware necessary to drive the XY stage motors and Z drive focussing motor can be seen under the microscope.

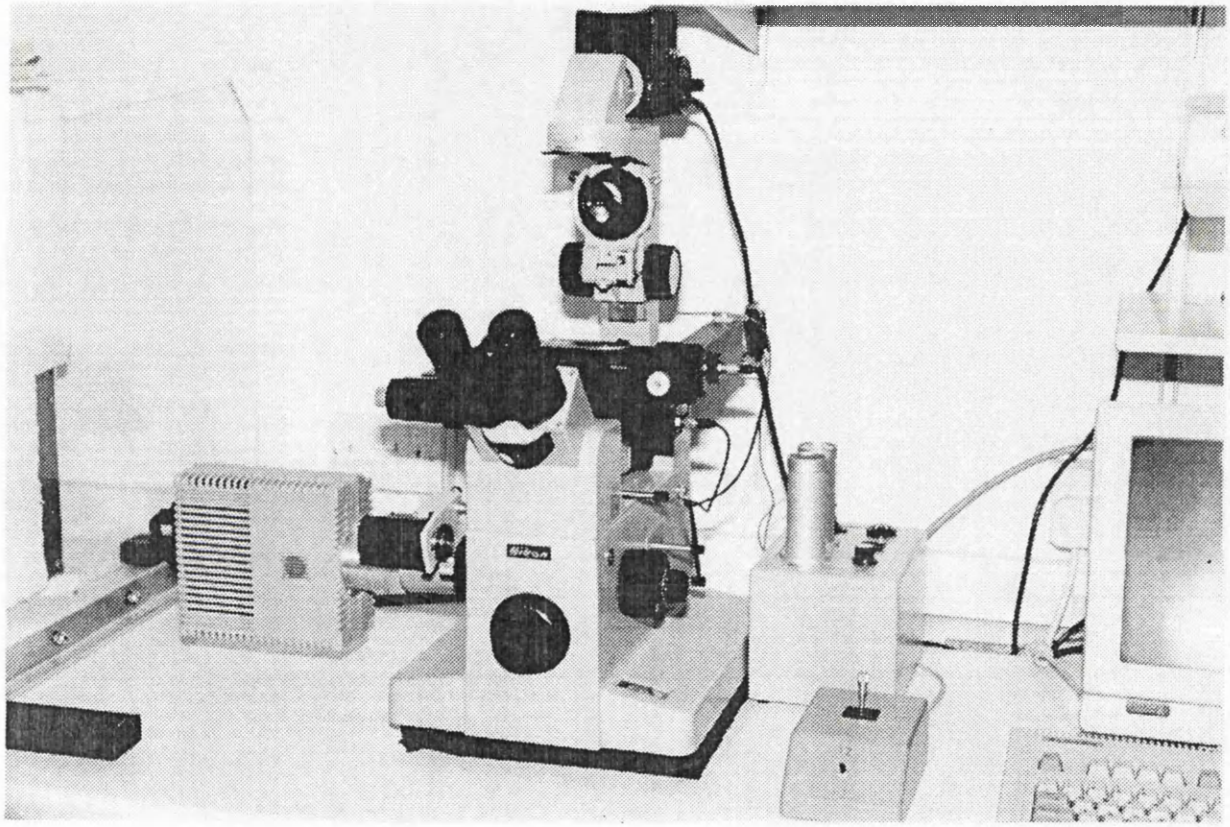

Fig. 2.2
The inverted microscope. The hot air blower and XY and Z control switches can be seen on the right of the microscope and the CCD camera mounted in the camera port on the left. The Z drive focussing motor can be seen between the CCD camera and the body of the microscope.

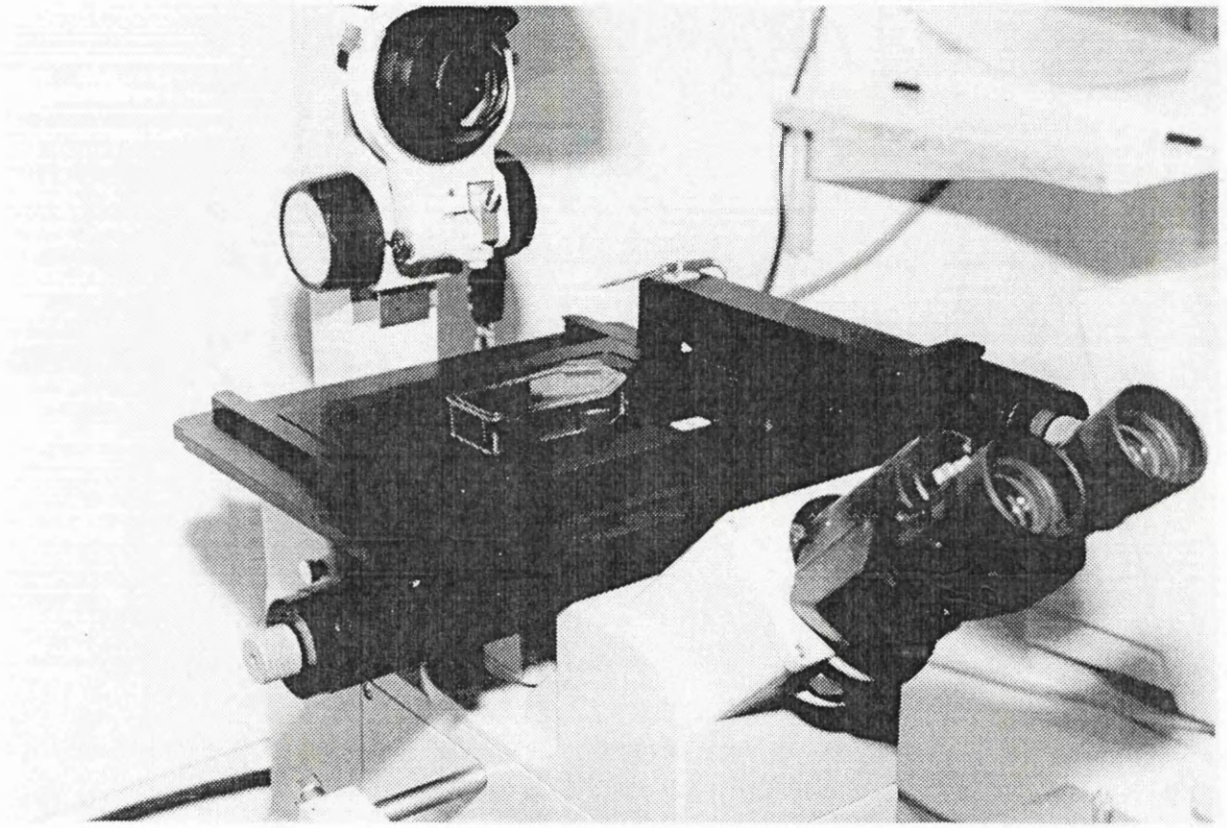

Fig. 2.3
A detailed view of the microscope stage. The XY motors which drive the stage can be seen protruding from the stage plate. The thermocouple which controls ambient air temperature is mounted on the far corner of the stage. The culture flask is held in position by a brass retaining-spring near the neck.

culture flask in a direction perpendicular to this linear array of sensors and sampling the light intensity. It had been found previously (Palcic and Jaggi 1986) that a single line scan across a cell with a pixel spacial resolution of 1.3 μm across the centre of a cell contains sufficient information to distinguish freshly-plated cells from debris and irregularities in the surface of the tissue culture flask. The interval at which scans are taken by the sensor (the step size) is dependent on the type of cell being investigated. Usually it is set to be no larger than the radius of the smallest cell in the population of interest to ensure that no cell can be missed by two successive line scans and therefore not be located. A large step size is favourable however as it allows for more rapid scanning of the flask. The time required to sense and process the image from the single line scan is independent of the step size but determined by the speed of the computer processor.

2.1.1.5 The stage incubator

The microscope and stage can be enclosed in a perspex incubator capable of maintaining a constant temperature around the culture flask. This allows a flask of cells to be kept at 37°C on the microscope stage during extended periods of observation. The temperature (± 1°C) is thermostatically controlled by a hot air blower circulating warm air, the thermocouple sensor is mounted on the stage plate.

2.1.2 Location and detection of cells

A 10 cm^2 area in the centre of the tissue culture flask is usually scanned. The middle of the culture flask is examined as this has a more uniform surface than the edges of the flask and therefore has better optical properties. The flask is scanned in 11 separate bands, 40 mm long × 2.25 mm wide. A step size of 4μm results in a total scanning time for a single culture flask of approximately 20-25 minutes including time for the automatic focussing procedure, and the acquisition and storage of the data.

The light intensity of each pixel is measured continually by the sensor as the stage moves the culture flask across the linear array of pixels. As an object crosses the scan line the light intensity reaching the pixels directly below the object is temporarily disrupted. A uniform structure such as a cell will produce a characteristic pattern of disruption in the background light level as it crosses the pixel array, whereas, irregular objects such as debris produce random fluctuations in the light

intensity. A freshly-plated cell produces a characteristic signal when illuminated by parallel light. The round, newly plated cell sits on the surface of the flask and acts as a small lens focussing the light towards its centre. This changes the refractive index of the interior of the cell compared with the background light level, producing a consistent image (see Figs. 2.4, 2.5). This image has a bright central peak, representing the centre of the cell, surrounded by dark edges produced by the outer edge of the cell. Irregular objects do not have a uniform image and the transmitted light is generally absorbed producing images below the background light level (see Fig. 2.6).

The image lines produced from the linear array are analysed by searching for a peak in the signal that is above the background light level by greater than a specified threshold. Once an object image is located, a 64-pixel segment from the scan line on which the peak is centred is isolated and the optical image is examined. Course primary analysis is performed on the optical image to look for the presence of cell-like characteristics in the image by comparing it with a master cell profile stored in the feature file. The optical images of the cell-like objects from this primary analysis are electrically digitised and transferred to the digital signal processor (DSP) for further detailed analyses, whereas optical images which contain no cell-like characteristics are disregarded. These digitised images are referred to as recognition signals. Several features of the signal are used to finally classify the objects into cells and non-cells. The features that are used to classify the objects can relate to physical characteristics (e.g. light scatter, refractive index, optical density) and also geometrical characteristics (i.e. object diameter and object width) (see Fig. 2.7). These simply-defined features, coupled with more sophisticated mathematical transformations of the signal, define the feature values for each object detected by the sensor. The normalised parameters of the 18 feature values of the signal are compared to previously determined values for the same cell line stored in the host computer in a master feature file. If all the feature values obtained from the located object fall between the lower and upper boundary levels of the master cell signal determined from a large sample of cells for that cell line, the object is recognised as, and scored, as a cell. Objects with features that do not meet these criteria are scored as non-cells.

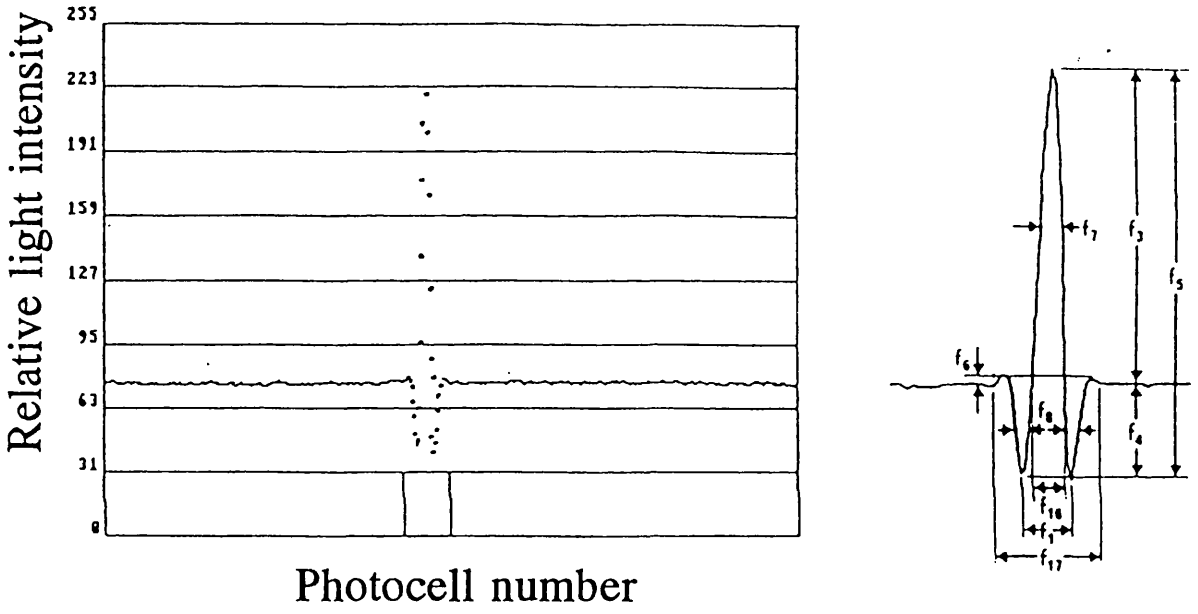

Fig. 2.4
A typical signal across the centre of a V79-379A cell measured in light intensity levels. The horizontal line represents the background light intensity; this level is changed when light passes through a cell. A schematic cell signal is shown on the right with some of the features used to characterise the signal. A list of all the features is shown in Fig. 2.7.

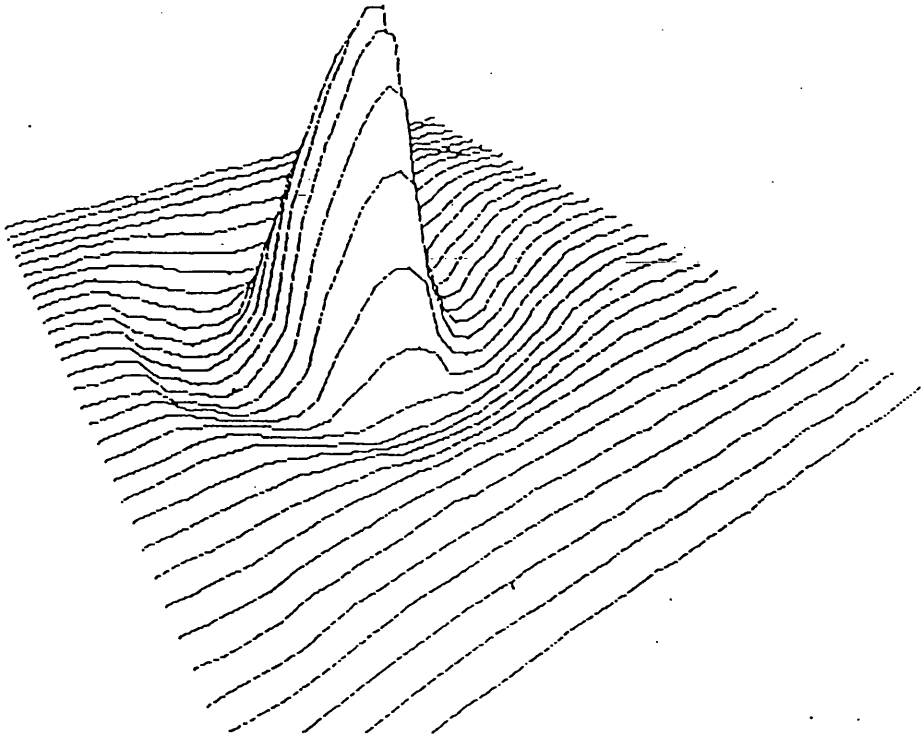

Fig. 2.5

A 3D image of a typical V79-379A cell constructed from single scan lines 1.3 μm apart. A freshly-plated cell attaches to the growth surface as a sphere and behaves like a small lens focusing the light from the inverted microscope towards its centre. The cell therefore has a bright centre and dark edges; this can be detected by measuring the light intensity transmitted through the cell. The bright centre of the cell is seen as a peak in the middle of the image surrounded by the dark edges of the cell. This image is surrounded by a constant light intensity representing the background light level.

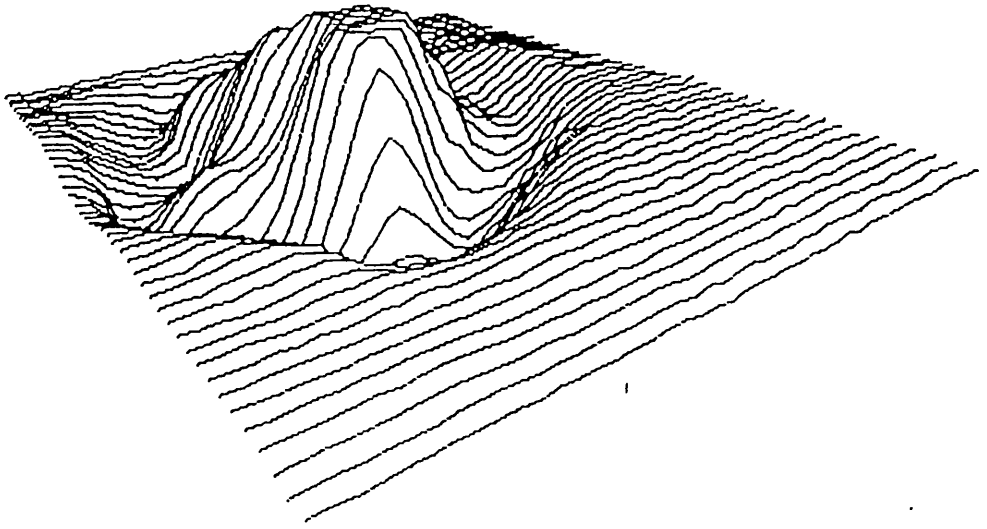

Fig. 2.6
A 3D image of a typical piece of debris. The culture medium is filtered prior to use to remove as much debris as possible. The majority of the debris is thought to come from the foetal calf serum, possibly proteins which have precipitated out of solution.

Feature No.	Feature Description	Units
f_1	distance between adjacent minima	pixels
f_2	maximum peak height between minima (relative to 0 intensity)	gray levels
f_3	maximum peak height between minima (relative to background)	gray levels
f_4	average depth of minima relative to background	gray levels
f_5	peak height relative to average minima depth	gray levels
f_6	brightness around cell relative to background	gray levels
f_7	peak width at half height relative to background	pixels
f_8	sum of minima widths at half the average minima depth relative to background	pixels
f_9	f_3/f_5	-
f_{10}	f_9/f_8	-
f_{11}	f_3f_7/f_4f_8	-
f_{12}	sum of absolute gradients along 64 pixel segment	gray level/pixel
f_{13}	auto-correlation of sample signal with 'master' cell signal	(gray level)^2
f_{14}	auto-correlation of (sample-background) with 'master' cell signal	(gray level)^2
f_{15}	f_{14}/f_3	gray levels
f_{16}	number of pixels above background in the peak	pixels
f_{17}	number of pixels between background levels bordering adjacent minima	pixels
f_{18}	number of pixels between the peak center and background level outside one of the adjacent minima (always measured in same direction)	pixels

Fig. 2.7

A list of all the 18 features that are used in the cell recognition signal. For an object to be classified as a cell the features derived from the object must fall within the upper and lower boundary values stored by the computer which are obtained by sampling a distribution of cells from the parental cell population.

Discriminant analysis is also performed before final classification to ensure that even an object whose features all fall between the upper and lower values for each of the 18 features has an overall image consistent with that of a true cell, as described by the recognition algorithm (see Fig. 2.8).

2.1.3 Recognition algorithm

Each cell line has a unique master recognition algorithm generated by combining the individual feature values from a large population of known cells. An example of a set of features was shown in Fig. 2.4. Several signal features are good for cell recognition purposes, whilst others are not so good. Signal width at background light level (feature f_{17}) is a good selective feature as it relates directly to cell size. An example of the upper and lower ranges of the 18 features of an asynchronous cell population is shown in Fig. 2.9.

2.1.4 Recognition files

The lower and upper boundary values of the 18 features of the master recognition signal used to discriminate cells from non-cells are contained in the feature file. Weighting factors are also stored which emphasize important features such as cell width. Also included in this file are values for a typical cell, characteristic of the cell line, stored as an optical image in light intensity levels, which are used for the primary classification of all located objects. Each individual cell line has a unique feature file, optimised to recognise cells particular to that cell line. The feature file is coupled with a parameter file containing the program information necessary to run the cell analyser specifically for that cell line, such as the width of the interval between successive scan lines.

2.1.5 Exclusion distance

The final position at which a cell settles on the flask surface is obviously a random process and the distance between individual cells is solely dependent on the number of cells actually plated, as the area of the culture flask remains constant. The actual number of cells recorded by the CSCAN program however is *not* solely dependent on the number of cells plated, because an exclusion distance parameter employed during the scan ultimately determines the number of cells recorded. The

exclusion distance ensures that cells recorded by the CSCAN program are sufficiently separated from all other cells so that they are still scored as discreet colonies in the time allowed for the assay. This prevents cells being selected which will ultimately grow to merge with other colonies in the incubation time of the assay. As the exclusion distance is increased, fewer cells are recorded by the CSCAN program. As some cells in the population may be incorrectly classified by the cell analyser and recorded as pieces of debris it is important that the exclusion procedure also excludes debris, as mis-classified cells may produce colonies that merge with the colony from a logged cell. It is important therefore that the exclusion distance can be manipulated to maximise the number of cells located in CSCAN, but minimise the number of these cells which produce merged colonies in SSCAN, for a given cell density.

2.1.6 Cell focusing

The recognition signal of a cell is sensitive to the focusing of the microscope. Precise focusing is therefore necessary to maximise the peak on the image signal obtained from the object. Automatic focusing of the culture flask is therefore a necessity. The focusing routine ensures the cell is kept with ± 30 μm of its optimum value by interactively adjusting the focus level at selected intervals during the scan. This procedure is essential as the base of the tissue culture flask may vary by up to ± 200 μm within the scanned area.

2.1.7 The software system (a box diagram illustrating how the individual programs interact is shown in Fig. 2.10)

2.1.7.1 General Scan (GSCAN)

This is a general purpose cell imaging program. The program is also used to calibrate the cell analyser by determining the centre of the linear array of pixels which is then synchronised with microscope crosshairs seen through the eyepieces. Eyepiece and CCD scanner focussing are also synchronised in GSCAN to ensure each located object is optimally focused for both the machine sensor and human operator. This is achieved by manually adjusting the focus control of the microscope to maximise the peak of the recognition signal from a located cell and then altering the focus on the eyepiece lens of the microscope until a sharp image is seen by the operator. This

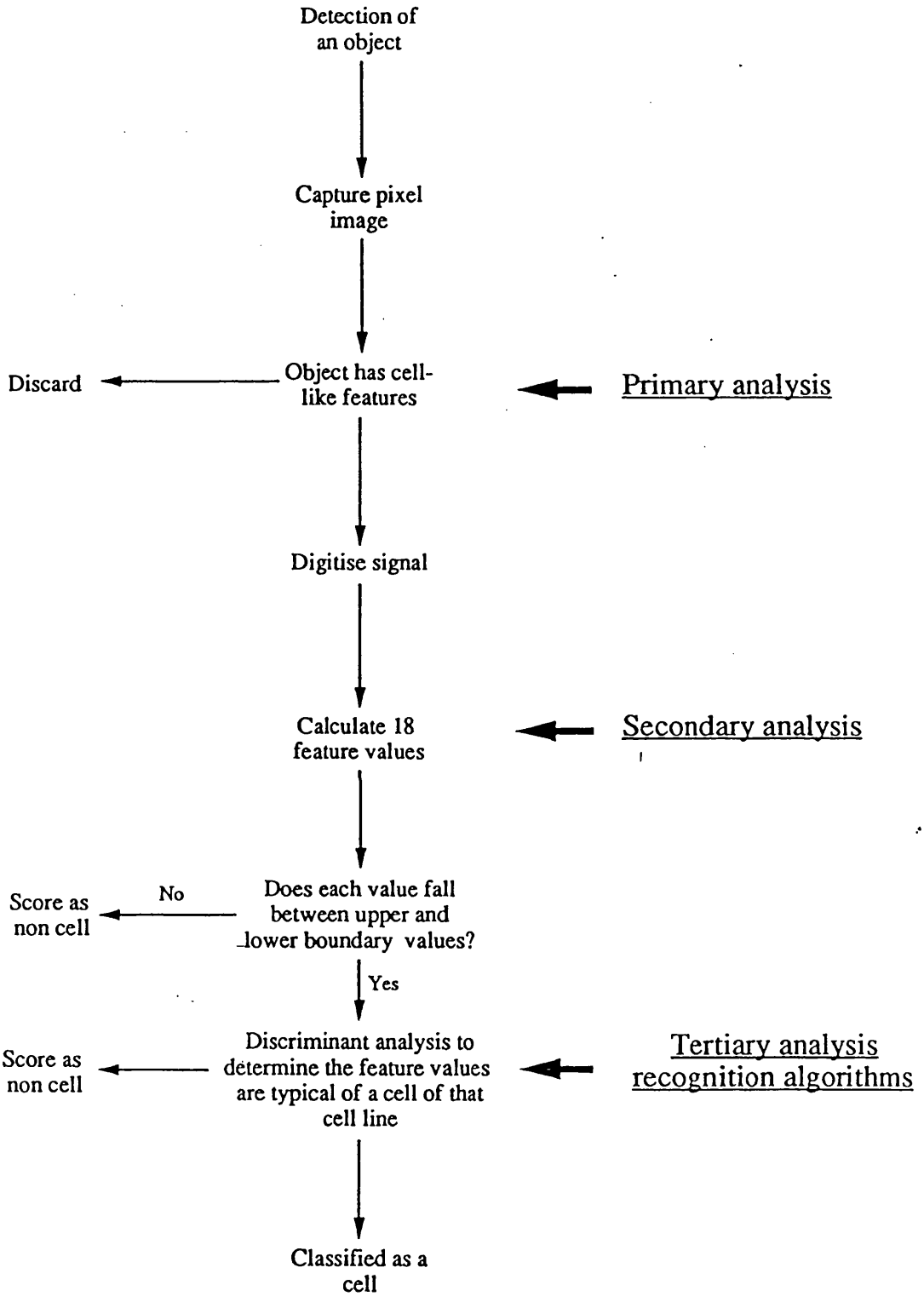

Fig. 2.8
A flow diagram of the automatic procedure to determine whether a located object is a cell.

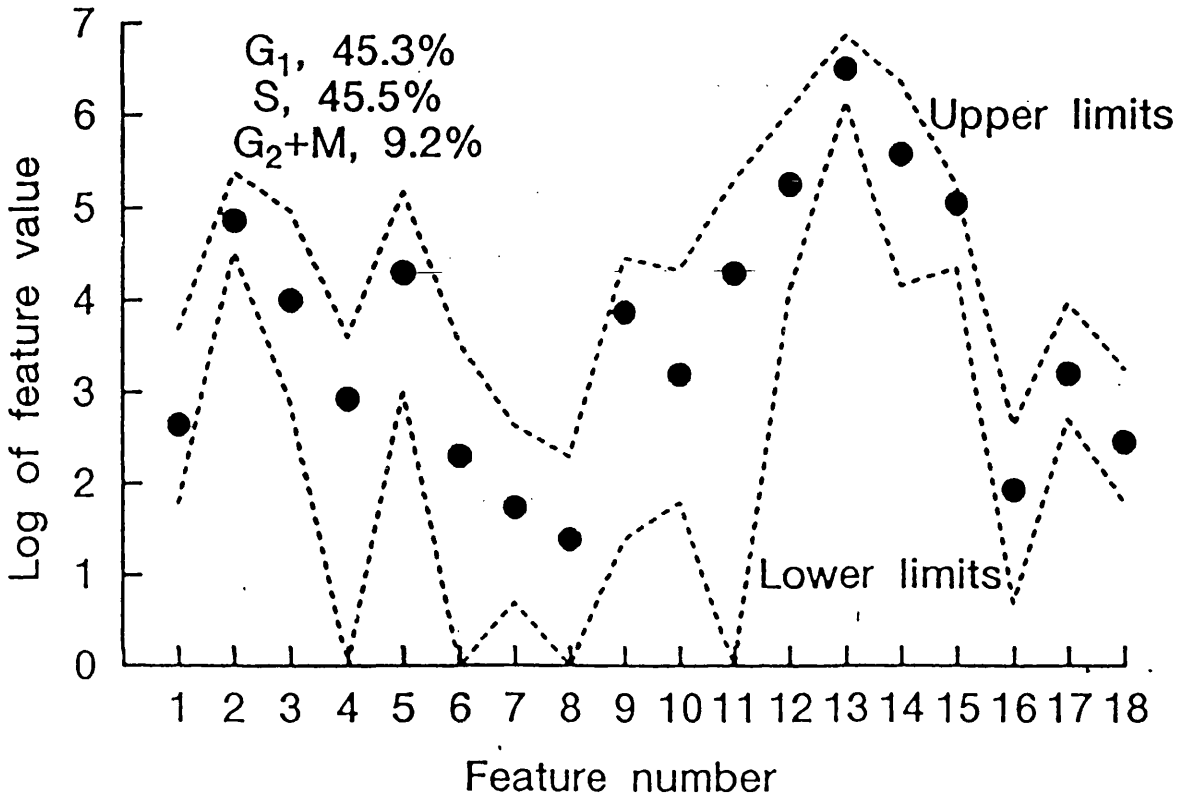

Fig. 2.9

This shows the numerical value of each feature plotted against feature number. A list of the features can be seen in Fig. 2.7. For an object to be classified as a cell each feature value obtained from the object must fall between the upper and low feature boundaries for that cell line. The upper and low boundaries are determined by manually capturing the features for >1000 cells and calculating the range of the values of each feature. Even when an object has met these criteria it is still only classified as a cell if all of its feature values are consistent with the master recognition algorithm i.e. the values of each feature are characteristic of a typical cell from that cell line.

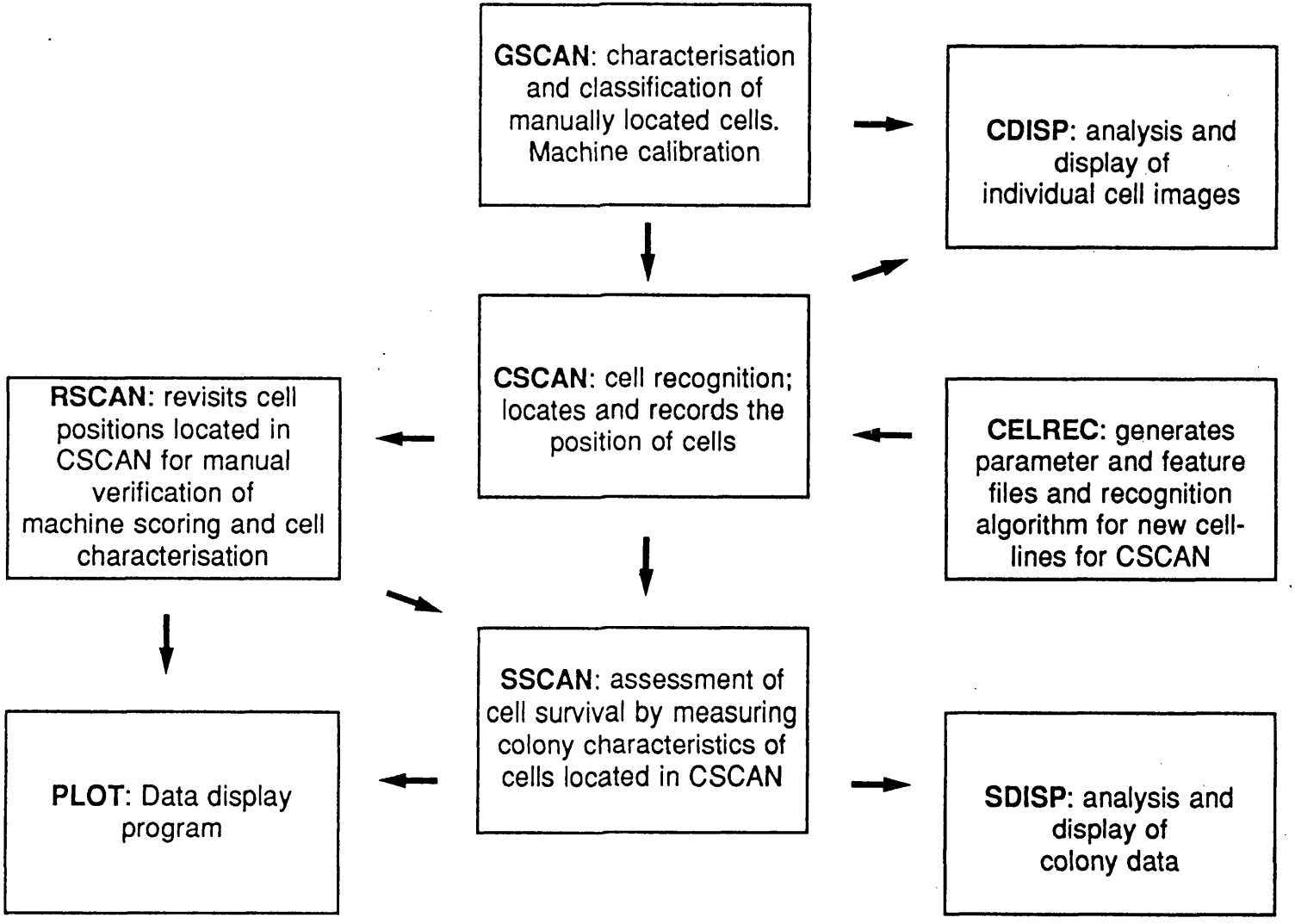

Fig. 2.10 A schematic flow diagram showing how the separate programs of the DMIPS cell analyser interact.

program has no discriminating capacity and it cannot distinguish between cells and debris. The cell imaging aspect of the GSCAN program is configured to capture, display and analyse detailed 2D and 3D images from any object located manually which can then be classified by the operator. The program is used routinely with a projection lens of 2.5× magnification and objective lens of 4× magnification but can be used at higher magnifications to obtain more detailed information. At 10× magnification the spatial resolution between the image array of pixels in the sensor is 1.3 microns (in the horizontal direction of the viewing field) and 4 microns between successive scan lines in the horizontal direction of the viewing field.

2.1.7.2 Cell Scan (CSCAN) (see Fig. 2.11)

CSCAN is the object location and cell recognition program. Using cell-line specific parameter and feature files, CSCAN is capable of locating and classifying different cell lines. These cell-line specific files are generated by the CELREC program. The parameter file synchronises the hardware components of the cell analyser, optimising the movement of the microscope stage with the capturing of the image by the sensor and the software processing of the image. The feature file contains information about the physical characteristics of the cells, which is utilised to determine whether a located object is a cell or non-cell. The culture flask is scanned by the CSCAN program in 11 vertical bands across the longest axis of the flask. The number of cells found and the total number of objects located are displayed at the end of each band as the data is stored. At the end of the entire scan a summary of the total number of objects detected and the number of cells located are displayed. On completion of the scan the locations of all the objects can be revisited for manual classification by the operator to verify the machine classification if required. The default scanning area is 10 cm^2 in the centre of the flask but this can be changed by altering the values in the parameter file. To scan a 10 cm^2 area of a culture flask using a step-size of 4 μm takes 20 - 25 minutes. The individual recognition signals of cells produced by the CSCAN program are stored in data files and can be analysed by the CDISP program. The X and Y co-ordinates of the objects logged as cells are saved for revisiting later by SSCAN to assess growth and survival.

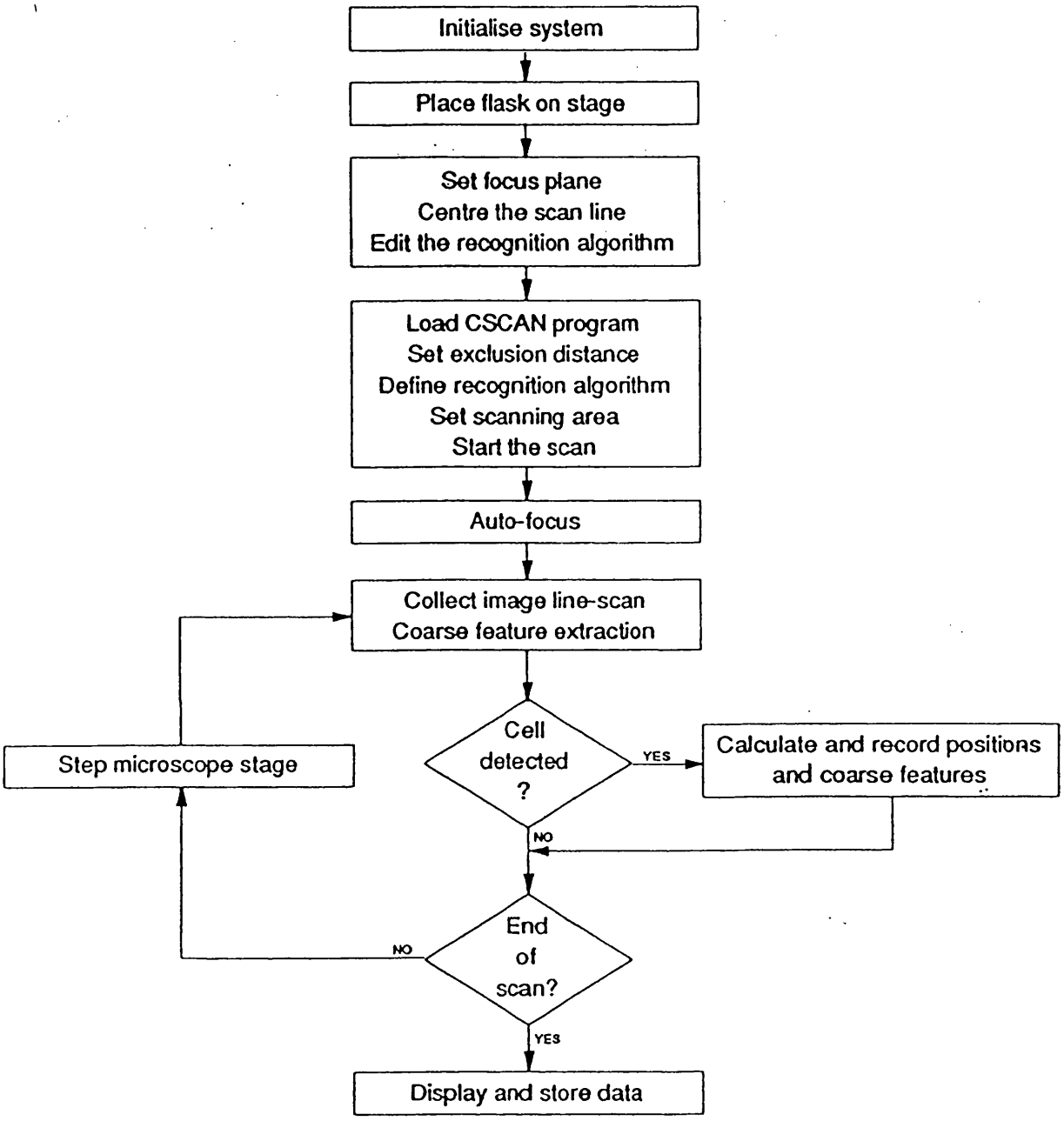

Fig. 2.11 *A schematic flow diagram of the cell location and recognition program (CSCAN).*

2.1.7.3 Revisit Scan (RSCAN)

This is a complex general purpose program configured to revisit cells, track cells or make repeated measurements of cell morphology. The program can track cells located manually or by a previous CSCAN, revisiting at a rate specified by the user. In the cell tracking mode the stage is driven to the last recorded position of the cell and an area around that point is scanned in 1μm steps. The data from the linear array of pixels is recorded and then the stage moves on to the position of the next cell. Once all the cells have been visited the file is appended and the flask is moved to an area out of the microscope light beam until the next set of scans begin. If a cell is not detected in the initial default scan area the position is revisited for another attempt at detection with an increased scan area. If the cell is still not found, it is classified as lost. Information on a range of cell features is measured during each scan (Table 2.1).

Cell information recorded by RSCAN	
Parameter	Feature recorded
1	area of cell or colony
2	volume/area of cell or colony
3	perimeter of cell or colony
4	circularity of cell or colony
5	XY movement of the cell

Table 2.1 *Some of the parameters recorded by the RSCAN program when revisiting cells.*

For each recorded cell the morphological features can be plotted against time, or against each other to give dynamic morphological images using the PLOT program, such as the increase in cell size with time from which the cell cycle time can be calculated (see Fig. 2.12). RSCAN provides the capability of revisiting files generated by CSCAN to assess colony growth.

2.1.7.4 Survival Scan (SSCAN) (see Fig. 2.13)

SSCAN is a menu driven program to measure the clonogenicity of cells located previously by CSCAN. This is achieved by scanning a user-specified area centred on the position of the cell located by the CSCAN program. If the cells are plated sparsely

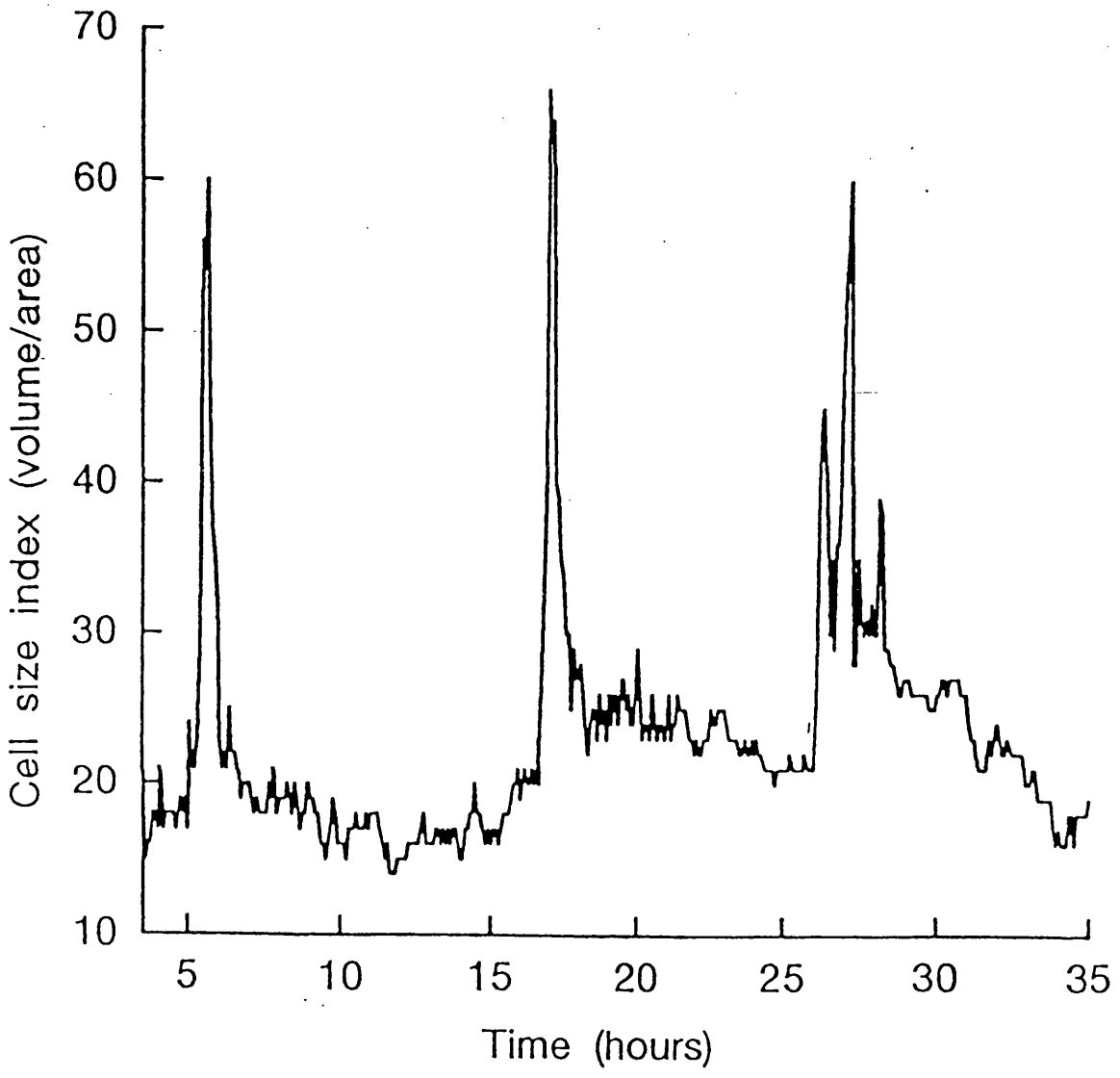

Fig. 2.12

An index of cell size measured as pixel volume/area. This parameter increases as the cells 'round-up' prior to division. The peaks therefore correspond to cell division and the distance between any two peaks is the intermitotic period.

and an appropriateexclusion distance is set during the CSCAN program then the SSCAN program will measure only discrete colonies. The sensor detects the colonies by detecting the perturbations in the background light intensity and calculates the number of pixels in the scanned areas which are above and below the background light level. This gives an index of colony size and is used to determine which cells are scored as survivors following radiation treatment. A number of colony features are recorded by the SSCAN program (Table 2.2) but clonogenicity is determined by the value of the colony area measured as the total number of pixels above and below the ambient light level. This parameter is calculated and determined by the SDISP program.

Colony features measured by the SSCAN program	
Parameter	Feature
1	number of peaks in the optical image
2	number of troughs in the optical image
3	area of signal more than 5 levels above background
4	area of signal more than 5 levels below background
5	volume of signal more than 5 levels above background
6	volume of signal more than 5 levels below background
7	total area of the image
8	total volume of the image in light intensity levels

***Table 2.2** The parameters measured from cell colonies by the SSCAN program.*

2.1.7.5 Survival Display (SDISP)

This is an interactive program designed to calculate the clonogenicity of cells located by CSCAN and assayed by SSCAN, by comparing the measured colony feature value with a previously determined value calculated from colonies which were manually scored to be greater than 50 cells. If the value of a specific colony feature measured by SSCAN is greater than the stored value then the colony is scored as representing a surviving cell.

2.1.7.6 Cell Display (CDISP)

CDISP is an interactive program for displaying individual object images. The

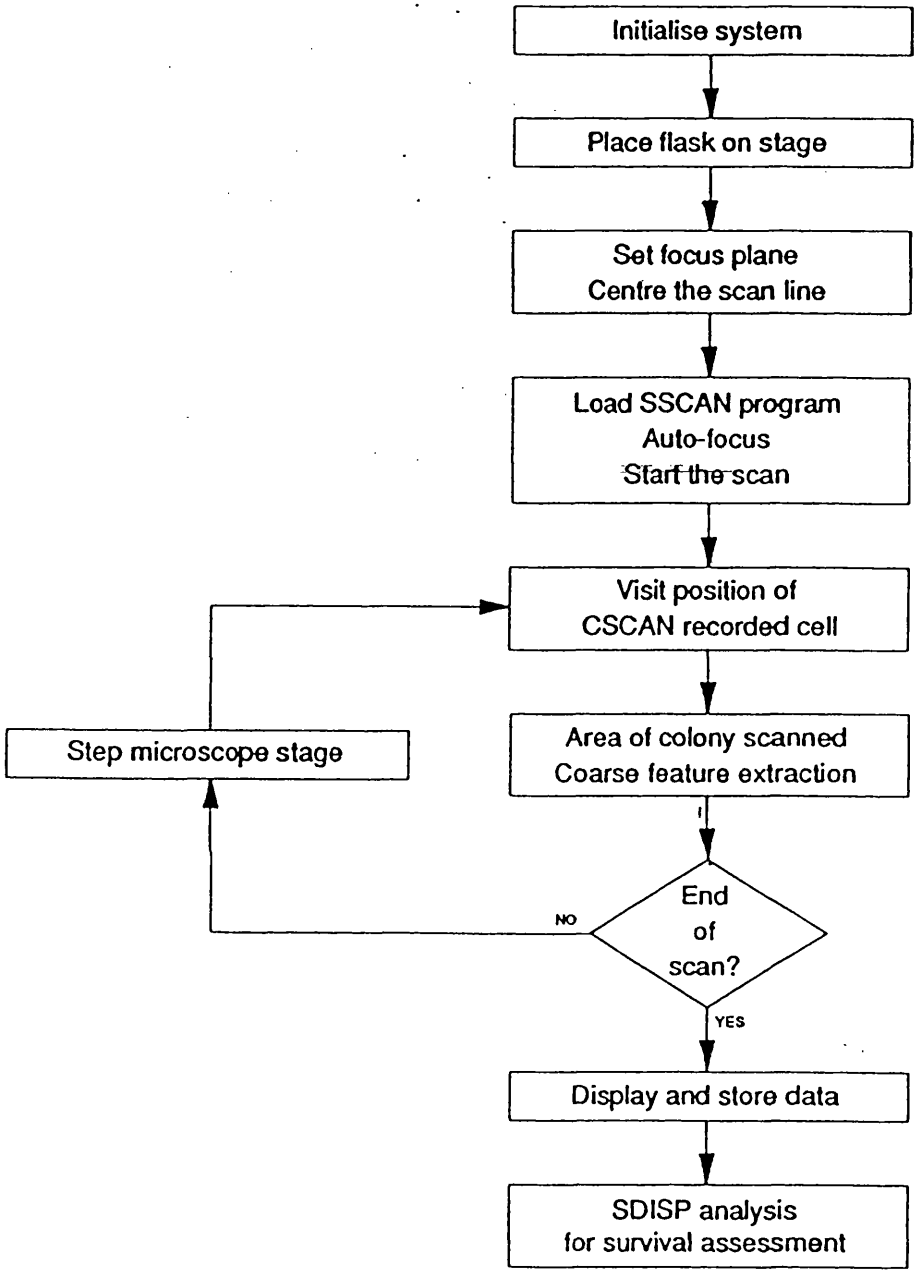

Fig. 2.13
A schematic flow diagram of the survival scan program (SSCAN), used to assess the size of colonies of cells located by the CSCAN program.

program plots the optical image of each logged object in light intensity levels, and assigns a machine classification value which is verified or not by the user.

2.1.7.7 Cell Recognition (CELREC) (see Fig. 2.14)

The CELREC program is an interactive system which generates the parameter and feature files used by CSCAN to perform cell recognition. CELREC generates the recognition algorithms by averaging the individual signals obtained from cells which have been located and scored manually. A small subset of cells is located initially and their optical images in light intensity levels are captured. The average signal obtained from these cells is temporarily stored and used by the program as a 'learning' image. An automatic procedure then scans the entire flask detecting each object which has an image resembling the averaged image obtaining from the learning subset of cells. Primary classification of all located objects from the automatic scan into cells and non-cells is performed automatically by the cell analyser using the transitional image generated initially as a master signal. The located objects are then revisited *manually* and classified by the user. This cell classification performed by the operator is then used to formulate the master recognition signal used by the CSCAN program. The average upper and lower feature boundary values derived from the 18 features of the cell image signal are calculated from the cell population and stored in a new feature file. Discriminant analysis is then performed between the objects scored as cells and non-cells to weight the individual feature boundary values. The discriminant weight values are also stored in the feature file. The newly generated feature and parameters files are named and saved.

2.1.7.8 PLOT Program

This is a general purpose program designed to plot cell image data from CSCAN, SSCAN and RSCAN.

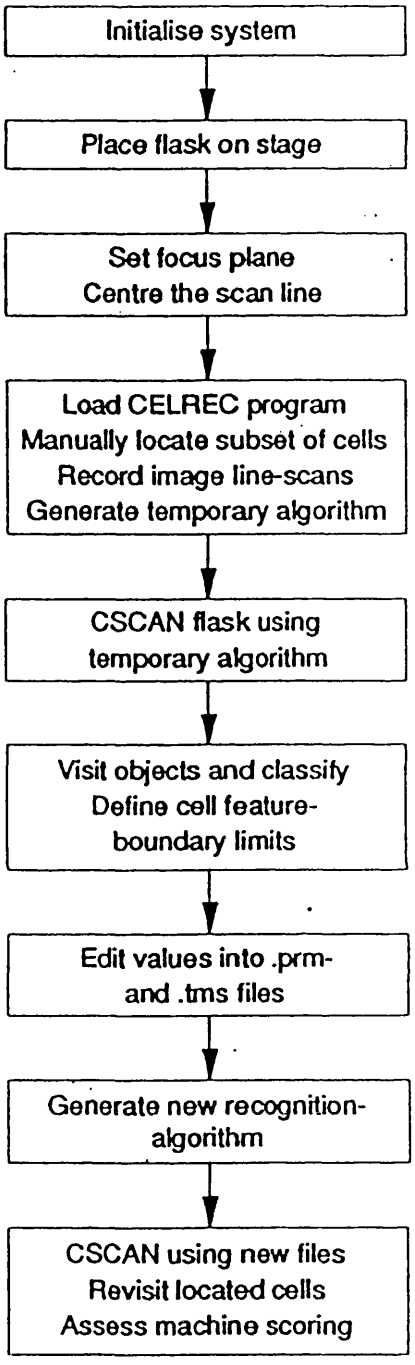

Fig. 2.14
A schematic flow diagram of the program (CELREC) used to 'teach' the DMIPS to recognise new cell lines.

2.2 Cell line

2.2.1 V79-379A Chinese hamster lung fibroblasts

The cell line was originally isolated in 1958 from the lung tissue of a mature Chinese hamster (*Cricetulus griseus*) for use in genetic studies and was designated the V strain. These cells were later sub-cloned and redesignated the V79 stain. A subclone of this was donated to Dr. L. Revesz at the Karolinska Institute, Stockholm and an aliquot from this culture was in turn donated to Dr. O.C.A. Scott at the Gray Laboratory in 1968 and is the V79-379A stain used in this study.

2.3 Cell culture techniques

2.3.1 Routine maintenance of the cell culture

Chinese hamster V79-379A cells were maintained as a log-phase spinner culture at 37°C in minimum essential medium, suspension modified, with 7.5% foetal calf serum. The cell concentration was maintained between 2×10^5 cells ml^{-1} and 6×10^5 cells ml^{-1}. A typical DNA distribution of the cell population at this cell concentration is shown in Table 2.3.

Phase of cell cycle	Cells in each phase (%)[+]
G_1	45
S	44
G_2 + M	11

[+] FCM analysis

Table 2.3 A typical DNA distribution of an asynchronous-exponentially growing population of V79-379A cells.

The culture of cells was diluted nightly with complete MEM-S culture medium to give a concentration of cells the following morning of 2×10^5 cells ml^{-1}. For weekend cultures, cells were diluted to 1×10^4 cells ml^{-1} on Friday evening which gave between 3-6 $\times 10^5$ cells ml^{-1} on Monday morning. Following the dilution of the culture with fresh medium, the cell suspension was gassed with a mixture of 95% air + 5% CO_2. Culture vessels were changed daily, excluding weekends. Cells were assayed as monolayer cultures in alpha-modified MEM medium, with 10% foetal calf serum.

2.3.2 Long term storage of the cell culture

Cells were maintained in liquid nitrogen for long term storage. Briefly, exponentially growing cells were washed and resuspended to a final concentration of approximately 1×10^7 cells ml^{-1} in complete growth medium containing 10% dimethyl sulphoxide (BDH Product No. 10323). One millilitre aliquots of this suspension were decanted into Nunc cryotubes (Cat No. 3-68632) and suspended over liquid nitrogen for approximately four hours until frozen. The samples were then immersed in the liquid nitrogen.

On retrieval from storage, the frozen samples were thawed rapidly and mixed with 10 ml of complete culture medium at 37°C and gassed with a mixture of 95% air + 5% CO_2. The cells were then washed twice by spinning down and resuspending in 5 ml of complete α-MEM medium and finally inoculated into suspension culture.

2.3.3 Standard plating procedure (SPP)

A 20 ml aliquot of cells taken from the stock spinner culture was centrifuged at 1000 rpm for 5 minutes. The pellet of cells was resuspended in 5 ml of complete - α-MEM culture medium. This procedure was repeated to wash the cells. The cells were finally resuspended to a density of $4\text{-}6 \times 10^5$ cells ml^{-1}. This cell suspension was serially diluted to a final cell density of 3000 cells ml^{-1}. Nunc T25 tissue culture flasks (Cat no. 152094) containing 4 ml of prewarmed α-MEM culture medium were seeded with 1 ml of this cell suspension. The inoculated flasks were incubated with loose lids, to allow gas exchange, at 37°C in a water saturated atmosphere of 95% air + 5% $C0_2$. The flasks were carefully removed from the incubator after a 90-120 minute period of incubation, during which time the cells attached to the growth surface. The initial 5 ml of culture medium were carefully poured out of the culture flask over the upper (non-cell) surface of the flask. The flasks were refilled slowly with complete α-MEM over the upper surface using a 25 ml pipette to minimise disruption to the cells attached to the opposite surface of the flask. Before the culture flask was sealed, all air bubbles in the culture medium were removed by gently agitating the flask until they rose to the top of the flask. The completely full flasks were maintained at 37°C prior to, and following, irradiation. Before a flask was scanned it was placed on its end in a vertical position for 15 minutes to allow any air bubbles still present in the

flask to float towards the top and out of the area to be scanned. This also allowed any debris and unattached cells to fall out of the scanning area to the bottom end of the flask. Cell location and recognition by the CSCAN program were performed at 37°C and on completion of the scanning procedure, the cell location data were filed and saved. All tissue culture flasks were returned to the incubator and clonogenicity was assessed using SSCAN after 84 hours of culture.

2.3.4 Culture medium recipes

α-Minimum Essential Medium (α-MEM)

A	α-MEM media powder (Gibco Cat No. 072-1100)
B	Sodium bicarbonate (Sigma Cat No. 55761)
C	15% w/v Penicillin (150 mg ml^{-1})[1]
D	12% w/v Streptomycin (125 mg ml^{-1})[2]
E	Foetal calf serum[3]
F	Amphotericin B 250 μg ml^{-1} (Gibco Cat No. 043-05290F)
G	Sterile water (residual ions << 1ppb)

To make one litre:

Dissolve 10 g of A and 2.2 g of B in 100 ml of G, add 0.5 ml of solutions C and D. Make up to 1 dm^3 with G. Sterilise by filtering (0.22μm pore size Flow Cat No. GSWP14250). Add 10% v/v of E and then 1% v/v of F. Adjust pH to be 7.5 ± 0.2. Store between 2-5°C. For the DMIPS recognition assay, filter again before use (0.45μm pore size, Flow Cat No. AW03 14250).

Minimum essential medium for suspension cultures (MEM-S)

A	10× MEM-S concentrate (Flow Cat No. 14-170-54)
B	Sterile water (residual ions << 1ppb)
C	1 N sodium bicarbonate (Flow Cat No. 16-883 2 g l^{-1})
D	L-glutamine 0.292 g l^{-1} (Flow Cat No. 16-801-49)
E	15% w/v Penicillin (150 mg ml^{-1})[1]
F	12% w/v Streptomycin (125 mg ml^{-1})[2]
G	Foetal calf serum[3]
H	Amphotericin B 250 mg ml^{-1} (Gibco Cat No. 043-05290F)

To make one litre:

Aseptically add 863 ml of B to 100 ml of A in a sterile one litre bottle. Add 27 ml of C. Filter (0.22 μm) solutions of E and F and add 0.5 ml of each. Finally add 7.5% v/v of G and 1% v/v of H. Adjust pH to 7.2 ± 0.2 and store at 4°C. Add 10 ml of D

immediately prior to use, swirl gently to mix.

1. Glaxo, Benzylpenicillin sodium BP
2. Evans Medical Limited, Streptomycin sulphate BP
3. Gibco, Flow

2.4 Radiation facilities

2.4.1 250 kVp X-rays

Cells were routinely irradiated at room temperature (18°C - 24°C). Prior to irradiation, the cells were maintained at 37°C and returned to 37°C immediately following irradiation. Cells were irradiated either in spinner culture (20 ml at 2-4 × 10^5 cells ml^{-1}) or as freshly-plated cell monolayers depending on the specific experimental design of the investigation. In each set-up the dose rate was dependent on the dose actually given (Table 2.4). The dose rate was changed by increasing the distance

Dose rate (Gy min^{-1})$^+$	Range of doses used (Gy)
0.016	0.01-0.50
0.44	0.20-0.50
1.7	1.0-10.0

$^+$(250 kVp, 15 mA, HVL = 1.46 mm Cu)

Table 2.4 The X-ray dose rates and the range of doses over which they were used.

between the sample and X-ray face plate. Dosimetry was performed using a 0.60 cm^3 Baldwin Farmer ionisation chamber.

2.4.2 2.5 MVp X-rays

2.5 MVp X-rays were produced by the Gray Laboratory Van de Graaff accelerator by focusing electrons onto a gold target. The electron beam current was varied between 7-200 μA, giving a range of dose rates. Dosimetry was carried out using a Baldwin Farmer 0.6 cm^3, ionisation chamber with a half-inch perspex shield. Cells were irradiated as attached monolayers at room temperature and maintained at

37°C prior to, and post irradiation.

2.4.3 d(4)-Be neutrons

Neutrons were produced from the Gray Laboratory Van de Graaff accelerator by bombarding a thick beryllium target with 4 MeV deuterons. This gave neutrons with mean energy of 2-3 MeV and dose mean lineal energy of 60-70 keV μm^{-1}. The neutron dose rate was 0.20 Gy min^{-1}. Cells were irradiated either as a 20 ml spinner culture or as attached monolayers. The irradiations were performed at room temperature (18-25°C) and the flasks were maintained at 37°C prior to, and post irradiation.

2.5 Irradiation protocols

Two irradiation systems were devised:

2.5.1 Spinner cultures of cells

An aliquot of cells taken from spinner culture was washed, and resuspended in α-MEM + 10% FCS at a concentration of $\approx 5 \times 10^5$ cells ml^{-1}. A 20 ml sample of this suspension was transferred to a sterile swan-necked glass irradiation vessel containing a magnetic stirrer bar. To ensure precise dosimetry, this was held in position, above a magnetic stirrer and below the X-ray face plate, by a specially-constructed irradiation jig. A 1 ml aliquot of cells was removed for each dose point.

2.5.2 Attached monolayers of cells

The desired number of cells was plated in complete α-MEM in accordance with the standard plating procedure (3000 - 4000 cells per flask). The flasks (by now completely full of culture medium) were held in position during the irradiation by a specially-constructed jig (when X-rays were delivered at the dose rates of 0.44 or 1.7 Gy min^{-1}). Flasks irradiated at the extremely low dose rate (X-rays - 0.016 Gy min^{-1}) were positioned on a shelf a at distance of 3 metres from the face plate. Accurate dosimetry was assured because a beam of laser light was used to position the culture flask and to ensure the X-ray face plate was perpendicular to the culture flask. A retaining system was employed to achieve accurate dosimetry during neutron irradiations.

2.6 Solutions

2.6.1 Trypsin (Flow Cat No. 28-203)

A 0.25% w/v solution of trypsin in Hanks buffered saline solution was used. This contained 200 IU ml^{-1} penicillin, 100 µg ml^{-1} streptomycin, 0.50 g l^{-1} sodium bicarbonate and calcium and magnesium.

Trypsin	
Ingredient	Concentration (µg/litre)
NaCl	8
KCl	0.4
D-Glucose	1
$NaHCO_3$	0.5
Na_2HPO_4	0.06
Penicillin	$2x10^5$ IU/litre
Streptomycin	$1x10^4$ IU/litre

2.6.2 Phosphate buffered saline (PBS) (Flow Cat No. 28-103-05)

Dulbecco's formula without calcium and magnesium

Phosphate buffered saline	
Ingredient	concentration (µg/litre)
NaCl	8
KCl	0.2
Na_2HPO_4	1.15
KH_2PO_4	0.2

Chapter 3: The radiation response of V79-379A cells

3.1 Aims

The experiments reported in this chapter were designed to measure the clonogenic survival of V79-379A cells with the DMIPS cell analyser using the cell plating methodology determined in the previous DMIPS studies performed at the Gray Laboratory (Marples, 1987).

3.2 Commissioning the DMIPS cell analyser

The cell-plating methodology and scanning procedures recommended initially for the DMIPS cell analyser were derived for a CHO cell line by Palcic and Jaggi (1984) at the British Columbia Cancer Research Center in Vancouver, along with the cell-recognition algorithm which enables the cell analyser to discriminate between freshly-plated cells and debris. These parameters were devised specifically for CHO cells because this was the cell line being used in the majority of the *in vitro* studies performed in the Vancouver laboratory at that time. However, cell culture studies carried out at the CRC Gray Laboratory were primarily on the V79-379A cell line and therefore the cell-plating procedures recommended for DMIPS by the Vancouver group had to be changed and optimised for the V79 cell line.

The cell-plating procedure that was used in the previous Gray Laboratory study was optimised for the CHO recognition algorithm because at that time the cell analyser could not be configured with a recognition algorithm specific for the V79 cells. This was because the software required to generate *new* cell-line specific recognition algorithms was still under development in Vancouver and was therefore unavailable. The development work to commission the cell analyser in order to measure cell survival for the V79 cell line therefore commenced with the CHO-specific algorithm. Although this situation was not ideal, the CHO algorithm recognised V79 cells because they are similar in size to the CHO cells (diameter 10-12 μm) and therefore the two cell lines are optically quite, but not exactly, similar.

3.3 Development of the cell plating procedure

Previous studies (Marples, 1987) developed and optimised the basic cell-plating procedures necessary to perform a clonogenic recognition assay using the cell analyser for the V79 cell line used at the Gray Laboratory. Briefly, cells grown and maintained routinely as a spinner culture were irradiated as a spinner culture before being plated to assess cell survival. Once irradiated, an aliquot of cells was serially diluted and approximately 3500 cells were plated in 25 cm^2 tissue culture flasks in 5 ml of culture medium. The culture flasks were then incubated for 120 minutes to allow time for the cells to sediment out of the culture medium and attach to the growth surface. After this period of incubation the culture flasks were removed from the incubator and the initial 5 ml of cell culture medium poured off to remove unattached cells and debris. The flask was then refilled totally with fresh culture medium and subsequently scanned to locate the attached cells.

Particular aspects of the cell-plating procedure which are not important in a conventional type of survival assay, such as the time allowed for cells to attach to the growth surface, are critical for the DMIPS recognition assay. Several parameters have to be strictly controlled in the DMIPS assay to ensure an accurate recognition of cells and therefore accurate measurement of the surviving fraction.

3.3.1 Late-sedimenting cells

Although the vast majority of the cells sedimented out of the culture medium and attached to the growth surface within the 120 minute period allowed, some 'late' cell sedimentation was found to occur *after* the scan of the culture flask had been completed. This presents an immediate problem, as 'late' sedimenting cells may settle in the vicinity of cells recorded in the original cell scan. When the position of the recorded cell is subsequently revisited to assess the level of cell survival a few days later, by measuring the size of the cell colony, the recorded colony may have already merged with a colony that arose from a late-sedimenting cell, thereby, producing a larger colony than expected normally from that single cell. Worse, this effect can result in an incorrect measurement of the survival of the original cell because the original logged cell may have been killed

by the radiation treatment and therefore not grow to produce a colony. The SSCAN program, however, will detect the colony that has arisen from the late-sedimenting cell at the location of the killed cell and assume it has arisen from the original cell. It will therefore falsely record the original cell as having survived the radiation treatment.

Late-sedimenting cells were found to arise from three sources:

1) Cells which did not attach to the surface of the flask during the 120 minute period of incubation and therefore remained free-floating in the culture medium.
2) Cells which had attached initially and then became detached.
3) Attached cells which were dislodged when the flask was refilled with fresh culture medium.

Incubating the culture flask in a vertical position 15 minutes prior to scanning was found to reduce substantially the problem of late-sedimenting cells. This was confirmed using the RSCAN program, by locating manually and counting all cells which had attached to a 5 cm^2 area of the growth surface of the culture flask following the standard 120 minutes of incubation. The cells were then incubated for 3.5 days to allow the them to grow into colonies and then the number of colonies in the marked area was counted (Table 3.1).

Approximate number of cells located	Unexpected colonies without vertical incubation (% ± SD)	Unexpected colonies with vertical incubation (% ± SD)
500	6.4 ± 5.4	1.2 ± 1.7

Table 3.1 *The number of colonies that arose from a cell which was not located at the time of plating. The 'unexpected' colonies arise from cells sedimenting out of the culture medium onto the growth surface. If this occurs after a cell scan, the survival assessment can be inaccurate.*

Assessing the number of cells which had initially attached to the growth surface and then detached as a direct result of the refilling procedure was difficult to determine because this possibility may have also occurred as a direct consequence of the radiation treatment. Therefore, the number of cells from an unirradiated sample which remained

attached immediately after refilling the culture flask with fresh medium was determined. It was found that the number of cells that were dislodged from the growth surface during the refilling of the flask was reduced somewhat by introducing the fresh culture medium over the upper (non-cell) surface of the culture flask rather than over the growth surface as this prevented the flow of medium directly onto the cells (Table 3.2)

approximate number of cells located	Refilling over upper surface (% ±SD)	Refilling over lower surface (% ± SD)
500	97 ± 4	91 ± 6

Table 3.2 The fraction of cells (%) that remained attached to the growth surface when the culture flask was refilled with fresh medium introduced over the upper surface (non-growth surface) and lower surface (growth surface) of the culture flask.

3.3.2 Number of cells plated

The greater the number of cells plated, the more accurate the measurement of cell survival because the binomial error on the estimate of the surviving fraction is dependent partially on the size of the sample population (Boag 1975). It is important therefore to maximise the number of cells located in each culture flask during a CSCAN. Increasing the number of cells in the sample, i.e. the number of cells plated in each culture flask, to reduce the sampling error does however introduce unique problems in the DMIPS recognition assay. Firstly, by increasing the number of cells per flask the final number of cells recorded by CSCAN may actually *decrease* because the cells will be closer together on the growth surface and therefore discarded by the exclusion distance criterion. Secondly, once the flasks have been refilled totally with culture medium and incubated they are not re-fed with fresh culture medium. This would be necessary if a larger number of cells are plated. Normally, approximately 3500 cells are plated per flask in 40 ml of culture medium. If the number of cells plated greatly exceeds this level then this volume of culture medium may not be sufficient to maintain an optimum growth of the cells. This could be detrimental, as poorly nourished cells may detach from the growth surface. Seeding approximately 5000 cells in a single flask which did not receive any radiation treatment produced a yellowing of the culture medium over the duration of the assay which was assumed to be due to the accumulation of acids in the culture

medium. Following this observation no more than 3500 cells were inoculated on control dishes; this gave no discolouring of the medium. However, flasks that were given neutron doses in excess of 1.5 Gy or X-ray doses > 5 Gy were seeded with more than 3500 cells (3500-6000 cells) because not all the cells would survive the radiation treatment (neutron $SF_{1.5}$ ≈0.3, X-ray SF_5 ≈0.25) and therefore the accumulation of acid in the culture medium from plating that number of cells did not present a problem.

3.3.3 Exclusion distance

It was found previously that a 350-400 μm exclusion distance gave a maximal number of cells recorded in CSCAN with minimal colony overlap in SSCAN when 3500 cells were plated (Marples, 1987). Using these two parameters, 350-400 cells are usually detected using the default 10 cm^2 scanning area in the centre of the tissue culture flask.

3.4 Results

3.4.1 Comparison of conventional and recognition assays

Experiments were performed on the same irradiated cell population to compare the survival estimates obtained using the DMIPS recognition assay with those obtained by a conventional clonogenic assay. The two assays produced similar measurements of surviving fraction over the X-ray dose range of 1-7 Gy and neutron dose range of 1-2 Gy (Fig. 3.1). However, as the dose was reduced below 1 Gy, the conventional assay gave more variable measurements of surviving fraction. In a number of instances, the values of surviving fraction that were obtained were often greater than the unirradiated control value, i.e. SF ≥ 1. This phenomenon was not seen using the recognition assay (Fig. 3.1). This was thought to be a consequence of the counting errors associated with the conventional assay and emphasized the difficulty in determining the surviving fraction of cells at low doses using this method.

In the conventional assay, the cells are plated by inoculating a culture dish with a volume of cell suspension of a known density which has been obtained by serial dilution from a stock culture. The assay scores the number of surviving colonies that have grown on the dish following irradiation and therefore it is desirable (statistically at higher doses and for the ease of counting at lower doses) to achieve a known number

of colonies on each culture plate irrespective of the dose given to that particular plate. If more cells than intended are transferred onto a culture dish through random errors in the counting, dilution and sampling procedures (see section 1.8.1), then at very low radiation doses, where little cell kill is achieved, more colonies may grow on that plate than the number of cells *believed* to be inoculated. If this error occurs with a culture dish that receives only a small radiation dose and not with the control plate of the same experiment, then a value of surviving fraction greater than 1 will be obtained at that dose level. This does not occur in the recognition assay because the cells are located after they have been inoculated and a precise number is therefore scored. During this series of experiments the CELREC program designed to generate new recognition algorithms became available and a V79 specific algorithm was produced by sampling over 4000 V79 cells. This new recognition algorithm was more efficient at recognising and discriminating V79 cells from debris than was the CHO algorithm; it had a lower frequency of false negative recognitions and located proportionally more cells in a finite sample (Table 3.3). The new algorithm was used therefore in all subsequent experiments.

Algorithm	Objects correctly classified as cells (%)	Objects correctly classified as debris (%)	False negative (cells classified as debris (%))	False positive (debris classified as cells (%))
CHO	92.7	84.4	15.6	7.3
V79	95.3	88.6	11.4	4.7

Table 3.3 *The recognition accuracy at the CHO algorithm obtained from Vancouver and the V79 algorithm generated in this study using the CELREC program. The table shows the number of objects that were correctly identified as cells and number of objects that were correctly scored as debris. The false positive parameter is critical as these objects are included in the cell sample.*

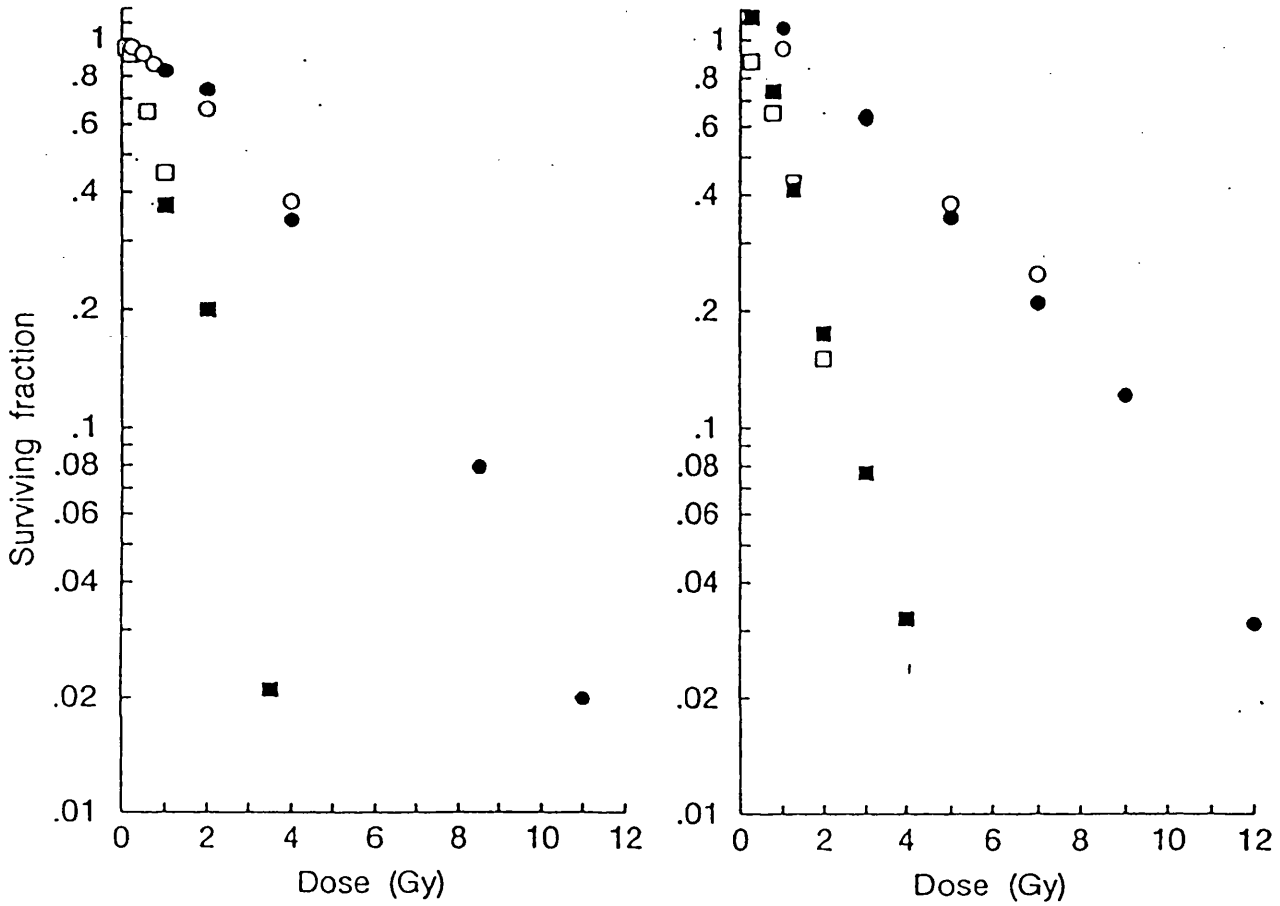

Fig. 3.1

The measurement of cell survival obtained using a conventional clonogenic assay and the DMIPS recognition assay for cells irradiated with 250 kVp X-rays (X, O recognition assay, ● conventional assay) and d(4)-Be neutrons (N, □ recognition assay, ■ conventional assay). Similar values of surviving fraction are obtained over the X-ray dose range 2-7 Gy but as the X-ray dose was decreased the conventional assay became imprecise which resulted in measurements of surviving fraction above 1. Each point represents one measurement of survival.

3.4.2 Change in the X-ray dose rate

In the initial study comparing the recognition assay with the conventional assay, the cells were irradiated in spinner culture using an X-ray dose rate of 1.7 Gy min^{-1}. However, for determining the survival of cells after exposure to small X-ray doses, a decision was made to reduce the X-ray dose rate when giving X-ray doses below 0.5 Gy. This was necessary to allow sufficient time during these short exposure periods for the X-ray set to reach 250 kVp. The X-ray set did not have a shutter, and at the full dose rate this would have resulted in a large proportion of the dose being given at energies below 250 kVp (e.g. a 0.5 Gy dose at 1.7 Gy min^{-1} takes ≈18 s to administer and the X-ray set takes ≈10 s to reach 250 kVp). The X-ray dose rate to the cell sample was therefore reduced to 0.016 Gy min^{-1} by increasing the distance between the X-ray source and the sample of cells (see Table 2.4). The reduction in dose rate had no significant effect on the cell survival over the X-ray dose range 0-1.5 Gy (Fig. 3.2). Similar values of surviving fraction were obtained at each dose level using the two dose rates of 1.7 Gy min^{-1} and 0.016 Gy min^{-1}. The neutron dose rate remained the same, for all experiments, at 0.20 Gy min^{-1}. Previous studies have showed that the shoulder of the X-ray survival curve is reduced with a reduction in dose rate, giving an apparent linear survival curve, if a large prolonged dose is given (Steel *et al.*, 1986). This has been explained by continuous repair of intracellular lesions during the low dose rate irradiation. This was not seen in this study because the exposure times were reasonably short (≤ 20 min) even at the low dose rate, because of the low doses given. For extremely low-dose radiation as given in this study, the radioresponsiveness is found to be largely independent of the dose rate because the measurements of surviving fraction are on the initial region of the survival curve.

3.4.3 Improvements in the method of cell plating

Although the DMIPS recognition assay gave consistent measurements of surviving fraction which were comparable with measurements made with a conventional clonogenic assay at X-ray doses above 1 Gy, some random variation in the survival was seen between individual experiments. To reduce any possible source of error that may

have arisen from clumps of multiple cells in the cell suspension, the plating procedure was modified to include a step whereby the cell suspension was passed repeatedly through a 19 gauge hypodermic needle until less than 1 doublet per 100 single cells was counted using a haemocytometer. This increased the proportion of single cells in the population and therefore reduced even further the small possibility of a doublet being scored as a single cell in the CSCAN routine, which would affect the measurement of surviving fraction. This procedure did not affect the plating efficiency of the cells.

The variation in RBE that was seen between individual experiments was further reduced by filtering the complete medium through a 0.45 μm filter prior to use. This was probably owing to an improvement in the degree of cell recognition since the slight possibility of a piece of debris being incorrectly classified as a cell was reduced, combined with a general improvement in the automatic focusing routine of CSCAN; less debris reduces the possibility of the optimal focus plane for the scan being assigned from a piece of debris rather than a cell. The number of recorded cells per flask was also increased by filtering out the debris as the number of objects that were eliminated by the exclusion procedure was reduced. It was noticed while observing the CSCAN routines, that the amount of debris in the culture medium correlated to the length of time the medium had been made and stored in the fridge. It was therefore decided that the medium should be used routinely within 4 weeks of being made up, and filtered the day before use through a 0.45 μm filter to minimised the amount of debris it contained. The majority of the debris were thought to come from the FCS. However, some debris were probably constituents of the culture medium that had crystallized out of solution.

Cell population	Number of cells scored (4 samples)	Plating efficiency (% ± SD)
A	1284	92 ± 5.7
B	1305	90 ± 4.1

***Table 3.4** The number of cells scored in 4 cell scans (CSCAN) from a population of cells (A) in which the cells were resuspended using a 19 gauge needle and for a population of cells (B) resuspended using a standard 10 ml pipette.*

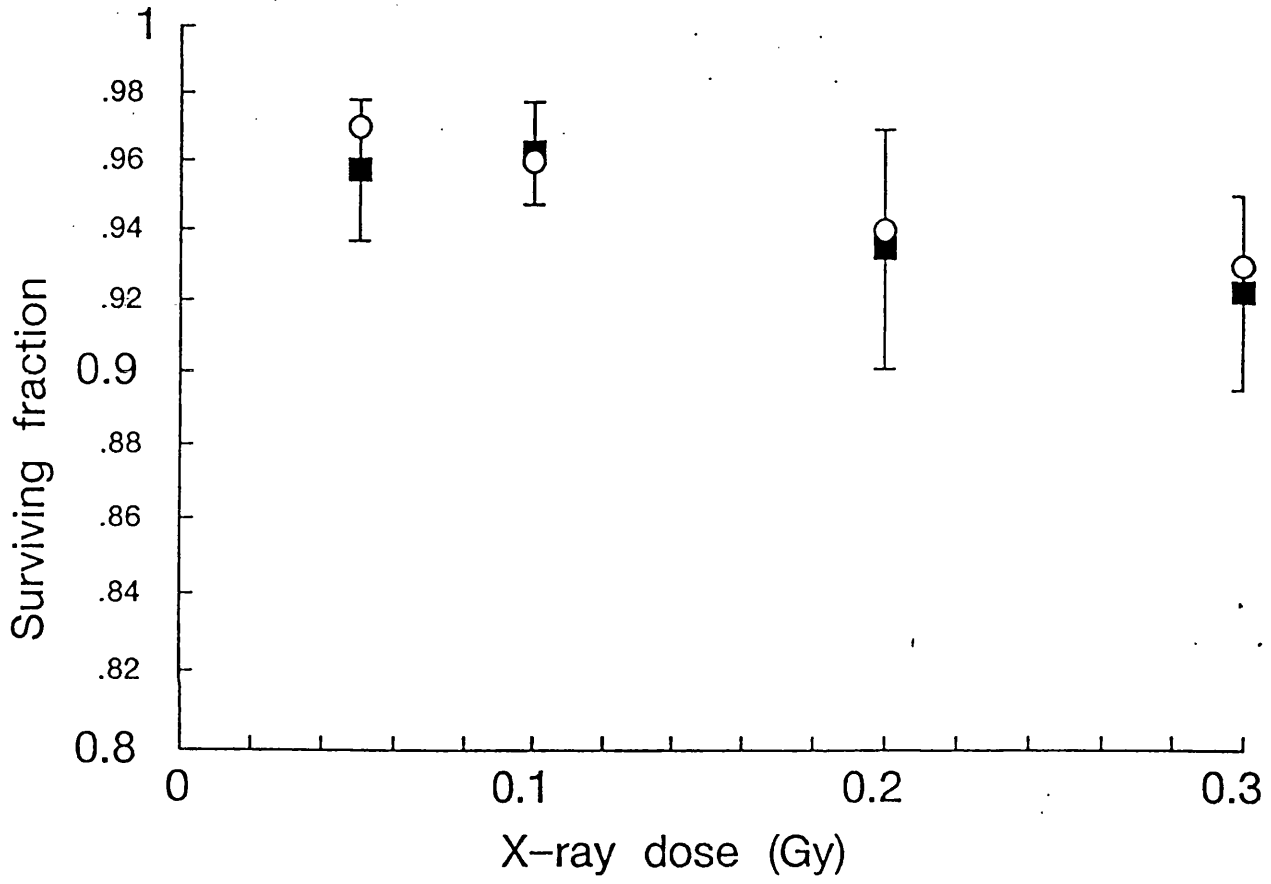

Fig..3.2

A comparison of the effect of radiation dose rate on cell survival. Reducing the X-ray dose rate from 1.7 Gy min^{-1} (O) to 0.016 Gy min^{-1} (■) did not effect cell survival and consistent measurements of surviving fraction were obtained at the two dose rates.

3.5 An improved recognition assay

3.5.1 Measurement of radiosensitivity

With all the improvements made in the methodological procedure, the radiation response of V79 cells could now be measured reliably down to X-ray and neutron doses of 0.01 Gy. The fraction of cells that survived a radiation treatment was calculated by dividing the value of the plating efficiency obtained from the SSCAN analysis of each irradiated flask by the plating efficiency (also from SSCAN) obtained for a sample of cells from the same experiment which were not irradiated. The values of surviving fraction were then plotted on a logarithmic scale against the corresponding dose on a linear scale (see Fig. 3.3).

The neutron response was always found to be an exponential decrease in surviving fraction with increasing dose and was fitted with a log-linear function (Fig. 3.3). The X-ray response was found to be biphasic (Fig. 3.3). Survival estimates over the X-ray dose range of 1-10 Gy showed a good fit to a linear quadratic (LQ) model, whereas for X-ray doses <0.30 Gy, a significantly increased X-ray sensitivity was observed with survival estimates below the LQ prediction. At the very lowest X-ray doses (0.01-0.2 Gy), X-rays were nearly as effective at killing cells as neutrons in some experiments.

These data can be presented in terms of relative biological effectiveness (RBE) (see Fig. 3.4). The RBE values were determined from the X-ray and neutron survival data obtained using the same parental cell population for each experiment. The RBE was calculated by relating the experimentally obtained survival measurements for each X-ray dose to the fitted neutron curve. In this way the results obtained from individual experiments can be compared readily, because slight changes in the cellular radiation response would presumably be similar for X-rays and neutrons and so would cancel in the calulation of RBE. The neutron line therefore acts as an internal biological standard. Therefore, despite the observed phenomenon of low dose sensitivity being only associated with the X-ray response, it is important that the neutron survival curve is obtained for each experiment in order to further increase the precision with which it can be described.

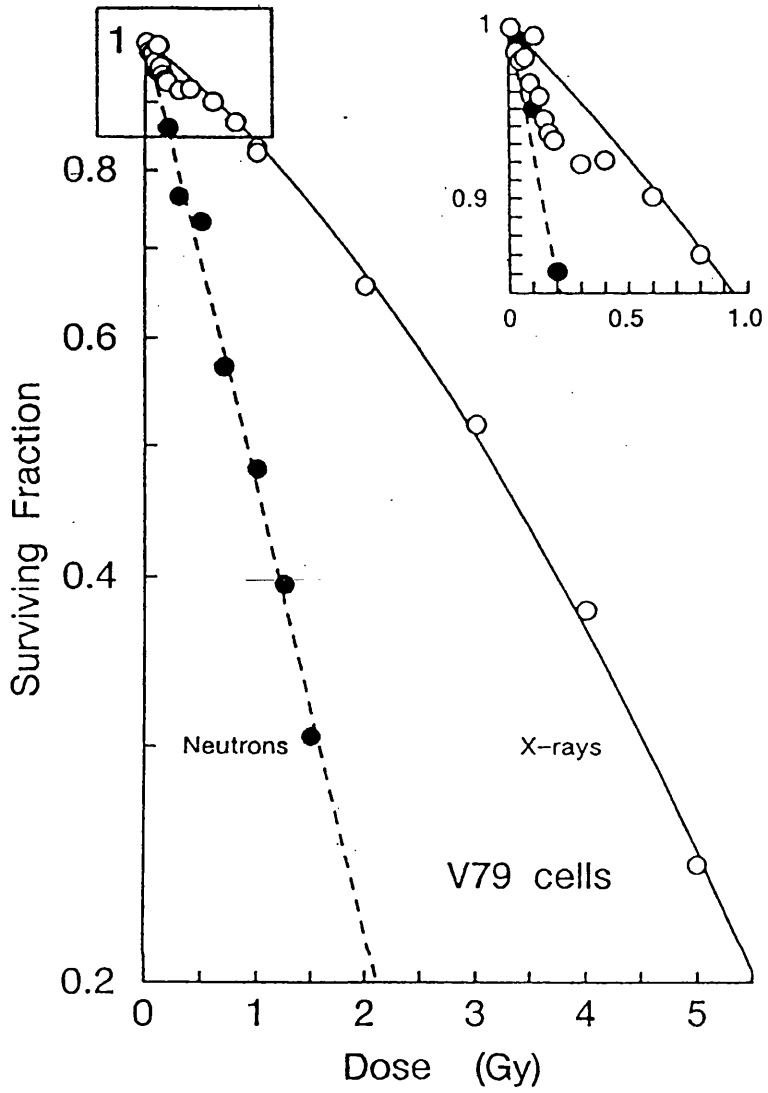

Fig. 3.3

Typical X-ray and neutron survival curves obtained for V79 cells irradiated as monolayer cultures. The radiation dose rate was changed in accordance with the values quotes in Table 2.4 to ensure the exposure time remained approximately constant at each dose level. Each point signifies a single flask and represents a measurement of survival made on 300-400 cells. Each flask takes 20-25 minutes to scan and 6-7 flasks are assayed as a single unit. These particular survival curves were obtained in a single experimental run, taking a total of 36 hours to plate and locate the cells and then 12 hours to revisit the colonies and assess survival 3.5 days later. The solid line represents a LQ fit to the X-ray data above 0.6 Gy and the dashed line is a single exponential fit to all the neutron data. The inset is a magnified view of the low-dose region. Over the X-ray dose range 0.2-0.6 Gy an increase in X-ray radioresistance is seen.

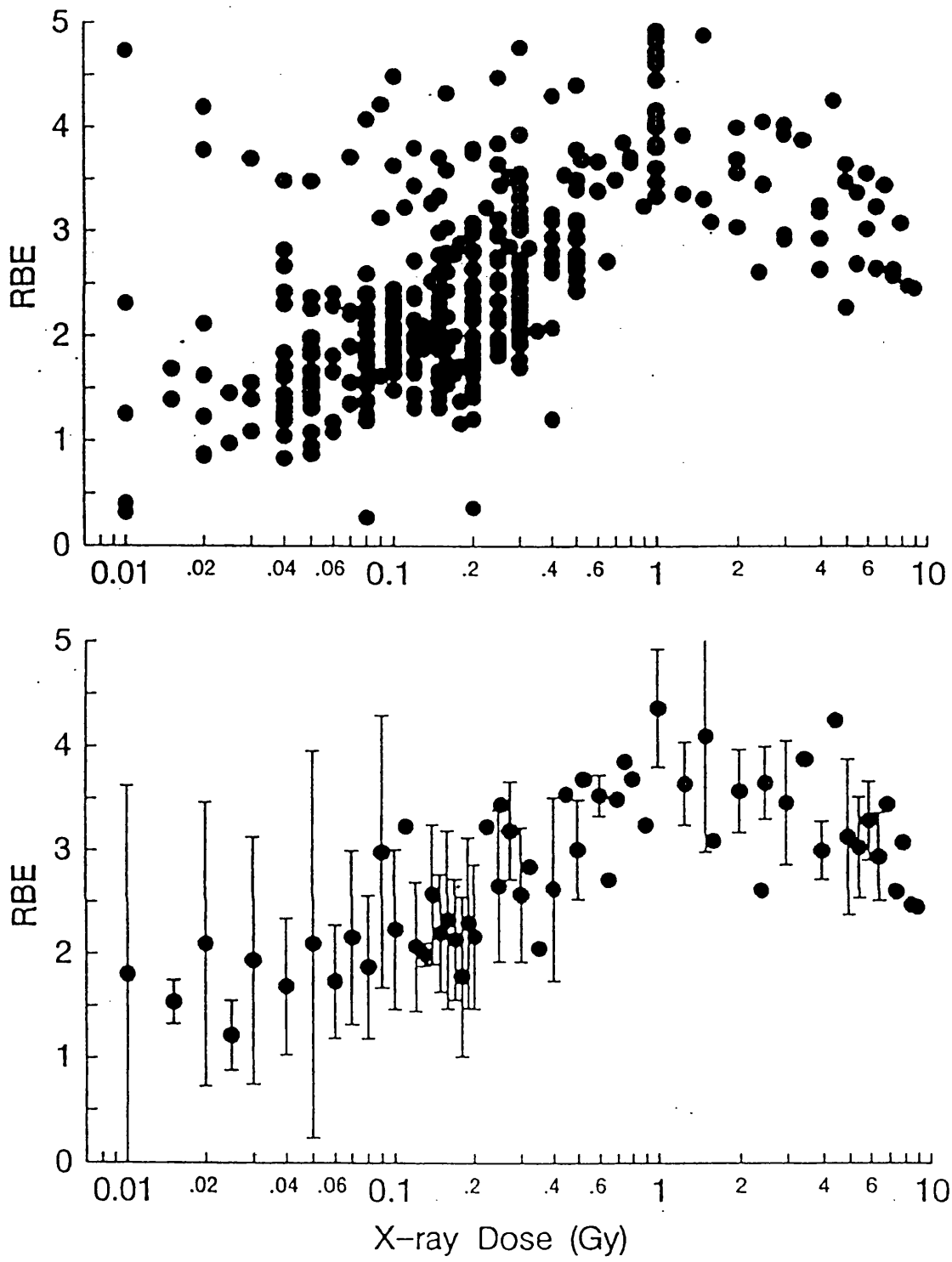

Fig. 3.4

RBE between 250 kVp X-rays and d(4)-Be neutrons given as single doses. The upper panel represents 403 individual measurements of surviving fraction and contains data for cells irradiated in spinner culture and monolayer culture. The lower panel is the mean RBE value at each level of dose (± SD). The increase in RBE over the dose range 0.2-0.6 Gy illustrates the increase in X-ray radioresistance over this dose range, as shown in Fig. 3.3.

3.6 Possible experimental artefacts

Despite the apparent increase in radiosensitivity at X-ray doses below 0.6 Gy being a consistent and reproducible effect, it only represents a small change in cell survival and this might be attributed to an experimental artefact in the X-ray irradiation procedure. It is unlikely that an artefact associated with the cell plating or scanning procedures could have been responsible for the biphasic X-ray survival curve because the same protocols were used to generate the neutron survival curve, which has been shown to be linear e.g. see Fig. 3.3. Experiments were therefore performed to investigate specific aspects of the X-ray irradiation procedure.

3.6.1 The effect of the pH of the culture medium

Exposing cell-culture medium to air leads to an increase in the pH owing to the gradual loss of CO_2 from the medium. The longer the culture medium is exposed the more basic it becomes. This can be seen as a change in the appearance of the culture medium from the orange-red colour of normally buffered medium to the more basic purple colour. To prevent changes in the pH of the culture medium during conventional large single-dose experiments (> 20 Gy) the cell suspension is usually gassed with a mixture of 95% air + 5% CO_2. This buffers the medium to the optimum pH level. In this study the cells were irradiated as a spinner culture in swan-necked vessels which were *not* gassed with 95% air + 5% CO_2 during the exposure period. This was thought unnecessary because the irradiation exposures were relatively short (≤ 30 min) and no change in the colour of the culture medium (indicating pH) was ever observed. However, the increase in radioresistance of the cell population, represented by the biphasic survival curve, occurred as a function of increasing X-ray dose i.e. it reflected the increase in the radiation exposure time during which the culture medium was exposed to air and presumably the pH of culture medium was therefore changing, if only very slightly. This may not have been detectable by a change in the colour of the culture medium, yet might ultimately have affected the radiosensitivity of the cells. This postulate did seem unlikely because the cells were plated in fresh culture medium immediately following irradiation and then incubated in a 95% CO_2 + 5% air atmosphere, which would have corrected any change in the pH of the culture medium which had occurred. This effect of a pH change

was unlikely to occur with neutron irradiations because smaller doses were given at a higher dose rate (0.20 Gy min^{-1}) resulting in short exposure times.

To test the effect of pH, experiments were performed in which three samples of cells were irradiated in spinner culture with culture medium of varying pH (Fig. 3.5). The colour of the medium was the same at each level of pH. The pH was increased by addition of 0.1 M NaOH and decreased by gassing with a mixture of 95% air + 5% CO_2. The data suggest that the pH of the culture medium during the irradiation procedure over the pH range 7.35-7.75 had no significant effect on the level of cell survival obtained, compared with cells assayed at pH 7.55; the three X-ray survival curves gave similar measures of surviving fraction (see Fig. 3.5).

3.6.2 The effect of the temperature of the culture medium

Slight variations in the temperature of the medium in which the cells were irradiated might also have affected the assessment of survival. The cells were irradiated in complete culture medium at room temperature (18°C-25°C). The temperature of the culture medium fell during the longest irradiation exposures from 37°C, at the start of the exposure, to between 34°C to 36°C. Experiments were carried out in which the temperature of the culture medium was kept constant during the radiation exposure by standing the irradiation vessel on a heated magnetic stirrer. Varying the temperature of the medium over the range 35°C to 39°C did not significantly alter the value of surviving fraction from that obtained at 37°C (Fig. 3.5). The effect on the measurement of surviving fraction of irradiating cells in culture medium above 37°C was investigated because the magnetic stirrer usually became warm after extended periods of use and this may have warmed the culture medium.

3.6.3 The effect of prolonged spinning

Irradiating the cells as a spinner culture and sequentially sampling cells as the dose increases, results in the cells receiving the largest doses being in suspension culture longer than the cells receiving the smallest X-ray doses. Therefore, they experience a longer spinning stress *while* in the irradiation suspension set-up. This set-up was a different arrangement from the suspension culture used to maintain the stock culture of

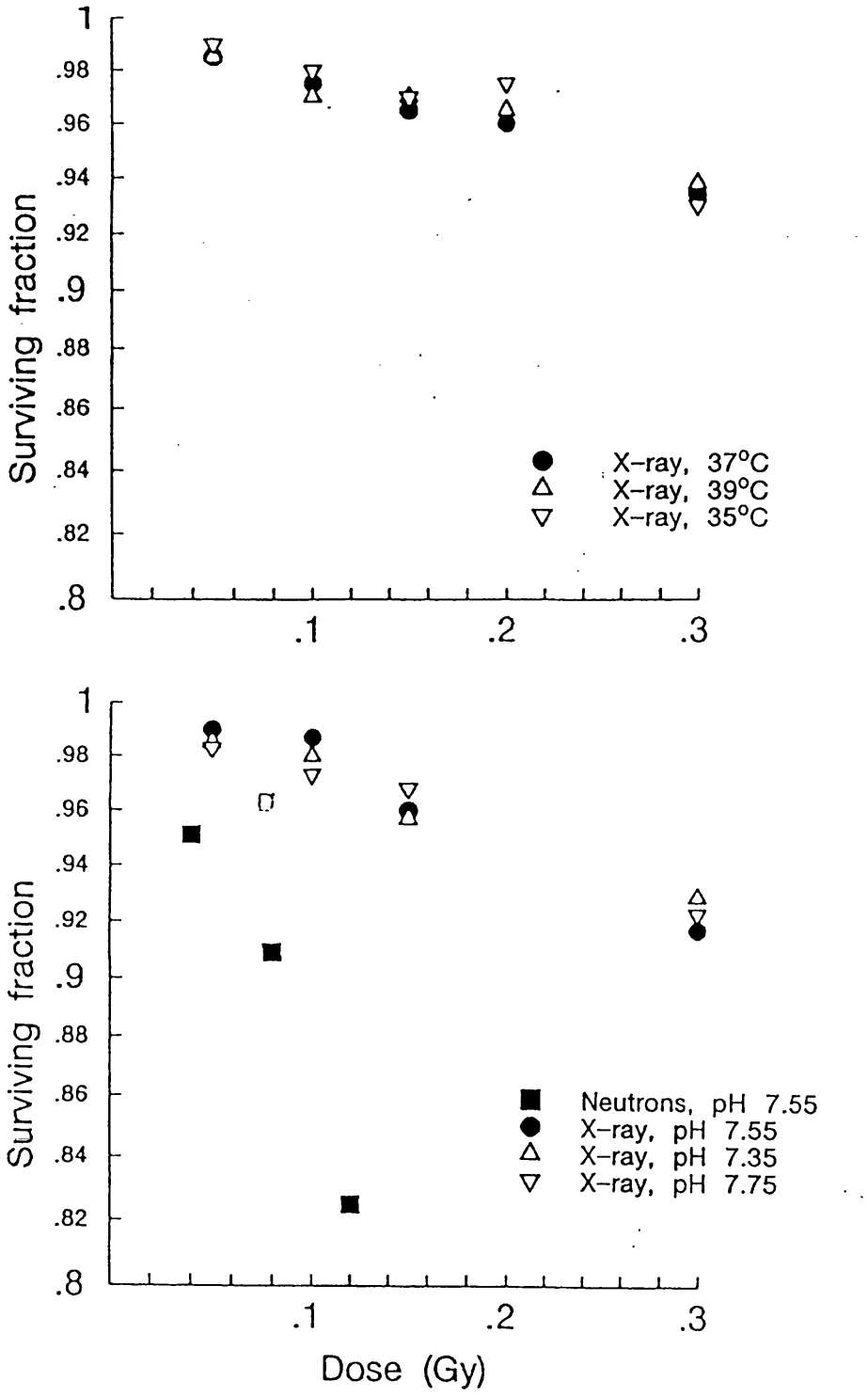

Fig. 3.5

A comparison of the effect of the pH (lower panel) and temperature (upper panel) on the measurement of surviving fraction of cells assayed in spinner culture. Slight modifications to these two parameters during irradiation had no significant effect on the level of surviving fraction compared with the standard pH (7.55) and temperature (37°C). The cells were always maintained at these standard conditions prior to irradiation and returned to them immediately following irradiation.

cells. The increase in spinning stress might have reduced the plating efficiency of the cells, affecting the survival measurement. This was investigated by establishing two spinner cultures of cells, in parallel, derived from the same parental cell population and irradiating only one of the cell samples. Over the dose range 0.1-0.3 Gy, corresponding to a range of exposure times from 7-20 min, the combination of the irradiation set-up and the spinning of the cell culture did not significantly effect the plating efficiency of the cells (Fig. 3.6).

3.7 Modifications of the DMIPS recognition assay

Despite the precisely-controlled methodology of the DMIPS recognition assay, a few values of RBE at the very lowest X-ray doses (<0.6 Gy) were not consistent with the majority of the experimental data (see Fig. 3.7). The variation may have been due to procedural artefacts which had not been considered previously or simply due to biological variation. In an attempt to reduce the range in the RBE values that were seen at the very lowest doses the recognition assay was modified further. To minimise further possible sources of error the number of procedural steps in the assay was reduced. This was achieved by changing the irradiation procedure from a spinner culture system to one in which cells were irradiated as an attached monolayer (see Figs. 3.8 and 3.9). In the new procedure a sample of cells was taken from the stock spinner culture and washed as usual, by repeatedly re-suspending the cells in fresh medium. In the spinner culture system the cells were then decanted into an irradiation vessel, irradiated and then plated. In the new monolayer system the cells were plated before being irradiated. Cells were first plated in 25 cm^2 tissue culture flasks (one flask per dose point) using an identical procedure to that in the old spinner culture system. When the cells had attached, the culture flasks were refilled to capacity with medium and irradiated. This irradiation protocol eliminated the requirement for the cells to be transferred to a unique irradiation vessel and as each flask was filled with fresh culture medium at 37°C no possible artefacts associated with the temperature and pH of the culture medium could occur. The neutron and X-ray irradiation procedures were both changed to accommodate this monolayer protocol (Fig. 3.9).

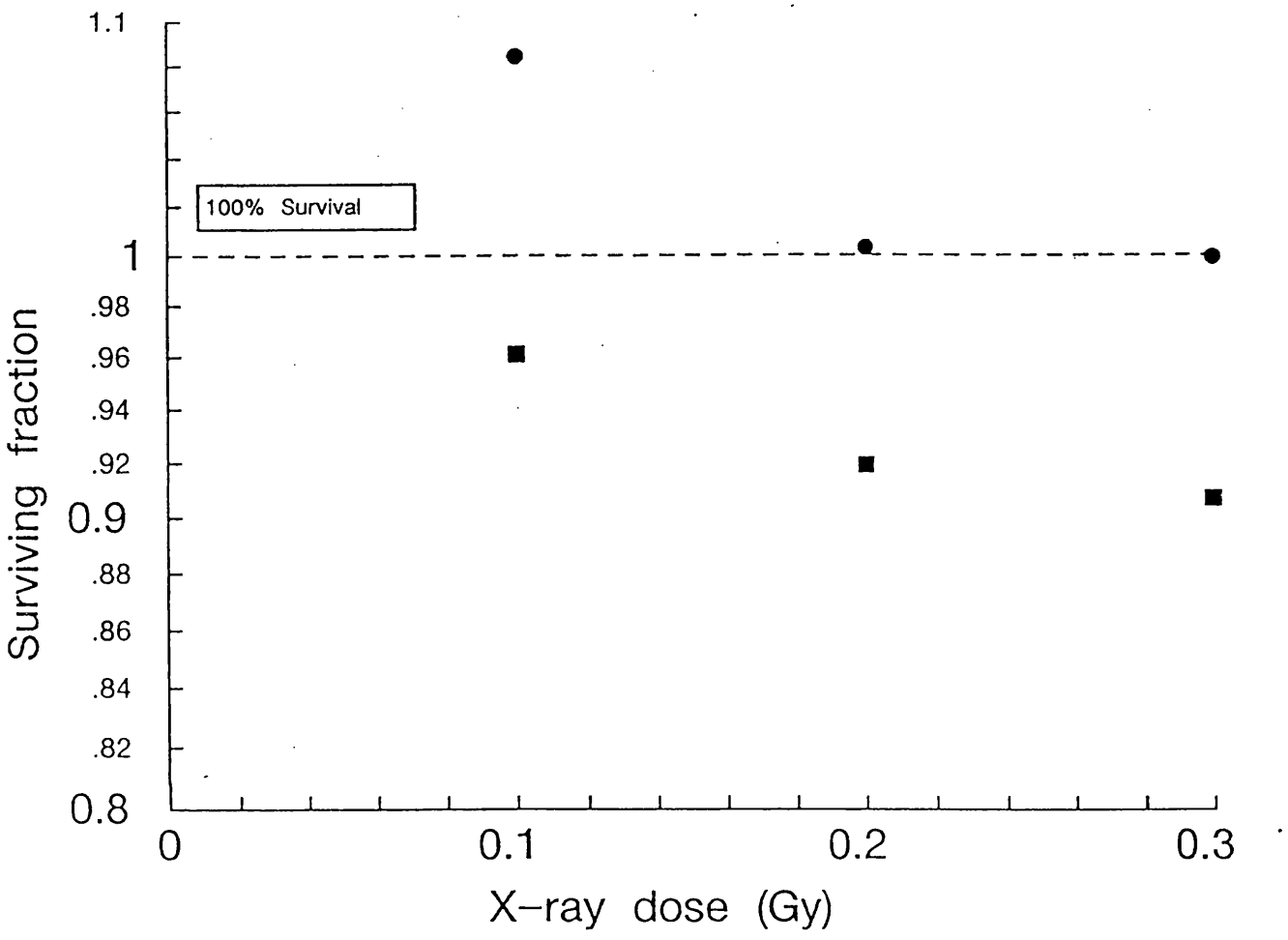

Fig. 3.6

The effect of 'spinning stress' on cells in suspension culture under the conditions of irradiation. Cells that were placed in an identical suspension culture arrangement to that used for X-ray irradiation but were not irradiated, had consistent plating efficiencies which were independent of the length of time the cells were in the irradiation set-up (●). These points have been plotted against an X-ray dose scale simply to compare them with cells assayed from a similar set-up but which <u>were</u> irradiated and sampled at the same time (■). The two cell samples therefore experienced a similar duration of suspension culture. This indicated that the increase in X-ray radioresistance that was observed over the dose range 0.2-0.6 Gy was not a reflection on the length of time the cells had been in suspension culture in the irradiation jig.

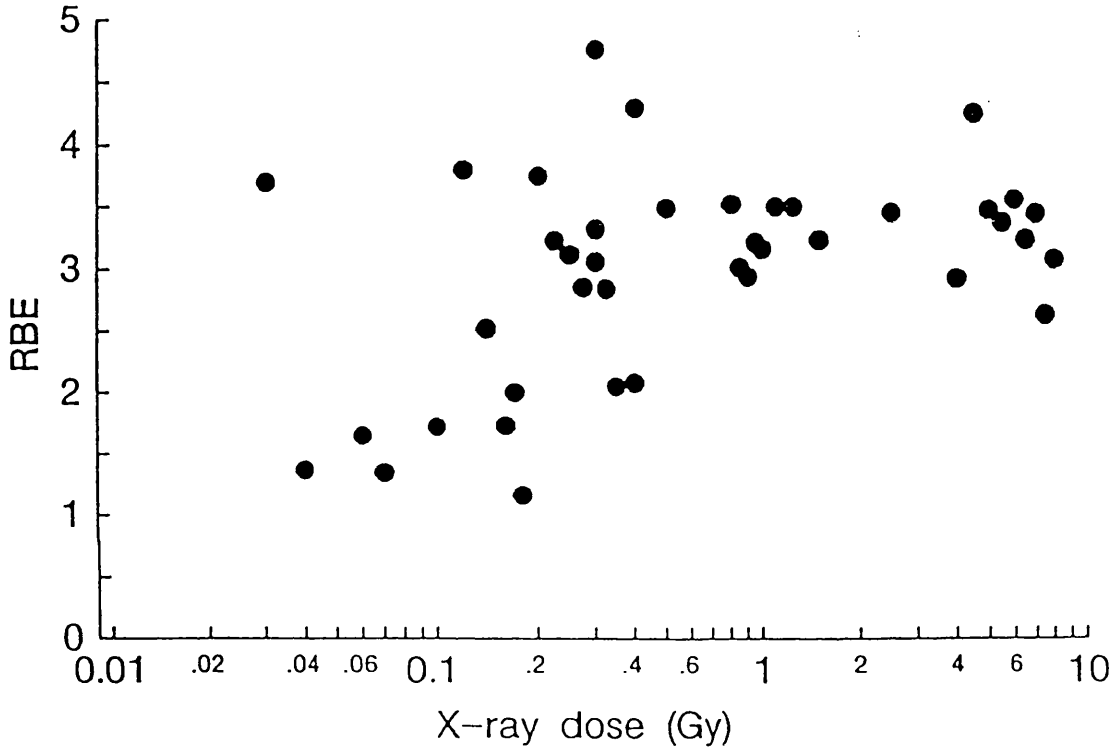

Fig. 3.7

RBE between 250 kVp X-rays and (d)4-Be neutrons given as single doses to cells in suspension culture. An increase in RBE is apparent as the X-ray dose increases above ≈0.2 Gy. The figure contains data from six experiments and each data point represents a single measurement of surviving fraction.

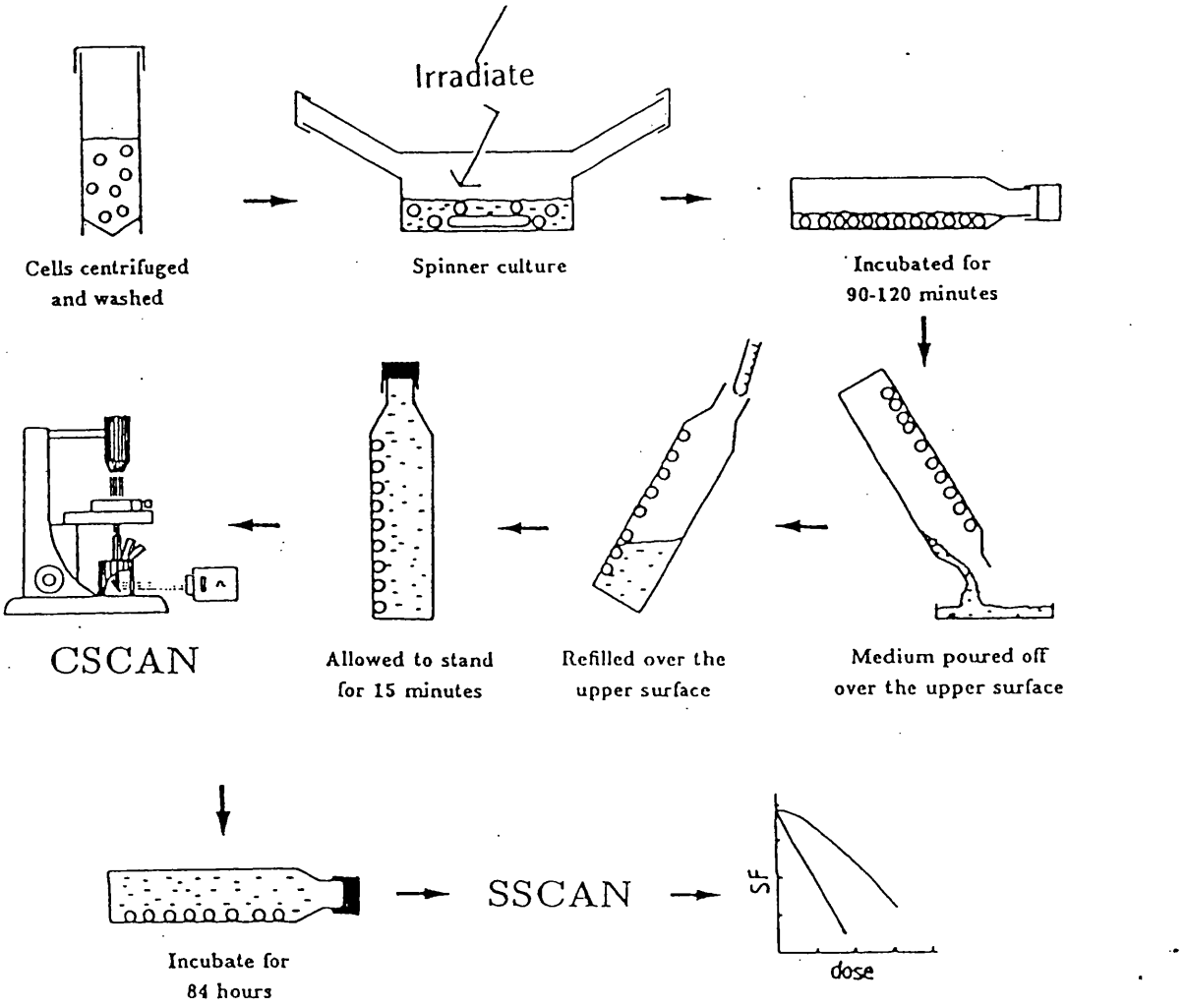

Fig. 3.8

Clonogenic recognition assay, spinner system: A sample of cells is taken from a stock cell culture and washed. A 20 ml volume of cells (2×10^5 - 4×10^5 cells ml^{-1}) is then irradiated as a spinner culture. 1 ml aliquots of cells are sequentially removed after successive doses and diluted (with fresh medium) to a concentration of 700 cells ml^{-1}. A 5 ml volume of this cell suspension is then plated (approximately 3500 cells). Following incubation at 37°C, the 5 ml of culture medium are removed and the flask re-filled completely with fresh culture medium. The flask is gently agitated to remove air bubbles and then sealed. The flask is placed vertically for 15 minutes prior to cell scanning. After re-incubation to allow for colony growth, the culture vessel is rescanned (SSCAN). The assessment of surviving fraction is calculated using the SDISP program with the unirradiated control flask providing the estimate of plating efficiency.

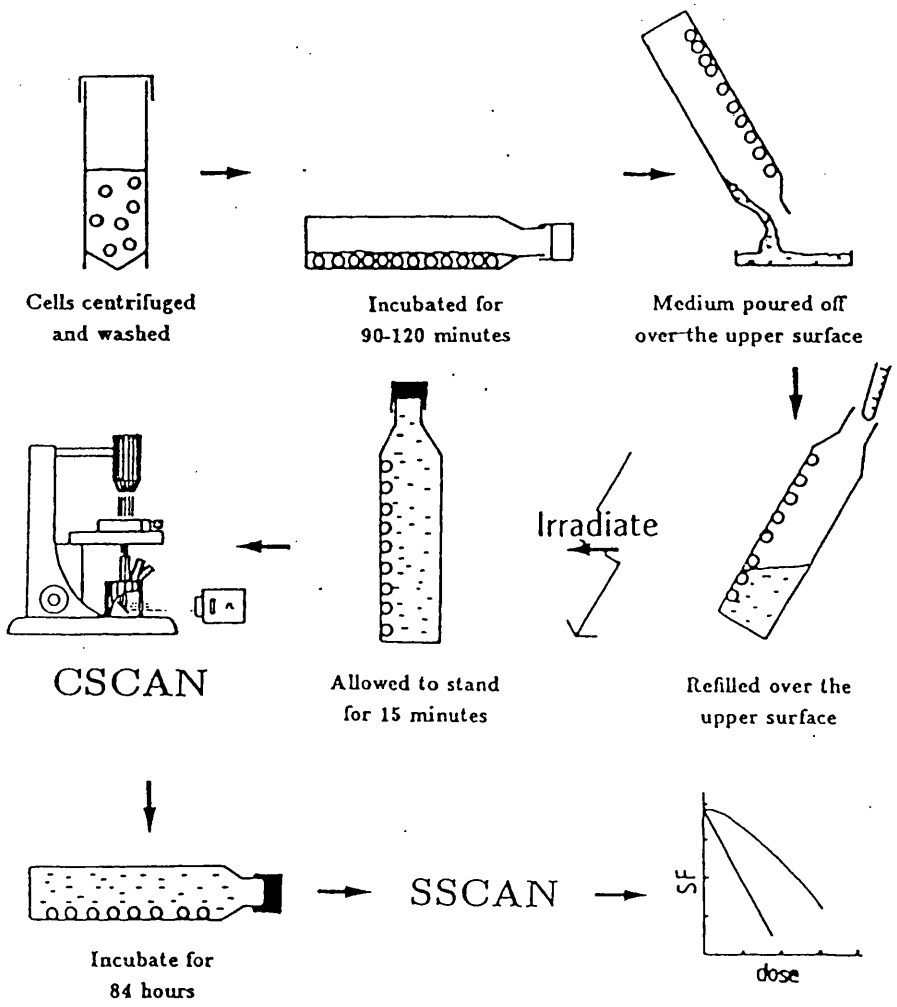

Fig. 3.9

Clonogenic recognition assay, monolayer system: A sample of cells is taken from a stock cell culture and washed. Approximately 3500 cells are plated in 5 ml of culture medium and incubated at 37°C in 95% air + 5% CO_2. This initial volume of medium is then removed and the flask totally refilled. The flask is gently agitated to remove any air bubbles and sealed. Following a 15 minute period of vertical incubation the flask is scanned (CSCAN). After re-incubation to allow colony growth the culture vessel is re-scanned (SSCAN) and values of surviving fraction are calculated using the SDISP program with the unirradiated flask providing the estimate of plating efficiency.

The increase in X-ray radioresistance that was seen in cells irradiated in spinner culture over the dose range 0.2-0.6 Gy was still observed when cells were irradiated as attached monolayers. However, the numerical range of the RBE values that were seen at each level of dose narrowed (see Fig. 3.10 c.f. Fig. 3.7). The precise reason why irradiating cells as a monolayer culture rather than as a suspension culture reduced the range of RBE values is not fully understood, but probably reflects the reduced number of steps in the monolayer protocol. The increase in X-ray radioresistance over the dose range 0.2-0.6 Gy was seen with both irradiation protocols, it is less likely therefore that the phenomenon of increasing X-ray radioresistance could have been caused by an experimental artefact associated with the method of irradiation. Another outcome of reducing the number of steps in the assay was that cells could be scanned earlier than possible previously when the cells were irradiated as a spinner culture. Using the spinner system for irradiation, the first culture flask was scanned 150-175 minutes after the start of the experiment whereas, using the monolayer system the first flask could be scanned routinely after only 120-130 minutes. The additional 20-25 minutes allowed an extra culture flask to be scanned per experimental run, thereby, increasing the amount of data for the same input of effort. Individual experiments were restricted in duration because once attached, the cells began to flatten, losing their recognition profile. The CSCAN program that locates and recognises the cells relies on each cell acting as a lens to distort the incidential light, thereby producing the characteristic image by which the cell is recognised (for a fuller description see section 2.1.2). Once flattened however, the cell has an irregular shape and image and cannot be located by CSCAN. It has been shown previously (Marples, 1987) that the V79 cell loses it's characteristic recognition image after approximately 300 minutes of monolayer culture. This permits a time window in which the cells can be scanned using the monolayer system of 120-300 minutes whereas, in the spinner system this range is smaller at 150-300 minutes. Searching for cells in a 10 cm^2 area takes approximately 20-25 min, and for the purposes of this example if the longer time of 25 min is used then 7 flasks can be scanned during the time-window of the monolayer system compared with 6 flasks in the spinner system. One flask is required for each survival curve to calculate the plating efficiency and is therefore not irradiated, typical survival curves therefore consisted of data obtained from 1 control

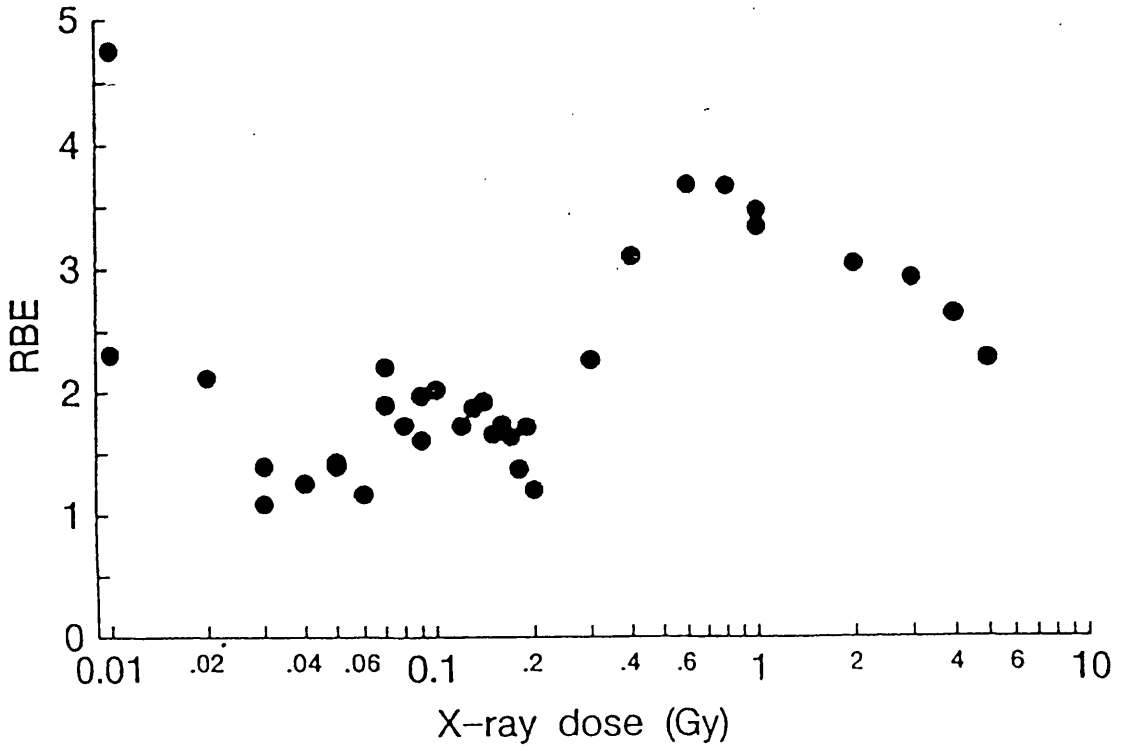

Fig. 3.10

RBE between 250 kVp X-rays and d(4)-Be neutrons given as single doses to monolayer cultures of cells. Once irradiated, the cells undergo no additional cell culture procedures; they are just cell scanned (CSCAN) and incubated. This may account for the reduced level of variation seen in the RBE values compared with data in Fig. 3.7 in which cells are irradiated as a suspension culture then diluted, plated and cell scanned.

flask and 6 irradiated flasks. When multiple survival curves were obtained in a single experiment the production of the individual survival curves was staggered to optimise the scanning of cells within the constrains of the time window. A typical experimental schedule is shown in Fig. 3.11. The experimental results in Fig. 3.3 took 36 hours of continuous experimentation with CSCAN to obtain.

3.7.1 Evolution of the V79 recognition algorithm

Throughout the course of work reported in this thesis the V79 cell-line recognition algorithm was modified frequently to improve the recognition efficiency and also to increase the data base for constructing the cell feature and parameter files. The V79 algorithm was manipulated to recognise cells at an optimum level after only 90 minutes had been allowed for the sedimentation and attachment of cells onto the growth surface, rather than the 120 minutes used previously. This reduction in incubation time was motivated by the desire to scan more flasks per experiment. This 30 minute reduction allowed one extra flask to be scanned because cell scanning could be performed earlier in the scanning time-window. The new recognition assay gave false negative and false positive values of 9% and 3% respectively. The improvement in the recognition efficiency over the values in Table 3.3 is due to the definition of more precise upper and lower feature boundaries and the improvement in the weighting factors used for the discriminant analysis. The cell recognition signal was similar for both attachment time intervals (see Fig. 3.12).

3.8 Mathematical description of the experimental data

As the size of the X-ray dose plotted in Fig. 3.4 increases, the RBE increases reflecting the increase in radioresistance that was seen in Fig. 3.3 over the X-ray dose range 0.2-0.6 Gy. These data which are not compatible with a LQ model, represented by the solid line in Fig. 3.3. These data can however be described by a modified LQ model developed by Joiner and Johns (1988), in which α, in the LQ model, is allowed to decrease with increasing X-ray dose.

Experimental protocol (23/11/89)

Neutrons

	Time	X-rays I		X-rays II	
obtain cells	8^{30}		Time		Time
count cells	8^{40}	obtain cells	10^{00}	obtain cells	12^{30}
plate cells	8^{45}	count cells	10^{10}	count cells	12^{40}
incubate-in	8^{45}	plate cells	10^{15}	plate cells	12^{45}
incubate-out	10^{00}	incubate-in	10^{30}	incubate-in	13^{00}
irrad.-start	10^{15}	incubate-out	11^{45}	incubate-out	14^{15}
irrad.-finish	10^{30}	irrad.-start	12^{00}	irrad.-start	14^{30}
CSCAN-start	10^{30}	irrad.-finish	12^{30}	irrad.-finish	15^{00}
CSCAN-finish	12^{30}	CSCAN-start	12^{30}	CSCAN-start	15^{00}
		CSCAN-finish	15^{00}	CSCAN-finish	18^{00}

Neutron doses		**X-ray doses**	
FN	control	FX	control
EN	0.05 Gy	EX	0.05 Gy
DN	0.10 Gy	DX	0.10 Gy
CN	0.15 Gy	CX	0.20 Gy
BN	0.20 Gy	BX	0.30 Gy
AN	0.25 Gy	AX	0.50 Gy
AAN	0.30 Gy	AAX	1.00 Gy

Neutrons: single full flasks 0.20 Gy min^{-1}

X-rays: single full flasks 0.016 and 0.44 Gy min^{-1}

Fig. 3.11

A typical experimental protocol to obtain 1 neutron and 2 X-ray survival curves. The location and detection of cells is only possible once the cells have attached to the growth surface. Five hours after plating, the cells flatten out and therefore lose their characteristic recognition signal. The recognition of these cells is, therefore, restricted to a period between 90-300 minutes of the plating procedure. This necessitates that the flasks for each survival curve be scanned sequentially. The protocol therefore provides approximate times for each stage in the production of three survival curves to ensure that maximum efficiency is achieved by the scanning procedure.

LQ model: $SF = \exp(-\alpha D - \beta D^2)$ (3.1)

modified LQ model: $\alpha = \alpha_{resistant}(1 + g.\exp(-d/t))$ (3.2)

Combining the data from all the individual single-dose V79 experiments described in the thesis and applying the modified LQ model in a calculation of RBE produces the fit shown in Fig. 3.13 represented by the solid line. The dotted lines representing the 95% confidence limits on the fit (See section 4.5 for a fuller description of the analysis). This model indicates that an approximate 2-fold difference exists between the very low dose response to X-rays (<0.2 Gy) and the high dose response (>>0.6 Gy). The same fit has also been added to a graph containing the mean RBE values ± SD calculated for the pooled data from the individual experiments for each dose level (Fig. 3.13, lower panel). The increase in X-ray radioresistance over the range 0.2-1 Gy, reflected by the increase seen in RBE over the same dose range is more apparent in this diagram (Fig. 3.13, lower panel) and it demonstrates that the response is a pronounced reproducible effect. Plotting the X-ray data as a function of effect per gray (EPG, which is defined as $1/D_0$) confirms that the increase in RBE value over the X-ray dose range 0.2-0.6 Gy is a consequence of changes in the X-ray response and not of the neutron response (Fig. 3.14).

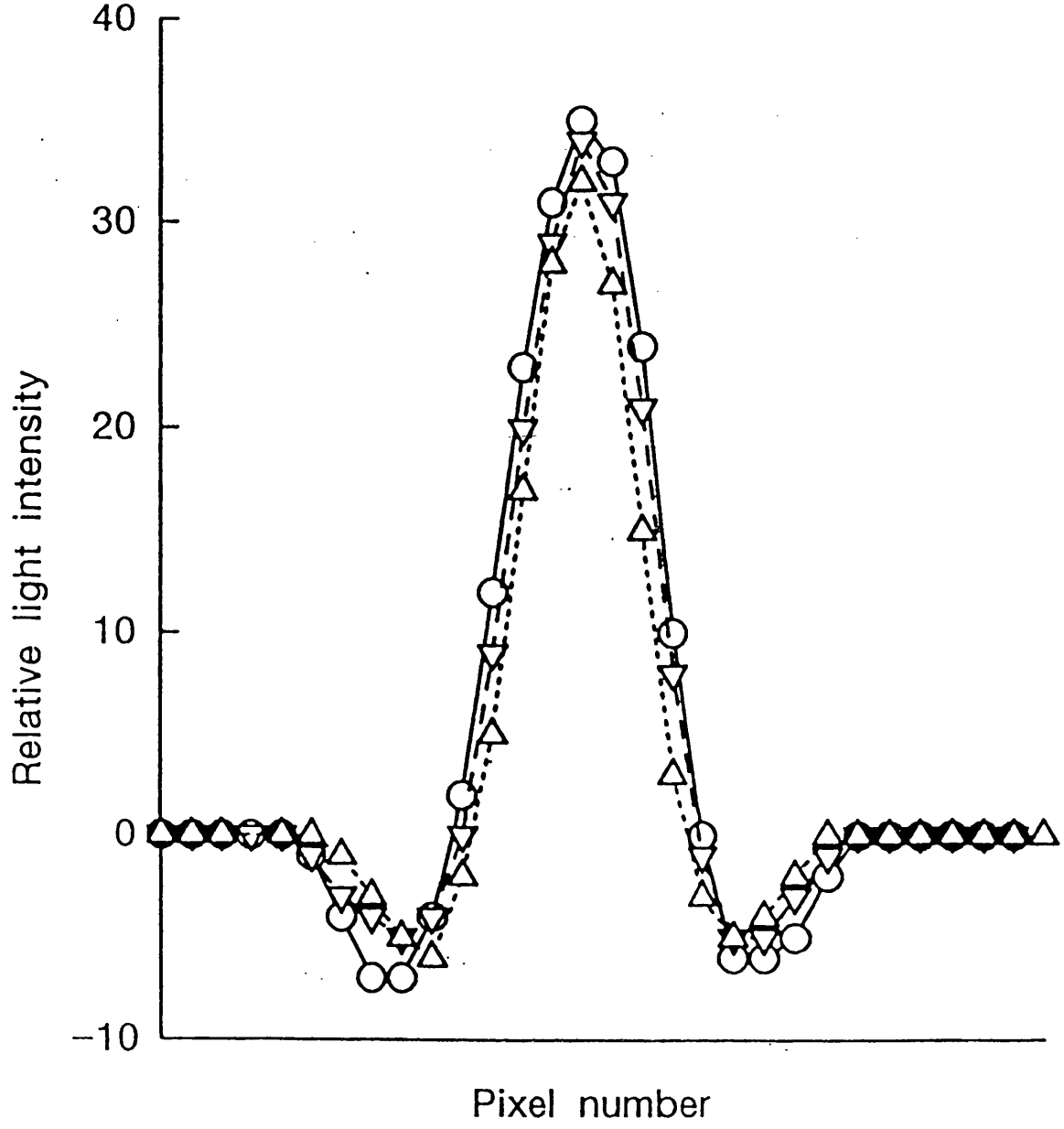

Fig. 3.12

Typical cell recognition signals from a CHO cell (△), V79 cell allowed 120 minutes to attach (▽) and a V79 cell allowed 90 minutes to attach to the growth surface(O). All three images were obtained by sampling 50 cells. The similarity between the CHO and V79 images explains why the CHO algorithm was able to locate and detect V79 cells. This image is used in the primary analysis referred to in Fig. 2.13 and is the most basic step in classifying located objects into cells and non-cells.

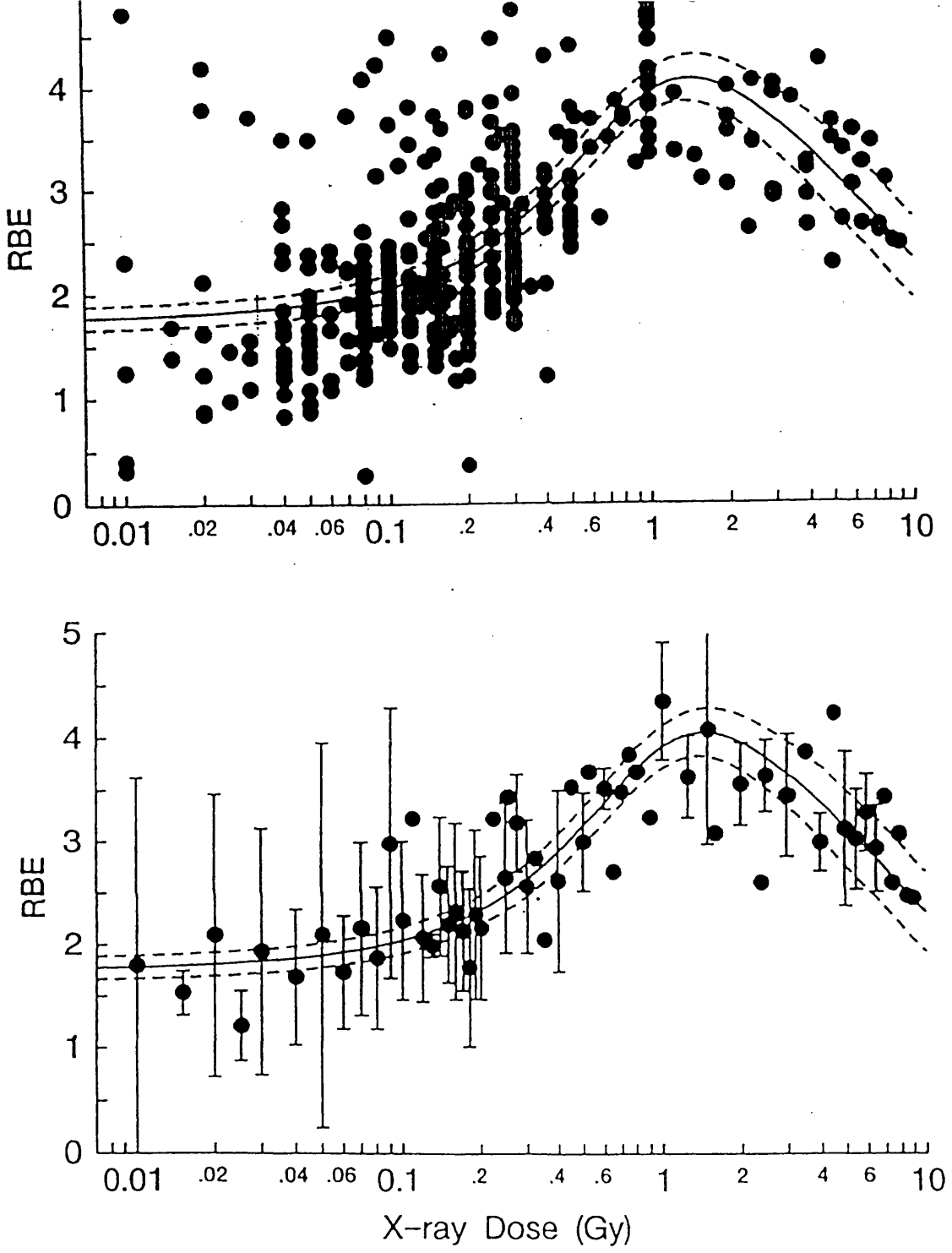

Fig. 3.13

RBE between 250 kVp X-rays and d(4)-Be neutrons for cell irradiated with single doses. The upper panel contains the raw data and the lower panel the mean value ± SD. The solid line on each panel represents the fit of the modified LQ model (Eqn. 3.2) incorporated in a calculation of RBE (see section 4.5) in which α is allowed to decrease with an increase in X-ray dose. The model suggests that the predominant change in RBE between the very low dose and high dose response occurs at an X-ray dose of ≈0.40 Gy and a two-fold difference exists between the two extremes. The dashed line is the 95% confidence limits on that fit.

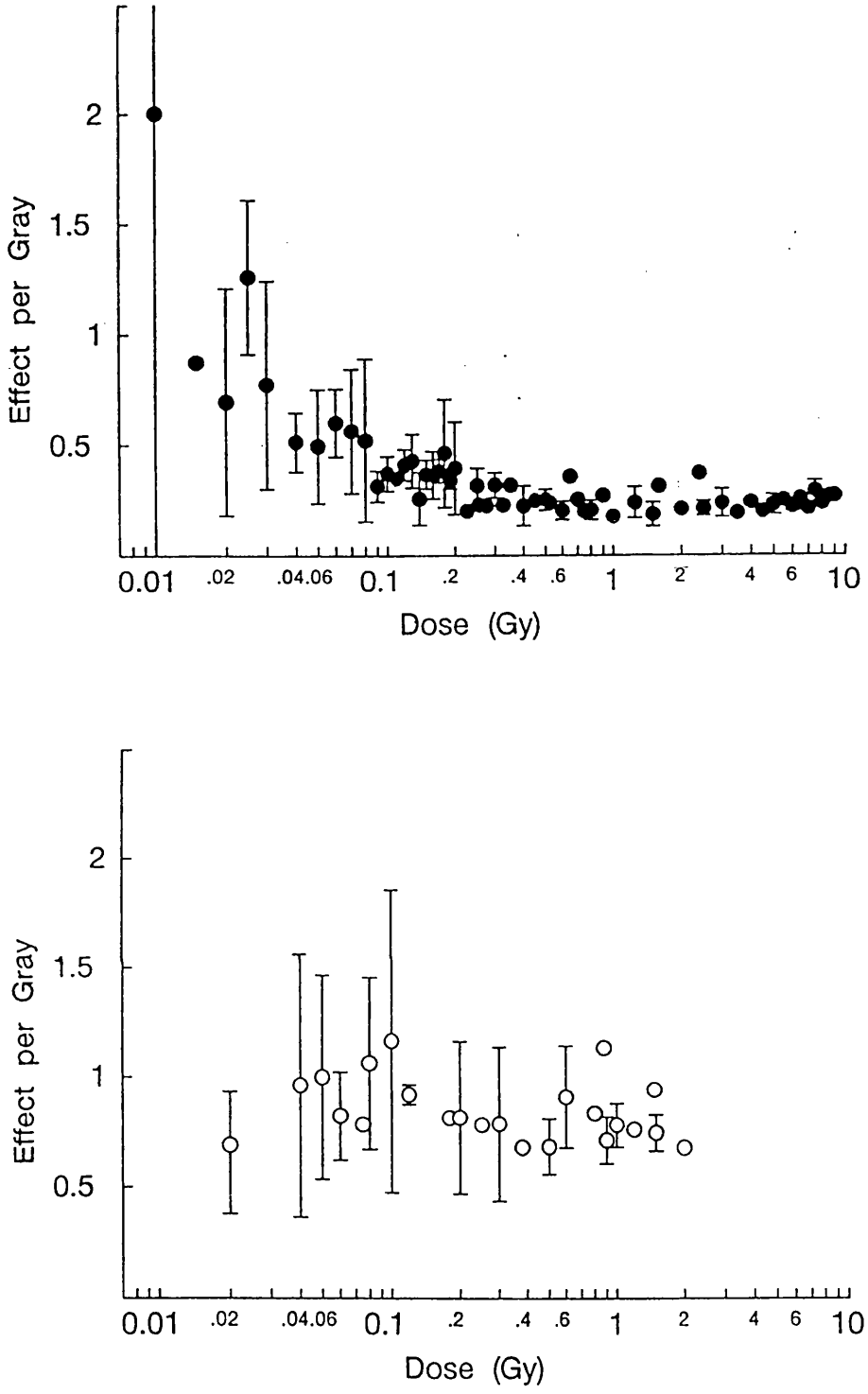

Fig. 3.14

The effectiveness per gray ($1/D_0$) for X-rays (upper panel) and neutrons (lower panel) indicating that the change in RBE reflecting the increase in radioresistance is due to an increase in the effectiveness of the X-rays at low doses and not the neutrons. The X-ray EPG increases as the X-ray dose decreases whereas the neutron EPG remains consistent over the whole dose range.

3.9 Summary

1) A good correlation was found between the survival estimates obtained using a conventional Puck and Marcus type clonogenic assay and the DMIPS clonogenic recognition assay over the X-ray dose range 2-7 Gy. Below 2 Gy, the conventional assay gave unreliable estimates of surviving fraction compared with the recognition assay, survival estimates were often greater than 1.0.

2) The recognition assay has been used to measure satisfactorily clonogenic survival down to X-ray doses of 0.01 Gy and to neutron doses of 0.02 Gy.

3) Cell survival after neutrons decreased exponentially with dose over the dose range 0.02-3 Gy.

4) The X-ray response was described by a linear quadratic model over the dose range 1-10 Gy but at X-ray doses <<1 Gy an unexpected increase in X-ray sensitivity was observed. In some experiments at the very lowest doses investigated X-rays were nearly as effective at killing cells as neutrons.

5) The increase in radioresistance that was observed over the X-ray dose range 0.2-0.6 Gy was probably not due to an artefact associated with measuring cell survival using the recognition assay. It is also unlikely that the phenomenon was due to changes in the environmental conditions of the irradiation set up (e.g. pH, stirring, temperature).

3.10 Discussion

The objective of these experiments was to obtain accurate measurements of the response of V79-379A cells to 250 kVp X-rays and d-(4) Be neutrons in the low-dose range (0-2 Gy). This dose range is becoming increasingly relevant in radiobiology because of the smaller doses of radiation that are being given in accelerated and hyperfractionated radiotherapy. Historically, measuring cell survival following low-dose

radiation treatment has proven difficult because the assays that have been used are imprecise at high levels of surviving fraction (Boag, 1975). Accurate measurement of low-dose survival was only possible in this study by using the DMIPS cell analyser.

The protocol for measuring low-dose cell survival using the DMIPS cell analyser has evolved during the course of this investigation. In the earliest experiments, the repeated measurement of surviving fraction at a particular dose level was associated with a consideration variation. However, the errors on the assessments of surviving fraction generated towards the end of the study were greatly reduced compared with the earlier work owing to methological improvements in the assessment of survival (see section 3.4.3). These included: first, the production of a better single cell suspension, achieved by passing the cell sample repeatedly through a 19-gauge hypodermic needle; second, the filtration of the culture medium to reduce the amount of debris, thereby reducing the slight possibility that a piece of debris would be incorrectly classified as a cell; third, the vertical incubation of flasks prior to, and following, CSCAN; fourth, the switch to a monolayer irradiation system (see section 3.7). Probably the most significant development was an improvement in the ability of the DMIPS cell analyser to locate and identify the V79 cells. Initially, a CHO cell recognition algorithm was used to detect the V79 cells. Although this was not an ideal situation, the algorithm proved satisfactory in the early stages of the work. This CHO algorithm was eventually replaced with a V79 specific algorithm when the CELREC program was commissioned. This newly-generated algorithm improved the recognition efficiency of the cell analyser for V79 cells (Table 3.3). The use of the CHO algorithm would have contributed to the variability in the assessment of survival that was seen in some of the early data obtained in the thesis.

When the X-ray survival data obtained in this study were fitted to a linear-quadratic model, the data below an X-ray dose of 1 Gy were below the predicted LQ response (e.g. see Fig. 3.3). This was found to be a consistent effect and has not been reported previously in this cell line. This low-dose X-ray hypersensitivity may not have been noticed previously because the conventional clonogenic assay used normally to measure cell survival lacks the necessary statistical precision to accurately determine cell survival over the dose range of the phenomenon. Measuring cell survival using the DMIPS cell analyser, reduces the cell counting and sampling errors usually associated

with the clonogenic measurement of low-dose (< 1Gy) cell survival (see section 1.8.1). The procedural errors which are usually associated with the repeated assessment of cell survival, and cause the variation in intrinsic radiosensitivity seen day to day, (see section 1.8.1) were also reduced in this study by comparing the cell survival measurement obtained after X-rays with that obtained after neutrons in the same experiment. Variations in radiosensitivity between individual experiments following X-irradiation would presumedly be the same after neutrons and therefore would be reduced by expressing the radiation response in terms of RBE (see section 4.5). Watts *et al.* (1986) measured cell survival down to X-ray doses of 0.25 Gy in this V79-379A cell line by extensive dose replication; however, the surviving fraction data were not sufficiently consistent to observe the change in radioresistance reported in this thesis. The low-dose hypersensitivity phenomenon might have been observed in the study of Watts *et al.* (1986) if the variation in response that was observed between the individual experiments was reduced by comparing the X-ray data with an internal control, such as the response of neutrons as in this study.

Low-dose X-ray hypersensitivity has been reported previously *in vivo* (Joiner & Johns, 1988). X-ray doses per fraction below 0.6 Gy were more effective per gray at causing normal tissue damage when compared with higher doses per fraction above 0.6 Gy. An *in vitro* study measuring the radiation response of insect cells also indicated an increased sensitivity to low doses of X-rays compared with high doses (Koval, 1984). A change in the radiation response of cells between the low-dose region and higher-dose region has also been reported for cell transformation (Hall and Millar, 1981). That study showed evidence that the transformation rate increases, when cells were irradiated with fission neutrons, over the lower dose range (0.1-0.3 Gy) remains constant up to 1 Gy and then increases again above 1 Gy.

Low-dose X-ray hypersensitivity manifested by the biphasic survival response observed in this study might be caused by the existence of an experimental artefact, the differential killing of a sensitive and resistant subpopulation of cells, or the manifestation of an induced repair response. Whatever the correct explanation for the biphasic cell survival curve the data reported in this chapter of the thesis clearly demonstrate that extrapolating the mathematical fit for survival data obtained from high doses of radiation

to predict the response of cells to low doses of radiation is not satisfactory. This is also evident for other radiobiological parameters that have been estimated for the low-dose region of the survival curve by extrapolation of the mathematical fit obtained from the high-dose response. Several authors report that the oxygen enhancement ratio (OER) decreases as a function of decreasing X-ray dose below 2 Gy (Alper, 1975; Palcic and Skarsgard, 1984), while others report that the sensitiser enhancement ratio (SER) for some radiosensitisers is also reduced at low X-ray doses (Chapman *et al.*, 1975).

It is unlikely that the low-dose X-ray hypersensitivity phenomenon was the result of an artefact of the scanning procedure as cell survival following exposure to neutrons, measured using the same assay, produced a linear survival response, with no hypersensitive response to low doses. A systematic error might be associated with the X-ray irradiation procedure however, this seems unlikely because extreme care was taken to ensure, as closely as possible, the identical treatment of all samples at each dose level. Three different X-ray dose rates were used to ensure that the radiation exposure time was approximately constant irrespective of the dose actually given (Table 2.4). Low-dose X-ray hypersensitivity was still observed when the irradiation set up was completely changed from a spinner arrangement to one where cells where irradiated as freshly-plated monolayer cultures (see section 3.7). These data further indicated that the phenomenon was unlikely to be the manifestation of an irradiation artefact. A dose-dependent experimental artefact which changes the radiation response markedly and consistently over such a large number of experiments is unlikely.

However, the biphasic survival response might reflect the existence of an intrinsically radiosensitive subset of cells in the whole cell population. This subset of cells might be an intrinsically radiosensitive subpopulation of cells that is genetically distinct from the majority of the stock cell culture or possibly an exquisitely radiosensitive component in each cell in the stock cell culture e.g. cells in a particular phase of the cell cycle. Sinclair (1968) reported that radiosensitivity was dependent on the phase of the cell cycle. The question of whether the biphasic survival curve simply reflects the differential killing of a radiosensitive subset of cells is investigated in depth in other chapters of this thesis. The possibility of a homogeneous, radiosensitive subpopulation of cells is investigated in chapter 4 while the dependence of

radiosensitivity on cell-cycle phase is studied in chapter 5.

Mathematical modelling of the X-ray survival data, expressed as RBE (see Fig. 3.13), indicated that a two-fold differential exists between the low-dose and high-dose responses (see Fig. 3.13). To account for this difference a process must exist that causes proportionally more cell kill at extremely low doses (<0.2 Gy) than at slightly higher doses (>0.6 Gy). The data could be explained by an 'inducible repair process': an increase in radiation-induced damage triggers a protective mechanism that becomes more effective over the dose range 0.2-0.6 Gy. The radiation response of the V79-379A cells was described accurately by a modified LQ equation (Eqn. 3.4) in which α was allowed to decrease with an increase in X-ray dose (Fig. 3.3). In the lethal, potentially lethal model (Curtis, 1986), α depends on the number of the initial induced lesions allowed to repair, therefore a biological explanation of a dose dependent α may be induced repair (Joiner, 1990).

Chapter 4: An effect of a sensitive subpopulation of cells?

4.1 Introduction

Mammalian cell survival curves are often described well by a linear-quadratic (LQ) equation over the dose range 2-20 Gy. The results of Chapter 3 demonstrate that the survival curve for V79-379A cells obtained using the DMIPS cell analyzer over the X-ray dose range 1-10 Gy was consistent with an LQ model. However, over the dose range 0.01-1 Gy the survival curve was biphasic and could not be described accurately by a LQ model. This observation has not been reported previously in this cell line and the accurate measurement of cell survival below X-ray doses of 1 Gy was only made possible in this study by using the DMIPS cell analyser to locate and identify cells.

The results of chapter 3 also indicated that the biphasic nature of the cell survival curve at low doses was unlikely to be due to the irradiation procedure or an artifact associated with measuring the clonogenicity of cells using the DMIPS recognition assay. It therefore must reflect a real change in radiation sensitivity.

4.1.1 Biological interpretations of a biphasic survival curve.

There are several possible ways of biologically explaining the occurrence of a biphasic survival curve. Historically, survival curves that have been multi-phasic have usually been interpreted as representing the response of a heterogenous mixture of cells, consisting of sub populations with differing radiosensitivities. An inflexion point on the survival curve was understood to mark the point where the survival response changed from reflecting predominantly one subpopulation to the other subpopulation of cells. Three possible explanations to account for the shape of the biphasic survival curve will be presented followed by some examples of each taken from the literature.

1) Static radiosensitive subpopulations of cells

A biphasic survival curve may indicate the existence of a small subpopulation

of cells that is more radiosensitive than the majority of the cell population. The radiation response of the sensitive component would dictate the overall response after small radiation doses producing an initial steep component to the survival curve. Following the small dose of radiation, the overall response of the whole cell population would then be determined by the remaining resistant subpopulation of cells, the sensitive subpopulation having been killed. The slope of the combined survival curve therefore becomes less steep as the response changes predominantly from the sensitive subpopulation of cells to that of the remaining resistant subpopulation of cells and therefore an inflexion is seen in the overall survival response. The biphasic survival does not represent a change in radiosensitivity of all the cells in the population, but simply the difference in the sensitivity of the two subpopulations of cells.

2) Dependence of radiosensitivity on cell-cycle phase

It is known that the response of cells to X-rays is dependent on the position of the cell in the cell cycle. Cells in G_2 and the mitotic phase of the cell cycle are more radiosensitive than cells in G_1 and S phase. The overall response of an asynchronous population of cells consists of the combined responses of the individual phases of the cell cycle. The total population of cells can therefore be viewed as a mixture of subpopulations of different radiosensitivities. As with explanation 1 one phase of the cell cycle may dominate the radiation response at low X-ray doses producing an initial steep region to the survival curve. When the sensitive component has been depleted the radiation response of the whole population changes and it appears that there is a *real* increase in the radioresistance of the whole cell population. This might produce an inflexion point on the survival curve of the whole population.

3) Induced repair

Increasing the degree of radiation insult produces greater levels of damage which may trigger a protective mechanism conferring radioresistance on the remaining cells in the population, therefore creating a biphasic survival curve. At the lowest doses little or no repair occurs and as the X-ray dose increases a repair system is activated which increases the repair of radiation induced damage. This produces an increase in the overall radioresistance of the remaining cells in the population and

consequently a decrease in the slope of the survival curve. This is seen as an inflexion on the survival curve.

4.1.2. Multi-phasic survival curves attributed to sensitive subpopulations of cells or the repair of radiation damage

Biphasic survival curves with distinct inflexion points have been observed for yeast (Beam *et al.*, 1954, see Fig. 4.1), in mammalian cells (Elkind and Sutton, 1959), algae (Horsley and Pujara, 1969) and insect cells (Koval, 1984, see Fig. 1.3). In the yeast and algal cell systems the inflexion point in the cell survival curve was attributed to the presence a small subpopulation of radiosensitive cells; budding cells in yeast (explanation 1) and S phase cells (explanation 2) in the algal population. The induction of an unidentified repair process was postulated to account for the multi-phasic survival curve seen in the insect cell study (explanation 3). Whitfield and Rixon (1960) reported biphasic survival curves over an X-ray dose range of 0.2-20 Gy in a strain of mouse cells isolated from connective tissue (Fig. 4.2). The shape of the survival curve was reported to be due to the presence of a radioresistant subline of cells in the parental cell population which was 4-5 times more radioresistant that the parental cell population. The survival curve for the resistant subline was not biphasic suggesting that the parental population of cells was inherently heterogenous and consisted of a mixture of cells with different intrinsic radiosensitivities (explanation 1).

4.1.3 Examples of multi-phasic survival curves attributed to differences in intrinsic radiosensitivity of an homogeneous population of cells.

Biphasic survival curves have been reported in two mammalian cell lines (Calkins *et al.*, 1989) and have been explained by postulating the repair of 'lethal mutations'. The existence of 'lethal mutations' was originally proposed (Mothersill and Seymour, 1989) to explain the lower plating efficiency that was seen in surviving cells which had been exposed previously to radiation compared with cells which had not been previously irradiated. The occurrence of 'lethal mutations' cannot explain the shape of the survival curves reported in this thesis because the stock culture of cells used for each experiment had not been exposed previously to radiation as far as is known.

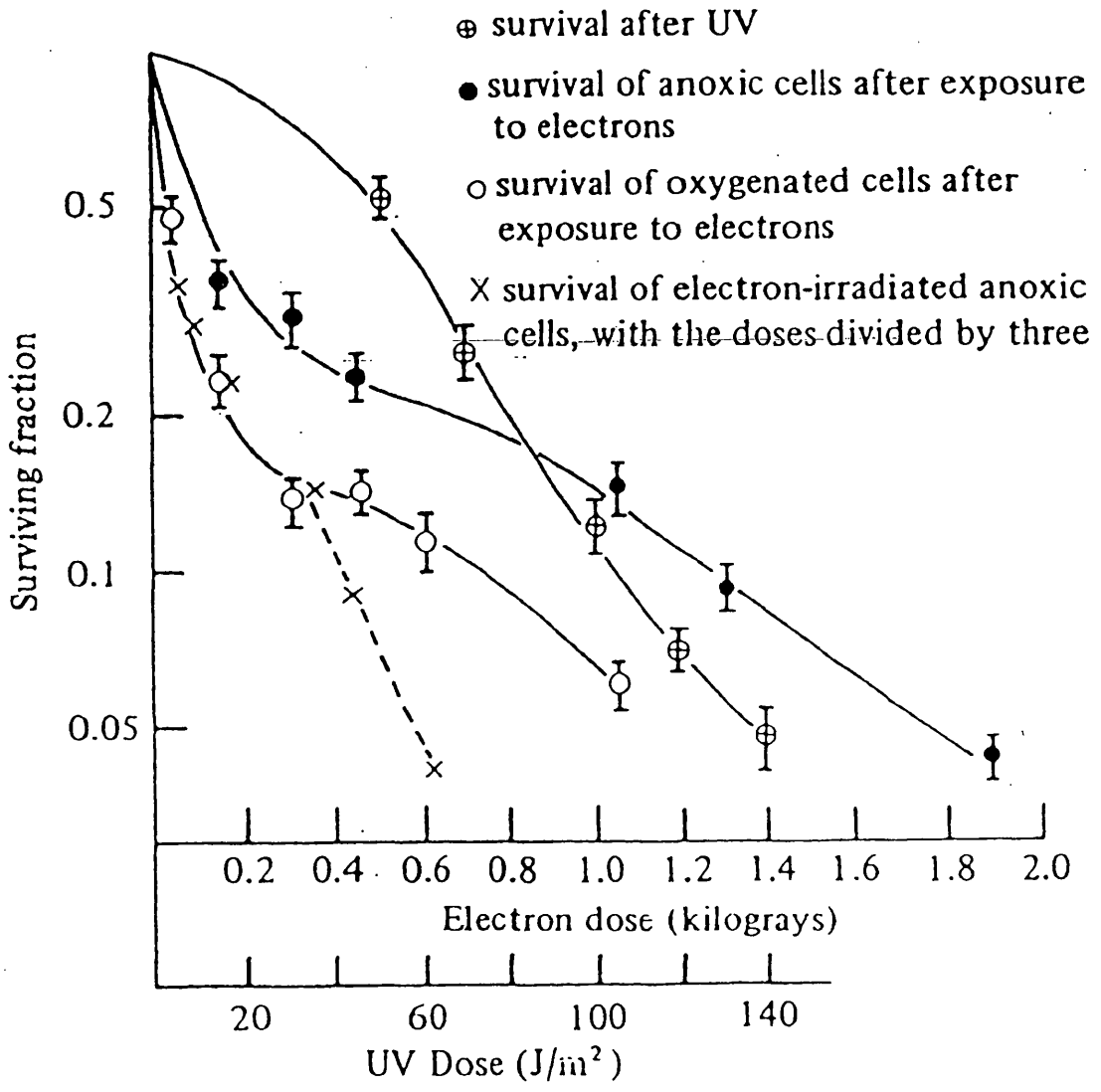

Fig. 4.1

Survival curves of haploid yeast cells exposed to ionising radiation and UV light. The biphasic survival curves of cells exposed to ionising radiation were attributed to the presence of radiosensitive budding cells in the single cell suspension (modified by Alper, 1979, from Beam et al., 1954).

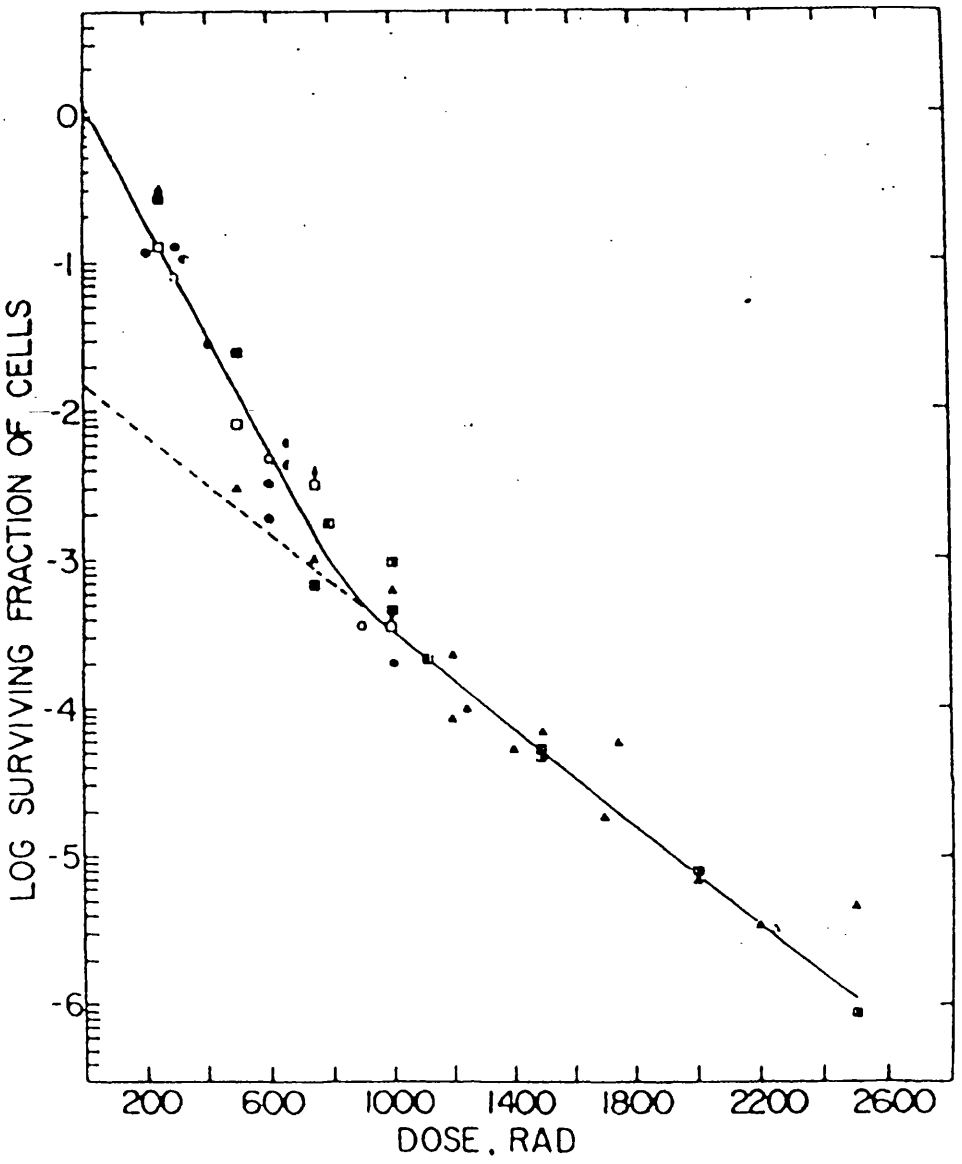

Fig. 4.2
A survival curve for 6C3HED mouse lymphosarcoma cells irradiated in vivo. The biphasic survival curve was attributed to a subpopulation of intrinsically radioresistant cells (reproduced from Whitfield and Rixon, 1960)

The radiosensitive *XRS* cell lines, derived from the CHO K1 cell line by treatment with EMS, also have multi-component survival curves (see Fig. 1.1) (Jeggo and Kemp, 1983). The radiosensitive mutants are not defective in single-strand break repair but have a reduced rate of double-strand break rejoining (Kemp *et al.*, 1984). It has been postulated that the parental cell line contains two copies of the *XRS* repair gene; only one copy of the gene is functional while the second is transcriptionally silent due to methylation control (Denekamp *et al.*, 1989). A mutation in the functional gene of the parental cell line abolishes the ability to repair, leading to the increased X-ray sensitivity seen in the *XRS* cell lines. The radiosensitive *XRS* mutant cells can revert a more resistant state when the silent gene is activated by de-methylation following treatment with 5 azacytidine, a potent de-methylating agent. The *XRS* 4, 5, 6 and 7 sublines have concave biphasic survival curves with a steep initial response, followed by a shallower response at higher X-ray doses. The biphasic response is a persistent feature of these cell lines and attempts to isolate a sensitive and resistant subpopulation of cells, which might have accounted for the shape of the curve, have so far been unsuccessful (Denekamp *et al.*, 1989) suggesting that the shape of the survival curve cannot be attributed to a subpopulation of intrinsically sensitive cells.

4.2 Aims

The biological explanation for the biphasic survival curve seen in this study was unknown. Throughout this thesis, various interpretations which could account for the biphasic nature of the survival curve are investigated. The possible effect of radiation dose-rate is investigated in chapter 6, the influence of phase of the cell cycle is studied in chapter 5 and the effect of inhibiting the repair of radiation-induced lesions on the shape of the survival curve is explored in chapter 7. This chapter is dedicated to investigating whether the biphasic survival curve over the dose range 0.04-1 Gy could be due to the existence of an inherently sensitive, genetically distinct subpopulation of cells in the parental V79-379A cell population, by examining the radiation response of cell populations 'cloned' from the stock V79 cell culture and also the radiation response of the progeny of a cell population exposed to an X-ray

dose of 1 Gy.

4.3 Materials and methods

4.3.1 Cloning the parental cell population

Cells were cloned from the stock culture of exponentially growing V79 cells. A aliquot of cells was diluted to a concentration of approximately 100 cells per 10 ml of medium. 0.1 ml of this cell suspension was added to each well in a 48 multi-well plate. The plates were then incubated at 37°C for 1-2 h to allow the cells to attach to the growth surface. Following the incubation period, the wells were examined microscopically to identify wells containing only one cell. The multi-well plate was re-incubated at 37°C. After a period of 5 days, two of the wells identified originally as containing only one cell were treated with trypsin, and the cell suspension transferred to a 50 ml culture vessel. The cell culture was maintained using standard culture techniques until sufficient cells had grown to assess cell survival.

4.4. Experimental results

4.4.1 Differences in intrinsic radiosensitivity

If the biphasic survival curve was due to intrinsic differences in the radiation sensitivity of a small subpopulation of cells in the stock culture of V79 cells, then a population of cells which had been cloned from the parental population would exhibit one of two responses. If the clone had originated from an intrinsic radiosensitive cell subpopulation the cells would have a very sensitive response to X-rays and therefore a steep survival curve over the whole X-ray dose-range, or alternatively the survival curve would be compatible with a LQ model over the entire dose range if the cloned population of cells had originated from the radioresistant subpopulation of cells. Fig. 4.3 shows the survival curves obtained for the two V79-379A clones and the parental cell population. The biphasic response present in the parental population was also evident in the cloned cell populations. All the survival curves had an initial steep region over the dose range 0.04-0.20 Gy followed by an increase in radioresistance as the X-ray dose increased to 1 Gy (Fig. 4.3). Plotting the data as RBE against X-ray dose to reduce the procedural error, the cloned cell populations have the same pattern of an increasing RBE with increasing X-ray dose as the parental cell population (Fig. 4.4).

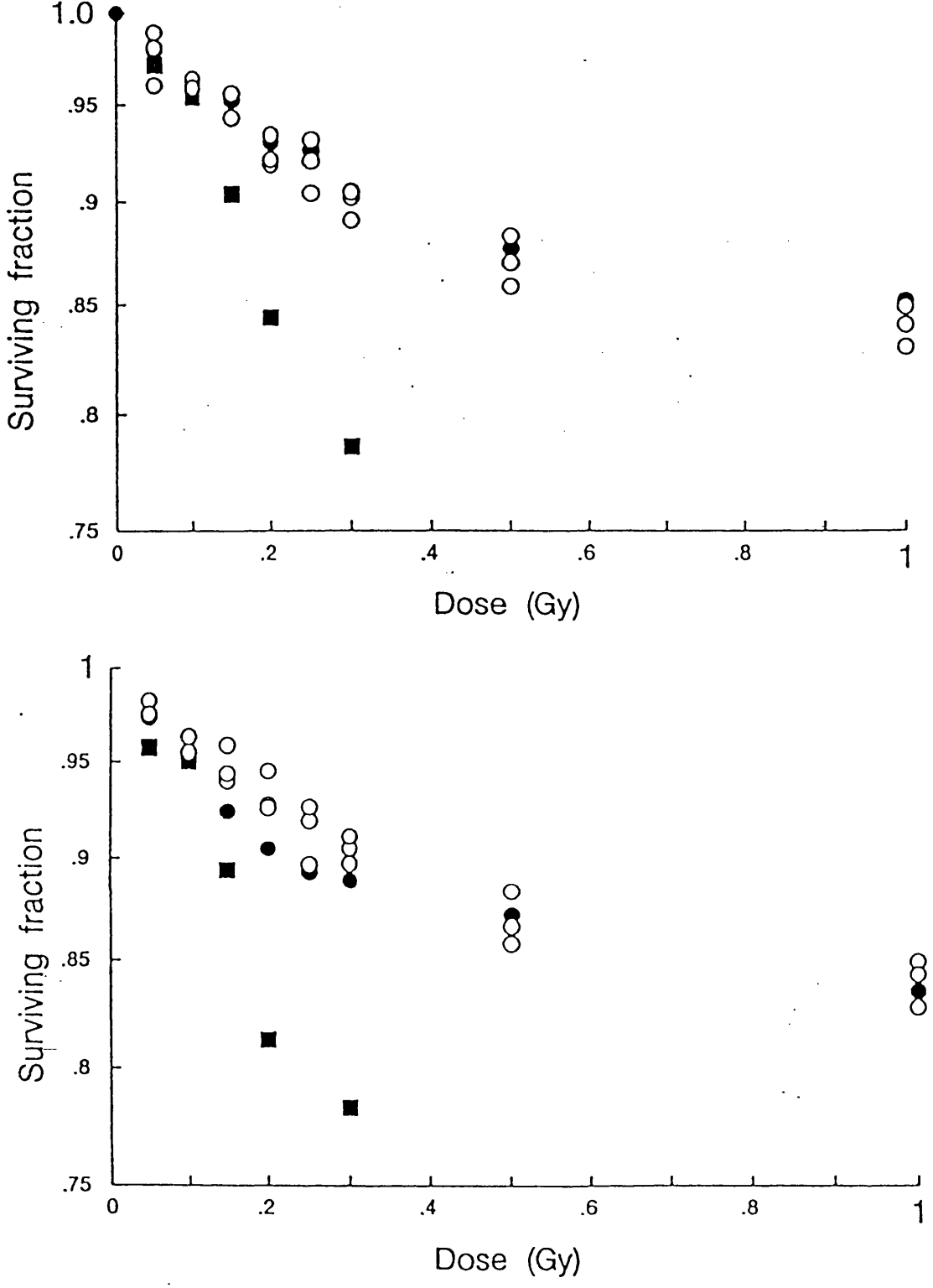

Fig. 4.3
Cell survival curves for 2 cell populations cloned from the stock culture of V79 cells. The upper panel contains the data from clone 1 and the lower panel from clone 2. The overall survival response of the cloned cell populations (O) *are the same as that of parental stock culture* (●). *The solid squares represent the neutron response.*

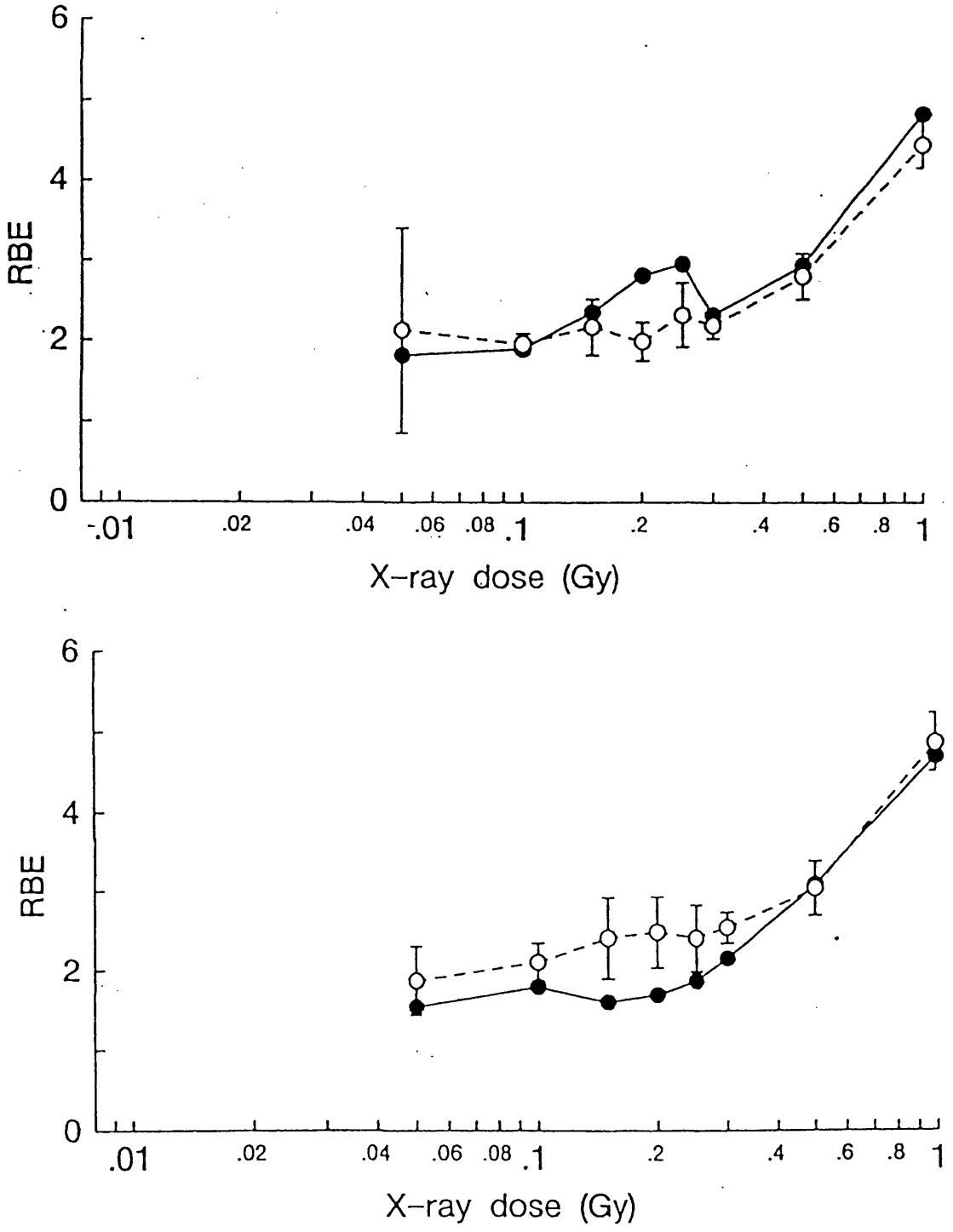

Fig. 4.4

RBE between 250 kVp X-rays and d(4)-Be neutrons for cells irradiated with single doses. The clone cell populations (O, *mean of 3 samples ± SEM) have the same pattern of RBE against X-ray dose as the parental stock culture of cells* (*control,* ●).

It is clear from these data that the biphasic survival curve, manifested by an increase in RBE with increasing X-ray dose over the range 0.05-1 Gy, is a persistent feature of the radiation response in each of the cloned populations of cells. This indicates that the biphasic survival response is unlikely to be a consequence of a static subpopulation of intrinsically radiosensitive genetically distinct cells in the parental cell population because all the cells in the population cloned from the stock culture are genetically identical.

4.4.2 Two subpopulations with different radiosensitivities

If the biphasic survival curve was a consequence of two subpopulations of cells whose individual responses, when combined, produced the biphasic survival curve then the initial steep region (below 0.6 Gy) would be caused by the more radiosensitive of the two subpopulations. If this sensitive-subpopulation hypothesis were correct, then the progeny of cells irradiated previously with an X-ray dose of 1 Gy would not have a biphasic survival curve because the sensitive subpopulation of cells which accounted for the initial steep portion of the combined survival curve would have been killed by the 1 Gy treatment. Figure 4.5 shows the survival response of cells, expressed as RBE, which had been irradiated 24 hours previously with 1 Gy of 250 kVp X-rays. These data obtained from two separate experiments, both show the same pattern of an increasing RBE with an increase in X-ray dose as control cells which had not been irradiated previously. Therefore, the assumption that a static-sensitive subpopulation of cells exists in the stock culture of V79 cells, which results in the initial steep region of the survival curve is not consistent with these data. The cell cloning and progeny experiments support the hypothesis that the shape of the survival curve that is obtained when V79-379A cells are irradiated with single doses of X-rays over the range 0.04-1 Gy is unlikely to be a consequence of an intrinsically radiosensitive subpopulation of cells within the parental-stock cell population .

4.5 Mathematical description of the experimental data

4.5.1 Survival data

A basic linear-quadratic model can be used to describe mammalian cell survival curves over the X-ray dose range 2-20 Gy.

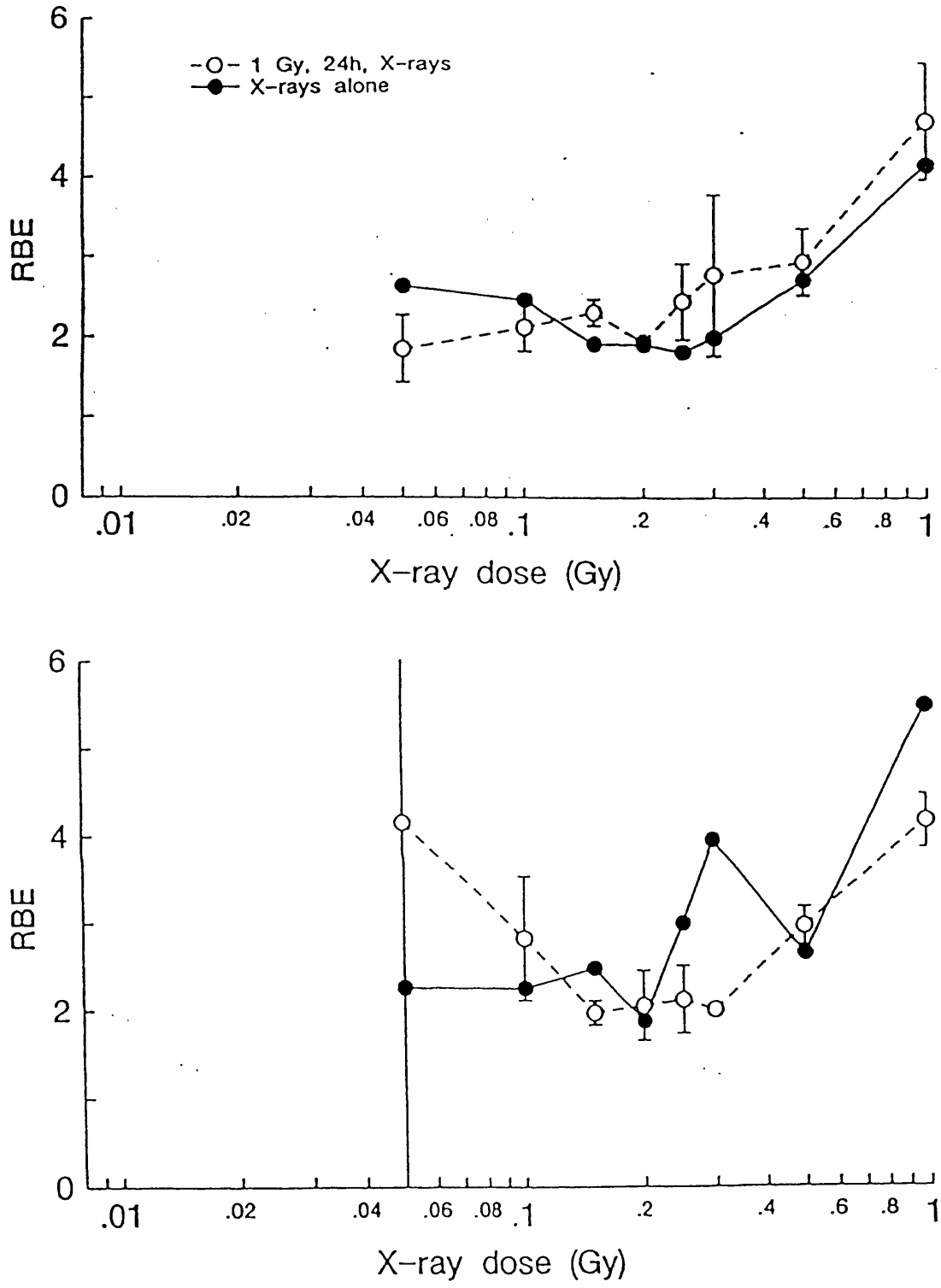

RBE between 250 kVp X-rays and d(4)-Be neutrons for cells irradiated with single doses. The same pattern of increasing RBE with increasing X-ray dose that is seen in the parental stock culture of cells (●) is also seen with two cell populations irradiated previously with 1 Gy of X-rays at a dose rate of 0.44 Gy min^{-1}, 24 hours prior to the single test X-ray doses (O, mean of 3 samples ± SEM). The two panels represent two experiments.

LQ model surviving fraction (SF) = $\exp(-\alpha D - \beta D^2)$ (4.1)

where α, β are constants

When cell survival was measured in this study following exposure to extremely small X-ray doses (0.01-1 Gy) using the DMIPS cell analyzer, a distinct deviation from a LQ model was seen below X-ray doses < 0.6 Gy (see Figs. 4.6 & 4.7). Fitting the LQ model to the typical experiment in Fig. 4.6 gives an α/β ratio of 5.82 (SF = $\exp(-0.15D - 0.02D^2)$). Applying this simple LQ model to all the experimental data for completeness results in a α/β ratio of ≈-935 (SF = $\exp(-0.24D + 2.52 \times 10^{-4}D^2)$). This clearly illustrates that a LQ model is inappropriate for describing these data. The fit of the LQ model is concave reflecting the negative β term.

	all experiment data			typical single experiment		
parameter	lower 95% conf. int.	value	upper 95% conf. int.	lower 95% conf. int.	value	upper 95% conf. int.
α	-0.25	-0.24	-0.23	-0.18	-0.15	-0.12
β	-0.003	2.52×10^{-4}	0.003	-0.03	-0.02	-0.01

Table 4.1: Results of a LQ fit to the experimental X-ray data.

The single experiment was described more accurately by an LQ model than all of the experimental data combined because of the variation in the values of surviving fraction at some dose levels and the disproportionate amount of data in the low dose range compared with the high dose range for the calculation of the β term. A more appropriate fit to the experimental data was achieved when the α term of the LQ model was allowed to decrease with increasing X-ray dose according to the modified LQ equation (Joiner and Johns, 1988) where α is defined as;

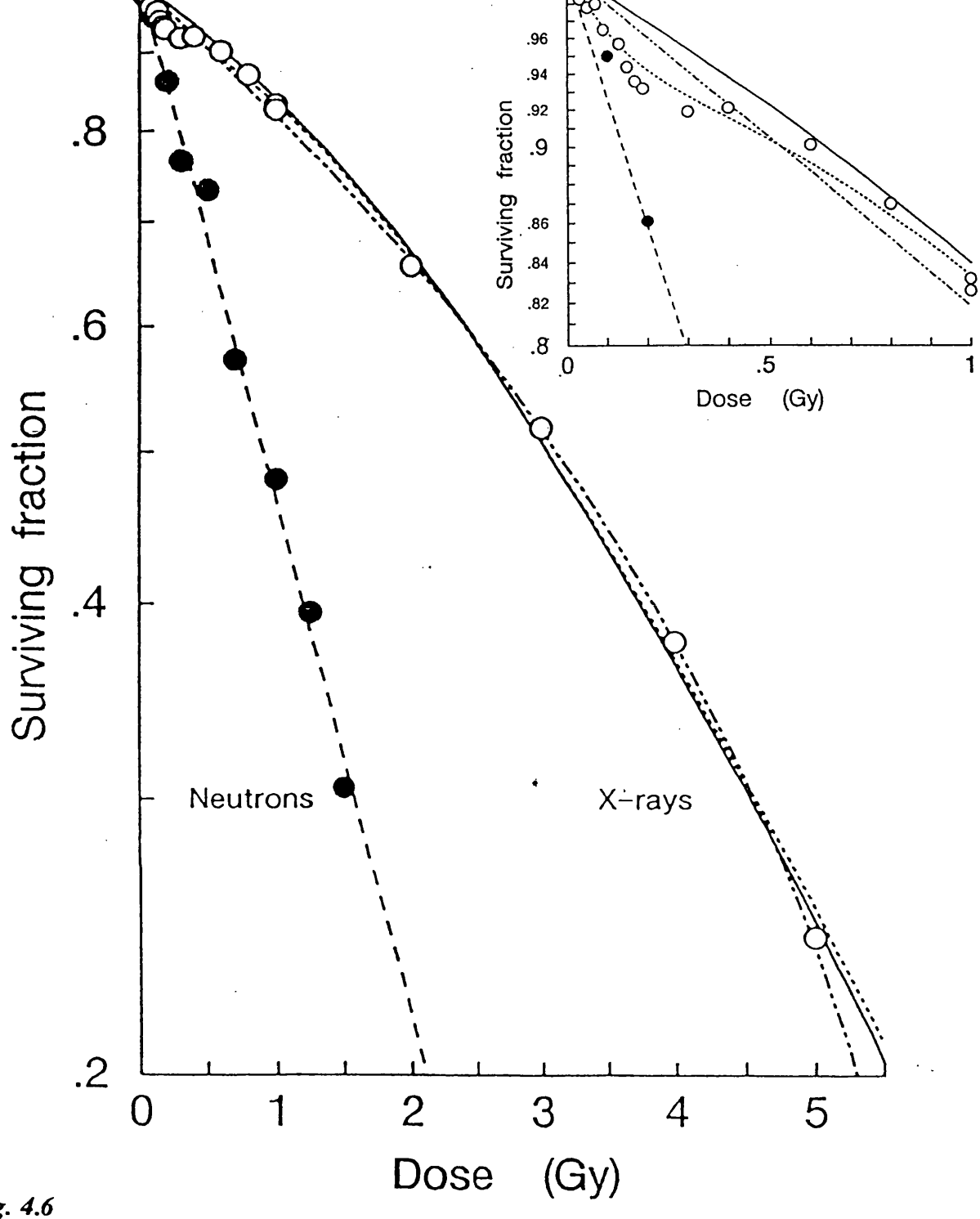

Fig. 4.6

Typical survival curves for V79-379A cells obtained in a single experiment following exposure to 250 kVp X-rays or d(4)-Be neutrons. The solid line represents the LQ fit to the X-ray data, which describes the high dose region with accuracy but over-estimates the radiosensitivity that was observed experimentally at low dose < 0.6 Gy. The dotted line represents the fit to the data using the modified LQ model (Eqn. 4.3), which describes the low dose response better than the simple LQ model (Eqn 4.1). The third fit (represented by the dot-dot-dashed line) is that of the two subpopulation model (Eqn 4.7).

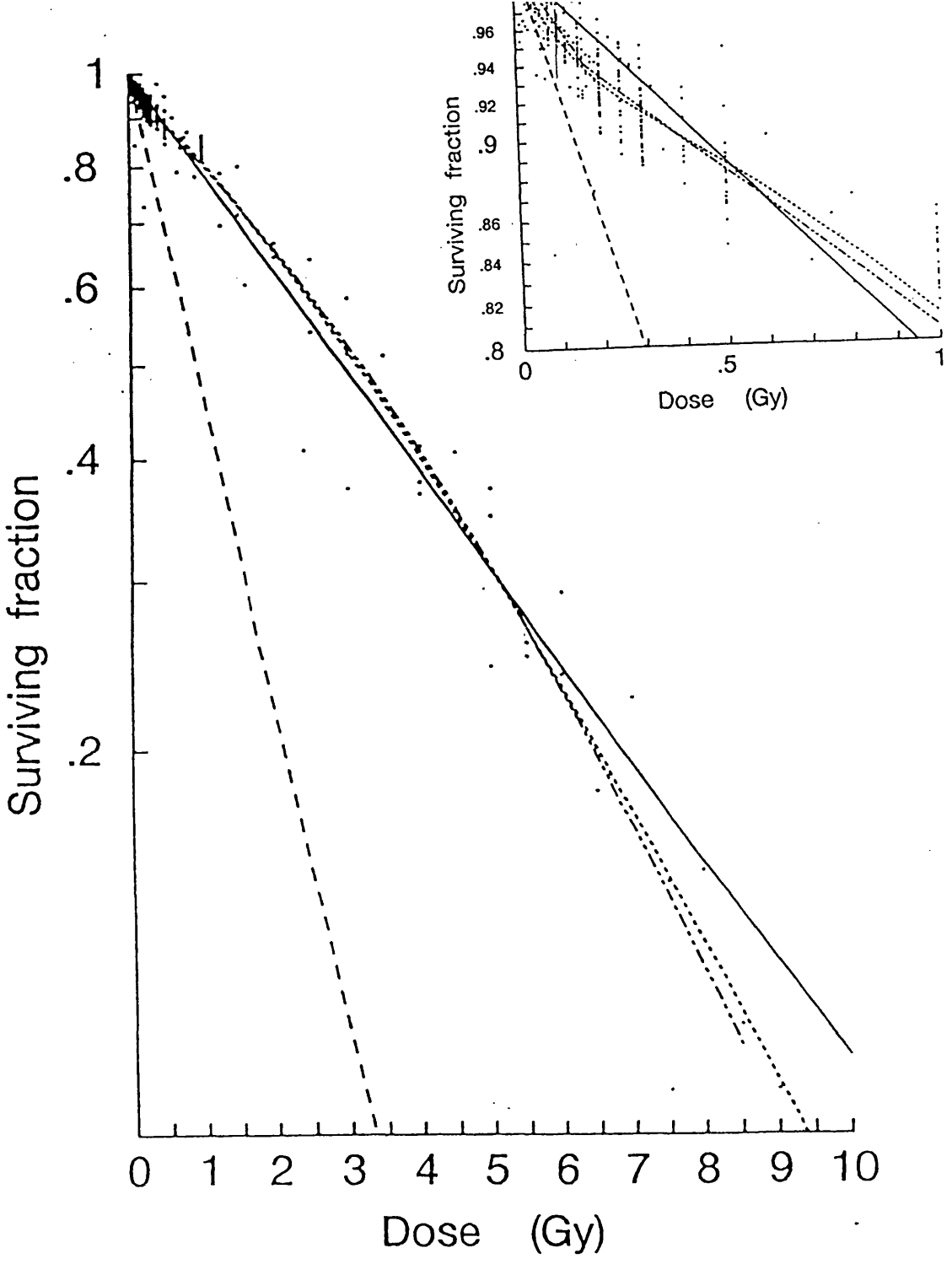

Fig. 4.7

All the experimental survival data for V79-379A cells exposed to single doses of X-rays (●, n = 403) and the fit to all the neutron data (dashed line). The solid line represents a LQ fit (Eqn. 4.1) to the X-ray data and the dotted line represents the fit obtained by the modified LQ model (Eqn. 4.3). The modified model gives a better fit at low and high doses. The linear quadratic fit is concave reflecting the negative value of β in this fit. The third fit is that of the two subpopulation model (Eqn. 4.7)(dot-dot-dashed line).

$$\alpha = \alpha_o(1 + g.\ \exp\ (-d/t)) \qquad (4.2)$$

where
- α_o - is the high dose α value
- g - is the factor by which the cells are more sensitive at very low X-ray doses compared with high X-ray doses
- t - critical dose for repair stimulation:

The α parameter in the modified LQ model was varied rather than the β term because the deviation from the LQ model was seen in the dose range where the αD response dominates over the βD^2 term in influencing the survival response.

The modified LQ model therefore becomes;

$$SF = \exp[(\alpha_o\ (1 + g.\exp(-d/t))D + \beta D^2)] \qquad (4.3)$$

The result of fitting this modified equation to all the experimental data and to a individual experiment can be seen in Figs. 4.6, 4.7 and Table 4.2.

	all experimental data			single experiment		
Parameter	Lower 95% con. int.	Value	Upper 95% con. int.	Lower 95% con. int.	Value	Upper 95% con. int.
g	1.57	2.07	2.56	0.87	2.16	3.44
t	0.15	0.21	0.27	0.06	0.23	0.39
α	-0.21	-0.20	-0.18	-0.18	-0.15	-0.12
β	-0.03	-0.02	-0.01	-0.03	-0.02	-0.01

Table 4.2 *Values of the parameters from the modified LQ model (Eqn. 4.3) fitted to the plot of surviving fraction versus X-ray dose for all the raw data (n = 403) and for a typical single experiment.*

The survival curve derived from the modified LQ model was biphasic and describes the experimental data better than the simple, two-parameter LQ model at the

lowest radiation doses (<0.6 Gy). In the single experiment, the fit of the modified LQ model describes the X-ray response below 0.6 Gy better than the LQ model. At higher doses above 1 Gy, both models produce reasonable fits to the data. The modified LQ model fitted to a typical experiment gives an α/β ratio of 6.51 Gy. Applying the modified LQ model to all the experimental data gives an α/β ratio of 25.07 Gy. Despite this high α/β value the experimental fit to the data is more accurate in both the low and high dose regions than was obtained by a simple LQ model. A more realistic α/β ratio might be obtained from all the experimental data in a single analysis if the procedural error which causes the inter-experimental variation was reduced. This can be achieved by fitting the modified LQ model to the RBE data rather than the SF data, as the X-ray response is compared with the neutron response in each experiment therefore slight changes in the cellular radiation response would presumably be similar for X-rays and neutrons and so would cancel in the RBE.

4.5.2 RBE data

The survival response following neutron irradiation was exponential and therefore it can be used as an internal biological standard in each experiment to which the X-ray response can be related as an RBE. Plotting the data as RBE instead of surviving fraction therefore allows a better comparison to be made between all the data from the many individual experiments without the diversity in X-ray radiosensitivity seen normally between individual experiments which arises from slight variations in the biology of the cell population and the efficiency of the recognition of cells by the DMIPS cell analyzer. The deviation from a LQ model below the X-ray dose of 0.6 Gy is more apparent in all the experimental data when the RBE values rather than surviving fraction are plotted against X-ray dose because the inter-experimental variation in X-ray radiosensitivity is reduced (Figs. 4.6 c.f. 4.5). A LQ model predicts a roughly constant RBE value over the dose range 0.01-1 Gy, however the experimental data clearly show *lower* RBE values at the lowest X-ray doses than predicted by a LQ model which reflects the increased X-ray sensitivity seen on the plots of surviving fraction.

The RBE value represents the ratio of the X-ray dose to the neutron dose at the same level of biological effect i.e.

$$RBE = \frac{X\text{-}ray\ dose\ (d_X)}{Neutron\ dose\ (d_N)} \qquad (4.4)$$

There are several ways of expressing the RBE equation. One method (Joiner and Johns, 1988) describes the RBE-X-ray dose relationship by incorporating Eqn. 4.3 into the RBE expression to allow for a decrease in α with increase in X-ray dose.

$$RBE = \frac{k + \sqrt{k^2 + 4\,k\,x\,(x/v + 1 + g.\exp(-x/t))/c}}{2(x/v + 1 + g.\exp(-x/t))} \qquad (4.5)$$

where c - α/β for neutrons
v - α/β for X-rays
k - α_N/α_X
x - X-ray dose
t - critical stimulation dose
g - extra-sensitivity factor

The fit of this model to the experimental data is shown in Fig. 4.8 and Table 4.3.

Parameter	Lower 95% Con. Int.	Value	Upper 95% Con. Int.
k	3.91	4.89	5.87
v	2.67	9.01	15.35
g	1.28	1.79	2.29
t	0.26	0.39	0.51

Table 4.3 *Values of the parameters from the RBE function given by Eqn. 4.5 fitted to the plot of RBE against X-ray dose for 405 individual measurements of surviving fraction.*

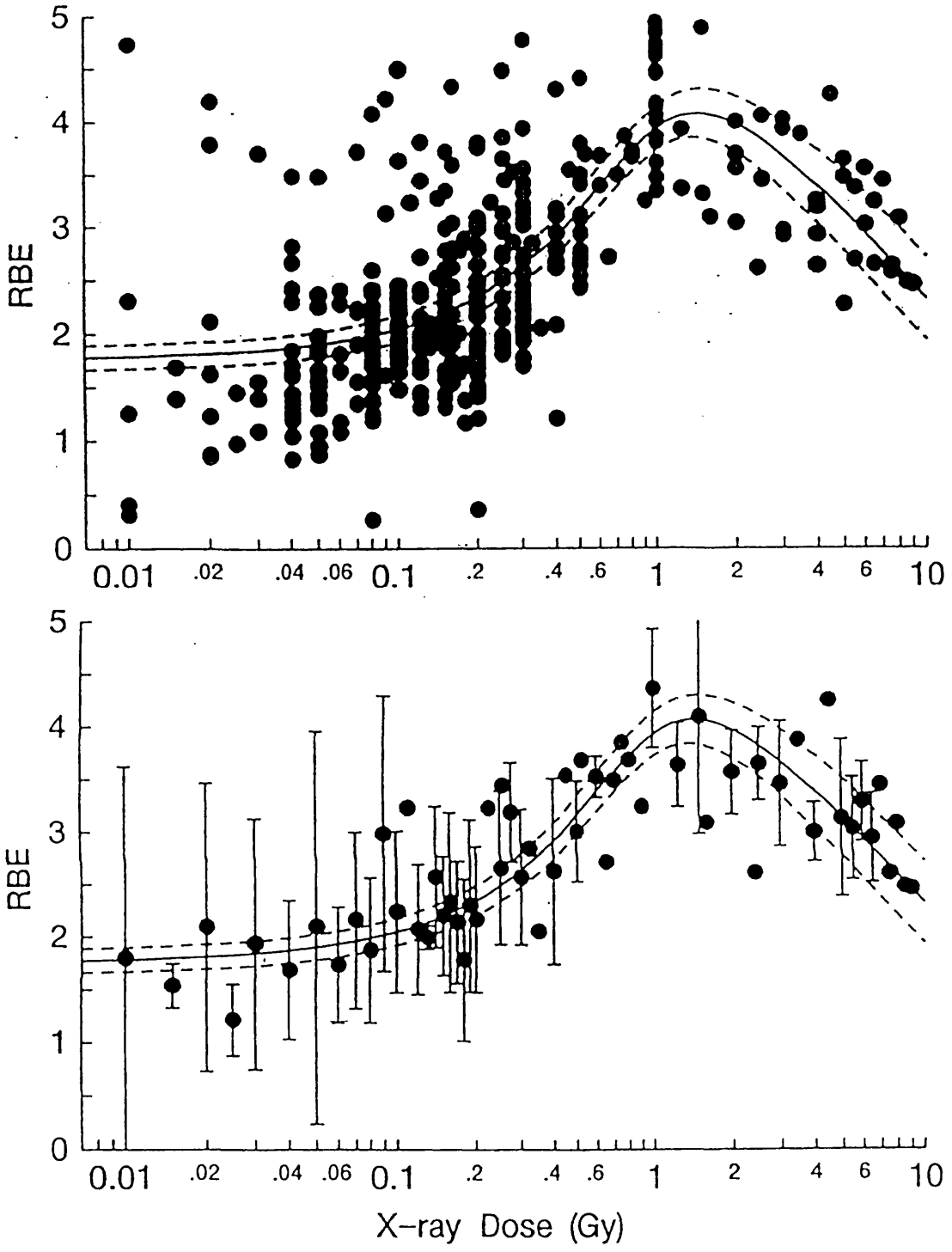

Fig. 4.8

RBE between 250 kVp and d(4)-Be neutrons delivered as single doses. The top panel shows the raw RBE data (403 data points from 56 experiments) and the lower panel the mean RBE (± SD). The solid line on both plots is the fit to the data from equation 4.5. The dashed lines represent the upper and lower 95% confidence intervals on that fit.

The α/β value obtained from this fit is 9.01. The critical dose at which the radiation response changes predominantly from the low dose values to the high dose values is approximately 0.39 Gy (upper 95% confidence interval (CI) = 0.26 Gy, lower 95% CI = 0.51 Gy). The difference in the radiation response at very low doses $<<$0.39 Gy and high doses $>>$0.39 Gy is a factor of 1.79 (upper 95% CI = 1.28, lower 95% CI = 2.29). These values of g and t are comparable with the values obtained when the modified LQ model was applied directly to the SF data (g = 2.07 (upper 95% CI = 1.57, lower 95% CI = 2.56), t = 0.21 Gy (upper 95% CI = 0.15 Gy, lower 95% CI = 0.27 Gy).

4.5.3 Interpretation of the modelling

The experimental data from the cloned-cell populations and from the survival after 1 Gy experiments are not consistent with the hypothesis that the biphasic survival curve is the consequence of a static-sensitive subpopulation of cells that dominate the radiation response at the very lowest X-ray doses, and that the change in radiation response occurs once this sensitive population of cells has been killed. However, it is worth exploring this argument further to see if a mathematical fit can be obtained for the experimental data assuming that the complete radiation response does consist of two distinct subpopulations of cells with one more radiosensitive to X-rays than the other. It is assumed that the two subpopulations have the same sensitivity to neutrons.

Assuming then that

$$SF_{\text{X-rays}} = b.SF_{\text{sensitive subpopulation}} + (1-b).SF_{\text{resistant subpopulation}} \qquad (4.6)$$

where b - proportion of sensitive cells (1-b) - proportion of resistant cells

The linear quadratic model can be expanded to include terms for each subpopulation of cells, and becomes

$$SF = b.\exp -(\alpha_s D + \beta_s D^2) + (1-b).\exp -(\alpha_r D + \beta_r D^2) \qquad (4.7)$$

where α_s - alpha for sensitive population β_s - beta for sensitive population
α_r - alpha for resistant population β_r - beta for resistant population

The result of applying this model to the SF data can be seen in Table 4.4

Parameter	Lower 95% conf. int.	Value	Upper 95% conf. int.
α_s	6.48	15.01	23.53
α_r	0.15	0.17	0.18
β_s	-2.59	-1.65	-0.70
β_r	0.01	0.01	0.02
b	0.027	0.036	0.045

Table 4.4 *Values of the parameters obtained when an expanded LQ model containing functions for two subpopulations of cells with different radiosensitivities was fitted to all the experiment data*

The result of applying this model to the data suggests that if the two subpopulation concept were correct then the sensitive subpopulation would comprise ≈3.6% of the cells and would be nearly 90 times (α_s/α_r) as sensitive to low dose radiation than the radioresistant subpopulation. The α/β ratio of the sensitive population of cells is -9.11 Gy and 14.15 Gy for the resistant subpopulation. The β_s value is negative which produces the concave shape to the survival curve at low doses whereas a positive value of β_r gives a convex shape to the survival curve at higher doses. If this two population concept is extended into an expression for RBE then the RBE-X-ray dose relationship can also be explored mathematically to determine if the fit that was obtained to the data achieved using equation 4.5 can be reproduced applying the concept that assumes the complete X-ray survival curve is composed of the responses from two populations of cells with different radiosensitivities.

Consider the following relationships;

$$SF_{\text{neutrons}} = \exp -(\alpha_N D_N) \tag{4.8}$$

$$SF_{\text{x-rays}} = b.\exp -(\alpha_s D + \beta_s D^2) + (1-b).\exp -(\alpha_r D + \beta_r D^2) \tag{4.9}$$

where α_s - alpha for sensitive population
α_r - alpha for resistant population

b - proportion of sensitive cells
β_s - beta for sensitive population
β_r - beta for resistant population
(1-b) - proportion of resistant cells
α_N - alpha for neutrons
D_N - neutron dose
D - X-ray dose

At the same level of biological effect, $SF_{neutrons} = SF_{X\text{-}rays}$, therefore

$$\exp -(\alpha_N D_N) = b.\exp -(\alpha_s D + \beta_s D^2) + (1-b).\exp -(\alpha_r D + \beta_r D^2) \quad (4.10)$$

re-arranging Equation 4.10

$$-\alpha_N D_N = \log [b.\exp -(\alpha_s D + \beta_s D^2) + (1-b).\exp -(\alpha_r D + \beta_r D^2)] \quad (4.11)$$

re-arranging equation 4.11 in terms of D_N,

$$D_N = \frac{\log[b.\exp-(\alpha_s D + \beta_s D^2) + (1-b).\exp-(\alpha_r D + \beta_r D^2)]}{-\alpha_N} \quad (4.13)$$

substituting in (D_X/RBE) from equation 4.4 in place of D_N, equation 4.13 becomes;

$$\frac{D_X}{RBE} = \log\frac{[b.\exp-(\alpha_s D + \beta_s D^2) + (1-b).\exp(-\alpha_r D + \beta_r D^2)]}{-\alpha_N} \quad (4.14)$$

re-arranging Eqn. 4.14 in terms of RBE

$$RBE = \frac{-\alpha_N . D_X}{\log[b.\exp-(\alpha_s D + \beta_s D^2) + (1-b).\exp-(\alpha_r D + \beta_r D^2)]} \quad (4.16)$$

An aim of the modelling exercise was to explore the function of neutron RBE plotted against X-ray dose to determine the value of each parameter in the two subpopulation model which would describe accurately the experimental data. As the increased X-ray sensitivity was seen in the low-dose region of the survival curve described by the α parameter in the LQ model it was decided to alter the α_s and α_r parameters and keep the β_s and β_r parameters constant and numerically equal for the purpose of this

exercise. This simplified the modelling exercise and is justified because the β_s and β_r terms only influence the survival of cells, and therefore RBE, at higher X-ray doses ($\approx$ 2 Gy and above) (see Fig. 4.9) and the aim of this exercise is to reproduce the low dose response. The effect of changing the numerical values of β_s and β_r on the terminal region of the RBE fit can be seen in Fig. 4.9. Changing the β_s and β_r parameter had little effect on the initial region of the RBE function.

Setting both the β values to 0.02 provides a reasonable comparison between the terminal slopes of the mathematically modelled fit and the actual fit (Fig. 4.8) to the experimental data achieved using equation 4.5. The influence of the α_r term on the model can be seen in Fig. 4.10, with all the other terms in the equation fixed reducing the value of α_r decreases the rise in RBE over the range 0.1-1 Gy. Increasing the α_r parameter increases the value of $(\alpha/\beta)_r$. A higher α_r value also results in a reduced sensitivity factor between the sensitive and resistant subpopulations which reduces the intercept value on the RBE axis. The effect of changing α_s can be seen in Fig. 4.11. This term has little effect on the terminal slope of the RBE plot because the parameter dominates the survival response of low X-ray doses. The slope of the initial region of the RBE plot is significantly altered by a change in the α_s parameter: reducing the α_s value reduces the steepness of the slope and effects the starting point of the curve of the RBE axis. From this modelling exercise it can be seen that the effect of the β term on the shape of the survival curve, and therefore RBE curve occurs above $\approx$2 Gy and that changing the α term influences the shape of the response below 2 Gy. The proportion of sensitive cells in the population has a large influence on the overall shape of the survival curve. Fig. 4.12 illustrates the effect of increasing the α_s value which increases the α/β ratio of the sensitive population of cells. As the value α_s increases towards 5 the modelled curves begin to resemble the fit to the experimental data. The α_s and $(\alpha/\beta)_s$ parameters effect the initial rise in the RBE value over the dose range 0.1-1 Gy. Reducing the proportion of sensitive cells in the population, assuming they are $\approx$50 times more sensitive to ionising radiation the resistant cells, to 6% produces a curve which is very similar to the experimental fit (Fig. 4.13). Applying this model (Eqn. 4.16) to the actual experimental data (Fig. 4.14) supports the conclusions of the modelling exercise that if the low-dose X-ray hypersensitivity

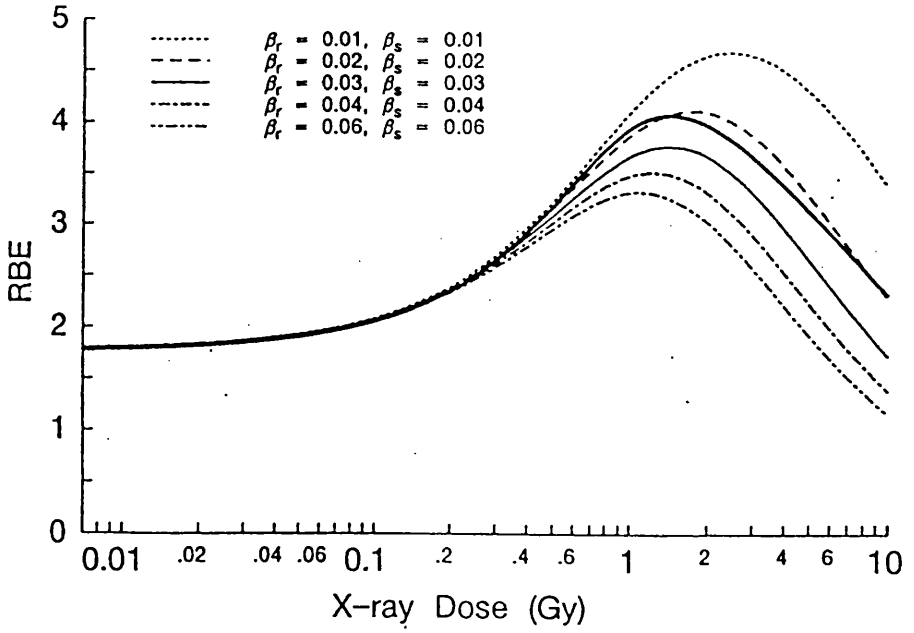

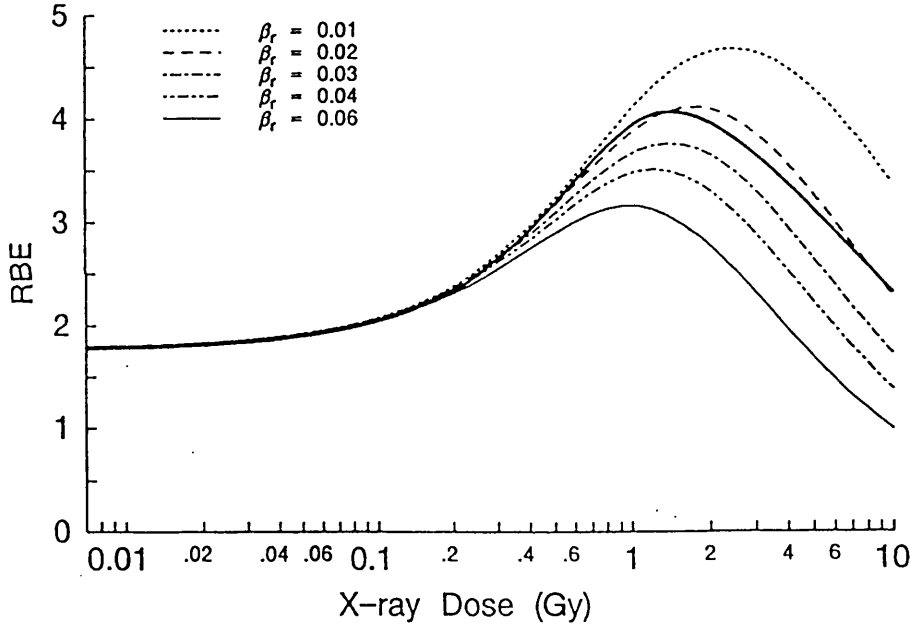

The effect of increasing β_r in the two subpopulation model. Increasing this parameter reduces the $(\alpha/\beta)_r$ and therefore decreases the RBE value as the X-ray dose increases. Modifying β_r had little effect on the initial low-dose region of the RBE against dose relationship. Changing both β_r and β_s simultaneously had a similar effect, altering only the terminal region of the RBE against dose relationship. The heavy solid line in each panel is the fit of Eqn. 4.5,
Upper panel: parameters in Eqn. 4.16, $b = 0.06$, $\alpha_s = 5$, $\alpha_r = 0.1$.
Lower panel: parameters in Eqn. 4.16, $b = 0.06$, $\alpha_s = 5$, $\alpha_r = 0.1$, $\beta_s = 0.02$.

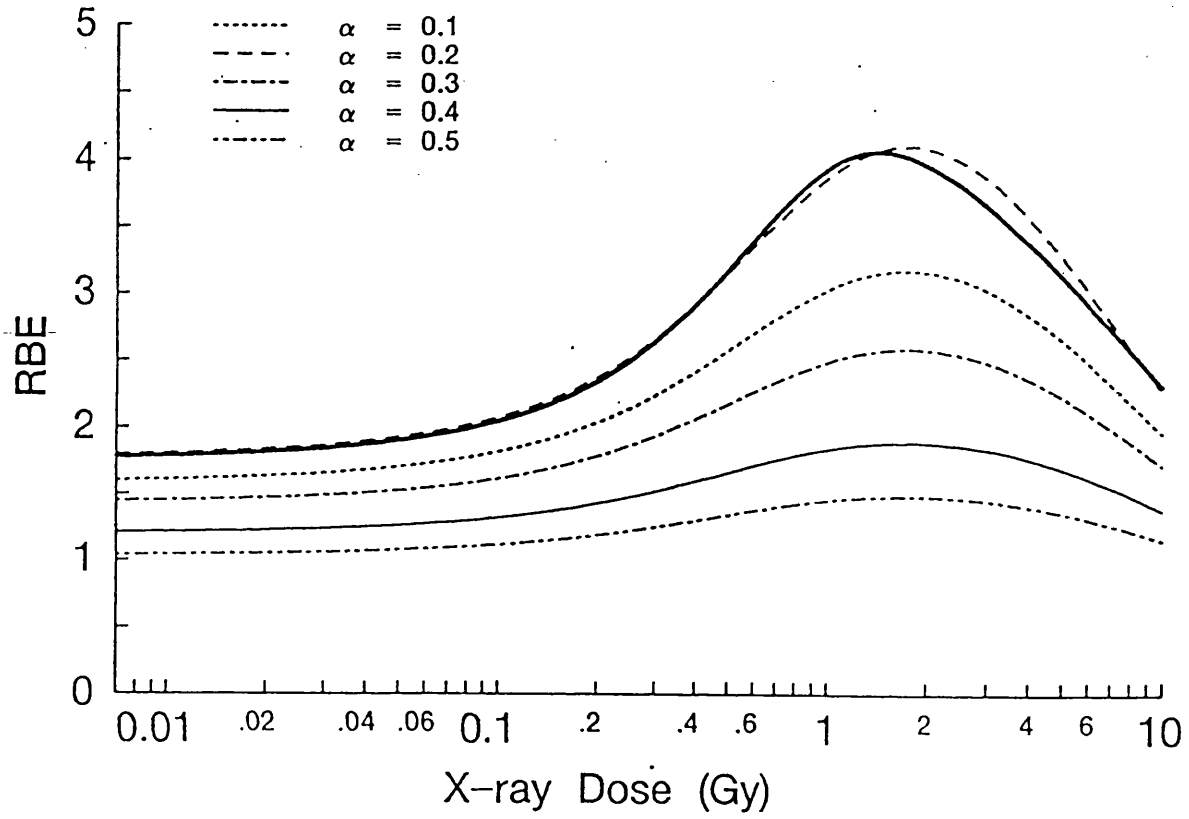

Fig. 4.10

The effect of increasing α_r in the two subpopulation model. This parameter alters the whole shape of the RBE function. Increasing the value of α_r decreases the $(\alpha/\beta)_r$ which affects the terminal slope and also changes the relationship between α_s/α_r: the low-dose sensitivity-difference between the two subpopulations. This affects the rate of increase of RBE with increasing X-ray dose and the value of the low-dose RBE. The heavy solid line is the fit of Eqn. 4.5. Parameters in Eqn. 4.16, $b = 0.06$, $\alpha_s = 5$, $\beta_r = 0.02$, $\beta_s = 0.02$.

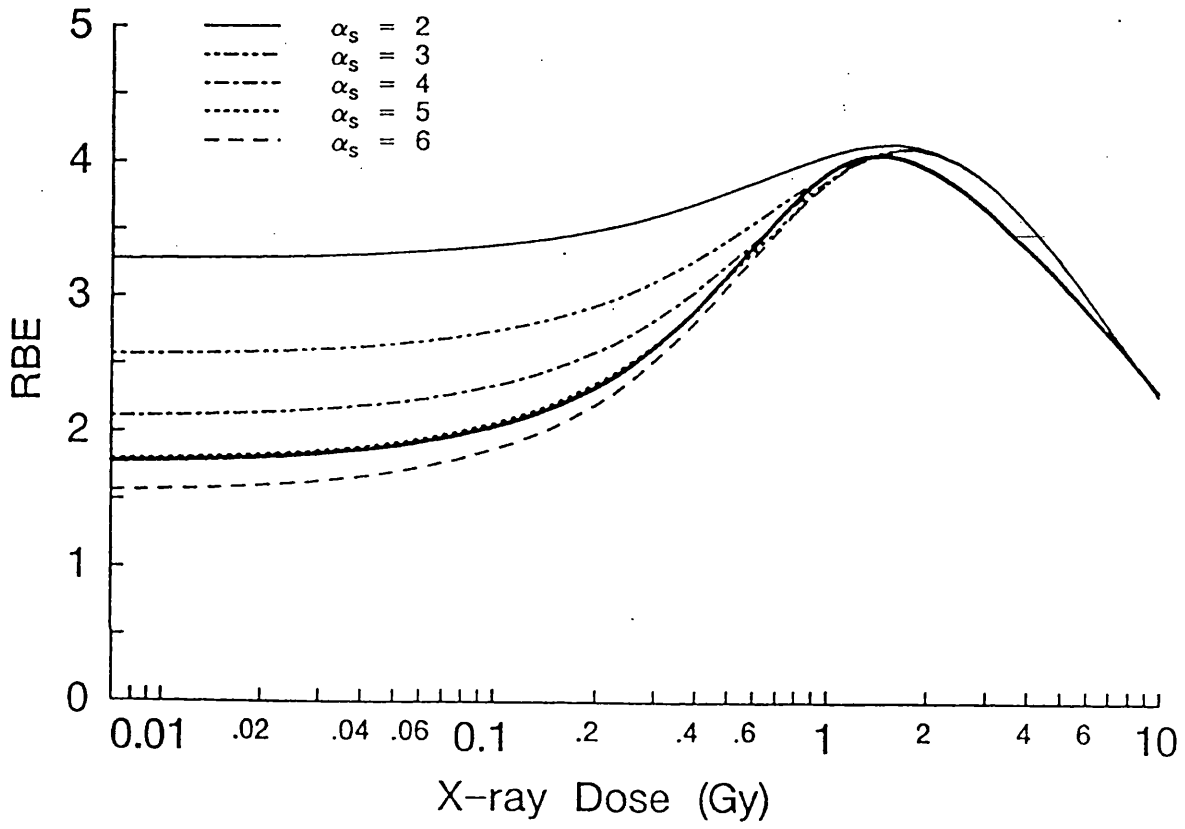

Fig. 4.11

The effect of increasing α_s in the two subpopulation model. Increasing this parameter reduces the $(\alpha/\beta)_s$ and therefore increases the X-ray sensitivity at low doses. This gives a lower starting value of RBE and therefore a large increase in RBE with increasing X-ray dose.

The heavy solid line is the fit of Eqn. 4.5. Parameters in Eqn. 4.16, b = 0.06, α_r = 0.1, β_r = 0.02, β_s = 0.02.

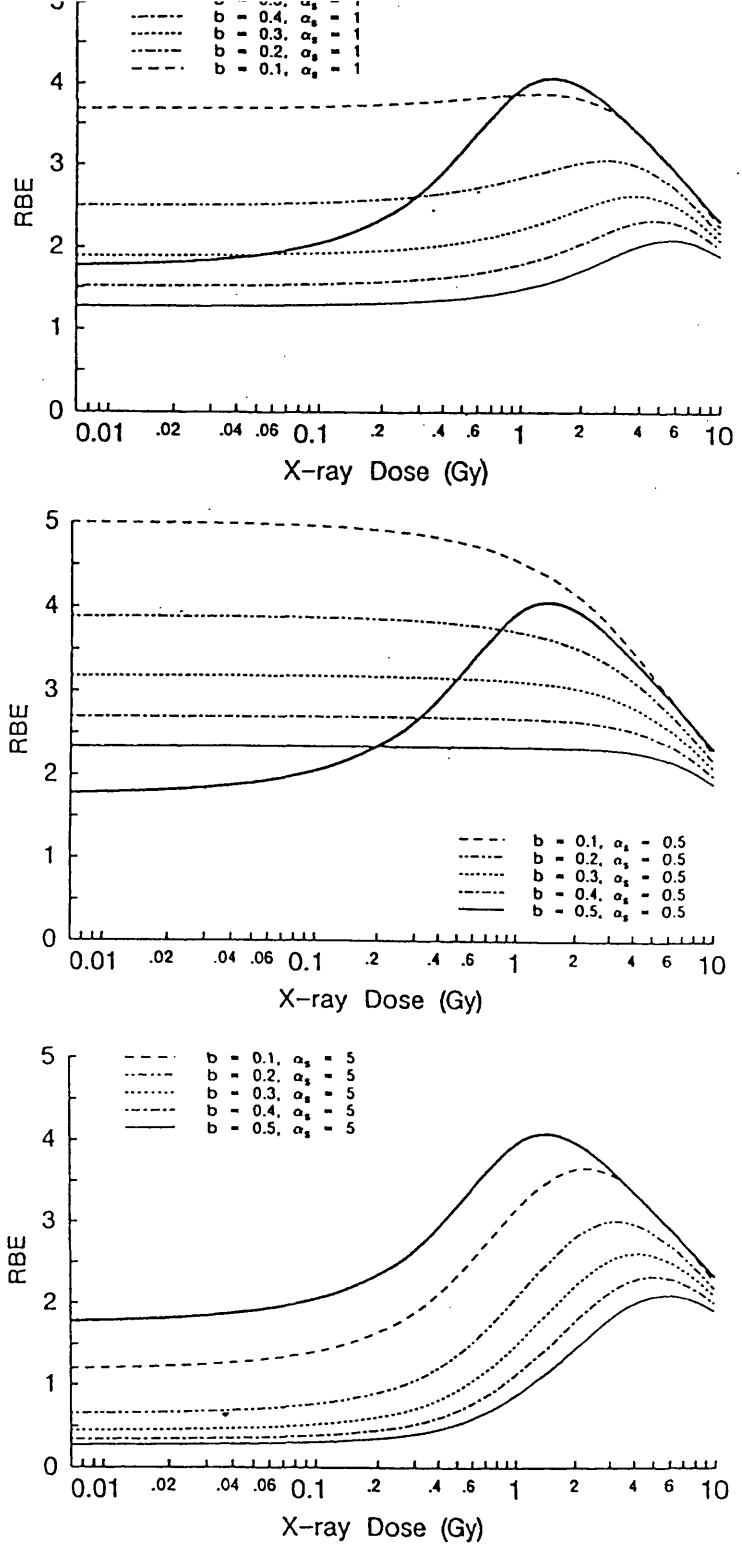

Fig. 4.12

The effect of increasing the proportion of the sensitive subpopulation of cells from 10%, 20%, 30%, 40% to 50% of the total cell population with increasing values of α_s. *Increasing b affects the proportion of sensitive to resistant cells while increasing* α_s *affects the sensitivity of the sensitive subpopulation of cells.*

All panels, heavy solid line is the fit of Eqn. 4.5 and the parameters in Eqn. 4.16 are $\alpha_r = 0.1$, $\beta_r = 0.02$, $\beta_s = 0.02$.

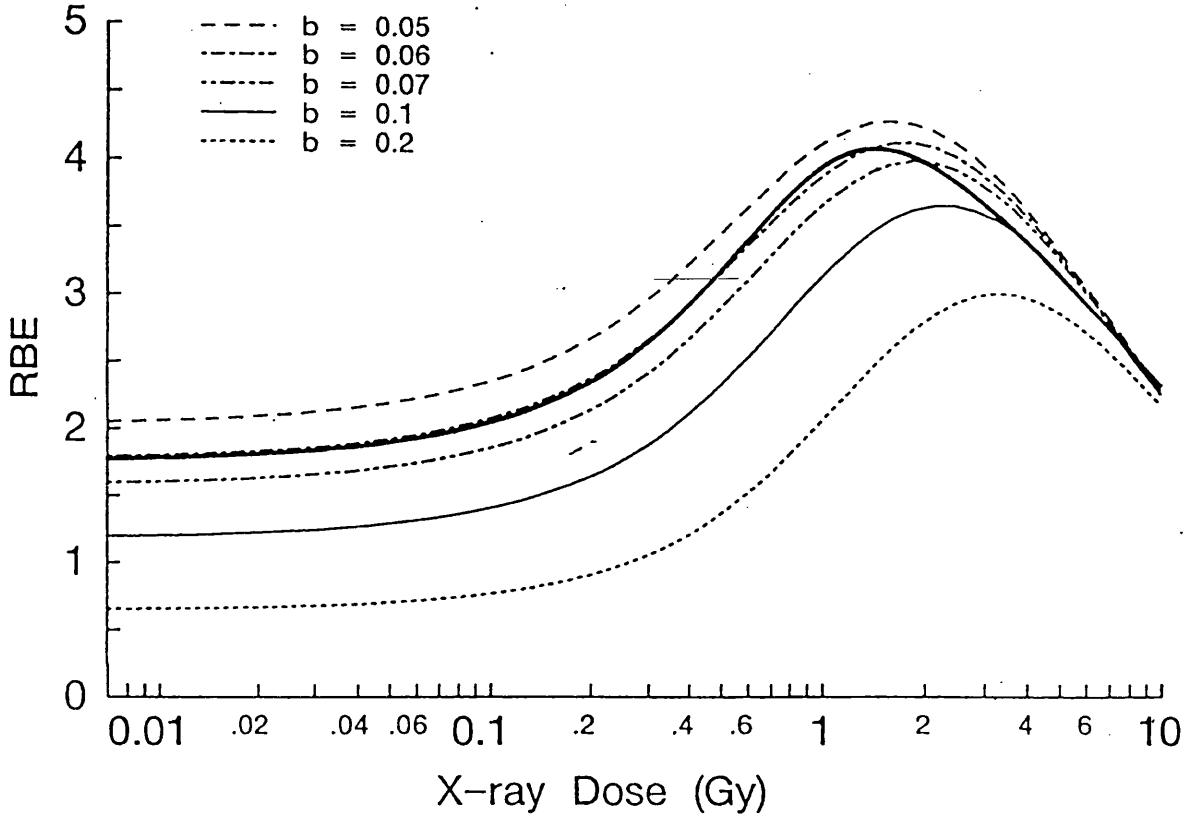

Fig. 4.13

The results of manipulating the parameters in the two subpopulation model. The fit to the experimental data using Eqn. 4.5 can be reproduced in a two subpopulation concept if the sensitive subpopulation is ≈50× more sensitive to X-rays than the resistant subpopulation and makes up ≈6% of the total population, assuming similar sensitivities to neutrons.

The heavy solid line is the fit of Eqn. 4.5 and the parameters in Eqn. 4.16 are α_r = *0.1,* α_s = *5,* β_r = *0.02,* β_s = *0.02.*

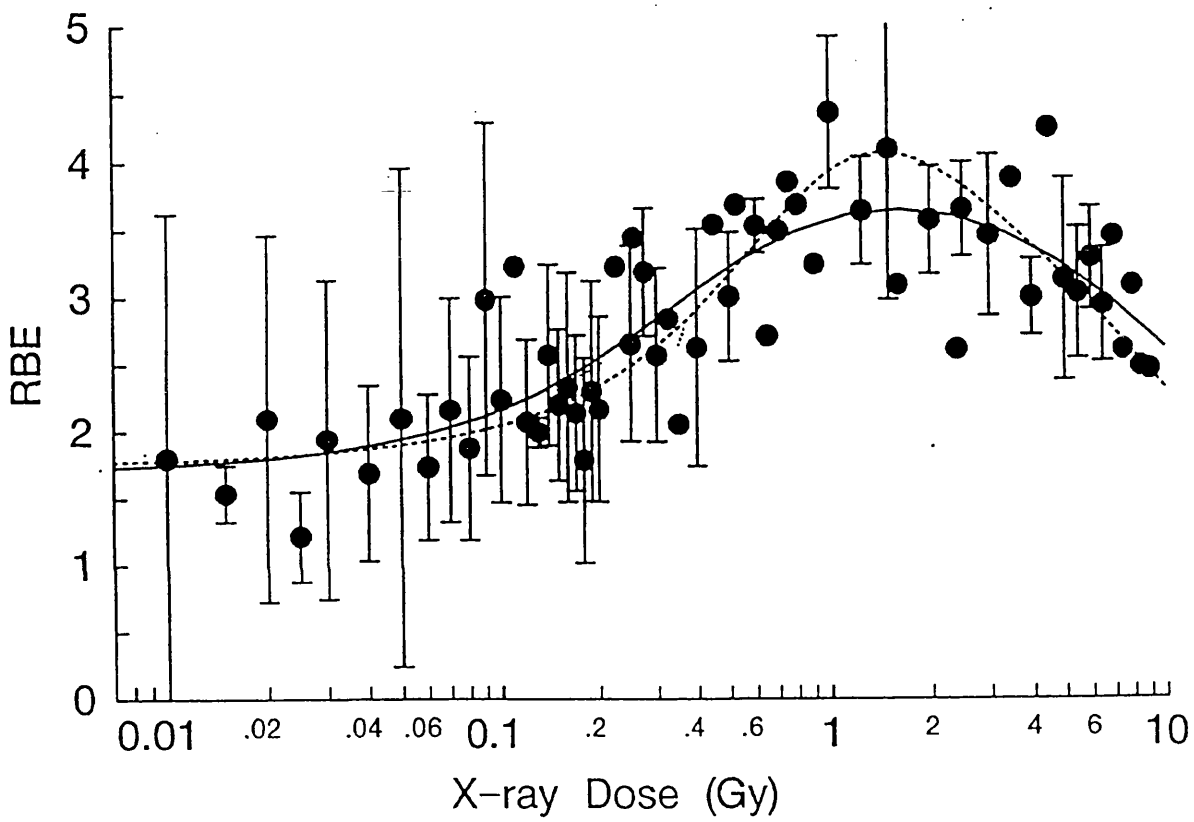

Fig. 4.14
The fit obtained when Eqn. 4.16 was applied to the RBE data (solid line). The two subpopulation model predicts values of $(\alpha/\beta)_s = 10.54$, $(\alpha/\beta)_r = 14.77$, $(\alpha_s/\alpha_r) = 58$ *and* $b = 2.9$. *The fit to the data using this model is not as good as that obtained using the modified LQ model (Eqn. 4.5) (dashed line).*

was due to the presence of a static subpopulation of intrinsically radiosensitive cells then this population would have to be 2.9% (Table 4.5) of the total population with a sensitivity of 58 times that of the balance of the population and this seems unlikely. These values are very similar to those obtained when the two subpopulation (Eqn. 4.7) was applied to all the experimental SF data (Table 4.5).

Parameter	Eqn. 4.7 on SF data	Eqn. 4.14 on RBE data
b	3.6	2.9
α_s/α_r	90	58

Table 4.5 *Values of two of the parameters (b = % of sensitive cells of the total population, α_s/α_r = difference in sensitivity between the sensitive and resistant populations) obtained when the two subpopulation model was applied to all the X-ray SF data using Eqn. 4.7 and applied to all of the X-ray data expressed as RBE Eqn. 4.14.*

The results of the modelling exercise suggest that the data can only be explained in terms of two subpopulations of cells if the sensitive subpopulation is small and very sensitive. This seems unlikely. Applying a two subpopulation model (Eqn. 4.7) to the *surviving fraction* data suggested that the sensitive population consists of 3.6% of the total cell population and these cells were 90× more radiosensitive than the resistance cells. Applying the two subpopulation concept (Eqn. 4.14) to the *RBE* data suggested a 2.9% sensitive subpopulation which was 58× more radiosensitive than the resistant subpopulation.

4.6 Summary

1. The same pattern of RBE against X-ray dose that was seen in the parental stock culture was also observed in two cell clones derived from the stock culture. This indicates that the biphasic survival curve of the parental population is unlikely to be due to a heterogenous cell populations of different radiosensitivities.

2. The same pattern of RBE against X-ray dose that was obtained from cells from the parental stock culture was also observed in two cell populations that were derived from a sample of the stock cell culture irradiated previously with 1 Gy of 250 kVp X-rays. This indicates that the biphasic survival response of the stock cell culture was unlikely to represent the combined response of two subpopulations of cells with different radiosensitivities.

3. Mathematical Modelling of the survival data suggests that the postulate of two subpopulations of cells of differing radiosensitivities, owing to, for example a subset of 'static' intrinsically radiosensitive cells, cannot explain the change in X-ray effectiveness over the dose range 0.1-1 Gy unless the sensitivities of the two populations differ by a factor of ≈50, which seems unlikely.

4. The RBE data are better described by the modified LQ model (Eqn. 4.5) than a model (Eqn. 4.16) which assumes the response consists of two subpopulations of cells (Fig. 4.14).

4.7 Discussion

This study demonstrates that the V79-379A cell line exhibits a multiphasic survival curve. In other studies multiphasic survival curves have been shown to be due to cells in different phases of the cell cycle (Beam *et al.*, 1954; Horsley *et al.*, 1967). Asynchronous-exponentially growing V79-379A cells were used in the majority of the investigations reported in this thesis. Such a population contains cells from all the phases of the cell cycle and each phase exhibits a different radiosensitivity (Sinclair, 1968) which might explain the data in this study. However, the dependence of cell-cycle phase on the effect of low-dose X-ray hypersensitivity is not considered in this chapter but instead, is addressed and documented separately in a different chapter of this thesis (see chapter 5).

The aim of this investigation was to determine if the shape of the V79-379A survival curve is a consequence of a small, intrinsically radiosensitive subpopulation of cells within the stock cell culture. A biphasic survival curve similar in shape to that of the parental cell population was observed when cell survival was measured for two separate cell populations cloned from the stock culture of parental cells (see section 4.4.1). The same survival response was also obtained from a cell population previously irradiated with 1 Gy of X-rays (see section 4.4.1). If the overall response of the parental cell population was due to two cell populations of different intrinsic radiosensitivities then a cell population cloned from the parental stock culture might either exhibit an extremely radiosensitive response over the dose range 0.04-1 Gy *without* the increase in radioresistance over the dose range 0.2-0.6 Gy or alternatively a completely radioresistant response *without* the hypersensitivity to X-rays doses below 0.6 Gy that is seen routinely in the parental population. As both cloned-cell populations exhibited the low-dose X-ray hypersensitivity followed by a subsequent increase in radioresistance over the dose range 0.2-0.6 Gy then each cell in the parental stock population has the same intrinsic radiation response which indicates that the biphasic survival curve that was obtained routinely for the stock-parental cell culture was unlikely to be due to the existence of two subpopulations of cells in the stock cell culture.

This phenomenon of hypersensitivity to low doses of X-rays followed by an increase in radioresistance with increasing X-ray dose is not a manifestation of the phenomenon of SLDR (Elkind and Sutton, 1959) or PLDR (Phillips and Tolmach, 1966) because it was seen following single doses of radiation (SLDR is a split-dose phenomenon) and did not require that the cells be held at a suboptimal growth condition for the increase in radioresistance to occur (a requirement of PLDR). This suggests that this phenomenon is the result of the action of a novel repair function. These data could be explained by an inducible repair system that is inactive at low doses and does not function in unirradiated or low-dose (<0.2 Gy) irradiated cells but is triggered or induced as the dose increases (>0.2 Gy) presumably by increasing levels of damage. The phenomenon may parallel similar effects which have been reported in other cell lines, in which unexpected levels of radioresistance have also been attributed to inducible repair systems (Koval, 1984; Calkins, 1967).

This V79 study however clearly shows a 'breakdown' of an LQ model at very low X-ray doses (<0.6 Gy) with an increased X-ray sensitivity than would be expected by extrapolation from higher X-ray doses using a linear quadratic (LQ) model. The experimental data points are persistently below the LQ prediction at X-ray doses of <0.6 Gy. Fitting a LQ model to a typical single experiment in this study (Fig. 3.3) produced an α/β value of 5.82 Gy (α = 0.15 Gy^{-1}, β = 0.03 Gy^{-2}) this compared with an α/β of ≈-935 Gy (α = 0.24 Gy^{-1}, $\beta = -2.52 \times 10^{-4}$ Gy^{-2}) for the same model applied to the pooled experimental data. This extremely high α/β ratio of the pooled data reflects the low negative value of the β term obtained in the fit. This was not unexpected because the vast majority of the experiment data were below the LQ fit (<1 Gy) making an estimate of the β term difficult. A more appropriate fit to the experimental data was obtained using a modified LQ model (Joiner and Johns, 1988). The model is formulated to allow a decrease in α with increasing X-ray dose. A similar value of α/β was obtained when the modified LQ model was fitted to the data of a single experiment (α/β = 6.51 Gy; α = 0.15 Gy^{-1}, β = 0.02 Gy^{-2}) compared with that obtained when the conventional LQ model was fitted to the same data. However, the α/β value estimated from all of the pooled experimental data using the modified LQ model was much lower and more realistic (α/β = 25.07 Gy; α = 0.20 Gy^{-1}, β = 0.01 Gy^{-2}) compared with the value that was obtained when the conventional LQ

model was applied to the data. A more realistic and probably more accurate estimate of the α/β ratio was obtained from the RBE data. This fit reduces the daily variation in X-ray radiation response between individual experiments by comparing the X-ray survival data with a neutron survival curve obtained during the same experiment. This derived approach reduced the variation in the assessment of cell survival that was seen between the individual experiments in the measurement of surviving fraction (Table 4.4 c.f. Table 4.1). Fitting Eqn. 4.5 to the RBE data produced an α/β value of 9.01 Gy (Table 4.1). This compares with α/β values for this cell line of between 8 and 10 derived by Watts *et al.* (1986) over a much larger range of doses from 0.25 Gy to 33 Gy.

Other studies have attributed biphasic survival curves to the presence of subpopulations of cells of different radiosensitivities (see section 4.1). The experimental data obtained in this study suggested that the biphasic nature of the survival curve for V79-379A cells is unlikely to be due to two subpopulations of cells. However, the experimental data were modelled assuming a two component radiation response in order to explore further this possibility. This exercise followed two approaches, firstly the experimental data were modelled assuming that the cell population comprised of a fraction of sensitive cells (b) and a fraction of resistant cells (1-b) (see equation 4.7). Application of this model to the surviving fraction data indicated that the sensitive subpopulation comprised 3.6% of the cells and that this component was nearly 90 times as sensitive as the resistant component. Applying the same model to the RBE data indicated that the sensitive subpopulation comprised 2.9% of the cells and was 58 times more sensitive than the resistant component. A homogeneous cell population which consists of cells differing in radiosensitivity by this degree has not been reported in the literature previously. The difference in the radiation response of cells of different cell cycle phase at this level of dose for example is maximally only by a factor of 10 (Sinclair, 1968).

The other approach in this modelling exercise was to manipulate the parameters in the two subpopulation model (equation 4.7) to reproduce the fit to the data that was obtained using the RBE equation 4.5, thereby, investigating the effect of each parameter in the model on the mathematical fit. This illustrated that changing

the α_r and β_r parameters in the model has little influence on the rise in RBE at the lowest doses. Only by reducing the fraction of sensitive cells and increasing differential in the sensitivity of α_s and α_r could the fit achieved using equation 4.5 be reproduced. This exercise supported the hypothesis of the linear survival response at low doses and a more curved survival response at much higher doses.

The different mathematical approaches to describe the experimental data present a dilemma of selecting the α/β value which should be used to describe the survival response of V79-379A cells. Should the low dose region be incorporated into the fit of the radiation response and the data fitted with the modified LQ or should the mathematical fit ignore the very low dose data and apply the LQ model to only the high dose data? This question is difficult to answer simply with the data available in this study because the vast majority of the data represent the X-ray response below 1 Gy, and any mathematical fit will disproportionally weight this area of the survival response. To select only one model would require significantly more data in the higher dose region and down to 2 or 3 decades of cell kill. The fit obtained using equation 4.5 probably represents the most appropriate fit to these data at this time, as each experimental X-ray point has been compared to a neutron standard thereby eliminating the daily variation in radiosensitivity and thereby giving a better value for the actual radiation response. The 95% confidence intervals on this fit are reasonable suggesting the fit of the model is an accurate representation of the data. This fit also includes both the low dose and high dose response and therefore this is the recommended way of mathematically describing these data.

Chapter 5: A phenomenon of the cell cycle?

5.1 Introduction

The growth of cells in culture can be divided into three stages: a 'lag' period of minimum growth as the newly seeded cells adapt to their new environment, a growth phase during which the cell number increases rapidly and usually exponentially, and a plateau or stationary phase during which the cell number remains constant owing to growth inhibition caused by nutrient depletion or density inhibition. A population of cells growing exponentially is distributed asynchronously throughout a cycle composed of four phases (Howard and Pelc, 1953):

- M: mitotic stage
- G_1: the first gap - the period before DNA synthesis starts
- S : the period of DNA synthesis
- G_2: the second gap - the period after the DNA synthesis has finished but before mitosis begins.

In the G_2 phase following DNA synthesis, the cell contains twice the DNA complement (4C) of the G_1 phase cell (2C). After mitosis the two daughter cells enter the G_1 phase and have a DNA content equivalent to that of the G_1 phase parent cell (2C).

The duration of the cell cycle is cell-line dependent. Variation in the length of the cell cycle time between mammalian cell lines is usually due to differences in the length of the G_1 phase. The G_2 and S phases of the cell cycle are generally similar in duration, and the length of mitosis lasts approximately 1 hour in the majority of mammalian cell lines. The cell cycle times of two commonly used cell lines, V79 Chinese hamster cells and HeLa human tumour cells, are shown in Table 5.1.

Cell cycle phase	V79	HeLa
Mitosis	1	1
G_1	1	11
S	6	8
G_2	3	4
Total time	11	24

Table 5.1 *The typical duration (in hours) of each phase of the cell cycle for V79 and HeLa cells.*

5.2 Measurement of the duration of the cell cycle

Autoradiography was used originally to determine the duration of the cell cycle (Howard and Pelc, 1953). The essence of this technique was to grow cells in culture medium containing radioactive DNA precursors, Howard and Pelc used radio-labelled phosphorus (P^{32}, 1710 keV) as this was one of the only radio-labelled compounds available at the time. Tritiated thymidine is now used commonly, as the shorter range of the beta-particles emitted by tritium (18 keV) makes the technique less hazardous and tritiated thymidine is more DNA specific. Cells in S phase actively synthesizing DNA integrate the radioactive label into their DNA in the same way as they do normal thymidine. After 2-3 hours, the culture medium containing the radioactively-labelled thymidine is removed and replaced with fresh, complete medium. Preparations of slides of the cells are then made, fixed and finally covered with a photographic emulsion. Beta particles emitted from the DNA-bound radioactive thymidine pass through the emulsion and produce silver grains. When the emulsion is developed, any area through which a beta particle had travelled is blackened, and these areas are over cells that were synthesising DNA at the time of the exposure to the radioactive label. The proportion of cells in S phase at the time of the exposure can therefore be calculated by counting the number of cells with black grains over their nuclei. The use of tritiated thymidine in this technique has been superseded by the use 5-bromodeoxyuridine (BrdUrd), which is similar in structure to the DNA precursor thymidine and is also assimilated by cells actively synthesising DNA in place of

thymidine. A fluorescent antibody specific for BrdUrd is then used to identify the cells in the culture containing BrdUrd i.e. any cells that were in S phase and synthesising DNA at the time of exposure to BrdUrd. The use of fluorescent antibodies reduces the time after which samples can be examined, because cells stained with BrdUrd can be fixed and scored within 20 hours of staining whereas cells exposed to tritiated thymidine require about a 5-6 week period of storage to allow time for the β-particles to produce a distinct image on the photographic emulsion. Flow cytometry is an alternative, more versatile and much quicker, method of cell cycle analysis. In this technique cultures of cells are stained with a fluorescent dye, e.g. propidium iodide (PI) that bind to the DNA. Each cell is then individually illuminated at a wavelength of laser light that 'excites' the dye and the resultant fluorescence is measured and recorded. The measure of fluorescence is proportional to the amount of bound dye, and therefore DNA, in each cell. A plot of the distribution of fluorescence against incidence for an asynchronous population of cells (see Fig. 5.1) consists of a peak at 1× DNA content produced by diploid G_1 phase cells (2C) and a second peak at 2× DNA content depicting G_2 phase and mitotic cells (4C). The region between the two peaks represents cells of intermediate DNA content where varying amounts of DNA have replicated i.e. S phase cells (2C-4C). The area of each sector in the distribution is proportional to the fraction of cells in the corresponding phase of the cell cycle and is determined by a computer analysis of the distribution.

5.3 Measurement and methods of producing cell synchrony

The majority of cell survival curves in this thesis have been delineated for asynchronous populations of cells. To study the radiation response of the cells in the individual phases of the cell cycle, the cells have to be synchronised so that the majority are in the same phase of the cell cycle. Ideally, synchrony should be achieved at a specific point in the cell cycle and the procedure should have little or no effect on the metabolic processes of the cell and produce synchronised cells in large numbers. Many methods have been developed to synchronise cells (see Nias and Fox, 1971). Nevertheless many do not achieve perfect synchrony but are a compromise aimed at achieving a high degree of cell synchrony with minimum disruption to the cell cycle.

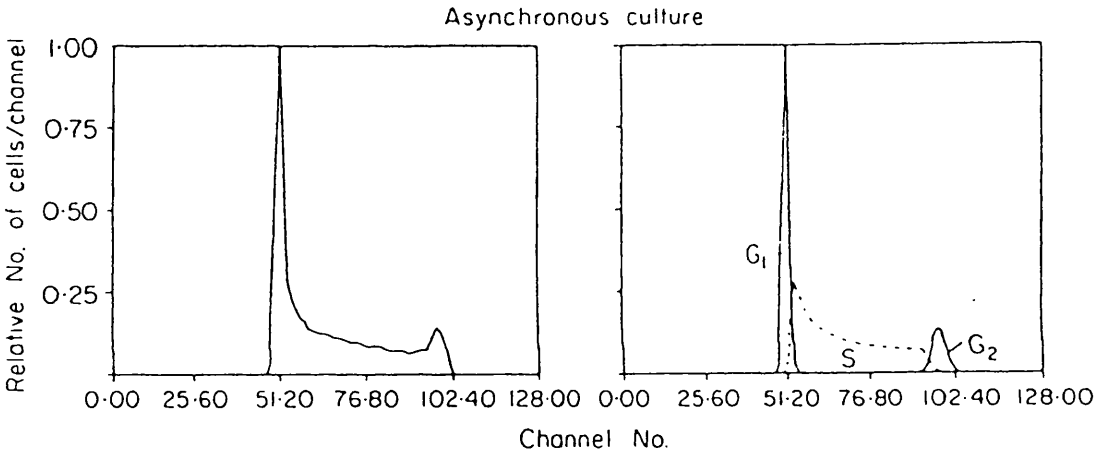

Fig. 5.1

A typical histogram of the DNA distribution of cells in an asynchronous cell population. The ordinate is a measure of the intensity of fluorescence per cell which is proportional to the amount of DNA in the cell and the abscisse measures the frequency of intensity. Computer analysis of the image reveals the proportion of cells in each phase of the cell cycle. The first peak represents the number of G_1 phase cells in the population. The G_2 phase cells which contain twice the DNA content of the G_1 phase cells are represented by the second peak. The region between the two peaks is characteristic of cells of intermediate DNA content, i.e. S phase cells.

Synchronisation can be achieved using two strategies, either a synchronous sample of cells of the same cycle phase can be selectively extracted from the asynchronous cell population or the asynchronous population of cells can be forced into synchrony. The former are generally mechanical non-cell cycle disruptive methods which exploit the change in the size of the cell as it progresses through the cell cycle, whereas the latter are often biochemical methods which inhibit a part of the cell cycle causing the accumulation of cells into the cell-cycle phase immediately prior to the chemical block.

5.3.1 Mechanical methods of producing cell synchrony

5.3.1.1 Mitotic harvesting

Terasima and Tolmach (1961) observed that cells were more loosely attached to the growth surface during mitosis than during other phases of the cell cycle and that gentle agitation of the culture flask detached the mitotic cells which were then harvested by removing the culture medium and isolating the cells. Synchronised populations of G_1, S and G_2 phase cells were obtained later by allowing a homogeneous population of mitotic cells to progress normally through the cell cycle. Using this technique, Terasima and Tolmach (1963) obtained populations of HeLa cells with a mitotic index of 50%-60% compared with a value of 2% from a typical asynchronous cell population of this cell line (the mitotic index is a measure of the number of cells in the population in mitosis at any one time).

A major limitation of the Terasima and Tolmach shake-off technique is the poor yield of synchronised cells that is achieved as only a small fraction of the cells in the population are in mitosis at any one time and are therefore able to be dislodged. The mitotic index of a population of HeLa cells in exponential growth rarely exceeds 2% and typically only 50% of these are harvested at any one time (Sinclair and Ross, 1969). To increase the yield of mitotic cells that can be obtained using this technique, repeated harvesting has been performed, shaking the monolayer culture every 10 minutes, storing and then combining the product of each harvest at 4°C to prevent any progression through the cell cycle (Peterson *et al.*, 1969).

The mitotic harvest technique can only be used for cell lines in which the

mitotic cells are weakly attached to the growth surface. To overcome this limitation, several modifications have been made to the original procedure to extend the technique to a broader range of cell lines that grow as monolayer cultures but do not have the required differential in the strength of attachment between mitotic and non-mitotic cells. Incubating cells in calcium-free medium has been reported to weaken the attachment link between the mitotic cell and growth surface, because the extent of the cell-substrate attachment is a consequence of the calcium concentration in the surrounding environment (Robbins and Marcus, 1964). Chilling the cell culture medium was also reported to improve the differential attachment between the rounded-up mitotic cells and flattened out cells (Lindahl and Sorenby, 1966) as has the use of low concentrations of trypsin to weaken enzymatically the cell-substrate binding protein (Sinclair and Morton, 1963).

5.3.1.2 Confluent cultures of cells

The procedures employed to maintain an established cell line as a spinner or monolayer culture are designed to propagate cells at their maximal rate. This is accomplished by supplying the culture with an optimum environment for growth, a regular supply of fresh culture medium and the removal of toxic metabolites. A failure to maintain this equilibrium ensures that the exponentially-growing population of cells eventually enters a stationary phase of growth owing to density-dependent growth inhibition, nutrient depletion (Griffiths *et al.*, 1972) or a build-up of toxic metabolites (Garcia-Giralt *et al.*, 1970). A population of cells that is retained in a stationary phase of growth by supplying some fresh culture medium becomes density-inhibited and accumulates into the G_1 phase of the cell cycle (Ross and Sinclair, 1972). Maintaining the density-inhibited culture can result in a synchronised population of G_1 cells. The stationary-phase culture, enriched in cells in the G_1 phase of the cycle, resumes exponential growth when diluted and transferred to fresh culture medium thereby producing synchronised cohorts of S and G_2 phase cells.

5.3.1.3 Centrifugal elutriation

Centrifugal elutriation is a method which separates cells according to their size and density by exploiting the change in the volume of the cell as it progresses through the cell cycle. In this technique (see Fig. 5.2), a centrifugal force which would

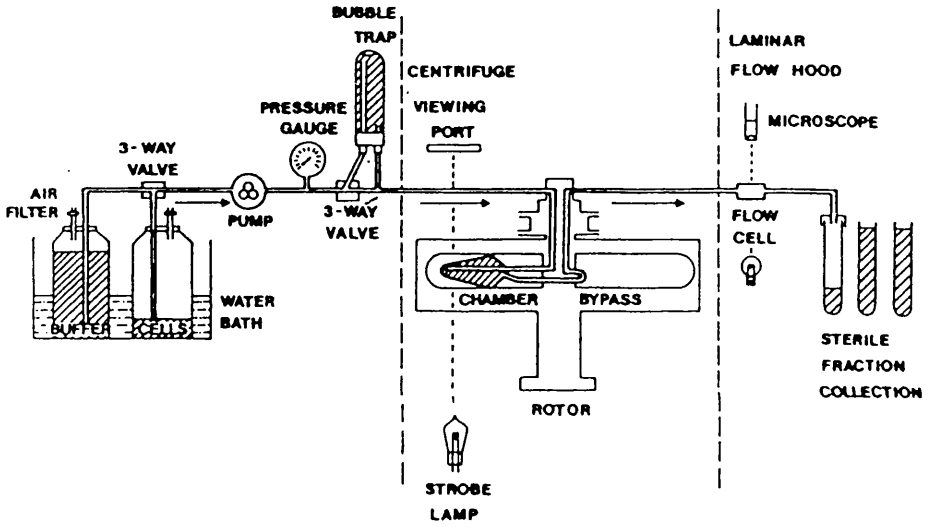

Fig. 5.2
Technique of centrifugal elutriation. The cells are held at equilibrium in the chamber by the counterbalancing of the centrifugal force and flow of eluting buffer through the chamber.

sediment cells in a separation chamber is counterbalanced by the force of an eluting buffer flowing through the chamber in the opposite direction. A narrow band of cells therefore forms across the width of the separation chamber, held in equilibrium by the two opposing forces. By increasing the flow rate of the buffer or decreasing the speed of the rotor (i.e. the centrifugal force) successive fractions containing relatively homogeneously-sized populations of cells are obtained. This technique has been reported to achieve a high degree of cell synchrony and an excellent homogeneity in the sizes of the separated cells for a whole range of cell types (Grdina *et al.*, 1984). Fractions of cells containing $\geq$ 90% G_1 cells, $\geq$ 70% S cells and $\geq$ 60% G_2 cells have been reported to be recovered routinely using centrifugal elutriation (Meistrich *et al.*, 1977).

5.3.2 Biochemical methods of producing cell synchrony

The biochemical approach to synchronising a population of cells entails the blocking or inhibiting of a step in the cell cycle, by a non-cytotoxic concentration of a drug. Cells therefore accumulate at a point in the cell cycle immediately prior to the block. Withdrawing the drug removes the inhibition and the normal progression of the cell cycle then continues with the cells in a synchronised cohort. However, the process of chemically inhibiting the cell cycle often induces gross perturbations in the biochemical balance of the cell which ultimately affect the subsequent progression of the cells through the cell cycle once the blocking agent has been removed. If the continued normal progression of the cell cycle is not one of the aims of the synchronisation process, then chemical modes of synchrony provide a quick and efficient method of producing large numbers of highly synchronised cells.

5.3.3 A comparison of mechanical and biochemical methods of producing synchrony

Each method of synchronisation has advantages and disadvantages. With respect to achieving minimal disruption of the cell cycle, mitotic selection is probably the best method, followed by centrifugal elutriation and lastly the biochemical methods. The major disadvantages of mitotic selection, however, are the specificity towards particular cell lines that grow as monolayer cultures and the low cell yield that is obtained (1% of the cell population at any time). The technique of centrifugal

elutriation is rapid, and large numbers of cells can be separated into subpopulations enriched in all phases of the cell cycle. Separation can be achieved at room temperature in culture medium with no exposure to cytotoxic or cytostatic agents. A major disadvantage is the complexity of the technique and the variability in the degree of synchrony that can be obtained owing to the inherent heterogeneity of cell sizes within each phase of the cell cycle. The precise nature of chemical synchronisation and the large cell yields which can be obtained are an obvious advantage but the methods are disadvantaged by the biochemical damage that might be induced in the cell which could affect the normal progression of the cell cycle and also the subsequent radiation response.

5.4 Radiation response of cells in the individual phases of the cell cycle

A variation in the radiation response of cells in the individual phases of the cell cycle was first reported in HeLa cells (Terasima & Tolmach 1963). A population of mitotic cells obtained using the technique of mitotic selection was incubated and allowed to progress through the cell cycle. At precise intervals following synchronisation, corresponding to a particular phase in the cell cycle, a sample of cells was removed and exposed to 3 Gy of X-rays. The fraction of cells that survived the 3 Gy dose increased rapidly with time after synchronisation as the cells progressed into S phase, survival then decreased as the cells moved out of S phase and into the G_2 phase (Fig. 5.3). This cyclic pattern of radiation response through the cell cycle has been found to occur in most mammalian cell lines although differences were observed in the radiosensitivity of the G_1 phase cells. Cell lines with a long G_1 phase had a resistant peak at the beginning of G_1 followed by a sensitive trough at the end of G_1, whereas cells with a short G_1 phase showed no appreciable change in the radiosensitivity throughout the phase. Despite the variation in the radiosensitivity that occurs in the response of G_1 phase cells, particular characteristics are common to all cell lines:

- The G_2 phase and mitosis are usually the most radiosensitive phases of the cell cycle.

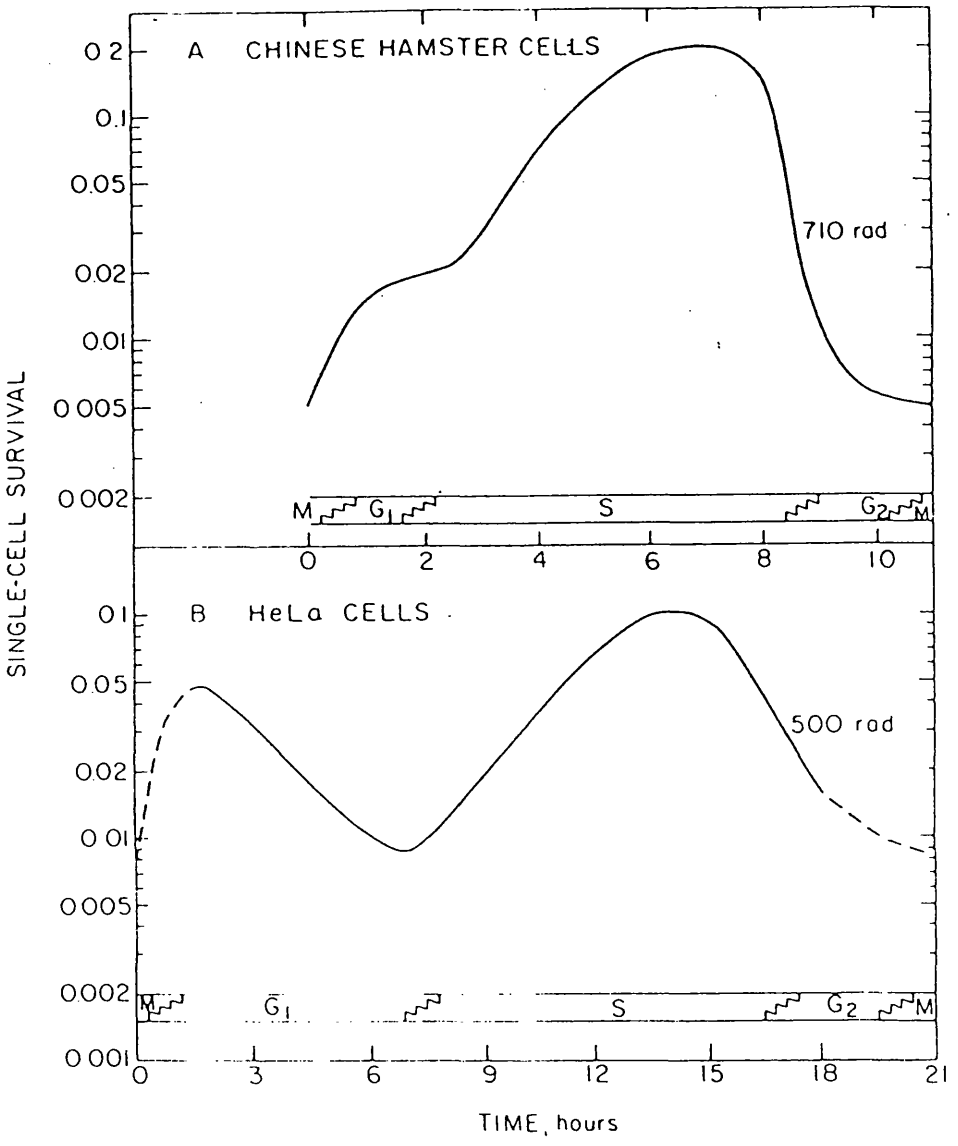

Fig. 5.3

The diagrams illustrate the form of the age response for cells with a short G_1 phase, represented by V79 hamster cells, and cells with a long G_1 phase, represented by HeLa cells. The time scales have been adjusted so that S phase has a comparable 'length' for both cell lines, and in doing so it is evident that the general pattern of cyclic variation is similar in the two cell lines. The main difference between the two cell lines is the extra structure during the G_1 phase in the HeLa cells (taken from Hall, 1978).

- Radioresistance is usually greatest in the latter part of S phase.

- If the G_1 phase comprises a significant proportion of the cell cycle then a resistant period is evident early in G_1 followed by a sensitive period towards the end of G_1.

Complete survival curves for each phase of the cell cycle were first generated by Sinclair (1968) (Fig. 5.4). Cells in mitosis and G_2 were characterized by steep survival curves with little or no curvature. Survival curves for cells in late S phase were less steep than at mitosis and G_2 and exhibited a broad 'shoulder' whilst G_1 and early-S phase cell survival curves were intermediate between the G_2/mitosis response and the late-S phase response. The reasons for the sensitivity changes throughout the cell cycle are not fully understood but could reflect radioprotective mechanisms. Sinclair noted that changes in the concentration of intracellular sulphydryl groups accompanied the changes in sensitivity (Sinclair, 1968). The highest concentration of sulphydryl groups was found in cells in late-S phase which had the greatest radioresistance, whereas the lowest concentration was found near mitosis. Sulphydryls are known radioprotectors and reduce the amount of indirect radiation damage by radical scavenging (Roots and Okada, 1972). It has also been proposed that changes in radiosensitivity throughout the mitotic cycle reflect shifts in the balance between the repair and fixation of potentially lethal lesions (Beetham and Tolmach, 1986; Iliakis and Neusse, 1983). The repair of potentially lethal lesions is thought to occur in all phases of the cell cycle whereas the fixation of radiation damage is thought to occur only at specific points. Cells repair potentially lethal lesions until these points in the cell cycle are reached where damage fixation predominates. The G_1/S border and mitosis have been identified as fixation regions which are postulated to account for their increased radiosensitivity compared to the other cell-cycle phases (Iliakis & Neusse, 1983, 1984).

5.5 Aims

In this study experiments were carried out to determine whether the increased X-ray sensitivity over the X-ray dose range 0.01-0.6 Gy seen in the asynchronous cell

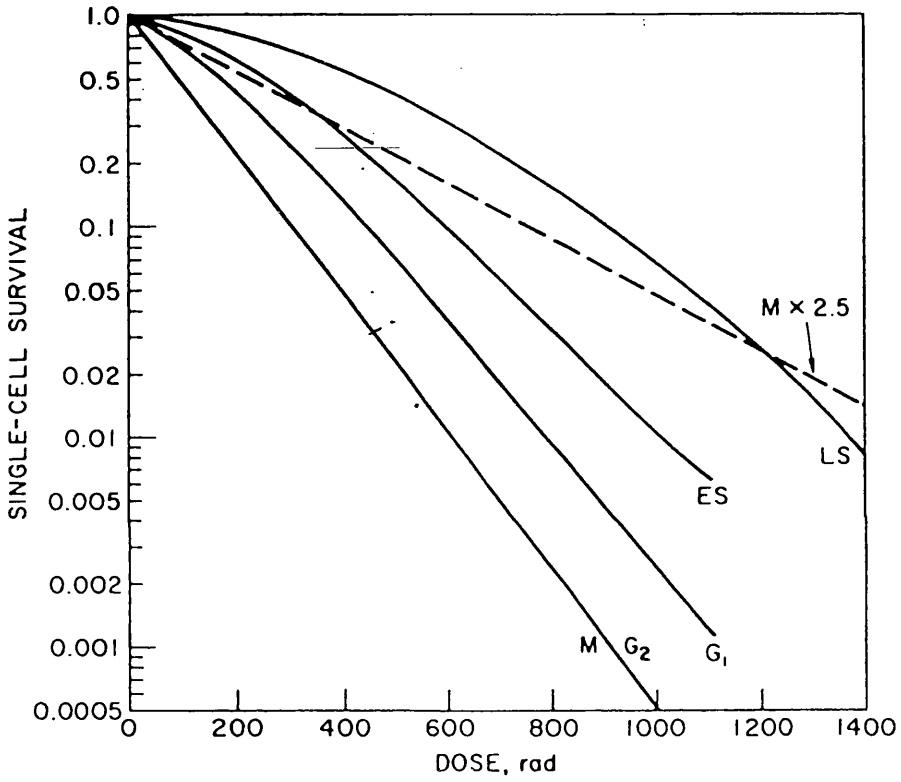

Fig. 5.4
Survival curves for Chinese hamster cells at various stages of the cell cycle. The survival curve for cells in mitosis is approximately exponential. The survival curve for cells in S is shallower and has an initial curved region at low doses. Cells in G_1 and early S are immediate in sensitivity between these two responses (from Sinclair, 1968).

population might be due to the response of a small subpopulation of cells in a particularly radiosensitive phase of the cell cycle (as outlined chapter 4). To investigate this the asynchronous cell population was synchronised to obtain populations of cells enriched in each phase of the cell cycle. Mechanical and chemical methods of synchrony were used in an effort to obtain high yields of synchronised cells with minimum disruption to the normal progession of the cell cycle. If a sufficiently homogeneous cell population could be obtained, parameter and feature files could then be generated using the CELREC program, so that in future studies survival estimates for each cell-cycle phase could be made from within an asynchronous cell population without the need for prior synchronisation.

5.6 Materials and methods

5.6.1 Elutriation methodology

The elutriator used in this study was a JE-6B Beckman System. To ensure that the smallest cells in the V79 cell population (the G_1 phase cells) were retained in the elutriator chamber, at the start of the procedure an initial flow rate of 20 ml min^{-1} of eluting buffer and a rotor speed of 2100 rpm were used. These values were selected using the information supplied in the manufacturers literature calculated for objects of comparable volume to the V79 cells used in this study.

5.6.1.1 Cleaning the system

When an elutriation run had been completed and the contents of the chamber collected, 200 ml of distilled water were pumped through the rotor. The elutriator system was then disconnected from the power and the rotor removed and dismantled. All the components were washed in distilled water, wiped and left to dry. The inflow and outflow lines and gasket seals were cleaned with alcohol and rinsed in PBS. The rotor was stored unassembled and maintenance was performed following procedures listed in the operations manual.

5.6.1.2 Sterilising the system

The rotor, tubing lines and buffer reservoir were sterilised with 70% ethanol. The system was assembled during the afternoon prior to a separation run. The sample

reservoir was rinsed and filled manually with 70% ethanol. Distilled water was pumped throughout the system (excluding the sample reservoir) and all air bubbles purged from the buffer lines. The sample reservoir valves were opened and the 70% ethanol pumped through the whole system and then the air purge was repeated. The system was then drained and the ends of the inflow and outflow lines were plugged and placed in 70% ethanol. The rotor was left in place overnight. On the morning of the elutriation run, 70% ethanol was pumped through the system and rinsed out with 2 litres of sterile water, followed by 500 ml of sterile PBS. The system was then refilled with running buffer and air purged.

5.6.1.3 Preparation of the cell sample

10^7 - 10^9 cells were loaded routinely. The volume of V79 stock spinner culture ($2\text{-}6 \times 10^5$ cells ml^{-1}) necessary to give the required number of cells was centrifuged, washed and resuspended in 10 ml of serum-free MEM-S medium. The resulting cell suspension was then examined using a haemocytometer to determine the number of cell doublets in the sample. The suspension was then passed repeatedly through a 19 gauge needle until less than one doublet was scored per 100 single cells. All these manipulations occurred at room temperature and the cell suspension remained at room temperature until loading.

5.6.1.4 Loading the cell sample

The rotor was pre-set to 2100 rpm and the system purged of air. The rotor speed remained at the initial starting value throughout the loading of the sample. To facilitate simple and rapid loading, the sample was injected through an injection valve in the tubing downstream of the sample reservoir. Extreme care was taken to prevent air entering the system. Loading was achieved by applying a constant pressure to the syringe plunger while simultaneously turning off the peristaltic pump used to drive the eluting buffer in the chamber. The pump was restarted when the loading of the sample was complete. A three way valve downstream of the injection site was used to remove any air bubbles introduced during loading. Elutriation commenced when a distinct cell boundary was clearly visible in the separation chamber.

5.6.1.5 The elutriation procedure

During the separation procedure, the centrifuge chamber and rotor head were maintained at 20°C by refrigeration. The buffer, pump, tubing lines and sample reservoir were at room temperature (18°C to 25°C). The flow rate of the eluting buffer remained constant at 20 ml min^{-1}. When a distinct cell boundary had developed in the separation chamber the collection of aliquots (fractions) of cells commenced. The 1st 50 ml fraction, usually containing only debris (i.e. the lightest particles), was discarded. A series of 50 ml fractions were then collected by incremental decreases in rotor speed (e.g. see Tables 5.2 and 5.3). Each 50 ml fraction contained 45 ml collected at the rotor speed designated for that fraction and 5 ml from the previous fraction. The volume of the outflow tubing was 5 ml. Occasionally, larger volumes were collected when harvesting the earliest fractions. After the final fraction had been collected the cells remaining in the chamber were washed out once the rotor had stopped. The yield of cells in each fraction was determined using a Coulter counter.

5.6.1.6 Analysis of the cell sample

Flow cytometry was used to analyse the percentage of cells in the G_1, S and G_2+M phases of the cell cycle. The cells collected from each elutriation fraction were centrifuged and washed in αMEM + 10% FCS and then resuspended in 10 ml of this medium. After syringing, to reduce the number of cell doublets, an aliquot of cells was taken to assess clonogenicity. The remaining cell suspension was centrifuged and resuspended in 2 ml of PBS containing 1 mg ml^{-1} ribonuclease (Sigma R-5503) and 20μg ml^{-1} propidium iodide (Sigma P-4170). DNA histograms were measured using an Ortho System Flow Cytometer. The fraction of cells in each phase of the cell cycle was determined by a computer analysis of the DNA histograms using a program written by Ormerod *et al.* (1987).

5.6.1.7 BrdUrd staining of a monolayer of cells

BrdUrd staining of monolayer cultures of cells was performed to directly determine the number of cells in S phase, using the following procedure:

1. Fix monolayers in 70% cold ethanol for at least 1 hour at 4°C.
2. Wash with phosphate buffered saline (PBS) twice (5 - 10 ml) 3 to 5 minutes each time.
3. Incubate with 10 ml of 2 M HCl for 30 minutes at room temperature.

Fraction Number	Volume collected (ml)	Centrifugation speed (r.p.m.)	Pump speed ml min^{-1}	Cell yield	Fraction designation
1	33	2100	20	1.1×10^4	debris
2	50	2100	20	3.2×10^3	G_1
3	50	2028	20	5.3×10^3	G_1
4	550	2028	20	1.3×10^3	S
5	50	2028	20	1.5×10^3	S
6	50	1850	20	1.2×10^4	S
7	50	1850	20	1.3×10^4	S
8	50	1900	20	2.7×10^4	S/G_2
9 (washout)	50	-	20	1.8×10^4	giant cells

Table 5.2 *Elutriation parameters for run ELU8 which aimed to achieve a high level of S phase synchrony (1.50×10^8 cells in 10 ml loaded into the chamber)*

Fraction Number	Volume collected (ml)	Centrifugation speed (r.p.m.)	Pump speed ml min^{-1}	Cell yield	Fraction designation
1	33	2100	20	-	G_1
2	50	2100	20	2.3×10^4	G_1
3	50	2028	20	3.9×10^4	G_1
4	500	1800	20	4.7×10^4	G_1
5	50	1350	20	4.9×10^4	S
6	50	1400	20	1.3×10^5	S/G_2
7	50	1300	20	1.3×10^5	S/G_2
8	50	1200	20	1.3×10^5	S/G_2
9 (washout)	50	-	20		giant cells

Table 5.3 *Elutriation parameters for run ELU9 which aimed to achieve a high level of G_1 phase synchrony (1.58×10^8 cells in 10 ml loaded into the chamber)*

4. Wash three times with PBS (as step 2).
5. Incubate with 1:20 dilution of monoclonal antibody in PBS containing 0.5% normal goat serum (NGS) at room temperature for 2 hours (Using just enough to cover monolayer).
6. Wash twice in PBS.
7. Incubate with 1:20 dilution of goat anti rat peroxidase conjugate for 60 minutes at room temperature (Just enough to cover monolayer).
8. Wash twice with PBS.
9. Stain with Diaminobenzidine-tetrachloride (DAB) (Make up 75 mg of (DAB) in 100 ml of 50 mM Tris buffer (pH 7.4) containing 0.1 mM imidazole and 15 ml H_2O_2 (100 volumes) just prior to use). Stain in DAB for 5 minutes or until colour reaction is complete.
10. Wash in distilled water.
11. Add haematoxylin for 20 to 30 seconds.
12. Wash in tap water for 5 minutes.
13. Add 5 ml PBS to flask to stop cells drying out and score.

5.7 Results of employing different methods to achieve cell synchrony

5.7.1 Measurement of the DNA profile

The level of cell-cycle phase synchrony that was achieved by each method of synchronisation was assessed from a DNA histogram obtained using an Ortho Flow Cytometer employing propidium iodide as a fluorescent DNA stain. A typical DNA histogram from an asynchronous, exponentially growing V79-379A cell population is presented in Fig. 5.5. The fraction of cells in each phase of the cell cycle was determined by computer analysis of the DNA profile.

5.7.2 Measurement of disruption caused to the size of cells by synchronisation

An asynchronous population of cells encompasses a large distribution of cell volumes, whereas a synchronised cohort of cells of the same cell-cycle phase consists of cells with a much narrower distribution of cell volumes. As a cohort of synchronised cells progress through the cell cycle, from mitosis to the end of G_2, the mean volume of the cells in the whole population increases but the distribution of the individual cell volumes remains narrow, until the synchrony is lost (Sinclair and Ross, 1969; Steen and Lindmo, 1978). The disruption caused to the size of cells by the synchronisation procedure can therefore be determined by measuring the heterogeneity

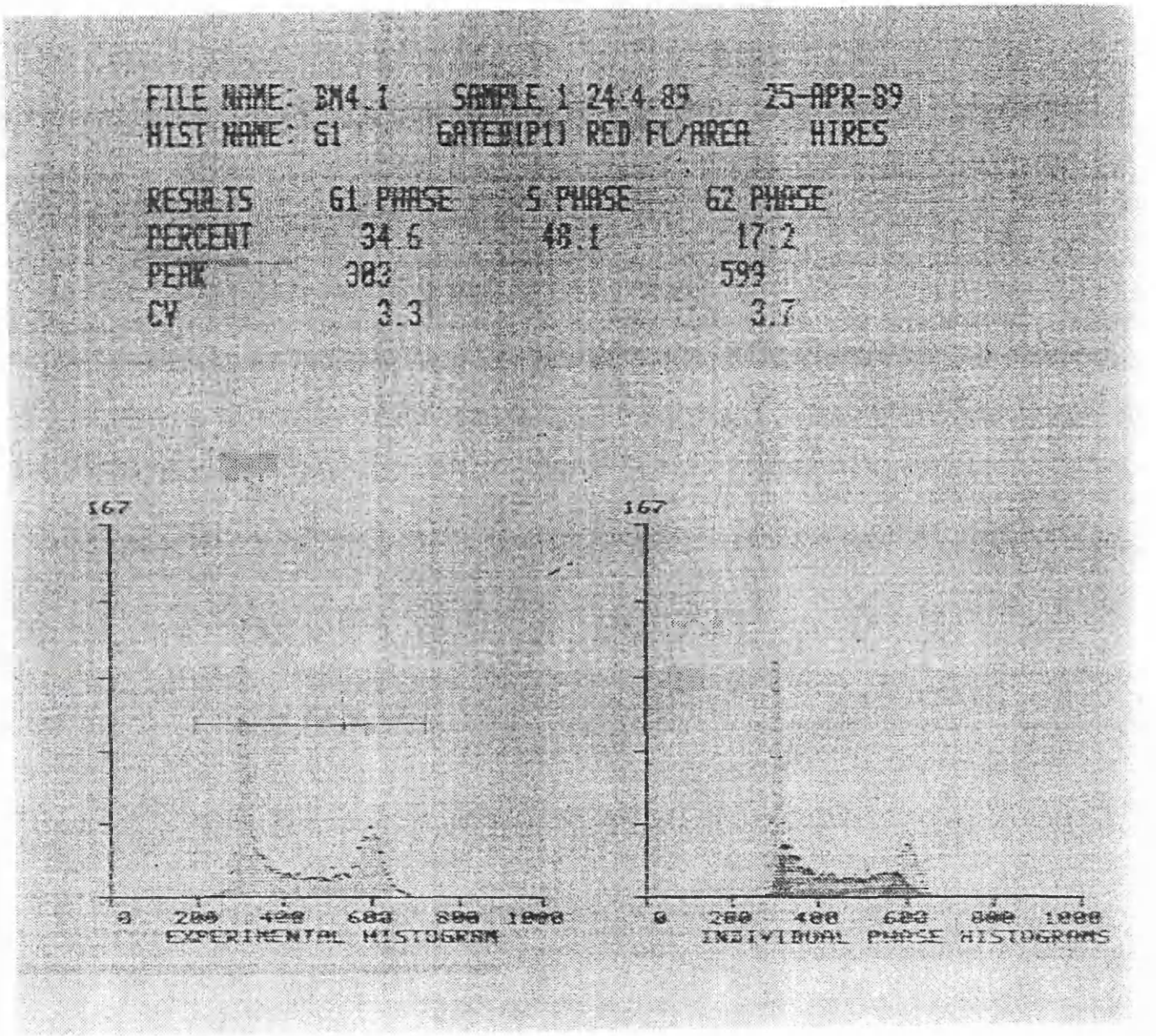

Fig. 5.5

A typical DNA histogram obtained from an asynchronous exponentially growing population of V79 cells. Incidence of light is plotted against relative intensity per cell. A range is placed on the profile marking the intensity of the two peaks (PEAK 303 and 599) to enable computer fitting of the profile. This profile contains 34.6% G_1 cells, 48.1% S phase and 17.2% G_2+M phase cells. The CV value measures the width of the two peaks. Low CV values indicate a highly homogeneous cell population.

of the cell volumes in the sample (Grdina *et al.*, 1984).

This heterogeneity was estimated using the CELREC program which individually locates and measures each cell in the population. A good visual estimation of the distribution of cell sizes in the population was given by the width of the band separating the upper and lower boundary values of the 18 features extracted from the cell signal (Fig. 5.6). An asynchronous sample of cells has a broader band between the upper and lower boundary values than a synchronised sample of cells owing to the greater range of cell sizes and volumes present in the asynchronous population compared with the synchronised population of cells (see section 5.7.6).

5.7.3 Mitotic harvesting

Attempts were also made to use the technique of mitotic selection (Terasima & Tolmach 1961) to obtain mitotic cells from an asynchronous population of cells grown as a monolayer culture. The V79 cell line used in this study was routinely subcultured in suspension but it can be grown as a monolayer culture using an alternative growth medium which provides the Ca^{++} required for attachment. When the mitotic harvest technique was applied to the V79 cell line used in this study, a poor cell yield was obtained (Table 5.4) and insufficient cells were harvested to perform reliable DNA analysis using flow cytometry.

Number of cells seeded	Cell yield (2nd harvest)	Expected Number of mitotic cells (%) in col 1^+	Number of cells actually scored in mitosis (%)
4.3×10^6	4.2×10^4	49	22
5.4×10^6	7.5×10^4	69	31
8.9×10^6	4.9×10^4	28	32
2×10^7	2.3×10^5	58	35

***Table 5.4** Results of the mitotic harvest ($^+$ assuming 2% mitotic index).*

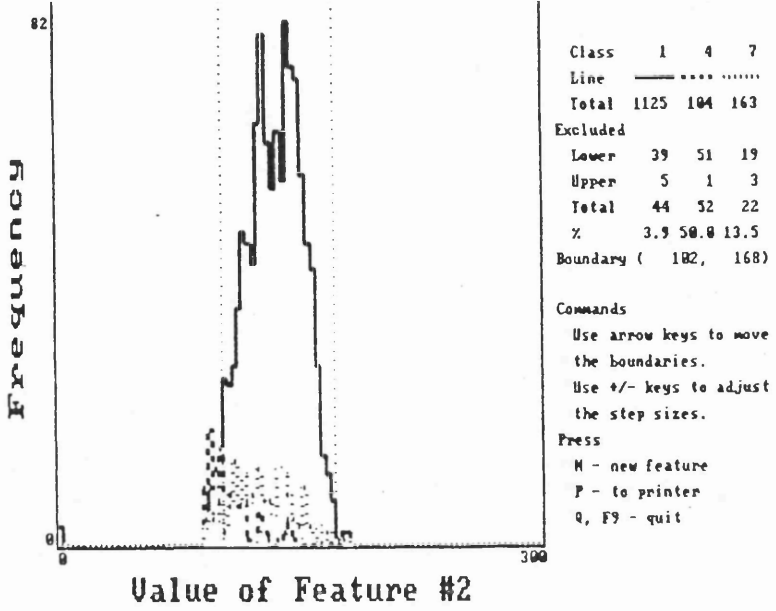

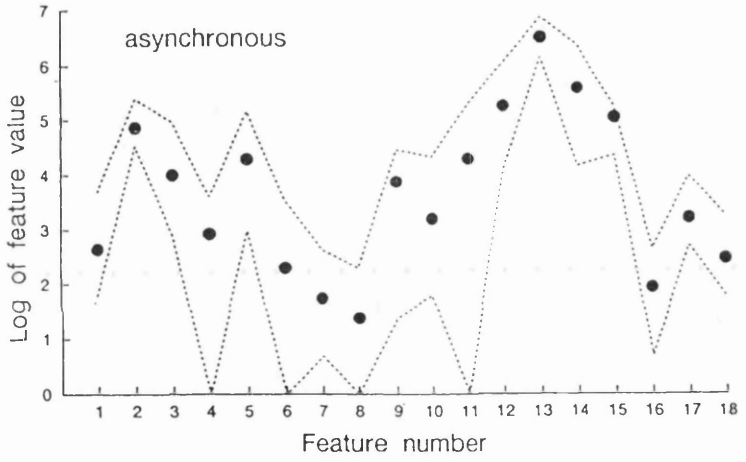

Fig. 5.6

The upper panel shows the selection of the upper and lower boundary values for feature 2 of the recognition image. Feature two is a measure of the maximum height of the peak of the image relative to background light level. The lower boundary limit (the left vertical dotted line) is set at a value of 102 and the right boundary limit (the right vertical dotted line) at 168. This excludes 3.9% of the cells, 50% of the debris and 13.5% of the objects classified as unknown. This feature alone therefore will exclude 50% of the typical debris in a culture flask. Combining this feature with all the other 17 features results in the vast majority of the debris being excluded, ensuring that only objects that have features that fall between all the upper and lower boundary values are scored as cells. The lower panel shows all the boundary limits for all of the features for a sample of V79 cells. The width between the upper and lower boundaries gives an indication of size heterogeneity of the cell population. A very homogeneous cell population will have a narrow band between the two lines.

The first harvest was discarded as typically this contained debris, unattached cells and dead cells, only cells from subsequent harvests performed at hourly intervals were counted and analysed for the presence of mitotic cells using the RSCAN program by manually revisiting the cells and recording the time of division. Despite seeding 2×10^7 cells in a roller bottle with a surface area of 400 cm^2, 24 h before harvesting, only 2.3×10^5 cells were recovered on the second harvest. This represented only 58% of the mitotic cells (mean of all the experiments = 55%, SD ± 8.3) present in the population at the time of harvesting, assuming a mitotic index in this cell line of 2%. Of these, only 35% (mean of all the experiments = 30%, SD ± 5.6) were actually in mitosis at the time of harvesting. This was determined by plating the cells obtained by mitotic selection and manually scoring the number which had divided within 2 hours of being harvested. Mitosis in this cell line lasts approximately 1 hour. Allowing 2 hours for the harvested cells to divide before scoring permitted some time for the cells to anchor to the growth surface following replating.

A mitotic enrichment of 35% obtained in this study compares with 95% for HeLa cells (Robbins and Marcus, 1964) and 95% for CHO cells (Tobey *et al.*, 1967). This indicates that the subline of V79 cells in this study is not amenable to mitotic shake-off. This is not surprising however because this particular sub line of V79 cells was developed to grow primarily as a suspension culture. Sinclair and Morton (1963) have reported mitotic harvests of 45% for one V79 cell subline. This was achieved by incubating log-phase cells at 4°C for 1 hour prior to harvesting in the presence of a dilute solution of trypsin to provide a better differential attachment between mitotic and intermitotic cells. However, employing a cooling and trypsinisation technique similar to the one used by Sinclair and Morton (1963) failed to improve significantly on the mitotic yield in this V79 cell sub-line (mean of all experiments = 38.2%, SD ± 6.9%). Replacing the normal culture medium with MEM-S growth medium containing less calcium (Robbins and Marcus and, 1964) improved the overall yield of cells (mean of all experiments = 37.3%, SD ± 8.4) but failed to improve significantly the number of cells scored in mitosis (mean of all experiments = 35.2%, SD ± 6.9) (Table 5.5). Therefore as the poor cell yield and low degree of cell synchrony could not be improved significantly and this method of obtaining synchrony was abandoned.

Number of cells seeded	Total cell yield	Expected number of mitotic cells (%) in col 1	Number of cells scored in mitosis (%)
6×10^6	1.6×10^5	33	27
5.2×10^6	1.2×10^5	28	39
6.4×10^6	2.1×10^5	41	38
7.1×10^6	2.7×10^5	47	26

***Table 5.5** Cell yield and the number of cells in mitosis, achieved in calcium reduced medium, calculated from an expected mitotic index in the V79 cell-line of 2%*

5.7.4 Biochemical methods

Hydroxyurea (HU) has both cytostatic, and at high concentrations for long exposure periods (in excess of two cell cycle times and in excess of 5 Mm in the V79 cell line) cytotoxic action, on cells grown *in vitro* (Sinclair, 1967). HU treatment at low concentrations for a fraction of the cell cycle time has been used as a method of inducing the synchronisation of cells. The drug inhibits DNA synthesis by suppressing the conversion of ribonucleotides to deoxyribonucleotides (Young and Hodas, 1964) which prevents the onset of S phase and therefore results in the accumulation of the cells at the G_1/S border. The cells remain arrested until the drug is removed whereupon a cohort of synchronised cells promptly enter S phase. Hydroxyurea was selected as a biochemical method of synchronising cells because it has been reported not to reduce the plating efficiency of V79 cells (Sinclair and Morton, 1963) after exposure to a drug concentrations of up to 1 mM for up to 8 hours. This was desirable as the recognition assay is dependent on cells attaching quickly, and remaining attached, to the growth surface for the CSCAN and SSCAN procedures.

A population of asynchronous cells was exposed to three concentrations of HU (0.33 mM, 0.5 mM and 1.0 mM) for 6 hours in order to achieve S-phase synchrony. HU has a differentially lethal action at different stages of the cell cycle (Sinclair, 1965) killing S phase cells synthesizing DNA at the time of exposure but not killing

G_1, G_2 or mitotic cells. An exposure period of 6 hours was selected because this was longer than the combined duration of the G_2, mitosis and G_1 phases of the V79 cell cycle (Table 5.1) and therefore allowed sufficient time for the cells in those phases to progress to the G_1/S border, after which time the drug was removed and the cells were allowed to progress into S phase as a synchronised cohort. Following the removal of the drug the cell suspension was washed with fresh culture medium and incubated for 1 hour to allow time for the cells to progress through the G_1/S border and into S phase before the DNA profile of the population was determined using propidium iodide staining and flow cytometry. The highest level of synchrony was achieved with the lowest concentration of drug used (Fig. 5.7). HU at a concentration of 0.33 mM yielded 80.3% of the cell population in S phase, 0.5 mM HU gave 70.5% S-phase cells and 1.0 mM HU resulted in only 48.8% of cells in S phase after 6 hours of drug exposure. It was unclear why the lowest concentration of HU was more effective at producing S phase synchrony. One possible explanation is that the cells treated with HU at concentrations of 0.5 mM and 1.0 mM needed a longer recovery interval before normal progression of the cell cycle could continue after the drug had been removed, and that the 1 hour used in this study was insufficient for the cells to progress from the G_1/S border into S phase. As the lowest drug concentration used (0.33 mM) produced a satisfactory level of synchrony with the least amount of disruption to the cell cycle of the three concentrations studied, it was decided to proceed using this concentration of drug. Complete cell synchrony might not have been achieved using a concentration of 0.33 mM HU because all of the cells in the population did not reach the G_1/S phase border in the initial six hour exposure period. The exposure time of the cells to the drug was therefore increased. This failed to improve the level of cell synchrony; doubling the exposure time of the cells to HU from 6 h to 12 h *reduced* the level of cell synchrony: the cell population contained only 65.2% S phase cells compared with 80.3% S phase cells after a 6 h exposure (Fig. 5.8). These data indicate that increasing the exposure time to the drug might have prevented the cells from progressing normally from the G_1/S boundary into S phase after the removal of the drug, in a similar manner as postulated when higher concentrations of the drug were used with a shorter exposure time. This was confirmed with the DNA distribution profiles of the cell sample: a large G_1/early S fraction occurred after the 12 h exposure compared with the much smaller G_1/early

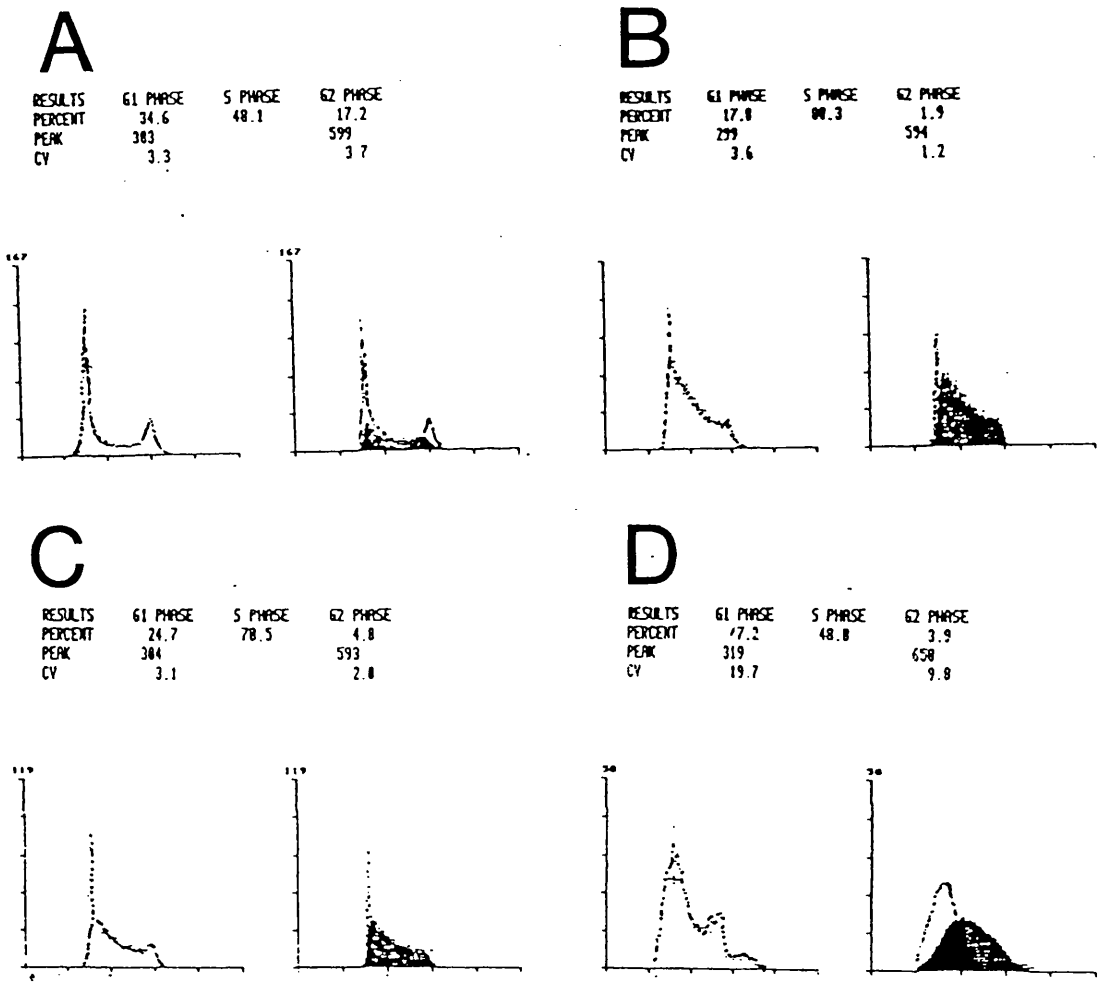

Fig. 5.7

DNA profiles for V79 cells exposed to three concentrations of HU for six hours. Panel A shows the DNA profile of an untreated cell population at the beginning of the experiment. The highest level of cell synchrony was achieved with 0.33 mM HU (panel B) followed by 0.5 mM (panel C) and 1 mM (panel D). As the drug concentration increased the DNA profile became atypical and at the highest concentration the data suggest a distortion of the cell size and shape, indicated by the large CV value of the first peak (19.7) compared with a value of 3.6 at a concentration of 0.33 mM.

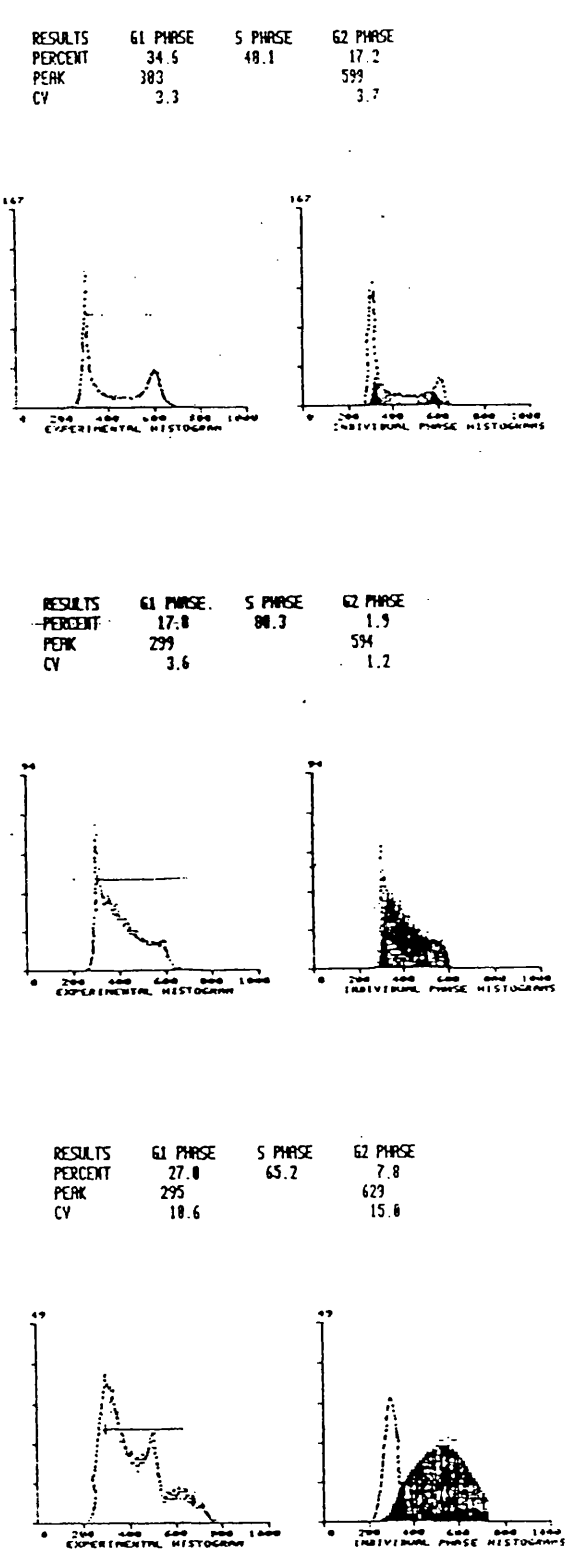

Fig. 5.8

DNA profiles of samples of cells exposed to a 0.33 mM concentration of HU for 6 or 12 hours. Increasing the exposure time of the cells to the drug did not improve the level of cell synchrony, with 65.2% S-phase (12 h HU) cells compared with 80.3% (6 h HU) and 48.1% (no drug). The increased exposure time elevated the level of distortion in the size and shape of the cells compared with the lower exposure time, indicated by a CV of 10.6 compared with 3.6 (6 h HU) and 3.3% (no drug).

S fraction in the cell sample exposed to the same concentration of the drug for 6 hours (see Fig. 5.8).

A more detailed study using a drug concentration of 0.33 mM HU was carried out in an attempt to improve the level of cell synchrony. The effect of the drug on the growth rate and DNA distribution of a population of cells was assessed and compared with a similar population of cells not exposed to HU. The total number of cells in the HU treated population remained approximately constant over the duration of the drug exposure compared with an increase in the number of cells in the population not exposed to the drug over the same period of time. The number of cells in the non-treated population increased rapidly (from $\approx 2 \times 10^5$ to $\approx 1.2 \times 10^6$ cells ml^{-1}) until a stationary phase of growth was achieved, 24 hours after sub-culture, indicated by the accumulation of cells in the G_1 phase of the cell cycle (35.7% to 63% Table 5.6). This was followed by a decline in the number of cells in the population after a further 24 hours of culture, due possibly to the depletion of nutrients in the culture medium. A doubling of the cell number from $\approx 1.2 \times 10^5$ cells ml^{-1} to $\approx 2.4 \times 10^5$ cells ml^{-1} was seen in the cell population treated with the drug, 16 h after the drug was removed. This suggests that the normal progression of the cell cycle was delayed by the drug treatment as a doubling in the number of cells would normally be expected 6-8 h after removal of the block i.e. the time taken for cells to progress from S phase to mitosis. The fraction of cells in the G_2+M phase of the cell cycle did not vary significantly between the two cell populations while the drug was present (Table 5.6).

		Phase of cell cycle		
Time (h)	Treatment	G_1	S	G_2+M
0	no drug	35.7%	54.3%	9.9%
0	HU	35.4%	53.5%	11.3%
24	no drug	62.0%	35.6%	7.5%
24	HU	3.2%	92.3%	4.48%

Table 5.6 *DNA profiles of a HU treated cell population and a non-drug treated cell population obtained by flow cytometry at the time of inoculation and at 24 hours of culture.*

The fraction of cells in S phase increased dramatically after the HU had been removed, whereas no change in the S-phase fraction occurred in the non-treated cell population. The increase in the S-phase fraction in the drug-treated population of cells was accompanied by a decrease in the fraction of G_1 phase cells. The elevated number of cells in S phase continued throughout the next cell cycle time (10-12 hours) which suggested that the cells were not progressing normally through the cell cycle, as a decrease in the S phase fraction and increase in the G_2 phase would have been expected over this period.

Although the degree of synchrony achieved using HU (97.8% S phase at best) was excellent the cell population was atypical in cell size and shape. A CELREC upper and lower boundary plot from a HU treated cell population gave a larger distribution of cell sizes (Fig. 5.9) than would be expected normally in an asynchronous cell population. A highly synchronised population of cells should ideally contain cells which have a narrow distribution of sizes; however this was not seen in the HU-treated population. The upper and lower feature boundary limits were considerably wider than those from an asynchronous cell population (see Fig. 5.9) which contain parameters for the recognition of larger G_2 phase cells. Another S-phase enriched population of cells obtained by centrifugal elutriation did have the narrow distribution of cell sizes that is expected of a highly synchronised cell population (Fig. 5.9). Slight distortion to cell size was expected in the HU-treated cell population because both G_1 and S phase cells have been reported to swell following exposure to HU, possibly owing to continued DNA synthesis and a failure to divide (Sinclair, 1967). However, the extent of the distortion seen in this study was unexpected and surprising. The explanation for the excessive swelling is unknown. Despite the very high level of synchrony attained using HU it was not suitable for synchronising cells to be assayed using the cell analyser because the change in optical image of the cell would result in the cells not being recognised by the CSCAN parameter file. Treatment with HU as a method of synchronising cells was therefore rejected because it was incompatible with the procedure of cell recognition used by the cell analyser. Pilot studies with other drugs, e.g. vinblastine, that were also being carried out, were also discontinued.

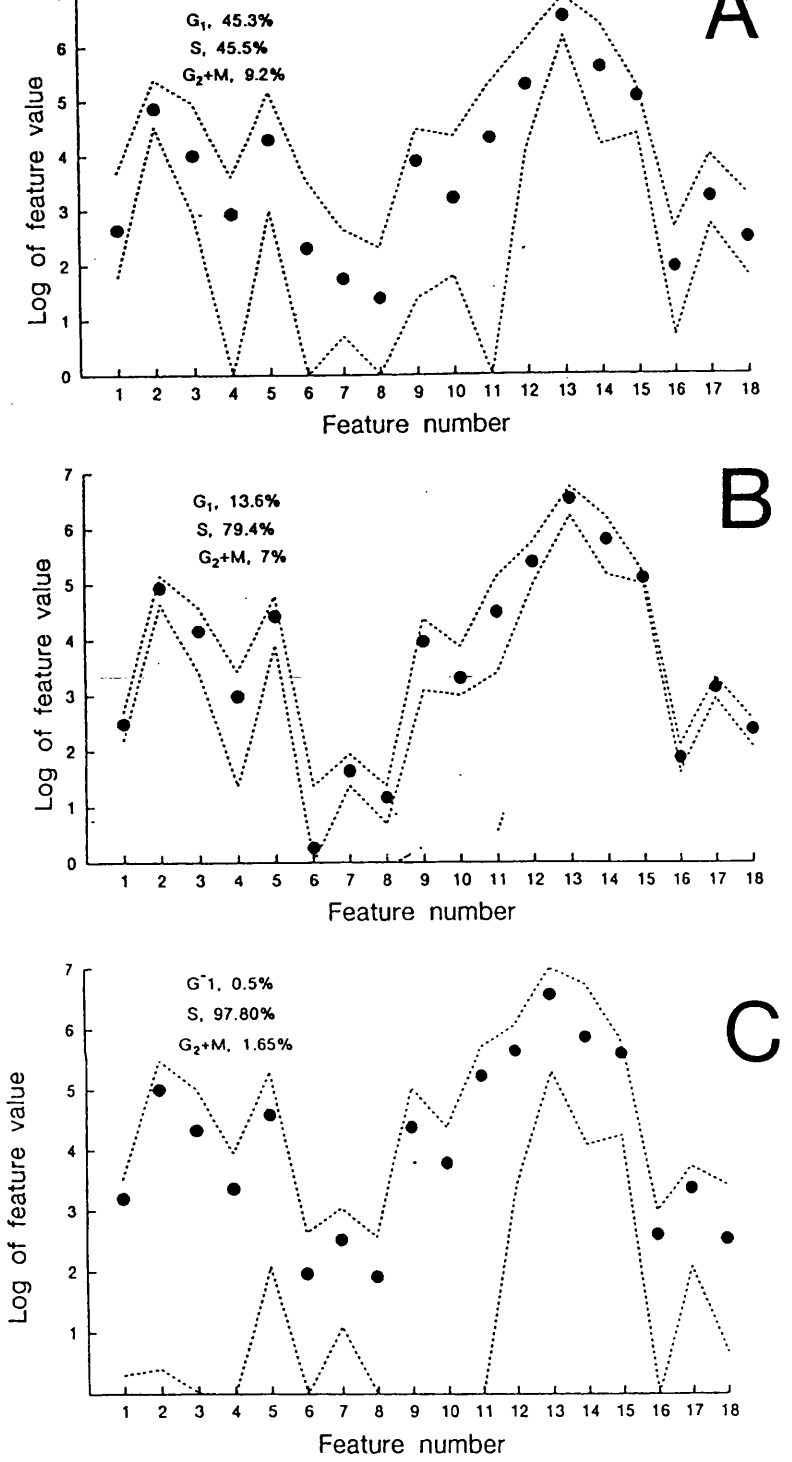

Fig. 5.9

Upper and lower cell boundary plots generated by CELREC for an asynchronous (panel A), eluted S phase enriched (panel B) and the enriched S phase cell population obtained by HU treatment (Panel C). The eluted cell population has a narrower band between the boundaries than the asynchronous population as would be expected from a more homogeneous cell population. The cell population synchronised by HU has a broad band between the boundary limits, illustrating the large size heterogeneity of the cells in the sample despite the high level of cell synchrony of 97.80% of S phase cells compared with 79.4% (eluted) and 45.5% (asynchronous).

5.7.5 Confluent cultures of cells

Figure 5.10 shows the growth curves for two populations of V79 cells, one grown as a spinner culture and the other as a monolayer culture (on an area of 25 cm^2) in the same volume of culture medium. The two cell populations were inoculated with a comparable number of cells and supplied with the same volume of culture medium; the difference in the final number of cells in each system is a result of the method of culture. In monolayer, the cells flattened rapidly after plating and formed discreet colonies which eventually merged as the area of the growth surface became covered totally with cells. In spinner culture however, a single cell suspension was maintained owing to the stirring movement of the culture. The growth inhibition of cells in the monolayer culture was therefore probably a consequence of contact inhibition and not nutrient depletion of the medium because the number of cells in the suspension culture, which was supplied with the same volume of culture medium, increased over the same time period.

The DNA distribution of the cells, obtained by flow cytometry, showed that the cells grown as a monolayer culture were arrested in the G_1 phase of the cell cycle (Fig. 5.10), whereas the cell population grown as a spinner culture did not accumulate into the G_1 phase until the cell number was approximately 3 times that of the monolayer culture. During the period 12-24 hours following the inoculation of the monolayer culture. The proportion of cells in the G_1 phase remained reasonably constant only increasing from 74.3% to 76.3% (Fig. 5.11).

The upper and lower boundaries of the feature values from cells synchronised by density inhibition (Fig. 5.12, panel A) indicated that the volume homogeneity was as narrow as obtained by elutriation (Fig. 5.10, panel B). Synchronising cells in spinner culture by nutrient deprivation produced a 70% enriched G_1-phase cell population which had a larger distribution of cell sizes that the two populations of cells synchronised by elutriation or contact inhibition confirming the lower degree of cell synchrony that was obtained (Fig. 5.12, panel C).

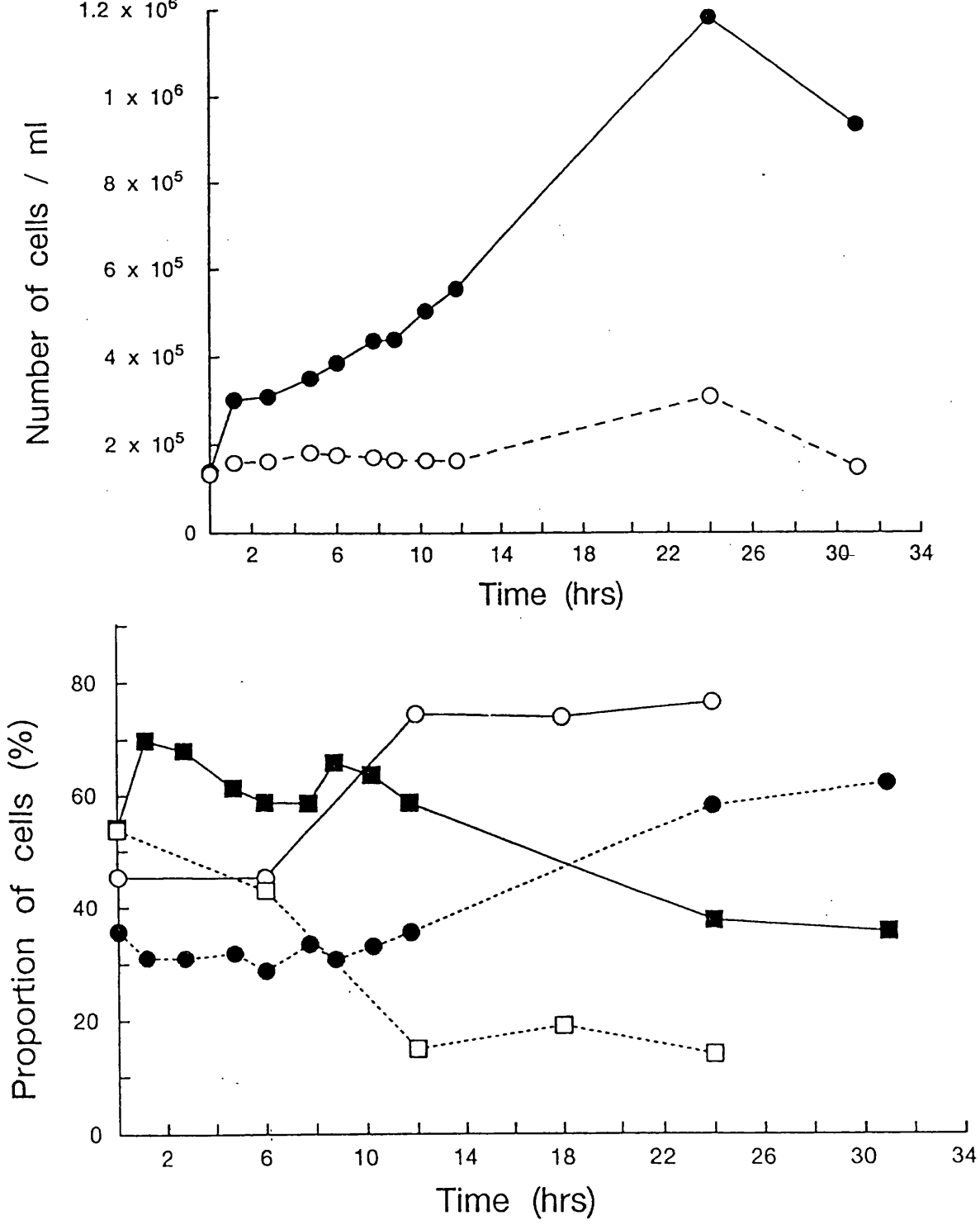

Fig. 5.10

Upper panel: The increase in cell number for two cell populations, a 45 ml spinner culture and 45 ml monolayer culture (25 cm² surface area). The number of cells in the monolayer culture only increased slightly over the first 24 hours of culture compared with the number of cells in the spinner culture, solid symbols represent spinner cultures, open symbols monolayer cultures. Lower panel: A DNA analysis of a sample of cells from the two cell populations obtained by flow cytometry. Solid symbols represent spinner cultures, open symbols monolayer cultures. (G_1 = ●, O; S = ■,□)

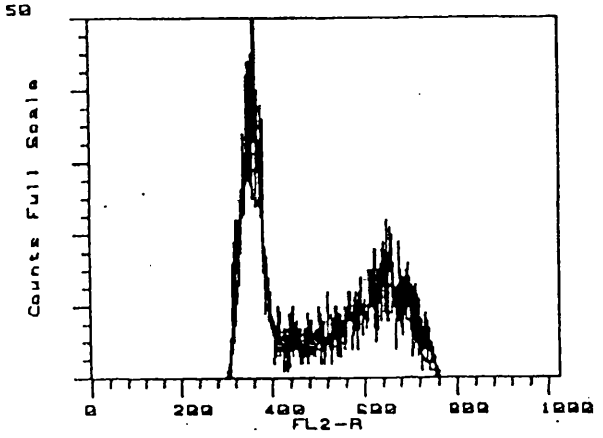

Calculation Parameters

	Initial	Final
G1 Peak :	355	356.5
G2+M Peak:	665	668.6
G1 CV :	6.1	5.8

Cell Cycle Statistics

Phase	Events	Percent	%SD
G1 :	1897	42.8	0.03
S :	1708	38.6	0.02
G2+M :	824	18.6	0.06
Total:	4429	100.0	

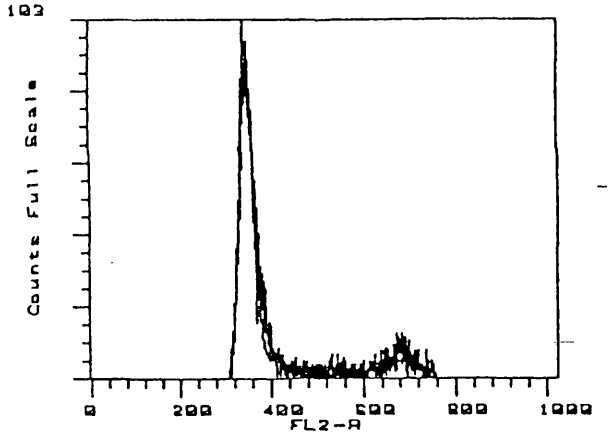

Calculation Parameters

	Initial	Final
G1 Peak :	345	348.4
G2+M Peak:	681	687.3
G1 CV :	3.7	4.3

Cell Cycle Statistics

Phase	Events	Percent	%SD
G1 :	3210	72.9	0.02
S :	843	19.1	0.02
G2+M :	352	8.0	0.07
Total:	4405	100.0	

Fig. 5.11

DNA profiles for cells grown to confluence as a monolayer culture. The upper panel shows the profile of the asynchronous cell population at the start of the experiment (1×10^5 cells ml^{-1}) and the lower panel shows the profile 26 hours later (1×10^6 cells ml^{-1}) when the proportion of cells in the G_1 phase has increased.

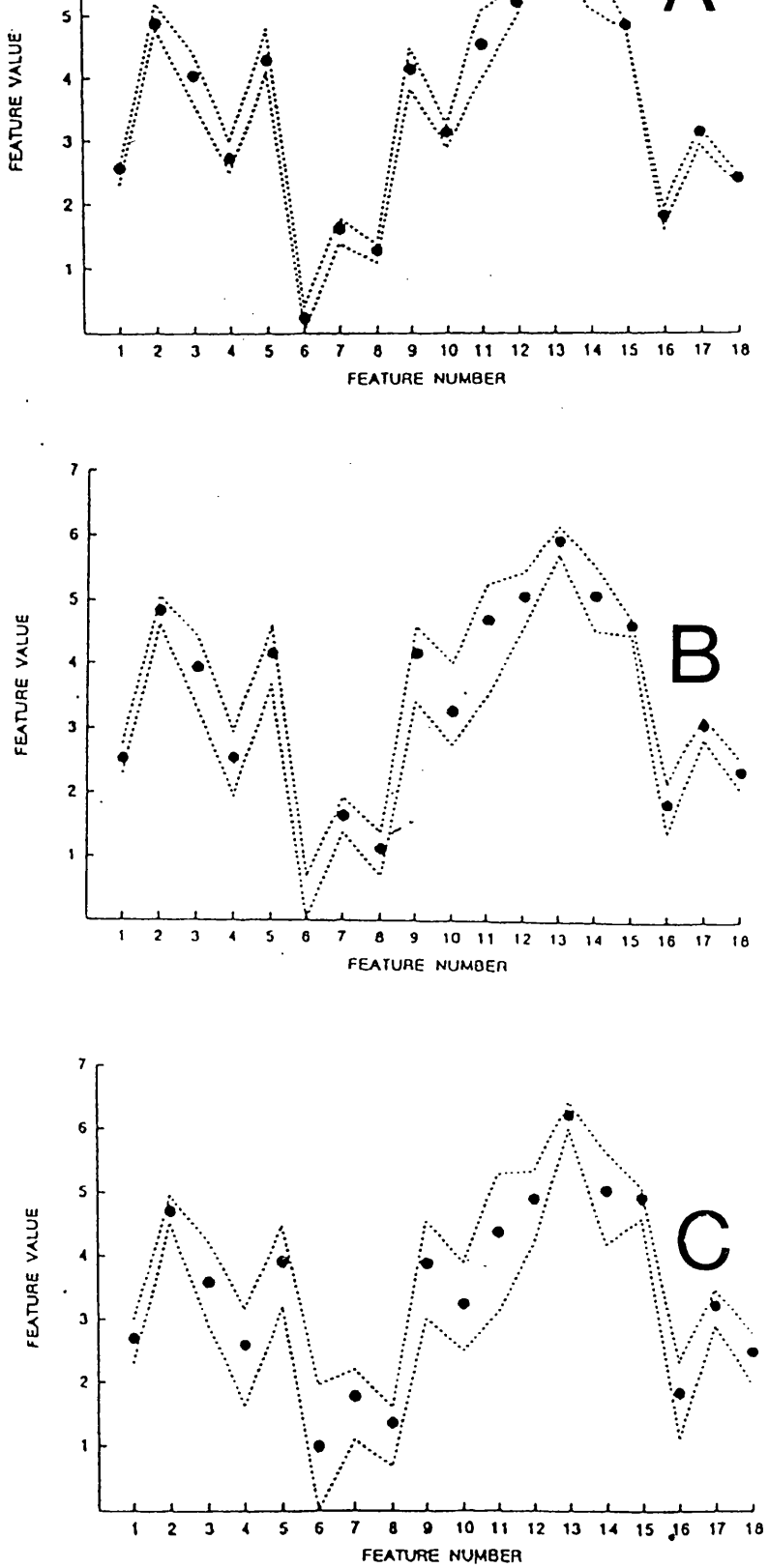

Fig. 5.12

Upper and lower boundary plots obtained using the CELREC program for a confluent monolayer of cells (panel A, G_1 = 75%), an eluted cell population (panel B, G_1 = 85%) and confluent spinner culture of cells (panel C, G_1 = 70%). All three samples have enriched G_1 fractions. The confluent monolayer of cells is the most homogeneous of the three cell samples in respect to cell size.

5.7.6 Centrifugal elutriation

5.7.6.1 Preparation of a single cell suspension

Centrifugal elutriation was carried out using a single-cell suspension. It has been reported that aggregates of cells in the cell sample affect the purity of cell separation (Meistrich *et al.*, 1977) and also increase the likelihood of a blockage developing in the separation chamber which inhibits separation. To improve the single cell purity of the sample the cell suspension was syringed through a 19 gauge needle immediately prior to loading. The cell sample was resuspended finally in MEM-S culture medium because it has a low calcium content. Calcium is known to be necessary for cell adhesion. Reducing the calcium concentration of the eluting buffer has been shown to reduce the degree of cell clumping and consequently improve the separation of cells (Sanderson *et al.*, 1977).

5.7.6.2 Development of the cell loading procedure

The method of loading the cells into the separation chamber that was recommended by the manufacturer was cumbersome to operate as it was designed primarily to prevent cells passing through the peristaltic pump used to drive the eluting buffer into the chamber. Using the recommended procedure often resulted in the introduction of air bubbles into the elutriator buffer lines which restricted the flow of eluting buffer into the separation chamber. After several unsuccessful attempts to load the sample using the recommended procedure, a new loading system was devised. Using this modified method, the sample was introduced through an 3-way injection valve directly into the eluting-buffer flowline, a procedure less prone to the introduction of air bubbles (see Fig. 5.13). Care was taken not to inject the sample too quickly as this would have increased the pressure within the system, a process which can fracture the joints in the buffer lines. To minimise further the build up of pressure during the loading of the sample the peristaltic pump was switched off once loading had commenced and restarted immediately once the procedure was complete. Using this method fewer air bubbles were introduced into the buffer lines and separation chamber and consequently fewer elutriation runs were terminated owing to air-bubble related blockages. Initially MEM-S culture medium was used as the eluting buffer and sample buffer which made it difficult to observe the cell sample entering the separation chamber. To overcome this problem the eluting buffer was changed to PBS

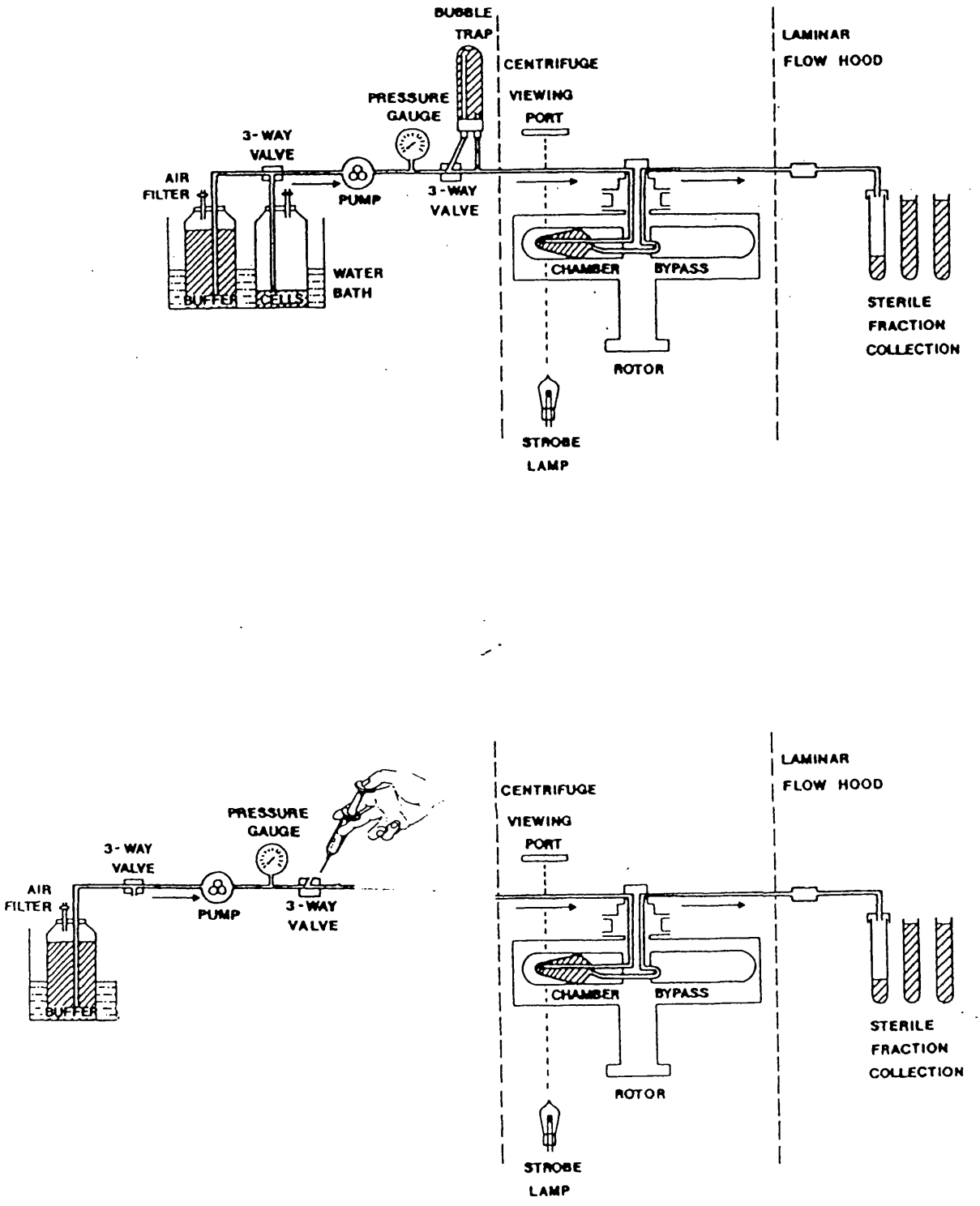

Fig. 5.13

Loading the cells into the elutriator. Upper panel: The recommended procedure for loading the cell sample into the elutriator. The cells are pumped through a bubble trap before entering the separation chamber. Lower panel: The modified procedure in which the cell sample was injected directly into the elutriation buffer line downstream of the pump and pressure value. This method eliminates the bubble trap.

which provided a discernable colour contrast from the sample medium.

5.7.6.3 Collection of cells eluted from the chamber

The cells reached equilibrium in the separation chamber forming a narrow band across it at an eluting-buffer flow rate of 20 ml min^{-1} in combination with a rotor speed (centrifugal force) of 2100 rpm. To elute cells, the rotor speed rather than the pump speed was reduced as this has been reported to be less disruptive to the cell boundary in the separation chamber (Keng *et al.*, 1980; van Es and Bont, 1980). Decreasing the rotor speed alters the balance of forces holding the cells in the separation chamber and therefore the smallest cells in the cell boundary are forced out of the chamber by the passage of eluting buffer through the chamber. The cells are harvested by collecting the eluting buffer as it leaves the rotor. A 50 ml volume of buffer was collected usually after each incremental decrease in rotor speed. To improve the proportion of S-phase cells in subsequent fractions 500 ml fractions of buffer were eluted occasionally after fraction 3 had been collected, in an attempt to remove all of the G_1 cells remaining in the chamber.

5.7.6.4 Determination of elutriation running parameters

Routinely the population of cells was separated into 9 fractions (designated F1-F9) and examples of the DNA distribution of the cells from each fraction are shown in Fig. 5.14. The cell cycle phase distribution of the population of cells to be separated was manipulated before the elutriation run by altering the growth conditions of the culture to enrich particular fractions. If an aim of the run was to harvest G_1 cells (e.g. elutriation run 7 and 9, see Fig. 5.14) then the starting population of cells was cultured at a high density to induce confluence (0.8-1.0 x 10^6 cells ml^{-1} of culture medium) thereby enriching the population in G_1 cells whereas for S phase elutriation runs (e.g. elutriation run 8) the culture was maintained at a lower density (4 x 10^5 cells ml^{-1} of culture medium) to ensure a log phase culture with a maximum S phase component. Generally, 90% of the cells loaded into the chamber were recovered in these fractions (F1-F9) the remaining 10% of cells were washed out of the chamber at the end of the run. The majority of the cells were eluted between fractions F2 and F7. The first fraction (F1) was usually discarded as this contained subcellular debris and most of the non-intact cells present in the original preparation. The last fraction (washed out

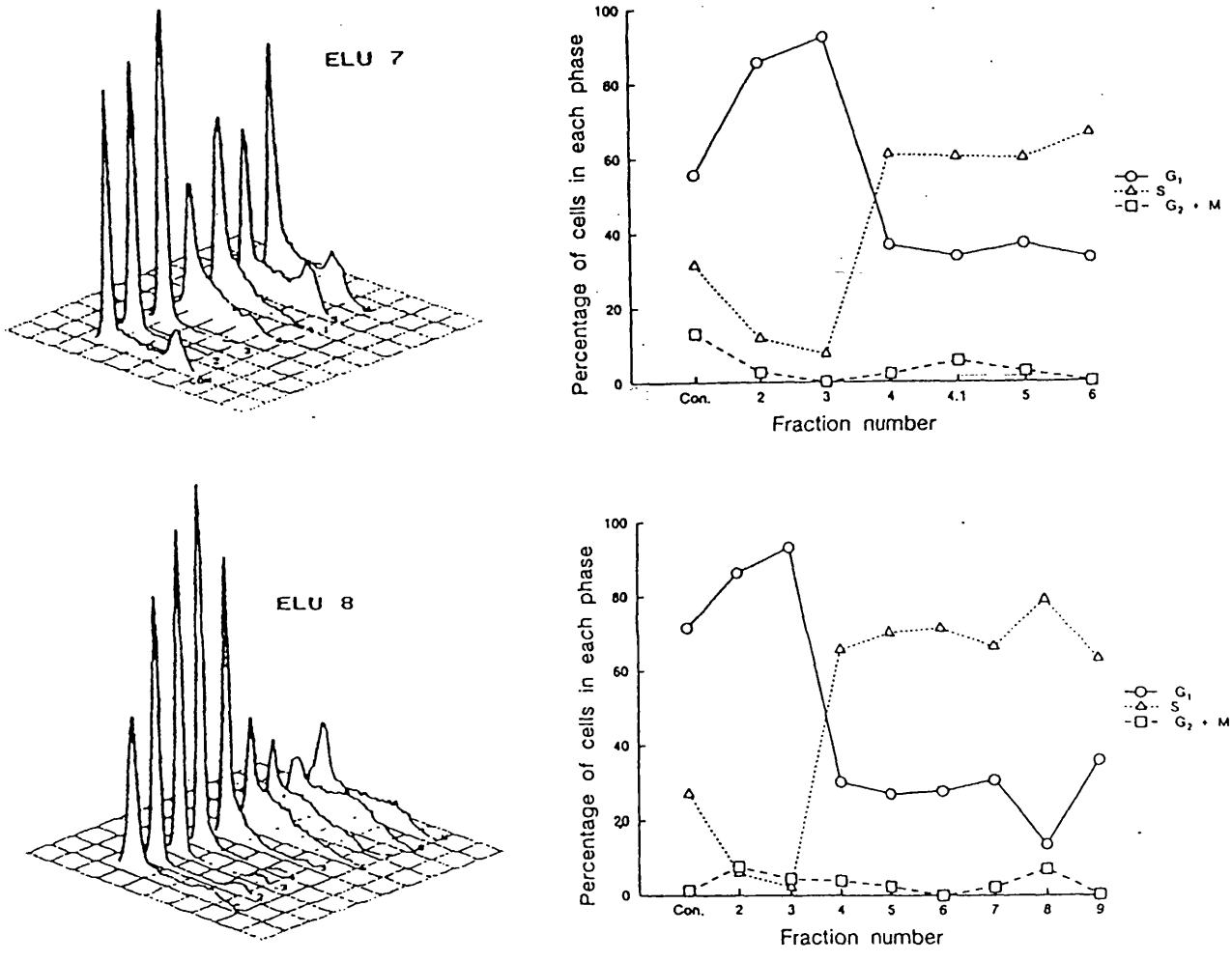

Fig. 5.14
DNA profiles and cell-cycle phase distributions of two typical elutriation runs, ELU 7 (upper panel) and ELU8 (lower panel).

at the end of the run) contained abnormally large cells and cells that were not eluted in the previous fractions. DNA histograms from three typical elutriation runs are shown in Fig. 5.14. The percentage of cells in G_1, S and G_2+M were calculated by the computer fit of these histograms and these are also shown. Fractions 2 and 3 typically contained few S or G_2+M phase cells. Fractions 4, 5 and 6 contained predominantly S phase cells. Fraction 8 of elutriation run 8 was the most enriched in S phase cells (over 75%). Fractions enriched in G2+M cells were rarely achieved. The experimental procedures of two typical elutriation runs to obtain G_1 phase cells (elutriation run 9) and S phase cells (elutriation run 8) are shown in Table 5.2 and 5.3. A flow rate of 20 ml min^{-1} of eluting buffer coupled with a centrifugation speed of 2028 rpm was most appropriate for collecting G_1 phase cells. A population enriched with 92.4% G_1 cells was obtained in elutriation run 8 (see Fig. 5.14). The most successful S phase harvest was achieved at 1400 rpm with a flow rate of 20 ml min^{-1}; 79.4% of the cells in the fraction were calculated to be in S phase. Despite reducing the rpm to below 1300 (elutriation run 9) the proportion of G_2 cells in any fraction could rarely be increased above 30%. This is probably due to the low initial proportion of cells in G_2+M in the starting population which rarely exceeded 10% of the total number of cells.

The distribution of the volumes of cells from an asynchronous cell suspension is broader than that from an early eluted (F3) and late eluted (F8) cell population (Fig. 5.15) as expected. The average volume of cells increased steadily with increasing fraction number as was evident by the broader distribution of feature values for cells from F8 compared to those from F3. The effect of separation by elutriation on cells was determined by incubating the cells in spinner culture for 3 days after which time a sample of cells was plated and the attachment efficiency determined. The clonogenicity of the cells was also assessed using the CSCAN program by scoring the number of cells which formed colonies of greater than 50 cells. No reduction in attachment efficiency, measured 3 days after separation, or clonogenicity, assessed over the period 3.5 days after separation, was seen for cells which had been eluted compared with non-eluted cells (Table 5.7).

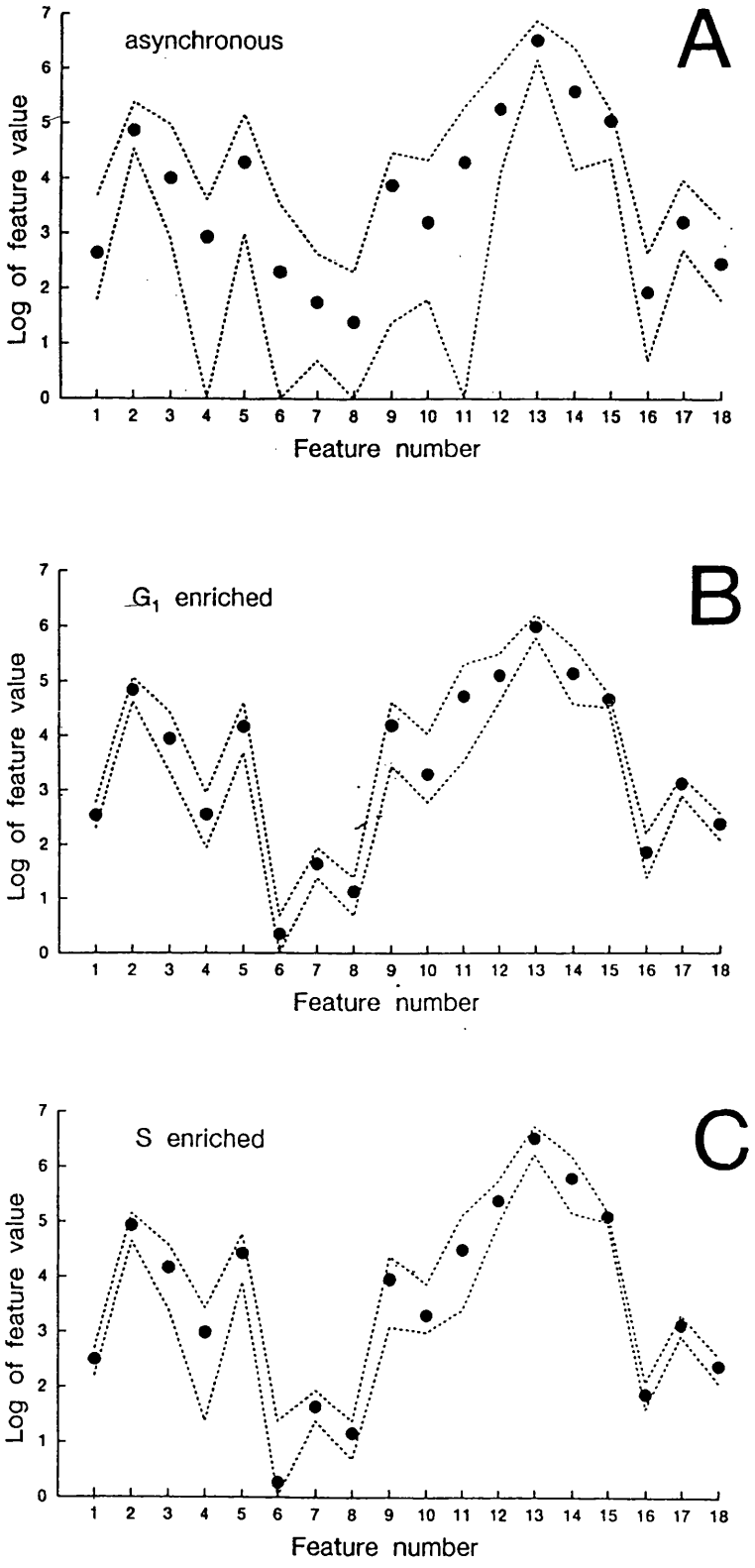

Fig. 5.15
Upper and lower boundary plots of an asynchronous (panel A), G_1 phase enriched (panel B) and S phase enriched (panel C) cell population. The G_1 and S phase cell populations have a narrow band between the upper and lower cell boundaries indicating a more homogeneous cell population with respect to cell size.

Cell population	Attachment efficiency	Clonogenicity(%)
Asynchronous	92 ± 4	98 ± 2
G_1 phase enriched (E6F3)	89 ± 6	96 ± 6
S phase enriched (E8F8)	90 ± 3	97 ± 9

Table 5.7 *Plating efficiency (% ± SD) and clonogenicity (% ± SD) for an asynchronous, G_1 enriched and S phase enriched cell population.*

The ability of cells to progress normally through the cell cycle following elutriation was assessed by measuring the DNA profiles of a sample of cells immediately following elutriation and from an aliquot of cell from the same sample, 4 and 20 hours after separation (Table 5.8).

	Cell cycle phase (%)		
time (h)	G_1 phase	S phase	G2+M
0	72.1	24.9	3.0
4	25.0	71.0	4.0
20	49.2	40.8	10.0

Table 5.8 *DNA distribution of the cell population immediately following synchronisation and at 4 and 20 hours post synchronisation.*

After 4 hours of incubation at 37°C following separation, the proportion of cells in G_1 had fallen to 25.0% from 72.1% measured at time zero while the proportion in S phase had risen from 29.9% to 71%. The distribution of the volumes of the cells in the population also increased as would be expected as S phase cells are larger than G_1 cells (Fig. 5.16). After 20 hours of culture the proportion of cells in G_1 and S were similar indicating a loss of cell synchrony.

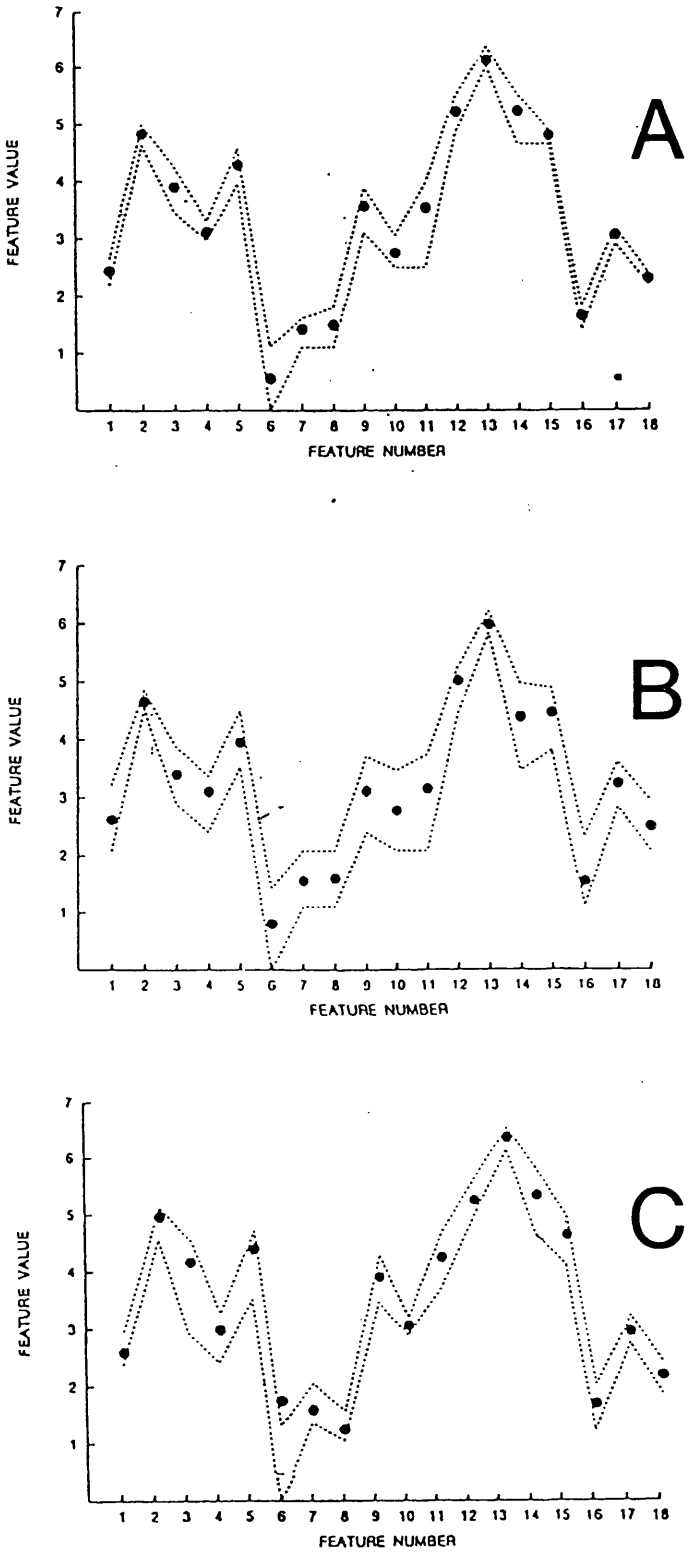

Fig. 5.16

Upper and lower boundary feature plots illustrating the loss of cell synchrony by an increase in the heterogeneity of the cell sizes in the sample. The width of the band between the boundary limits increases with time, 0 h (panel A), 4 h (panel B) and 20 h (panel C).

Using the DMIPS cell analyser it was found that the G_1-enriched cell sample showed negligible cell division for up to 8 hours after separation as would be expected, because insufficient time had elapsed for the cells to progress through the S and G_2 phases of the cycle to mitosis. However, 12 hours after separation, 87% of cells were assessed as having divided. This was determined using the RSCAN program by plating the cells, locating them and then scoring manually the number of cells which had divided to produce two daughter cells (Table 5.9). Approximately 74% of cells from fractions enriched in S phase cells had divided within 6 hours of separation and 94% within 12 hours (Table 5.9).

	Time after plating (h)		
Cell cycle phase	6 h	8 h	12 h
G_1 phase	-	15%	87%
S phase	74%	-	94%

Table 5.9 *Percentage of cells scored manually as having divided 6, 8 and 12 h after cell plating.*

5.8 Method of synchrony selected to construct DMIPS recognition algorithms

The cell analyser identifies objects by comparing the optical image from the located object with a master signal generated from a large sample of cells representative of that cell line. Consequently, synchronisation procedures which distort the shape of a cell are not desirable as they affect the optical properties of the cell and therefore the recognition accuracy of the cell anaylser. The aim of this part of the thesis was to measure the dependence of the radiation response of cells on the phase of the cell cycle over the dose region 0.2-0.6 Gy. It was therefore necessary to investigate methods of synchronising cells (section 5.7) to obtain samples enriched in each phase of the cell cycle. Essential requirements of synchrony were that the shape of the cell was not disrupted and that the normal progression of cells through the cell cycle was not affected. Disrupting the shape and size of the cell reduces the possibility of the cell being recognised by the cell analyser. The only methods of cell synchrony

that did not change the shape and size of the cells were centrifugal elutriation and growing cells to confluence. However, synchronisation via confluent culture was not reproducible, despite the high levels of cell synchrony that were often achieved. Enriched populations of cells obtained by elutriation were therefore used as a 'learning' population of cells to construct new cell-cycle phase-specific recognition algorithms. Enriched populations of G_2 and mitotic cells could not be obtained with a high degree of purity using any of the synchronisation methods investigated. Therefore, cell-cycle specific algorithms could not be constructed to identify G_2 or mitotic cells.

5.9 Development of algorithms for recognising individual phases of the cell cycle

The ultimate aim of synchronisation was to investigate the dependence of the measurement of surviving fraction on the phase of the cell cycle and to construct new recognition algorithms using the CELREC program so that cells from particular phases of the cell cycle could be located from within an asynchronous cell population. The eluted cell populations with the highest degree of cell synchrony were used as test populations to construct new cell-cycle specific algorithms. Although other methods of synchrony achieved phase-enriched cell populations the size distributions of cells in these samples was poor or they were not reproducible and therefore not ideal for constructing new algorithms.

5.9.1 Testing the new recognition algorithms

The efficiency of the new algorithms was tested using the CSCAN program on asynchronous, G_1 phase enriched and S phase enriched cell populations (Table 5.10).

	Phase of cell cycle (%) measured by flow cytometry		
Eluted cell population	G_1	S	G_2 + M
G_1 enriched	89.0	10.5	0.5
S enriched	15.5	71.6	12.8
asynchronous	51.3	43.1	5.6

Table 5.10 The DNA distributions of cell populations determined by flow cytometry which were used to test the new recognition algorithms The table shows the fraction (%) of cells in phase of the cell cycle.

The DMIPS S phase parameter file recognised 71% of the cells in the S phase-enriched cell population obtained by elutriation but only 14% of the cells in the G_1 phase enriched cell population. Several feature values of the G_1 cells were smaller than the lower boundary of particular features that make up the S phase parameter file explaining why the G_1 cells were not recognised by the S phase algorithm. The G_1 phase parameter file recognised 80% of the cells in the G_1 phase enriched cell population but only 12%, on average, of the S phase cells. The larger S phase cells did not fall within some of the upper boundary limits of the G_1 phase parameter file and consequently were not recognised. The asynchronous parameter file recognised 90-95% of cells in both of the S and G_1 phase enriched cell populations.

Additional experiments were performed to compare the identification of cells from within an asynchronous cell population by the phase specific recognition algorithms with S phase specific staining and manual scoring of G_1 phase cells. The fraction of cells in each phase of the cycle in the asynchronous, G_1 and S phase enriched cell samples used to test the recognition algorithms was determined by flow cytometry. Staining with BrdUrd was used to determine the number of cells in S phase in a monolayer culture of cells and the number of cells in G_1 was measured by scoring the number that had divided after 8 hours but before 12 hours. The G_1 algorithm scored 80% of the cells in the G_1 enriched cell sample as being in G_1; 87% of these were manually scoring as having divided in the 8-12 h period. Flow cytometry indicated that 89% of the cells in the sample were in G_1. The S phase algorithm detected 71% of the cells in the S phase enriched cell population as being in S phase, BrdUrd staining suggested that 84% of these scored cells were in S phase. Flow cytometry measured 71% of the cell sample as being in S phase.

5.9.2 Testing the S phase and G_1 phase parameter files

Cell survival curves were generated for G_1 and S phase-enriched cell populations obtained by elutriation and RBE values calculated. The following day cell survival curves were produced for G_1 and S phase cells selected from within an asynchronous cell population using the DMIPS cell-cycle phase-specific recognition

algorithms. The pattern of RBE against X-ray dose that was obtained was similar in both experiments (Fig. 5.17). The increase in radioresistance that occurs over the X-ray dose range 0.2-0.6 Gy, reflected by an increase in RBE over the same dose range is therefore unlikely to be due to a radiosensitive subpopulation of cells from one of the phases of the cell cycle. If the increase in radioresistance over the dose range 0.2-0.6 Gy was due to the response of cells in a single, radiosensitive phase of the cell cycle then it is likely that only the radiosensitive cell cycle phase would show the increasing radioresistance over the range 0.2 -0.6 Gy and that the other phases would exhibit a response comparable with an LQ model i.e. without the low-dose X-ray hypersensitivity. As the increase in radioresistance was seen experimentally to occur in two distinct phases of the cell cycle the phenomenon of an increasing radioresistance over the dose range 0.2-0.6 Gy is unlikely to be due to a single phase of the cell cycle and therefore the phenomenon is probably in dependent of the phase of the cell cycle.

The method of measuring cell survival using the phase specific recognition algorithms, by selecting cells of a particular phase of the cell cycle from within an asynchronous population, produced quantitatively similar results to measuring the survival of synchronised populations of cells using an asynchronous paramater file (Fig. 5.18, 5.19).

Cell-cycle phase recognition algorithms were not constructed for G_2 or mitotic cells as a sufficiently-synchronised unperturbed population of cells could not be obtained.

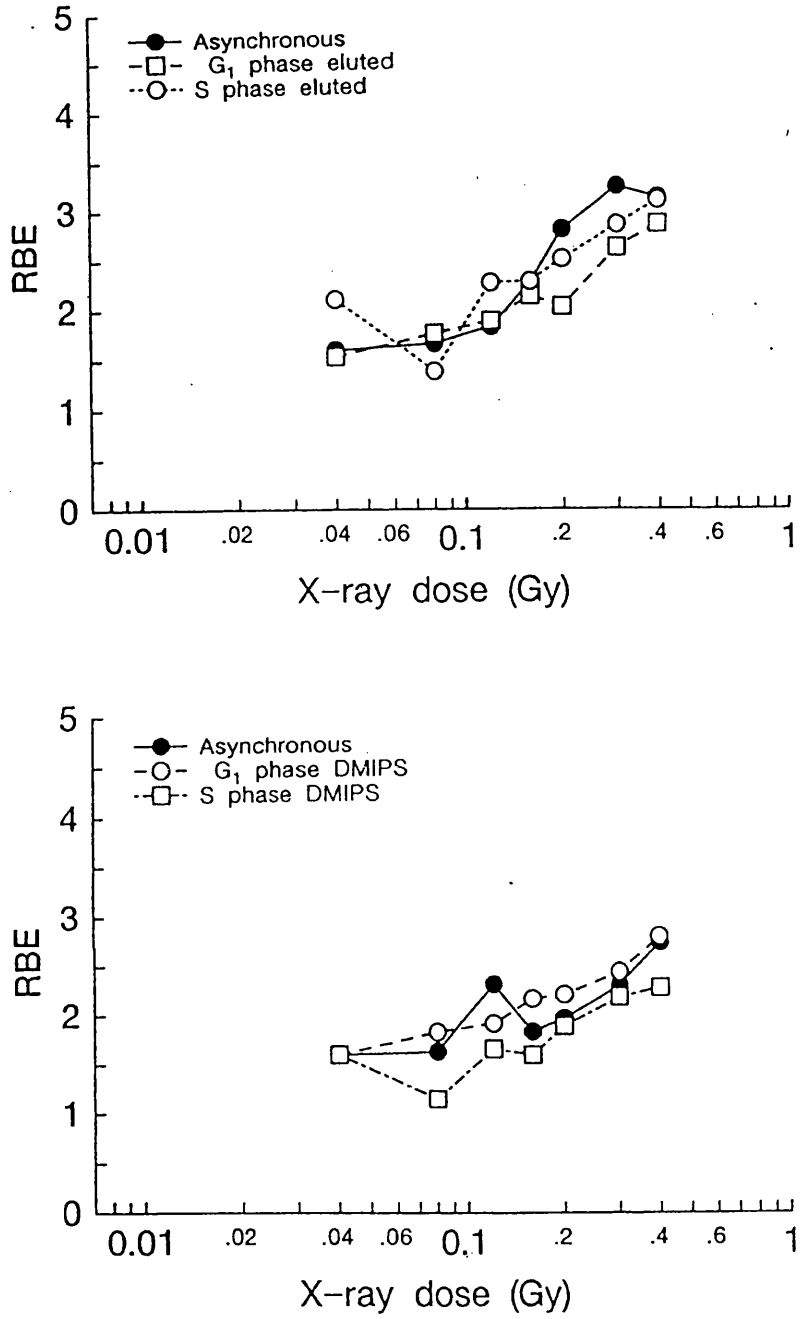

Fig. 5.17

RBE values between 250 kVp X-rays and d(4)-Be neutrons for asynchronous, G_1 enriched and S enriched cell populations. The data in the upper panel was generated using an asynchronous parameter file on each of the three cell samples obtained by elutriation whereas the lower panel was generated with the cell-cycle phase recognition algorithms on three comparable cell samples. The increase in RBE over the X-ray dose range (0.04-0.4 Gy) reflects an increase in X-ray radioresistance over the same range occurs. The same pattern of RBE against X-ray dose is seen in the enriched cell populations obtained by elutriation and the asynchronous cell population.

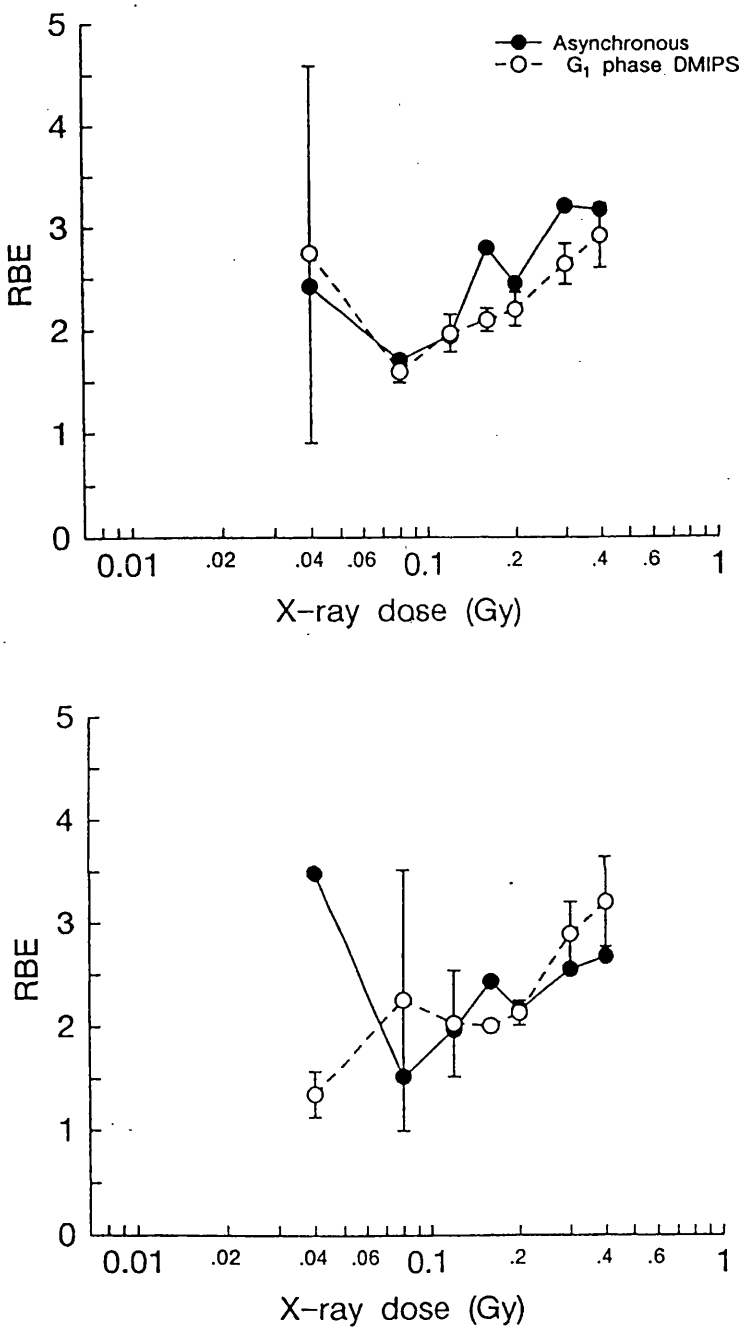

Fig. 5.18

RBE between 250 kVp X-rays and d(4)-Be neutrons for asynchronous cells, and G_1 cells recognised using the DMIPS G_1 phase recognition algorithm. The algorithm eliminates the need to synchronise the cells as it locates and recognises G_1 phase cells from within the asynchronous cell population. The increase in RBE over the dose range 0.4-1 Gy was seen in the G_1 phase cells (open symbols mean ± SEM) and in the asynchronous cells. The two panels represent two separate experiments.

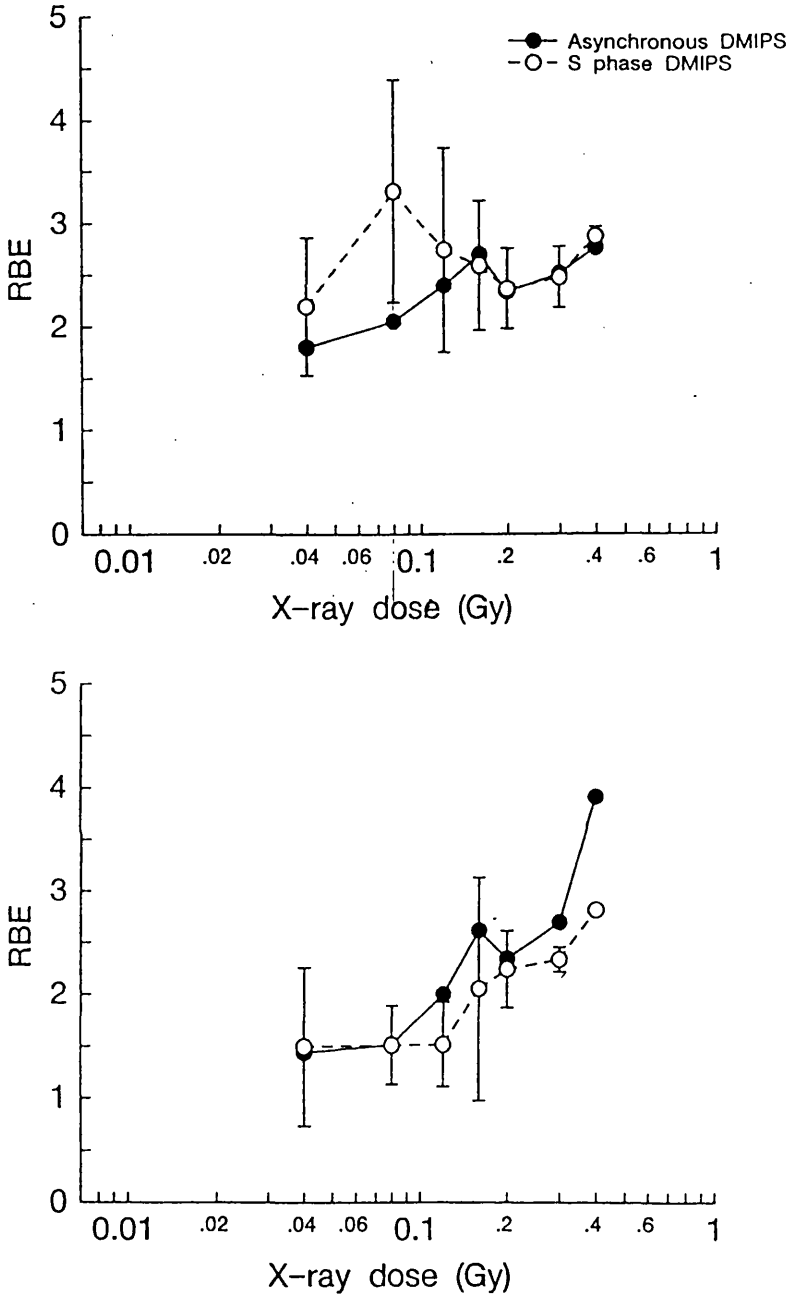

Fig. 5.19

RBE between 250 kVp X-rays and d(4)-Be neutrons for asynchronous cells, and S cells recognised using the DMIPS S phase recognition algorithm. The algorithm eliminates the need to synchronise the cells as it locates and recognises S phase cells from within the asynchronous cell population. The increase in RBE was seen in the S phase cells (open symbols mean ± SEM) and in the asynchronous cells. The two panels represent two separate experiments.

5.10 Summary

1. The technique of mitotic selection was not suitable for the cell line used in this study. Repeated attempts at harvesting mitotic cells failed to produce a highly synchronised cohort of cells. This highest level of synchrony achieved was a 39% enrichment of mitotic cells.
2. A high degree of cell synchrony was obtained when spinner and monolayer cultures of cells were grown to confluence. The G_1 fraction was enriched to 77% at maximum. However, this method was not a reproducible or consistent method of producing highly synchronised cells.
3. The highest degree of cell synchrony was obtained using hydroxyurea (0.33 mM for 6 hours), with 97% of cells in S phase. The cells were atypical in size and shape however, and therefore, this method of synchrony was not compatible with assessing cell survival using the DMIPS cell analyser.
4. Centrifugal elutriation was found to be the most reproducible and reliable method of producing large numbers of synchronised cells without causing any distortion to the size and shape of the cells.
5. Using centrifugal elutriation, enriched populations of G_1 phase cells (92% at maximum) and S phase cells (80% at maximum) were routinely obtained.
6. G_1 and S phase specific recognition algorithms were constructed from enriched cell populations obtained by elutriation, enabling G_1 and S phase cells to be located and recognised from within an asynchronous cell population *without* the need for synchronisation.
7. Enriched populations of G_2 and mitotic cells were not obtained by any method of synchronisation used, therefore cell cycle specific recognition algorithms for G_2 and mitotic cells could not be developed.
8. The proportion of cells in the G_1 phase of the cycle, determined by the phase specific recognition algorithm, compared favourably with the actual number of G_1 phase cells in the cell sample as determined by flow cytometry. DNA analysis indicated 89% of cells in a particular cell sample were in the G_1 phase and the G_1 specific algorithm scored 80% of located cells as being in G_1.

9. The S phase specific recognition algorithm detected 71% of the cells in a S phase enriched cell population as being in S phase while BrdUrd staining which is specific for S phase cells suggested that 84% of the *scored* cells were in S phase.

10. The increase in radioresistance over the X-ray dose range 0.2-0.6 Gy that was observed in the asynchronous cell population was also seen in G_1 phase enriched and S phase enriched cell samples. The same pattern of RBE against X-ray dose that was obtained for the synchronised cell samples that were obtained by elutriation was also seen using the cell cycle specific recognition algorithms.

11. The production of cell cycle specific recognition algorithms removed the need to synchronise the cells to assess the radiation response of specific phases of the cell cycle.

12. As the increase in radioresistance over the X-ray dose range 0.2-0.6 Gy was seen in G_1 phase and S phase cells then the phenomenon of a change in radiation resistance with increasing X-ray dose is unlikely to be due to cells in a single radiosensitive phase of the cell cycle.

5.11 Discussion

In mammalian cell lines which have a short G_1 phase, the cells in late S are typically the least radiosensitive while those in mitosis are the most sensitive (Sinclair and Morton, 1966). The biphasic survival curves observed in this thesis might therefore be due to the differential killing between sensitive mitotic and G_2 phase cells and resistant late S phase cells in the asynchronous cell population. If this is the explanation for the biphasic survival curve then the initial steep region of the survival curve (< 0.2 Gy) would reflect the response of the radiosensitive subpopulation of mitotic or G_2 cells. However, mathematical modelling of the experimental data using a two subpopulation model (see chapter 4) suggested that the sensitive subpopulation must be ≈3% of the entire asynchronous cell population and the cells must be nearly ≈50x more radiosensitive than the resistant cell population (e.g. late S or G_1) for the data to be explained by this concept. The largest differential reported in the literature for differences in radiosensitivity between cells in each phase of the cell cycle for a

mammalian cell line *in vitro* exposed to low dose radiation was approximately 10 fold (Sinclair, 1968). At higher X-ray doses however a larger differential was reported. This is significantly lower than required to explain the data in this study which suggests that the biphasic survival is unlikely to be the manifestation of the killing of a sensitive subpopulation of cells in a particular phase of the cell cycle.

However, an assumption of the two subpopulation model used in chapter 4 was that the two subpopulations of cells were static i.e. they were not progressing through the cell cycle. This situation does not reflect the true experimental situation. Cells in the two subpopulations would be continually cycling through the mitotic cycle entering and leaving radioresistant and radiosensitive phases. The radiation-induced arrest of the progression of cells in the cell cycle is a well recognised phenomenon during low dose and low dose-rate irradiation (Doida and Okada, 1969). Irradiated cells will progress through the cell cycle until they reach specific points where subsequent progression will be inhibited e.g. at the G_1/M boundary and in regions of the G_2 and mitotic phases of the cell cycle (Walters and Petersen 1968, Leeper *et al.* 1973). This phenomenon can result in the accumulation of cells in a radiosensitive and radioresistant phases of the cell cycle during prolonged irradiation. The cell-cycle redistribution following irradiation has been suggested as an important factor in the radiation response of cells to low X-ray dose rates ranging from 1 - 5 cGy min^{-1} (Mitchell *et al.*, 1979). The lowest dose rate used in this study falls into this range. The data reported in this thesis might therefore reflect a situation where at low dose rates normal progression of the cell cycle in a radiosensitive phase may be differentially delayed compared with a radioresistant phase of the cell cycle resulting in an accumulation of cells in that particular radiosensitive phase of the cell cycle and thereby producing an extra radiosensitive component in the cell cycle not considered by the static two subpopulation model. The hypersensitive, low dose X-ray response over the X-ray dose range 0.01-0.6 Gy might represent the response of such a cell population, if it exists. Therefore, it was important to investigate the radiation response of synchronised populations of cells as it has been reported that in some cell lines that cell cycle redistribution after low dose-rate irradiation in exponentially growing cultures of cells appears to be a more important factor than repair in determining the dose-rate effect (Oftebro and Nordbye, 1969) and to eliminate effects of the cell cycle

as a cause of the hypersensitive response.

Before the dependence of radiosensitivity on cell-cycle phase could be determined, samples of cells had to be obtained which were enriched in the various phases of the cell cycle. Many of the methods of achieving cell synchrony cited in the literature involve the blockage of cells in a specific phase of the cell cycle by either cytotoxic and/or cytostatic agents or the deprivation of essential nutrients from the culture medium (see Nias and Fox, 1970). However, these methods of synchrony often cause perturbations in the progression of cells through the cell cycle and give rise to cells atypical in size (Grdina *et al.*, 1984; White *et al.*, 1984). In the low dose DMIPS recognition assay alterations to the size and shape of the cell as a result of the synchronisation process are important. The cell analyser locates, recognises and characterises cells based on their optical properties which reflects the physical shape and size of the cells. Therefore, disruption to these parameters will affect the efficiency of cell recognition. This will be particularly important if, for example, a particular method of synchronisation disrupts only a small subset of cells in the total cell population e.g. cells in a particular phase of the cell cycle as these cells will be discriminately excluded from any cell sample that is assayed using a recognition algorithm. This effect of synchronisation is not usually critical in a conventional clonogenic assay because the cells are not individually located and therefore this represents a unique problem for the recognition assay compared with other methods of studying the cell cycle. It is imperative that any methods of cell synchrony that are used in conjunction with the DMIPS recognition assay do not disrupt the size and shape of the cells.

A change in the distribution of the volumes of the cells in the synchronised cell sample can be used to give an index of disruption to the cell size and shape caused by the synchronisation procedure (Meistrich, 1977; Grdina *et al.*, 1984). This distribution is usually determined using a Coulter counter and multichannel analyser. In this method, when a cell is recorded by the Coulter counter an index of cell volume is instantly obtained by measuring the alteration to the current across the two electrodes. A new method was used in this study. A large sample of cells was located manually using the cell analyser and the 18 features of the recognition signal

measured using the CELREC program. The statistical range of the values from each cell feature was then used as an index of the cell sample homogeneity (see section 5.7.2). A large range of feature values indicated a large size and shape heterogeneity and therefore poor synchrony (see Fig. 5.6).

In this study, commonly used methods of cell synchrony were compared with each other by measuring the level of synchrony achieved and any disruption that was caused to the size and shape of cells as a result of synchronisation. Analyses of mitotically selected cells indicated a poor level of cell synchrony (30-50% of mitosis) but very little disruption to the volume homogeneity of the cells. In contrast, the G_1 cell populations obtained by centrifugal elutriation, HU treatment and from confluent cultures of cells were highly synchronised (see section 5.8). The results of the mitotic selection were disappointing because the technique was experimentally simple and gave no significant disruption to the cell size which are ideal attributes for the recognition assay. Higher levels of synchrony have been achieved using this method in other studies. In some cases populations of 95% mitotic cells have been obtained routinely from a CHO cell line (Robbin and Marcus, 1964) and 80-90% in V79 cell lines (Peterson *et al.*, 1969) However, mitotic selsection was not suitable for synchronising the V79 subline used in this thesis probably because this particular subline has been developed originally to grow as a spinner culture.

Synchrony by HU treatment (Sinclair, 1967) caused gross perturbations to the size and shape of cells as indicated by the feature boundary plots (Fig. 5.9) and the DNA analysis of the cell samples (Fig. 5.7) (see section 5.7.4). This was unfortunate because large numbers of highly synchronised cells were obtained using this method. This result was not unexpected however, as HU treatment has been reported previously to cause cell cycle disruption (Sinclair and Morton, 1963). Although a good level of synchrony was obtained this method was not suitable for use with the recognition assay because the cells that were harvested were atypical in size, shape and optical properties and therefore would not be recognised as cells by the DMIPS recognition parameter file.

The methods investigated of achieving cell synchrony using confluent cultures of cells produced large numbers of highly synchronised cells with little disruption to the cell (see section 5.7). These methods combined the advantages of HU treatment (high yield, see section 5.7.4) and mitotic shake off (little disruption to the size of the cells, see section 5.7.3) without the disadvantages of these methods. However, as a method of achieving synchrony confluence was inconsistent and unreliable. It was also difficult to predict the time cell confluence would be achieved and therefore the onset of cell synchrony. To harvest the synchronised cells from the monolayer cultures of confluent cells trypsinisation treatment was required. This procedure was observed to effect the optical properties of cells which in turn effected the procedure of cell recognition. Some cells were therefore were less likely to be recognised by the cell analyser following trypsination.

Centrifugal elutriation proved to be the most reliable and consistent method of producing large numbers of synchronised cells (see section 5.7.6). It was also possible to obtain cells in two different phases of the cell cycle within a single experiment, G_1 and S, which was an immediate advantage over the other methods of synchrony investigated. Cell synchrony by elutriation offered several other advantages. The method was rapid, in that large numbers of asynchronously grown cells could be separated within 30 - 45 minutes into subpopulations enriched with cells in various stages of the cell cycle. The cells are separated at room temperature in culture medium and are therefore not subject to any cytotoxic or cytostatic agents. One disappointing feature of this method was the failure to synchronise cells in the G_2 or M phases of the cell cycle, since other workers have reported reasonable degrees of synchrony of G_2 phase cells by elutriation (Keng *et al.*, 1981). This failure was probably due to the inherent heterogeneity of the size of cells in the G_2 phase. Centrifugal elutriation was the only method of cell synchrony investigated that was reproducible, predictable and gave consistently large numbers of highly synchronised cells with no disturbance to the volume heterogeneity of cells. In a study comparing different methods of cell synchrony Grdina *et al*,. (1984) also report that centrifugal elutriation was an excellent method of obtaining large numbers of synchronised mammalian cells with little disruption to the size of the synchronised cells. This method was therefore used in order to synchronise cells to be assayed using the DMIPS recognition assay.

The pattern of survival obtained from synchronised populations of G_1 and S phase cells was similar to that obtained for the asynchronous cell population obtained by elutriation. All three cell samples had biphasic survival curves (illustrated by the increase in RBE over the dose range 0.2-0.6 Gy) and exhibited an increase in radioresistance with increasing X-ray dose over the range 0.2-0.6 Gy. These data indicate that the low-dose X-ray hypersensitivity reported in this thesis (<0.2 Gy) was unlikely to be due to a radiosensitive subpopulation of cells from one cell-cycle phase. If either, the G_1 or S phase cells were responsible for the hypersensitivity at low doses then only *one* of these cell samples would exhibit the hypersensitive response while the other would exhibit a response compatible with a LQ model i.e. no evidence of a hypersensitivity response. However, as cells from both the G_1 and S phase enriched cell populations exhibited the hypersensitivity to low doses of X-rays then it is unlikely that this phenomenon is due to the response of a cells from a single radiosensitive phase of the cell cycle.

The aim of this chapter was not merely to measure the radiation response of synchronised populations of cells but also to calibrate the cell analyser to locate automatically and recognise cells in particular phases of the cell cycle. However, synchronised populations of cells were required to develop the cell-cycle phase recognition algorithms. It was for this reason that two aspects of cell synchronisation were addressed when examining the cell synchrony data; first, if a given synchronisation technique produced large numbers of highly synchronised cells and second, if the synchronisation technique caused disruption to the normal optical properties of the cell. Disruption to the cell cycle was assessed qualitatively by locating microscopically many cells by eye and quantitatively by measuring in excess of 1000 cells using the CELREC program. Of all the methods employed, only centrifugal elutriation provided high levels of cell synchrony and minimum disruption to the cell cycle yielding a homogeneous cell population with respect to cell size. This was also reported by White *et al.* (1984) in a study comparing elutriation with mitotic selection, flow cytometry cell sorting and mitotic selection in conjunction with mitotic selection. The size homogeneity of each cell sample separated by elutriation was expected as the procedure utilises the increase in cell size through the cell cycle (Anderson *et al.*, 1969; Glick *et al.*, 1971) as a criterion for separation. The cell-cycle

phase specific recognition algorithms were therefore formulated on cell populations synchronised by elutriation.

The cell-cycle phase specific recognition algorithms that were generated for G_1 and S phase cells using the CELREC procedure had a comparable recognition efficiency compared with the parameter file used to locate and recognise asynchronous cells (see section 5.9). The cells located by these recognition files were confirmed to be in the required phase by BrdUrd staining in the case of the S phase cells and time of division for G_1 phase cells (see section 5.9.2).

The efficiency of these recognition algorithms enabled accurate measurements of surviving fraction to be calculated *without* the need for the prior synchronisation of cells. This was important because the hypersensitivity to low doses of X-rays represented only a small change in radiation response and any synchronisation procedure which altered the normal biology of the cells might have effected the accurate measurement of cell survival and therefore reduced the increase in radioresistance that was seen over the X-ray dose range of 0.2-0.6 Gy. The same pattern of survival response was obtained for G_1 and S phase cells assayed using the cell-cycle phase recognition algorithms from within an asynchronised cell population and for a population of cells which had been enriched into a particular cell-cycle phase by elutriation. Both sets of data indicated that the phenomenon of low-dose X-ray hypersensitivity is independent of cell cycle phase and therefore is unlikely to be due to cells in a radiosensitive phase of the cell cycle.

Chapter 6: A phenomenon of X-ray dose rate?

6.1 Introduction: Dose-rate phenomena

Dose rate is an important factor in determining the effectiveness of ionising radiation. In the experiments described in this thesis so far, the dose rate has varied from 0.016 Gy min^{-1} to 1.7 Gy min^{-1} to ensure precise dosimetry (see section 3.4.2). Over this range of dose rates several factors have been reported to effect the radiosensitivity of cells (Hall, 1972) (Fig. 6.1). In a review of radiation dose rate effects (Steel *et al.*, 1986) three critical processes were identified. The precise dose rate for each of these processes will be cell line dependent.

6.1.1 Repair of radiation-induced lesions

A change in the biological effectiveness of a given dose of sparsely-ionising (low LET) X-rays has been reported to occur over the range of dose rates used in this V79 study: lower dose rates were less effective at cell killing than higher dose rates (e.g. Mitchell *et al.*, 1979)(Fig. 6.2). This reduction in cell killing results in a reduction in the slope of the cell survival curve. This necessity for an 'extra' radiation dose to achieve the same degree of cell kill was attributed to the repair of a greater proportion of radiation-induced lesions during the longer exposure period associated with the lower dose rate.

6.1.2 Redistribution through the cell cycle

As the dose rate is lowered the exposure time required to give an acute dose of radiation may approach a time equivalent to the length of the cell cycle. Often when this occurs perturbations to the normal progression of cells through the cell cycle can be detected. Lowering the dose rate further a critical dose rate is reached where any additional reduction in dose rate becomes more damaging, giving an increased level of cell kill rather than being less effective as would have been predicted owing to dose-rate sparing (see Fig. 6.3). This apparent increase in radiosensitivity is due to a phenomenon known as the inverse dose rate effect (Bedford and Mitchell, 1973; Mitchell *et al.*, 1979).

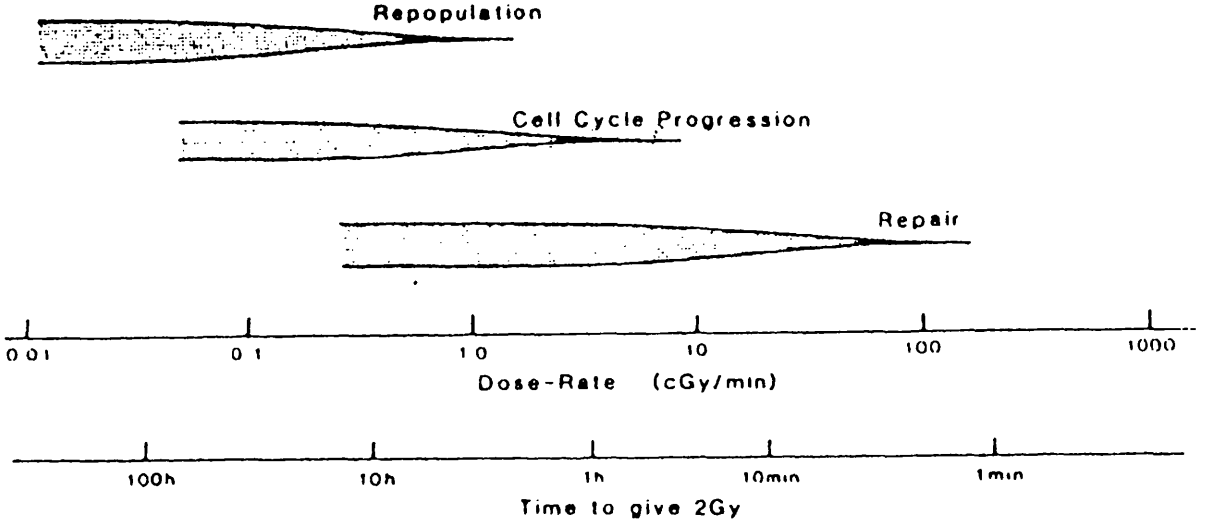

Fig. 6.1

The three principal processes that influence the response of cultured cells to low dose-rate irradiation. The horizontal axis indicates the range of dose rates and duration of exposure (for a dose of 2 Gy) at which each of the processes becomes important (reproduced from Steel et al., 1986).

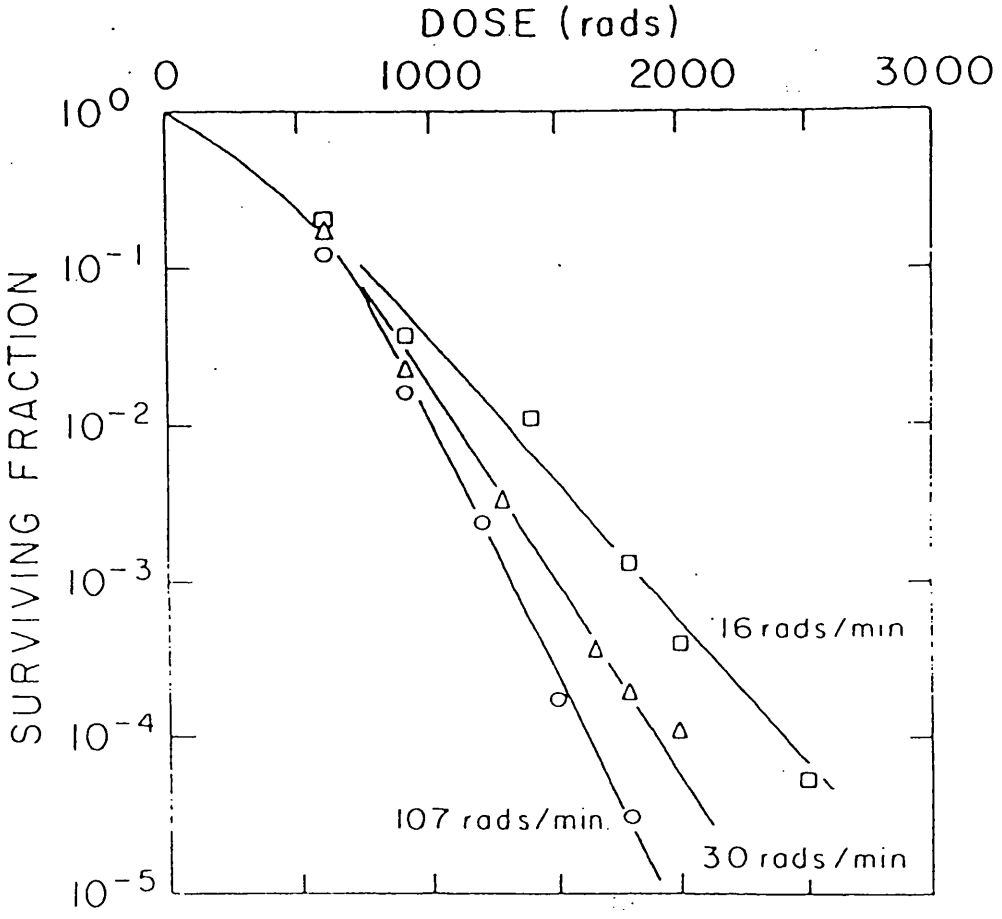

Fig. 6.2

The survival of Chinese hamster cells after exposure to ^{60}Co γ-rays at three radiation dose rates. The decrease in the slope of the survival curve with a decrease in dose rate is due to the repair of proportionally more radiation-induced lesion during the period of the radiation exposure (from Hall, 1972).

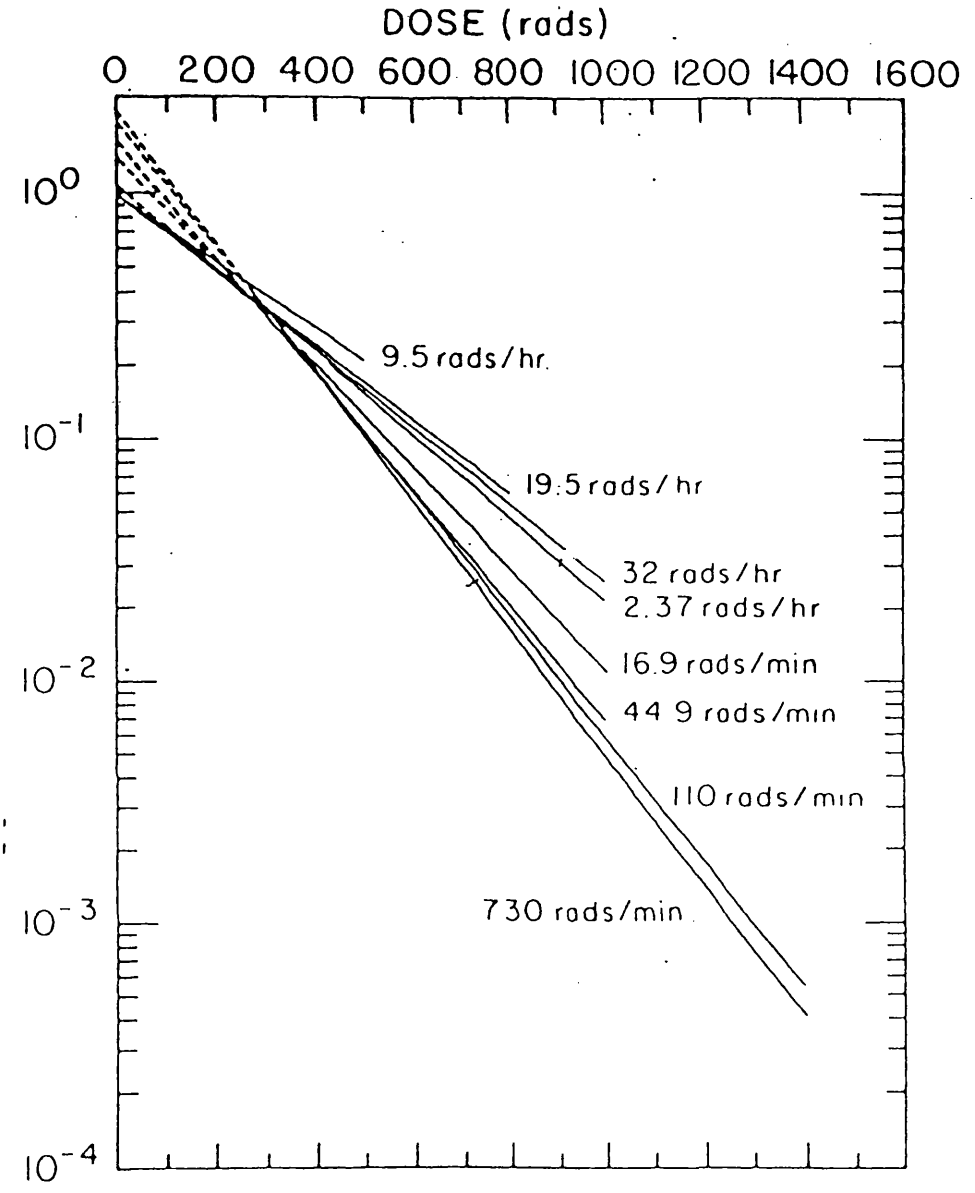

Fig. 6.3
Survival curves for HeLa cells exposed to X-rays over a range of dose-rates. A dose-rate of 32 rads/hr is less effective per unit dose at killing cells than a dose-rate of 2.37 rads/hr. This has been attributed to the inverse dose rate effect (reproduced from Hall, 1972).

The precise dose rate at which the inverse dose rate effect occurs will be cell line dependent. In general terms however, above a dose rate of 5 cGy min^{-1}, the progression of the cell cycle is usually inhibited and the overall radiation response of the cell population is the sum of the individual responses of each phase of the cell cycle. As the dose rate is reduced below 5 cGy min^{-1}, the progression of cells through the cell cycle is no longer inhibited and cells begin to proceed through the intermitotic stages of cell cycle. Mitosis, however, still remains inhibited leading to an accumulation of cells at the G_2/M boundary in the G_2 phase of the cell cycle. The G_2 phase of the cell cycle is particularly radiosensitive compared with the other phases of the cell cycle, and as the majority of the cells are accumulated in this phase an increase in the radiosensitivity of the total cell population is seen. Consequently, cells irradiated with a dose rate below 5 cGy min^{-1} have steeper cell survival curves, than those survival curves obtained from cells irradiated at a higher dose rate of 5 cGy min^{-1} reflecting the increased radiosensitivity. As the dose rate is reduced further to approximately 2 cGy min^{-1}, mitosis is no longer inhibited and proceeds normally. Therefore, the cell population will redistribute through all the phases of the cell cycle as cell progression occurs. The undamaged cells in the population pass through mitosis and enter more radioresistant phases of the cell cycle characterised by shallower survival curves. The slope of the survival curve derived for the total cell population is therefore seen to increase and then decreases as the dose-rate is reduced from above 5 cGy min^{-1} to below 5 cGy min^{-1}, giving the 'impression' that a lower dose rate is more effective at killing cells than a higher dose rate.

6.1.3 Cell proliferation

At dose rates below about 2 cGy min^{-1}, cell progression is not inhibited and cell proliferation can occur during long radiation exposures. 'New' cells can then be born into the population to replace some cells killed by the radiation. To achieve the same level of cell killing when cells are irradiated with an extremely low dose rate (<2 cGy min^{-1}) compared with a higher dose rate ($>>2$ cGy min^{-1}) a greater dose has to be given to compensate for this. The biological effects of exposure to continuous very low dose rate radiation *in vitro* are assessed usually by measuring the disruption caused to the normal growth-rate of the cell population. Nias and Lajtha (1964) reported that the exposure of HeLa cells to β-rays from tritiated water at dose rates

of 30 to 300 cGy day^{-1} only reduced slightly the number of cells expected after 11 days of culture compared with a sample of non-irradiated cells cultured over the same period. This was because cell death resulting from the radiation exposure was compensated for by the proliferation of cells during the exposure period. Courtenay (1965) however, reported an increase in the cell cycle time of mouse lymphoma cells from 10.8 hours, measured in non-irradiated cells, to 14.3 hours when irradiated continuously at a dose-rate of 72 cGy day^{-1} for a period of 8 months.

In this study an increase in radioresistance has been reported to occur over the X-ray dose range 0.20-0.60 Gy (see Fig. 3.3). However, cell survival was assessed routinely over this dose range using two X-ray dose rates, namely 0.016 and 0.44 Gy min^{-1} (Table 6.1). It is important, therefore, to determine if the increase in radioresistance seen over this dose range was due to an artefact of changing the X-ray dose rate or a consequence of the different exposure times that resulted from the change in X-ray dose rate.

6.2 Aims

The experiments reported in this chapter of the thesis were designed to compare the measurement of cell survival using the conventional experimental procedure, in which the dose rate is dependent on the dose actually given (Table 6.1), with the measurement of cell survival obtained using the three individual X-ray dose rates (0.016, 0.44 and 1.7 Gy min^{-1}, Table 6.2) over the X-ray dose range 0.04-1.0 Gy. A second series of experiments were designed to compare the measurement of cell survival obtained using the conventional experimental procedure in which the exposure time was dependent of the dose given (Table 6.1) with the measurement of survival obtained using three fixed exposure times at each level of dose (10sec, 2 and 10 min, Table 6.3) achieved by altering the X-ray dose rate. These experiments would determine if the increase in radioresistance over the X-ray dose range 0.20-0.60 Gy was dose-rate dependent or exposure-time dependent.

6.3 Materials and methods

Cells were irradiated either with 250 kVp X-rays (see section 2.4.1) (Table 6.1) or 2.5 MVp X-rays produced by the Van de Graaff accelerator (see section 2.4.2) (Tables 6.2 and 6.3). The delivery of the radiation dose can be more accurately controlled using the Van de Graaff accelerator than it can be using the Westinghouse X-ray set by altering the electron beam current. The ability to control the electron beam current allows the radiation exposure time to be kept short while still maintaining a high degree of accuracy in the delivery of the radiation dose. This permits a larger range of dose-rates to be used, more accurately, than can be obtained with the Westinghouse X-ray set.

Dose rate (Gy min^{-1})	Dose range (Gy)
0.016	0.01 - 0.5
0.44	0.2 - 5
1.7	1 - 10

Table 6.1 *The three standard dose rates employed using the Westinghouse X-ray set (250 kVp X-rays) and the dose range over which they were used.*

Dose rate (Gy min^{-1})	Exposure time
0.016	2.5 - 63 min
0.44	5 - 136 s
1.7	1 - 35 s

Table 6.2 *The range of exposure times required to give a dose of 2.5 MVp X-rays over the range 0.04-1 Gy using the Van de Graaff accelerator at the three standard dose rates.*

Exposure time	Dose rate (Gy min^{-1})
10 s	0.24 - 6
2 min	0.02 - 0.5
10 min	0.004 - 0.1

Table 6.3 *The range of dose rates used to maintain fixed exposure times for cells irradiated with 2.5 MVp X-rays over the dose range 0.04-1 Gy.*

6.4 Results

6.4.1 Fixed dose rate, variable exposure time

The surviving fractions of cells from three separate populations irradiated with 2.5 MVp X-rays over the dose range 0.04-1 Gy using the fixed dose rates of 0.017, 0.44 or 1.7 Gy min^{-1} at each level of dose is shown in Fig. 6.4. Also shown are the values of surviving fraction obtained from cells exposed to 250 kVp X-rays irradiated using the conventional irradiation procedure in which the dose rate used was dependent on the dose given (Table 6.1). The data are presented as surviving fraction against X-ray dose rather than RBE against X-ray dose which is used commonly in this thesis because it was not possible to produce 2.5 MVp X-rays and neutrons from the Van de Graaff accelerator during a single experiment on the same parental cell population owing to the time required to switch between the two radiation modalities. The increase in radioresistance seen normally after exposure to 250 kVp X-rays using the conventional irradiation procedure over the dose-range 0.2-0.6 Gy was also evident in the data obtained from cells exposed to 2.5 MeV X-rays at one of the three standard dose rates. These data suggest that the increase in radioresistance over this dose range is independent of radiation dose rate. Below a dose of 0.5 Gy, similar values of surviving fraction were obtained from cells irradiated with 250 kVp X-rays and 2.5 MVp X-rays. A difference in relative biological effectiveness would normally be expected between these two X-ray energies, but it was not detected in this study. Above a dose of 0.5 Gy slightly less cell kill was obtained for cells irradiated with 2.5 MVp X-rays at a dose rate of 0.016 Gy min^{-1} compared with cells irradiated with the same energy X-rays at dose rates of 0.44 and 1.7 Gy min^{-1}. At the lowest dose rate used, the exposure time required to give 1 Gy was 63 minutes. This is approximately equivalent to the half-time of repair of potentially lethal lesions quoted in the literature (Iliakis, 1980). The increase in survival that was observed was therefore probably due to the repair of proportionally more radiation-induced damage during the longer dose exposure. The amount of dose-rate sparing that occurred at the lowest dose rate can be seen in Fig. 6.5.

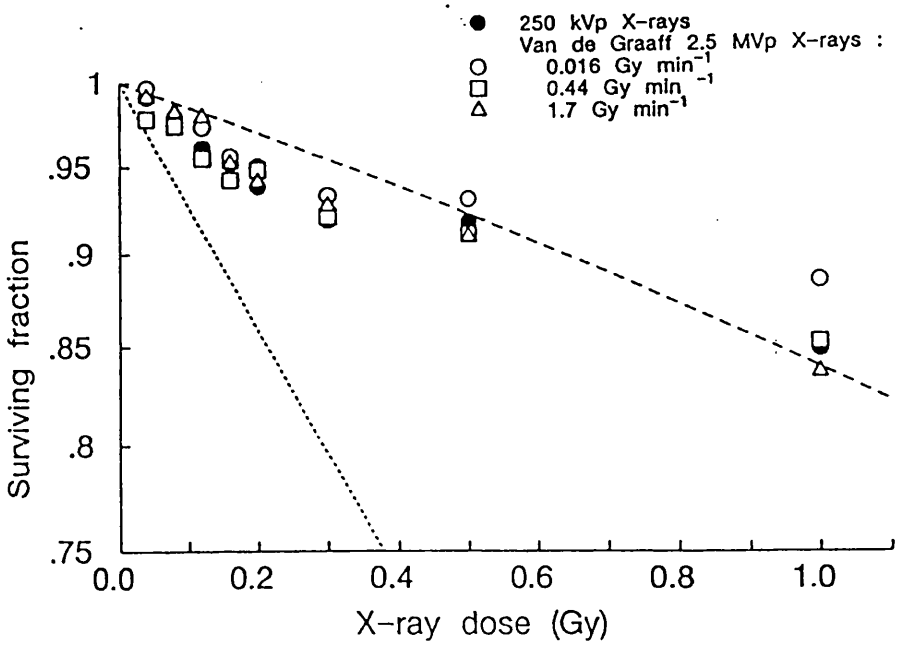

Fig. 6.4

Survival curves for V79 cells irradiated with single doses of 250 kVp X-rays using a dose-rate that is dependent on the actual dose delivered (●) (Table 6.1) and 2.5 MVp X-rays produced by the Van de Graaff accelerator at a dose-rate of 0.016 Gy min^{-1} (O), 0.44 Gy min^{-1} (□) and 1.7 Gy min^{-1} (Δ). Each X-ray survival curve is biphasic and exhibits an increasing radioresistance with increasing X-ray dose over the range 0.2-0.6 Gy. The dashed line is a modified LQ fit (with LQ prediction at low doses) to all the experimental X-ray data and the dotted line is a least squares regression fit to all the experimental neutron data.

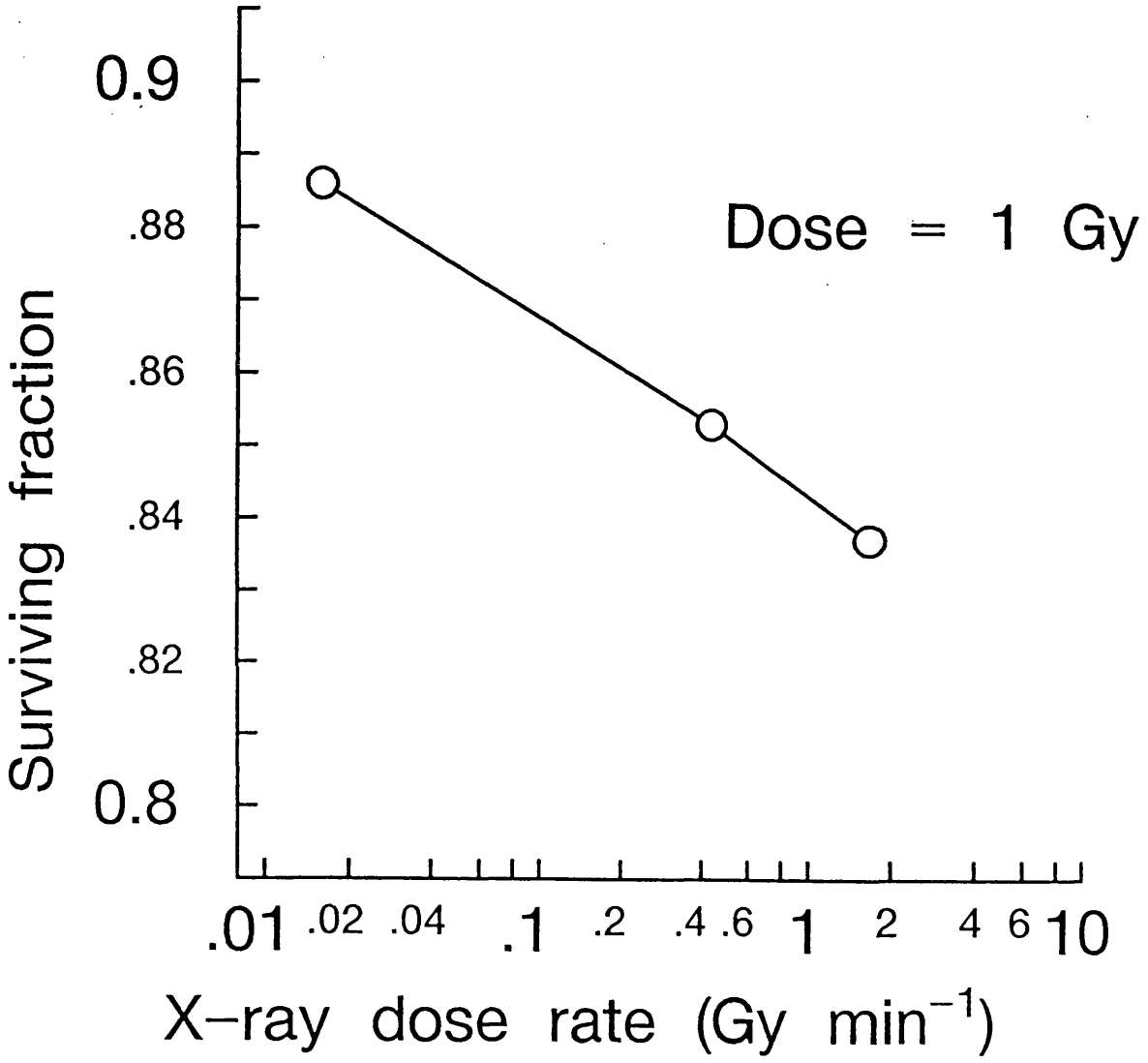

Fig. 6.5
This plot illustrates the level of dose-rate sparing that was seen in this study when 3 samples of cells were irradiated with 1 Gy of X-rays at dose rates of 0.016, 0.44 and 1.7 Gy min^{-1}.

6.4.2 Variable dose rate, fixed exposure time

Using 250 kVp X-rays the increase in radioresistance occurred with an increase in radiation dose and, therefore, increasing exposure time over the dose range 0.04-0.5 Gy (0.016 Gy min^{-1}). The longer exposure times necessary to give the largest doses using these conditions have the greatest potential for proportionally more dose-rate sparing to occur. The increase in radioresistance over this dose range might therefore be attributable to this potential for an increased level of dose-rate sparing. However, a biphasic survival response was evident when the radiation exposure time was fixed at either 10 s, 2 min or 10 min (Fig. 6.6). The results from a more extensive study using a 10 s exposure time at each level of dose are shown in Fig. 6.7. These data demonstrate that the increase in radioresistance over the range 0.2-0.6 Gy seen when cells were irradiated with 250 kVp X-rays is unlikely to be a consequence of the differences in radiation exposure time at each level of dose. These data also suggest that the low-dose X-ray hypersensitivity phenomenon is unlikely to be due to the accumulation of cells in a radioresistant phase of the cell cycle during the radiation exposure owing to a dose-dependent inhibition of the cell cycle because these small fixed exposure times at each level of dose do not allow insufficient time for for significant cell cycle blocking to occur.

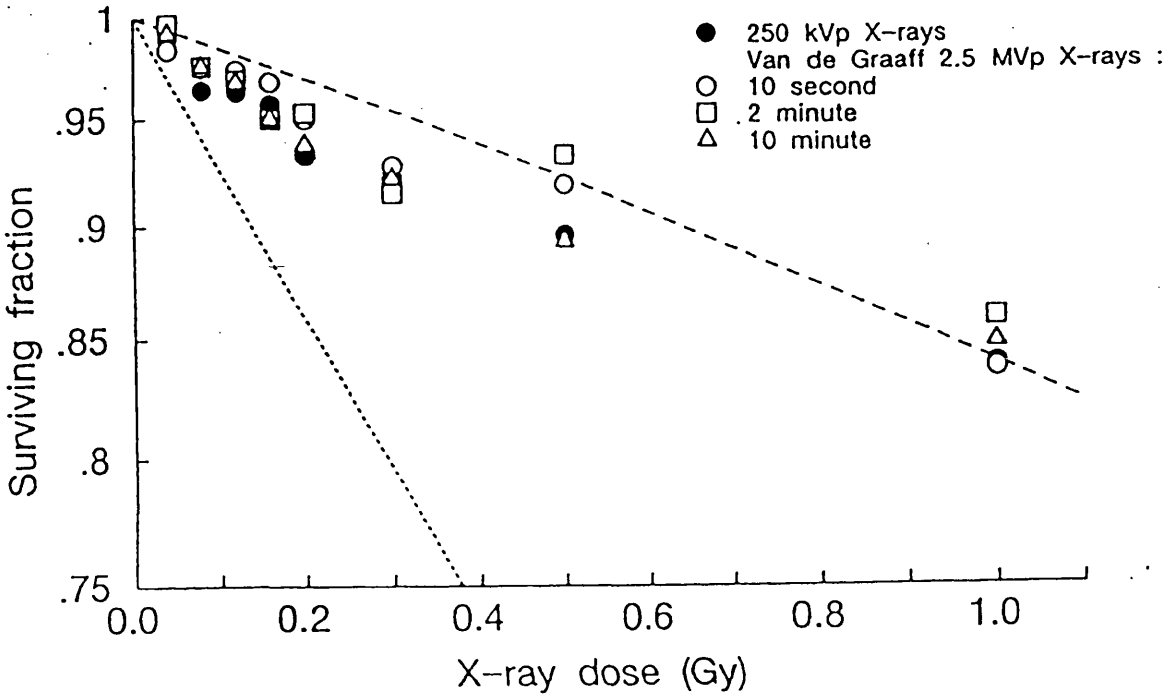

Fig. 6.6

Survival curves for V79 cells irradiated with single doses of 250 kVp X-rays using a dose-rate that is dependent on the actual dose delivered (●)(Table 6.1) and 2.5 MVp X-rays produced by the Van de Graaff accelerator in which the dose rate was changed to ensure a fixed exposure time of 10 seconds (O), 2 minutes (□) and 10 minutes (Δ). The survival curves are biphasic and exhibit an increasing radioresistance with increasing X-ray dose over the dose range 0.2-0.6 Gy. The dashed line is a modified LQ fit (with LQ prediction at low dose) to all the experimental X-ray data and the dotted line is a least squares regression fit to all the experimental neutron data.

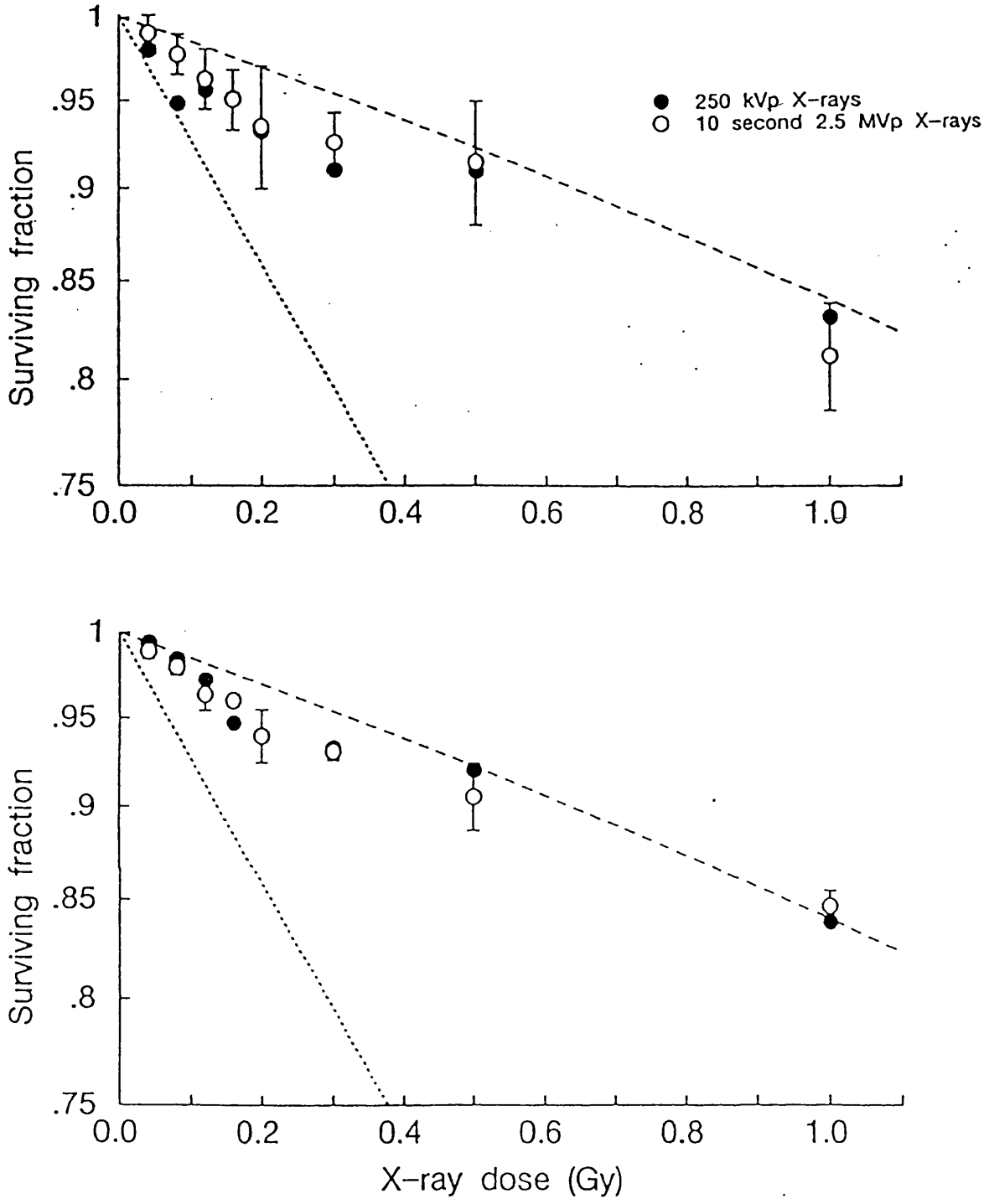

Fig. 6.7

Survival curves for V79 cells irradiated with 250 kVp X-rays using a dose-rate that is dependent on the actual dose delivered (●)(Table 6.1) and 2.5 MVp X-rays produced by the Van de Graaff accelerator with a fixed exposure period of 10 seconds (O, mean of 3 samples ± SD). The survival curves are biphasic and exhibit an increasing radioresistance with increasing X-ray dose over the dose range 0.2-0.6 Gy. The dashed line is a modified LQ fit (with LQ prediction at low doses) to all the experimental X-ray data and the dotted line is a least squares regression fit to all the experimental neutron data. The two panels represent two experiments.

6.5 Summary

1. Similar values of surviving fraction were obtained over the X-ray dose range 0.04-0.5 Gy for cells irradiated at dose rates of 0.016, 0.44 and 1.7 Gy min^{-1}. This indicates that the increase in radioresistance seen routinely over this dose range is unlikely to be a consequence of changes in X-ray dose rate that were necessary to deliver accurately these small doses using the Westinghouse X-ray set.
2. At a higher X-ray dose (1 Gy) dose-rate sparing was observed when cells were irradiated at the lowest dose rate used in this study (0.016 Gy min^{-1}). This corresponded to an exposure time of 62.5 minutes.
3. The low-dose X-ray hypersensitivity that was observed routinely at doses below 0.2 Gy using 250 kVp X-rays was also seen when the radiation exposure time at each level of dose was fixed at either 10 seconds, 2 or 10 minutes. This indicates that the increase in radioresistance over the dose range 0.2-0.6 Gy is probably independent of the radiation exposure time.

6.7 Discussion

A decrease in the biological effect of a given dose of sparsely ionising X-rays with decreasing dose rate is due to the repair of radiation-induced lesions during the irradiation (Hall, 1972; Steel *et al.*, 1986). The more protracted the irradiation, the more repair can occur, further reducing the biological effect of the dose. This effect is most dramatic as the dose-rate is reduced over the range 1.0 Gy min^{-1} to 0.01 Gy min^{-1} (Hall, 1972). In this study, for dosimetric reasons the radiation dose rate used was dependent on the dose actually delivered. It was important therefore to investigate the dependence of radiosensitivity on the radiation dose rate and length of the exposure period as the increase in radioresistance might be attributed to change in X-ray dose rate or a change in duration of the radiation exposure.

The hypersensitivity to low doses of X-rays and the subsequent increase in radioresistance over the dose range 0.2-0.6 Gy was observed when the X-ray dose-rate

was fixed at 0.016, 0.44 or 1.7 Gy min^{-1}. This indicated that the phenomenon of low dose X-ray hypersensitivity and the subsequent increase in radioresistance with increasing X-ray dose was not due to a dose-rate dependent effect, at the dose-rates used in this study.

The low-dose X-ray hypersensitivity was also observed when the irradiation exposure time at each level of dose was fixed at 10 s, 2 min and 10 min. These data indicate that low-dose X-ray hypersensitivity and the change in radioresistance over the dose range 0.2-0.6 Gy was not due to the increase in exposure time necessary to deliver the largest doses at the lowest dose rate. These data indicate therefore that dose-rate sparing is probably not the source of the increase in radioresistance seen in this study. Dose-rate sparing was observed in this study when a 1 Gy dose was given at a dose-rate of 0.016 Gy min^{-1} compared with the same dose given at 0.44 and 1.7 Gy min^{-1} (Fig. 6.5). These data also indicate the phenomenon of increasing radioresistance over the dose range 0.2-0.6 Gy was not due to a temporary blocking or inhibition of the normal progression of the cell cycle causing the accumulation of cells into resistance phase of the cycle because insufficient time would have elapsed with a 10 second exposure period for this to occur.

In order to perform the experiments described in this chapter the dose rate had to be varied over a range of 0.004-6 Gy min^{-1}. A change in the X-ray set-up was therefore necessary, from the Westinghouse X-ray set to a system using X-rays generated from the Van de Graaff accelerator. This change ruled out any other possible experimental artefacts associated with the Westinghouse X-ray set that may have contributed to, or caused the low dose X-ray hypersensitivity.

Chapter 7: Modification of the radiation response of V79-379A cells

7.1 Introduction

7.1.1 The primary target for radiation-induced cell killing

Hofer *et al.* (1975) have demonstrated that intense irradiation of the cytoplasm of the cell using ^{67}Ga-citrate was ineffective at killing cells, illustrating that the cytoplasm was not a radiosensitive site responsible for cell death. There is considerable evidence, however, that the radiation-induced lesions responsible for cell death occur in the nucleus (Painter, 1980). One of the strongest pieces of evidence that suggests DNA is the primary target for radiation-induced killing of mammalian cells comes from studies with ^{125}I-iododeoxyuridine, which is incorporated randomly into the DNA base sequence in place of thymidine (see Fig. 7.1). Local irradiation of the surrounding DNA by the ^{125}I-iododeoxyuridine base analogue was extremely effective in killing mammalian cells (LD_{50} = 60 decays/cell), whereas, irradiation of the plasma membrane from ^{125}I-concanavalin A was not as lethal to the cell (LD_{50} = 19600 decays/cell) (Warters *et al.*, 1977). Datta *et al.* (1976) reported experiments using ionising radiations of different penetration depths that indicated that the level of cell kill was more pronounced if the nuclear membrane rather than the centre of the nucleus was irradiated, possibly indicating the existence of radiation-sensitive DNA attachment sites on the nuclear membrane. It therefore appears that radiation-induced cell lethality results primarily from nuclear damage at the DNA level and the contribution to cell killing from any damage to the cytoplasm is minimal.

7.1.2 DNA lesions responsible for cell death

It is generally accepted that chromosome aberrations are a principal cause of cell death in irradiated cells (Carrano, 1973; Natarajan *et al.*, 1980). Chromosome aberrations may be such that cells are fully viable and function normally until the next mitosis. At that time, however, the damage may become evident. Unequal asymmetric mitoses may occur which result in aneuploidy and death. It is possible that the daughter cells themselves may be viable and functional, although carrying chromosome aberrations, but that the second or third mitosis may be unsuccessful. Thus with most cells the expression of radiation damage is mediated through reproductive sterilisation.

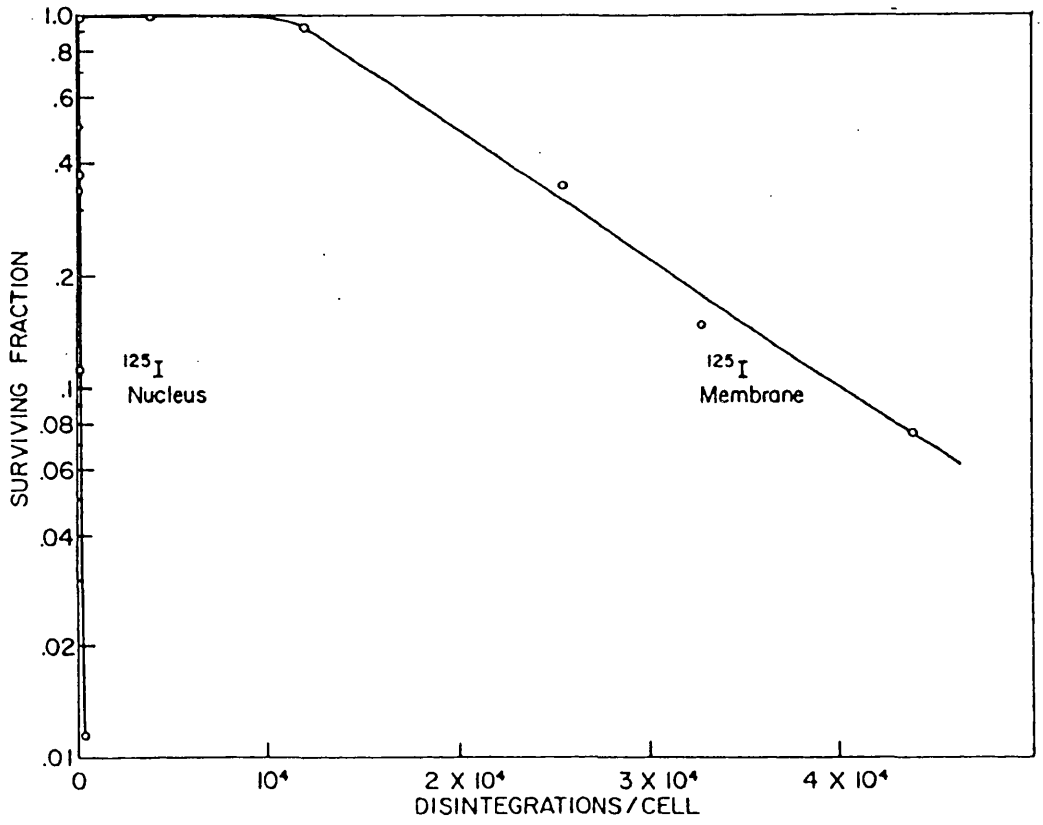

Fig. 7.1

The effect of the decay of ^{125}I iododeoxyuridine in the DNA or ^{125}I-labelled concanavalin A in the cell membrane, on the proliferative capacity of Chinese hamster ovary cells. The steep survival curve obtained when the nucleus was irradiated compares with the much more radioresistant response seen when only the membrane of the cell was irradiated (reproduced from Warters et al., (1977).

A chromosomal aberration necessitates a fracture of the DNA filament, which suggests that the DNA lesion that precedes and precipitates a chromosome aberration is an unrepaired break in the DNA (Bender *et al.*, 1974). Using restriction enzymes that split the DNA at specific bases sequences, Bryant (1984) showed that chromosome aberrations were associated with double strand breaks (DSBs). Evidence supporting the hypothesis that DNA DSBs are lethal to a cell came from studies using radiosensitive cells. The X-ray sensitive Chinese hamster ovary cell lines, *xrs* 1 to *xrs* 7 (Jeggo & Kemp, 1983) are more radiosensitive than the parental CHO cell line and all have a reduced capacity for repair of DSBs compared with the parental line (Kemp *et al.*, 1984). Data from a yeast cell line totally deficient in DSB repair support the premise that one unrepaired DSB leads to cell killing after irradiation (Resnick, 1978; Frankenberg *et al.*, 1981).

Although it is generally believed that unrepaired or mis-repaired DNA DSBs are the dominant cause of cell death after exposure to ionising radiation, a number of other important lesions are produced in DNA following irradiation, such as DNA single strand breaks (SSBs), damage to the DNA sugar-phosphate backbone, alterations to nucleotide bases and the formation of DNA protein crosslinks (Frankenberg-Schwager, 1989) (Fig. 7.2). Solitary lesions of the types listed above may not necessarily be lethal to a cell, but these lesions may contribute to cell killing following irradiation when combined with other lesions as a component of a locally multiply damaged site (LMDS) (Ward, 1986).

7.1.3 Mechanisms of DNA repair

The potential significance of a particular radiation-induced lesion is a reflection on the ability of the cell to successfully repair it. A solitary damaged base or a single strand break on one side of the DNA molecule can be excised and replaced correctly using the opposite strand of DNA as a template in a process termed excision repair. To repair the altered base, a cut needs to be introduced, by an incision enzyme, into the oligonucleotide chain carrying the lesion. The damaged base is then enzymatically removed and the apurinic/apyrimidinic site excised, leaving a gap in the nucleotide sequence on one strand of the DNA molecule. As with the repair of SSBs, the ends of the two nucleotides adjacent to the break in the base sequence may need further

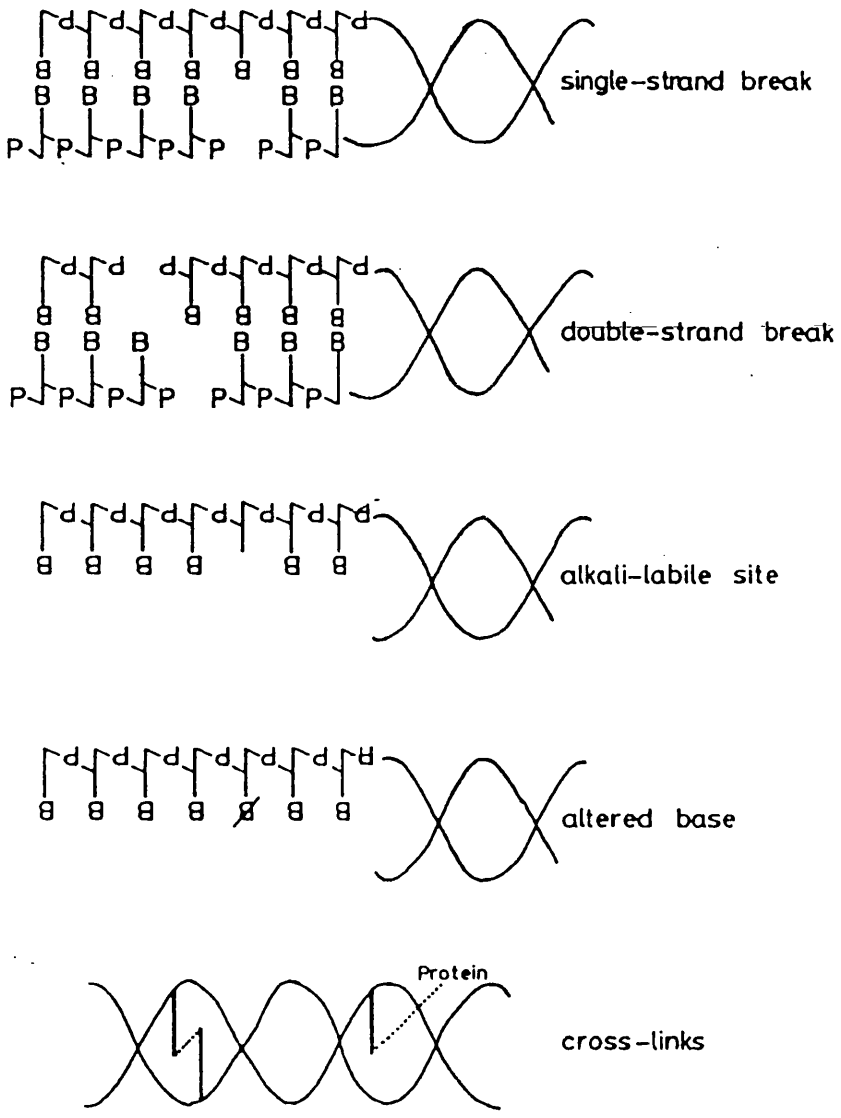

Fig. 7.2
A schematic diagram illustrating different types of DNA damage inflicted by ionising radiation. In the example of the double strand break, the deleted bases are offset from one another and this type of DSB is referred to as a 'sticky-ended' break. Double strand breaks in which opposite base pairs are deleted are known as a 'blunt-ended'. A locally multiply damage site (LMDS) may consist of a combination of these singular lesions (reproduced from Collins, 1987).

trimming by excision enzymes before the oligonucleotide chain can be reassembled by polymerase enzymes using the opposite strand of DNA as a template. Two polymerases are thought to exist, polymerase α which requires a large stretch of single stranded DNA to be exposed before it is able to operate (20-30 nucleotides), and polymerase β which can initiate the synthesis of nucleotides at a small nick in the DNA. Once the new bases are in place, the polynucleotide chain is sealed by ligase enzymes.

A consequence of the intricate packaging of DNA in the nucleus is that the repair of DNA double strand breaks (and also LMDS) is a more complex procedure than the repair of SSBs or damage to individual nucleotides. A DSB fractures the DNA duplex, producing conformational and structural changes in the packing of the DNA as well as the loss of base sequence information. Structural damage to the DNA is repaired with the aid of topoisomerase enzymes. These enzymes unwind the DNA, opening the double helix therefore making the lesion more accessible to repair enzymes. The topoisomerase enzymes are able to pass a DNA duplex through a second duplex by making and sealing a double strand break and such activity is clearly important in the repair of radiation-induced DNA damage in the highly ordered cell nucleus and also in DNA replication and transcription. The nature of the double strand break may dictate its mode of repair. If the constituent single strand breaks that form the DSB are offset from one another, as in the lesion known as a cohesive or 'sticky-ended' break, no immediate loss of sequence information occurs. However, during the repair of the first SSB lesion, a number of nucleotides may be removed before the new nucleotides are inserted to reconstitute the base sequence. If this excision process, removing the first damaged SSB, occurs past the site of the second SSB on the opposite strand of DNA, there is a loss of sequence information (Ahnström and Bryant, 1982). A priority of repair may therefore exist to maintain the integrity of the base sequence for this type of repair. A blunt-ended double strand break in the DNA involves the loss of opposite nucleotides, the base sequence is irrevocably lost and no template remains from which the correct sequence can be reconstructed. Correct repair may then only occur by a recombinational process involving a homologous chromosome. Recombinational repair is thought to occur in prokaryotes but has not been conclusively demonstrated in eukaryotic systems

(Resnick, 1978; Rydberg, 1984).

7.1.4 Modification of DNA repair

Metabolic inhibitors and inhibitors of DNA synthesis can be used to dissect repair pathways and provide an understanding of the sequence of events involved in the repair of radiation-induced damage. The ideal inhibitor of repair is one that is highly specific, so that any effect the drug may have in modifying the response of the cell to the DNA damage can be attributed safely to a particular enzyme or biochemical pathway.

Much of the current information regarding the mechanisms of action of repair modifiers has been obtained from studies on the inhibition of repair in cells following exposure to ultraviolet (UV) radiation (Collins and Johnson, 1984) and cytotoxic chemical agents (Teoule, 1987). These insults often produce a singular type of damage at a specific site in the DNA, unlike ionising radiation which produces a spectrum of damage randomly throughout the nucleus. The interpretation of the effects of a repair modifier on the repair of UV or chemical induced damage are therefore easier to determine than the effect on the repair of ionising radiation-induced damage because the initial types of DNA lesions are known. The large diversity of lesions that are produced after exposure to ionising radiation presumably demands that several types of repair process function simultaneously, making it difficult to discriminate between the inhibition of different repair pathways, in the entire repair process.

7.1.4.1 Inhibition of repair

Several repair inhibitors are known to affect different sites in the major repair pathways (Fig. 7.3).

Novobiocin is thought to act at an early stage in base and nucleotide excision repair, probably through the inhibition of a pre-incision step mediated by type II DNA topoisomerase (Mattern and Painter, 1979). The inhibition of repair may be due also to an effect on ATP metabolism by affecting the structure of the mitochrondia in the cell (Downes and Johnson, 1988).

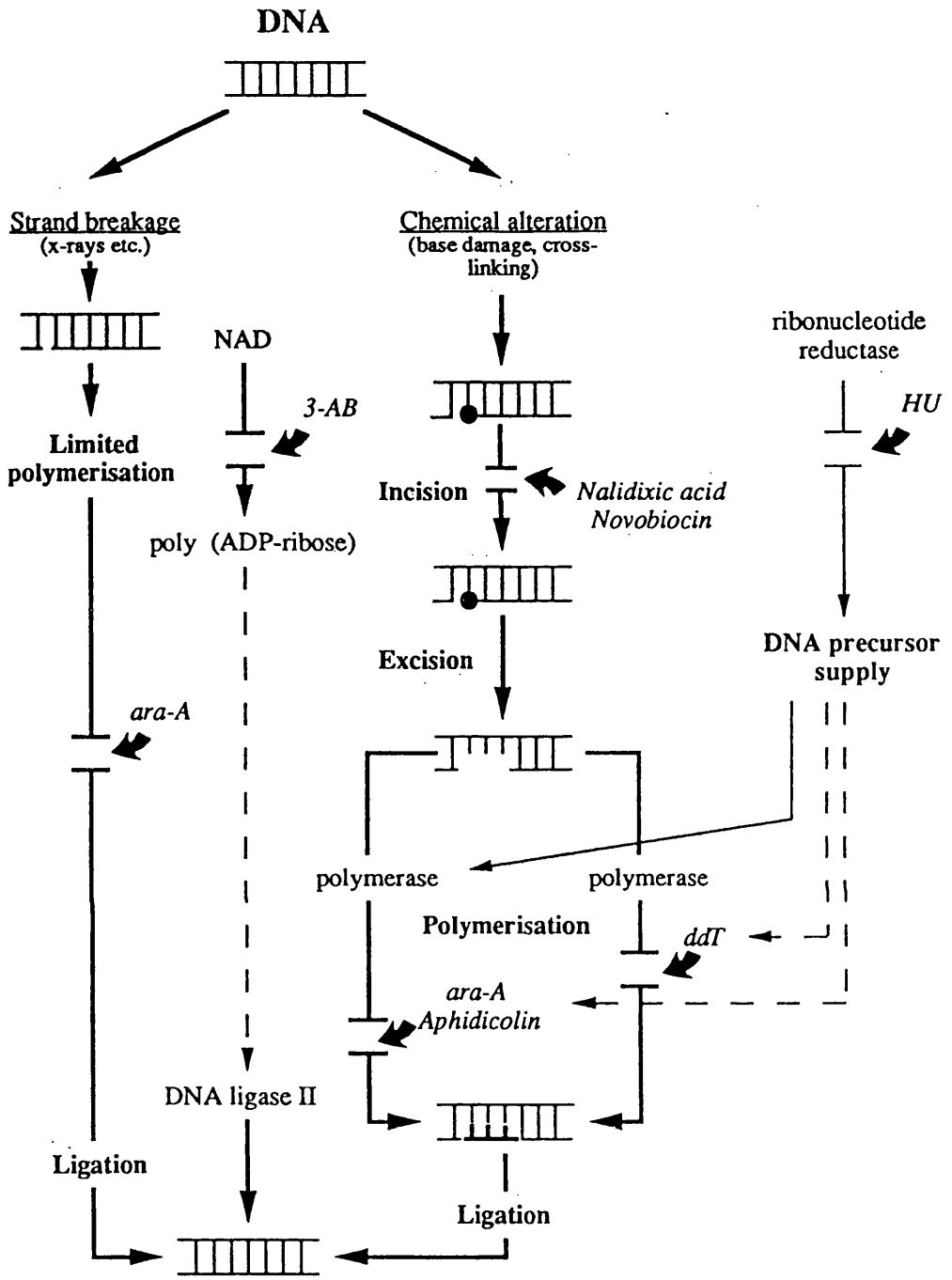

Fig. 7.3

The major DNA repair pathways with sites of inhibition by various drugs. The broken lines (---) indicate activation or competition. A break in a solid line indicates inhibition. Enzymatic processes e.g. incision of the DNA backbone are marked by the bold text and the drugs are identified by italic text. The solid circles signify damaged bases.

β-arabinofuranosyladenine (β-ara-A), an analogue of deoxyadenosine, exerts its effect on repair inhibition through competitive inhibition of α and β polymerases (Muller *et al.*, 1975). After phosphorylation of β-ara-A to the nucleotide (ara-ATP), competition occurs between the ara-A nucleotide and unaffected nucleotide, ATP. Incorporation of ara-ATP into the polypeptide chain in place of the normal ATP is thought to cause a termination of the polymerisation process which inserts new nucleotides.

3-aminobenzamide is a competitive inhibitor of NAD. The synthesis by ADP-ribosyltransferase (*adprt*) of large amounts of poly-(ADP-ribose), using cellular NAD as a substrate, is a common response to DNA damage (Shall, 1984). 3-aminobenzamide prevents the synthesis of poly-(ADP-ribose) by its competition with NAD and this may inhibit DNA ligase activity which is thought to be stimulated by the ADP-ribosylation in response to DNA damage. Poly-(ADP-ribose) is synthesised early in the repair process and is thought to be associated with euchromatin (or active regions of DNA) and therefore poly-(ADP-ribose) may regulate the accessibility of the DNA to other proteins (Bohr and Hanawalt, 1984).

Hydroxyurea (HU) prevents the production of nucleotide precursors in the cell by inhibiting the enzyme ribonucleotide reductase (Synder *et al.*, 1984). Continued synthesis of DNA will eventually lead to a depletion of the pools of dNTP (deoxyribonucelotide triphosphate) in the cell. The repair of radiation-induced damage is inhibited therefore because of a lack of nucleotide precursors owing to the reduced level of nucleotide synthesis.

7.1.4.2 Stimulation and induction of repair

In the bacterium *Escherichia coli* exposed to sublethal concentrations of the chemical mutagens N-methyl-N-1-nitro-N-nitrosoguanidine (MNNG) or N-methyl-N-nitrosourea (MNUA) an error-free repair system is induced that confers increased resistance to the lethal effect of subsequent doses of the same compound (Samson and Cairns, 1977). The main mutagenic lesion produced by agents like MNNG is O-6-methylguanine, which leads to GC and AT transitions during DNA replication and transcription (Coulonidre and Miller, 1977). The adaptive response is due to the

increased ability of the pretreated *E. coli* cells to remove O-6-methylguanine residues from their DNA owing to the increased synthesis of the enzyme DNA methyl-transferase, which demethylates O-6-methylguanine (Bridges and Lehmann, 1982).

An adaptive response which is possibly enzyme mediated has also been reported in V79 cells (Ikushima, 1987) and insect cells (Koval, 1984) following exposure to ionising radiation. In several studies human lymphocytes exposed to low (priming) doses of ionising radiation have been shown to be less susceptible to damage from a second higher (challenge) dose of radiation given a few hours later. (Olivieri *et al.* 1984, Wienke *et al.* 1986, Shadley and Wolff 1987, Shadley *et al.* 1987, Wolff *et al.* 1989). The low-dose pretreatment resulted in fewer chromatid breaks in pretreated cells than in cells given only the large challenge dose of X-irradiation. These authors showed that the low-dose pretreatments did not select against radiation sensitive populations of lymphocytes and so prevent them from contributing to the yield of aberrations found after the high challenge doses given a few hours later. It was postulated that the low radiation doses induced a repair mechanism that, if in place at the time of a subsequent high-dose exposure, caused the primary DNA damage to be repaired more efficiently so that fewer chromosome breaks were seen. Such a repair induction process cannot be attributed to the synthesis of an alkyltransferase enzyme as in the case of prokaryote chemical adaption, because the major DNA lesions responsible for cell death after exposure to ionising radiation are probably double strand breaks which lead to the formation of chromosome aberrations (Natarajan *et al.*, 1980) and not solitary DNA base damage. It is thought therefore that another enzymatic repair process is being induced by low-dose ionising radiation. The biphasic survival curves that were reported when insect cells were irradiated with single doses of X-rays (Koval, 1984) have also been attributed to a similar inducible repair process.

Hydrogen peroxide (H_2O_2) has been shown to produce single strand breaks in DNA akin to those caused by ionising radiations (Ward, 1985). In bacteria, pretreatment with H_2O_2 resulted in a decreased sensitivity to gamma rays (Demple and Halbrook, 1983) compared to non-drug treated cells. Mammalian cells exposed to non-toxic levels of H_2O_2 had a reduced sensitivity to subsequent doses of H_2O_2, gamma

rays and MNNG but not to UV radiation (Gupta and Bhattacharjee, 1988), indicating an inducible protective response. UV radiation does not produce direct strand breaks in DNA, unlike the other three modalities used; instead, the major lesion in DNA following UV exposure is the pyrimidine dimer (Smith and Hanawalt, 1969) which suggests that the protective response induced by the other agents may be associated with the repair of DNA strand breaks.

If the change in radioresistance over the X-ray dose range 0.2-0.6 Gy seen in this thesis is also the manifestation of an inducible protective mechanism which is triggered by increasing levels of damage, then this protective mechanism should also respond to stimulation by cytotoxic insults such as small priming doses of radiation, or H_2O_2 in a similar way to the activation of repair processes in the adaptive response reported in lymphocytes (Shadley and Wienke, 1989) and V79 cells (Ikushima, 1987). Treatment with H_2O_2 or small doses of X-rays might therefore be able to eliminate the increased X-ray sensitivity seen below 0.2 Gy, by stimulating the repair process, or processes, triggered at higher X-ray doses but not normally active in the low-dose range.

7.2 Aims

The experiments reported in this chapter of the thesis were designed to investigate the effect of chemical modifiers of DNA repair on the radiation response below X-ray doses of 1 Gy, and to investigate the effect of pretreatments with X-rays or H_2O_2 in an attempt to stimulate or induce DNA repair processes.

7.3 Materials and Methods

7.3.1 Chemical repair modifiers

The assessment of cell survival was determined using the DMIPS cell analyser as described in section 3.7. Drugs were made up to the appropriate concentrations in sterile PBS, and passed through a 0.22 μm filter for sterilisation. For each inhibitor drug, preliminary experiments were performed on unirradiated cells to determine the maximal concentration of drug which could be used without causing a significant reduction in plating efficiency. The action of each inhibitor was assessed by adding

the drug 1.5 hours prior to irradiation and removing it 6 hours following irradiation (Fig. 7.4), after which the monolayer of cells was washed gently in 5 ml of PBS (3 washes) and the flask refilled with complete medium. In this way, adequate time was permitted for the drug to enter the cells before radiation treatment. More specifically, a 1.5h pre-irradiation exposure period was used because this could be incorporated readily into the standard plating methodology without the need to modify the procedure. A consequence of this approach was that the cells had to attach to the growth surface of the culture flask in the presence of the drug, however this did not effect the attachment or flattening of cells. After the cells had attached, and the initial 5 ml of medium had been poured off, removing any debris and unattached cells, the flask was filled completely with culture medium containing the drug at the required concentration and then irradiated. This culture medium was removed from the flask 6 h after the radiation exposure and replaced with fresh, complete growth medium. The survival of cells following X-ray treatment determined in the presence of the drug was corrected for the reduction in survival of unirradiated cells owing to the presence of the inhibitor.

For hydrogen peroxide treatment, cells taken from an asynchronous, exponentially growing spinner culture were washed and resuspended to a density of 3-5 x 10^5 cells ml^{-1}. A 20 ml volume of this cell suspension was placed in a spinner vessel and cooled in an ice-water bath for 5 minutes. Hydrogen peroxide was added to the spinner culture in sufficient amounts to give a final 25 ml of culture at the required concentration. After 20 minutes, the H_2O_2 was removed by washing twice with fresh complete medium pre-warmed to 37°C. The cell suspension was then plated and assayed as described in section 3.7 (Fig. 7.4).

7.3.2 Radiation treatments

Pretreatment with X-rays (priming treatments) was given at a dose rate of 0.016 Gy min^{-1} (0.05, 0.20 Gy) or 0.44 Gy min^{-1} (1 Gy) in suspension culture. The cells were maintained in suspension culture following irradiation for a period of time that ensured the subsequent doses of radiation (challenge doses) were given to attached monolayers of cells 4 hours after the priming dose had been administered (6 hours with a 1 Gy priming dose), remembering that 1.5 hours were required for the

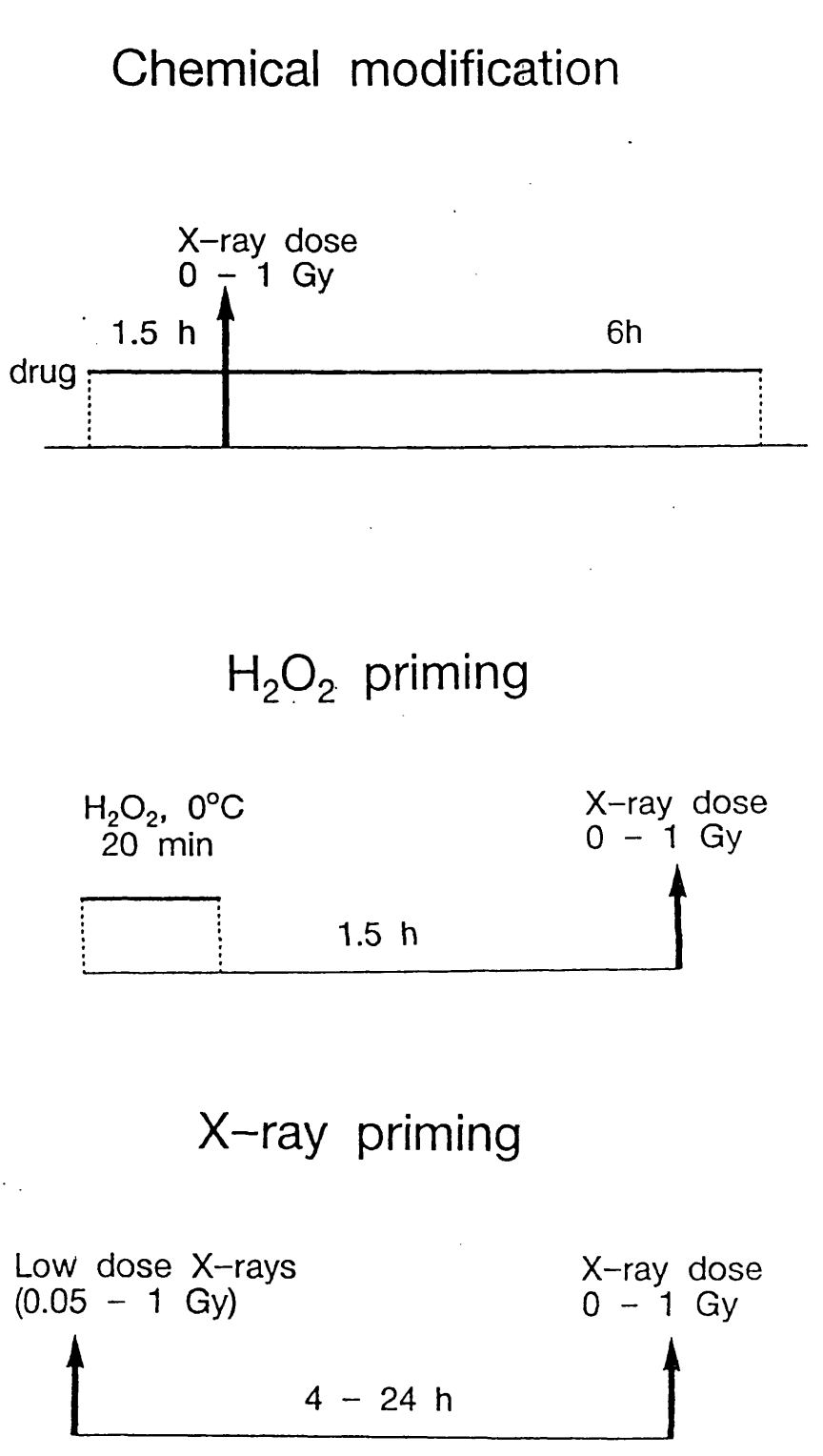

Fig. 7.4
Summary of drug and radiation-priming treatments

cells to attach to the culture flask after being transferred from suspension culture (Fig.7.4).

7.4 Results

7.4.1 Inhibitors of repair

A 6 h post-irradiation period was used because this would normally be the time necessary to complete full repair. A longer period of exposure to the drug might have had a detrimental effect on the normal replicative DNA processes of the cell. Removing the medium containing the drug, washing with PBS and refilling the flask with fresh complete medium had no significant effect on the attachment efficiency (AE) of the cells compared with cells assayed using the procedure for the conventional recognition assay which did not include the washing with PBS and change of culture medium (Table 7.1).

Assay method	Cells located initially	Cells remaining attached (%)
SPP	267 ± 17.3	94.2 ± 2.3
Change in culture medium	279 ± 32.3	92.7 ± 6.7

Table 7.1 *Number of cells located by CSCAN (Mean of four samples ± SD) and the number of these cells remaining attached after 12 hours, using the standard plating procedure (SPP) and a procedure that required the replacement of the culture medium (and 3 PBS washes) 6 hours after irradiation.*

The attachment efficiency of cells is a critical parameter in the recognition assay because colony survival is assessed by revisiting the precise point in the culture flask where an attached cell was located previously by CSCAN. Any treatment that results in attached cells detaching from the growth surface is therefore undesirable as this will influence the plating efficiency of the untreated sample of cells and therefore the measurement of cell survival for cells exposed to radiation.

7.4.1.1 Concentration of repair inhibitor used

For each inhibitor, preliminary experiments were performed on unirradiated cells to determine the highest concentration of drug that could be used without causing an appreciable reduction in the plating efficiency. As the concentration of each drug was increased the PE of cells decreased because cells which had attached initially to the growth surface, detached (Table 7.2). The precise reason for this was not clear but presumably at the highest concentrations of drug used, the inhibitor effects the routine replication of the cells and as the cell begins to round up during mitosis it detaches from the growth surface.

Inhibitor	Concentration (μM)	Cells located initially	Cells remaining attached (%)
3AB	1000	335 ± 40	76.2 ± 5.6
	8000	350 ± 14	60.7 ± 15.1
Novobiocin	100	384 ± 50	84.8 ± 9.1
	600	304 ± 28	71.2 ± 10.6
Hydroxyurea	80	346 ± 34	70.3 ± 8.2
	180	321 ± 33	38.2 ± 21.5
β-ara-A	50	352 ± 47	86.4 ± 7.4
	1000	338 ± 32	52.9 ± 17.3
cycloheximide	10	364 ± 31	93.0 ± 11.9
	70	362 ± 32	74.1 ± 9.2

Table 7.2 *Number of cells located by CSCAN (Mean ± SD of three samples) and the number of cells remaining attached to the growth surface of the culture flask after 12 hours (comprising 6 hours in the presence of the drug and 6 hours following the removal of the drug).*

The final concentration of drug that was used is shown in the Table 7.3 and represented the highest concentration of drug that did not significantly reduce the plating efficiency of the cells.

Concentration of drug used	
Inhibitor	Concentration
3AB	5 mM
Novobiocin	350 μM
HU	100 μM
ara-A	120 μM
cycloheximide	33 μM

***Table 7.3** The concentrations of the repair inhibitors used in the cell survival experiments.*

7.4.1.2 Modification of survival response

The effect of each repair inhibitor on the radiation response has been calculated by assessing the RBE relative to non-drug treated cells exposed to neutrons. The X-ray response (plotted as RBE against X-ray dose) over the range 0.04 -1 Gy can be altered in three ways by the presence of the repair modifiers from the usual pattern that is seen over the same dose range for non-drug treated cells. Figure 7.5 shows a schematic explanation of these alterations in terms of induced repair, if in fact the increase in RBE seen with an increase in X-ray dose is due to induced repair.

3-aminobenzamide, an inhibitor of poly (ADP-ribose) transferase, reduced the increase in RBE that occurred in non-drug treated cells, as the X-ray dose was increased over the range 0.2-0.6 Gy (Fig. 7.6), suggesting an inhibition of the inducible radioprotective mechanism. β-ara-A, an inhibitor of α and β polymerases, sensitised the cells to X-rays over the entire dose range (Fig. 7.7). Novobiocin, an inhibitor of DNA topoisomerase type II, and hydroxyurea an inhibitor of ribonuclease reductase, had little effect on the radiation response (Figs. 7.8 and 7.9), although there was some evidence of induced radioresistance, possibly by a stimulation of the protective mechanism at the lowest doses after exposure to novobiocin. The effect of the various inhibitors suggest that the repair induction brought about by levels of damage that result from an X-ray dose above 0.6 Gy, manifested by an increase in RBE, may be specific to a DNA repair pathway or stress response that is modified by

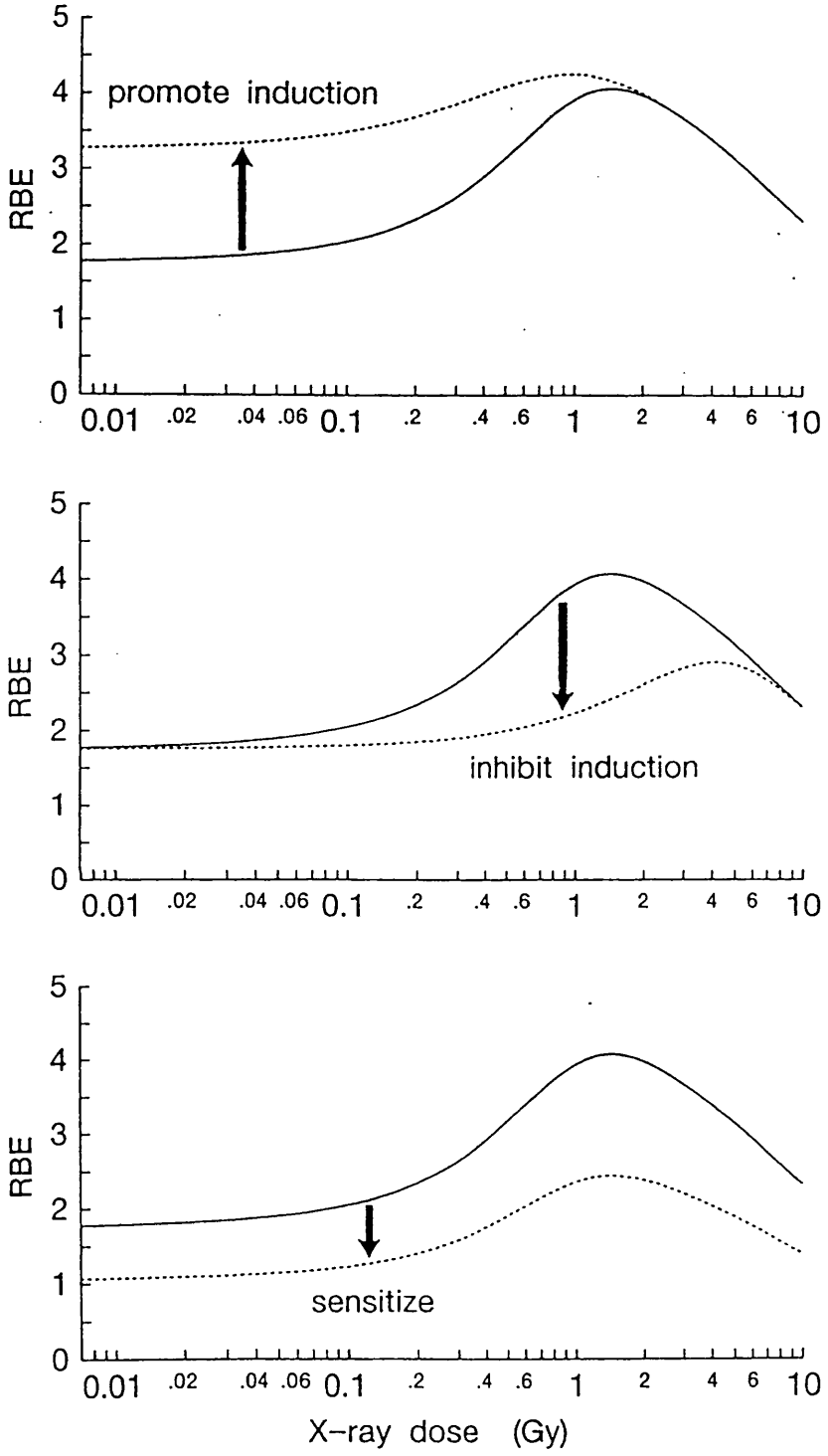

Fig. 7.5
Three hypothetical ways in which the pattern of RBE against X-ray dose can be modified.

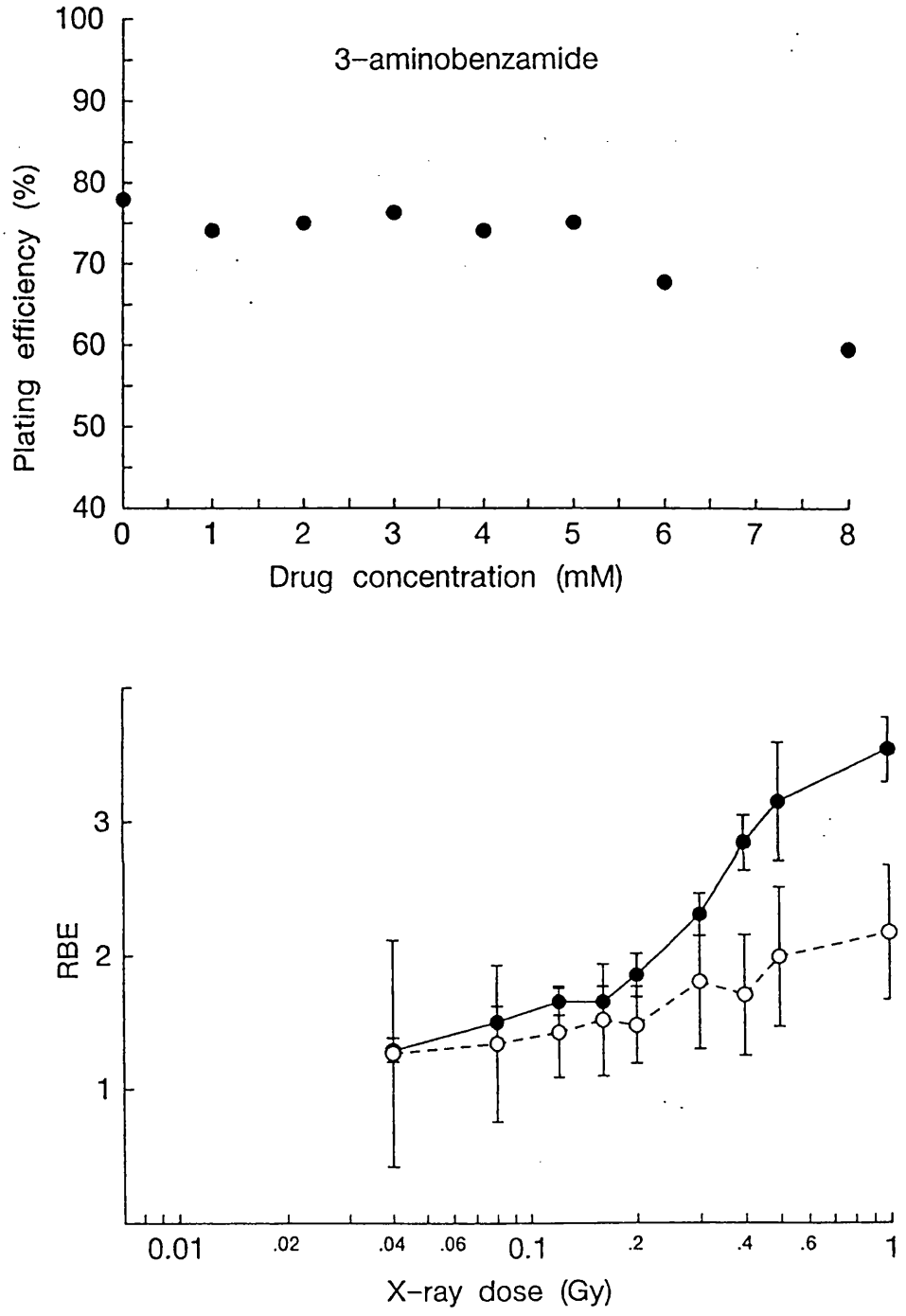

Fig. 7.6

Upper panel: The effect of drug concentration on the plating efficiency of unirradiated cells exposed to 3-AB. As the concentration of the drug increased above 5 mM the plating efficiency decreased.

Lower panel: RBE between 250 kVp X-rays and d(4)-Be neutrons (mean of 6 or more samples ± SEM) delivered as single doses alone (●) and with exposure to 5 mM 3AB (O). Cells were exposed to the drug 1.5 h prior to, and 6 h following irradiation.

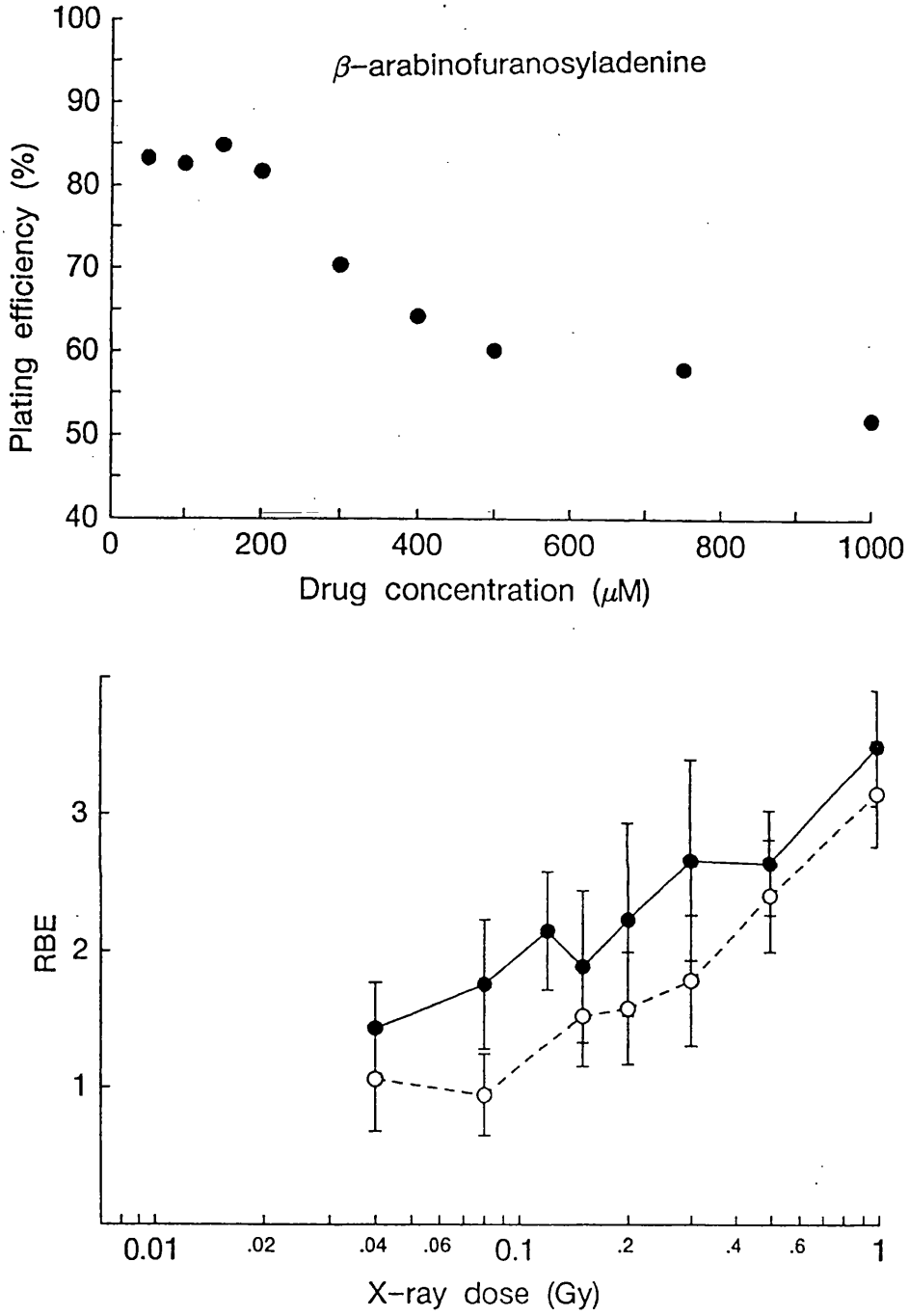

Fig. 7.7

Upper panel: The effect of drug concentration on the plating efficiency of unirradiated cells exposed to β-ara-A. As the concentration of the drug increased above 120 μM the plating efficiency decreased.

Lower panel: RBE between 250 kVp X-rays and d(4)-Be neutrons (mean of 6 or more samples ± SEM) delivered as single doses alone (●) and with exposure to 120 μM β-ara-A (O). Cells were exposed to the drug 1.5 h prior to, and 6 h following irrdiation.

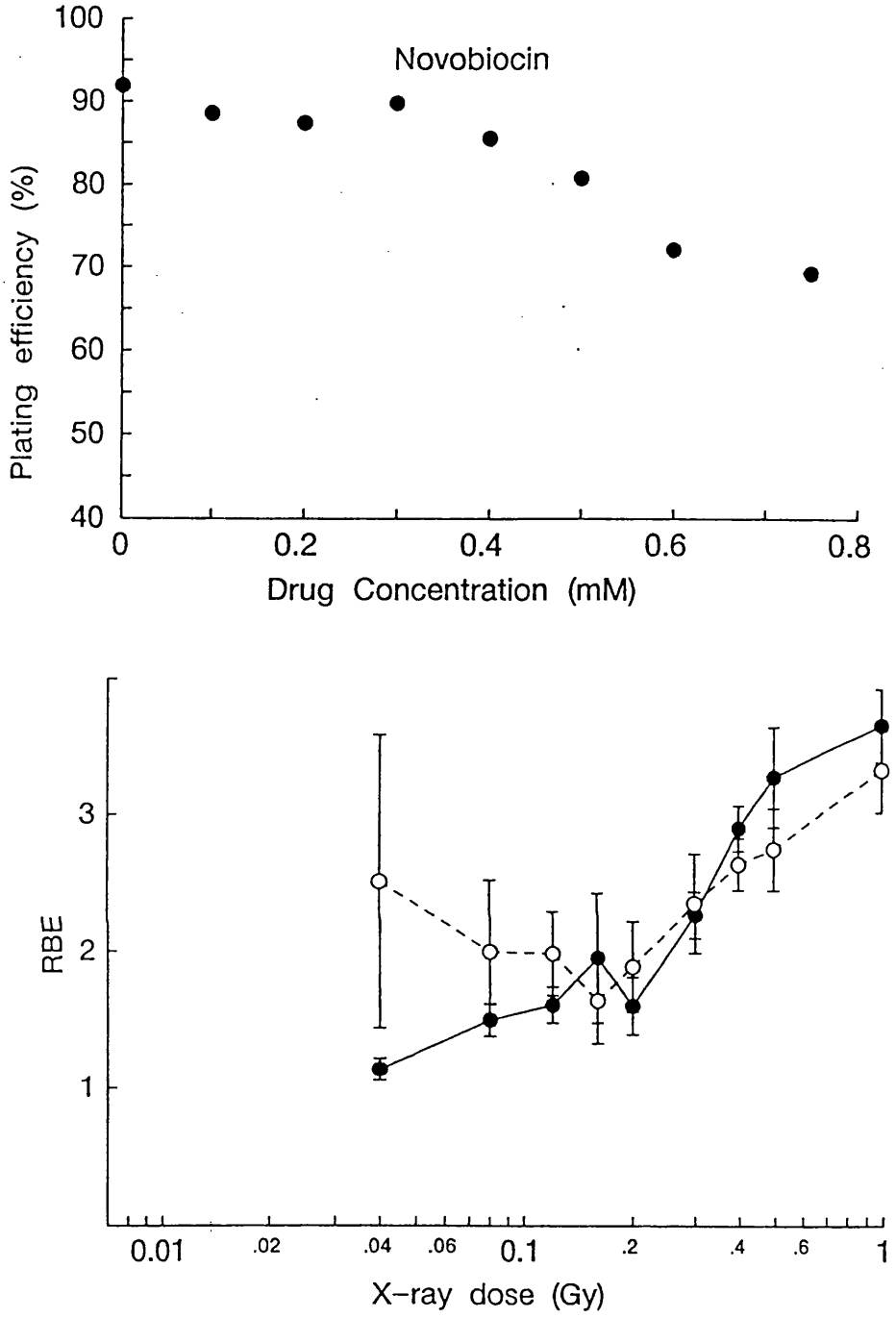

Fig. 7.8

Upper panel: The effect of drug concentration on the plating efficiency of unirradiated cells exposed to novobiocin. As the concentration of the drug increased above 350 μM the plating efficiency decreased.

Lower panel: RBE between 250 kVp X-rays and d(4)-Be neutrons (mean of 6 or more samples ± SEM) delivered as single doses alone (●) and with exposure to 350 μM novobiocin (O). Cells were exposed to the drug 1.5 h prior to, and 6 h following irradiation.

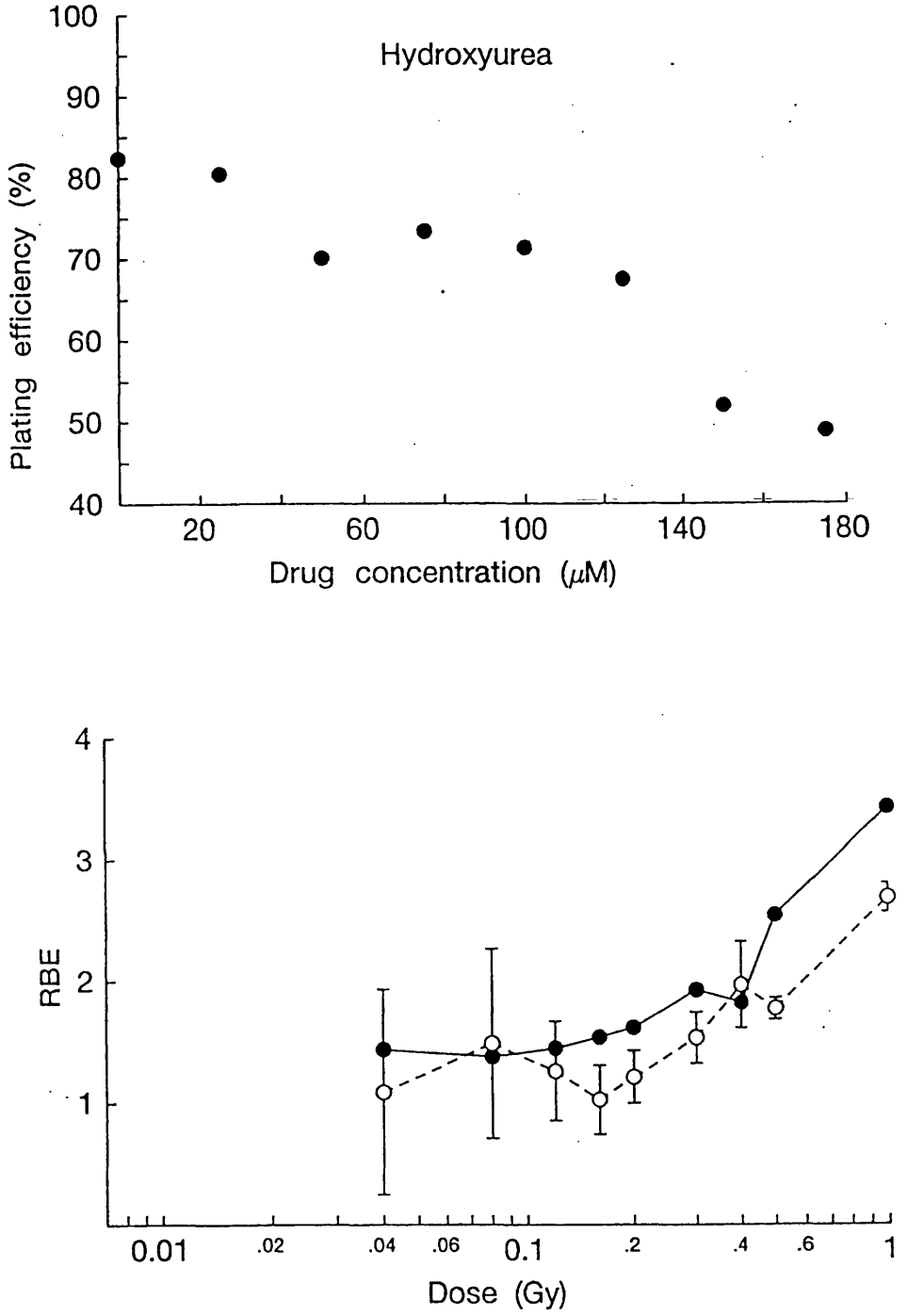

Fig. 7.9

Upper panel: The effect of drug concentration on the plating efficiency of unirradiated cells exposed to HU. As the concentration of the drug increased above 100 μM the plating efficiency decreased.

Lower panel: RBE between 250 kVp X-rays and d(4)-Be neutrons (mean of 6 or more samples ± SEM) delivered as single doses alone (●) and with exposure to 100 μM HU (O). Cells were exposed to the drug 1.5 h prior to, and 6 h following irradiation.

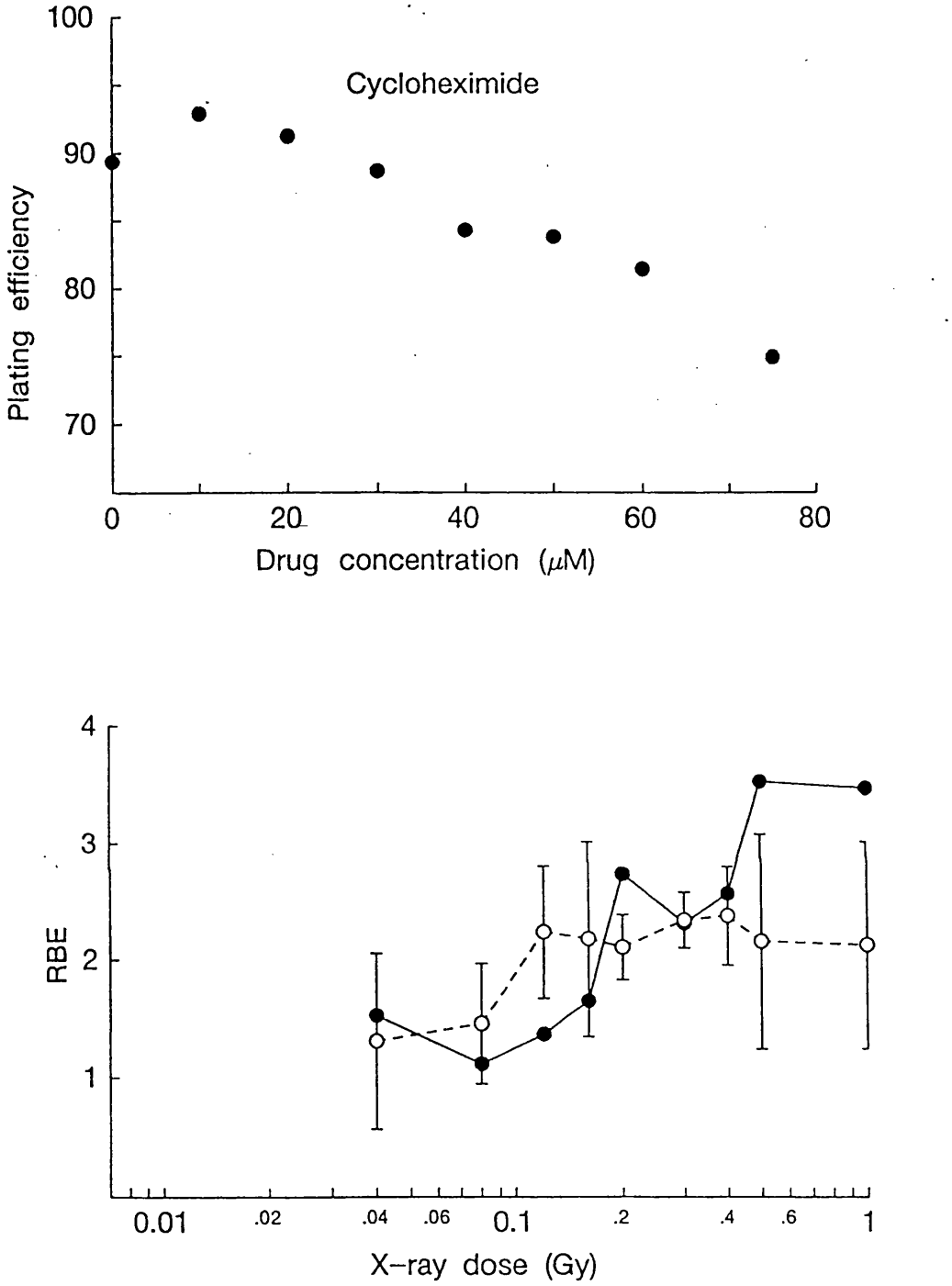

Fig. 7.10

Upper panel: The effect of drug concentration on the plating efficiency of unirradiated cells exposed to cycloheximide. As the concentration of the drug increased above 33 μM the plating efficiency decreased.

Lower panel: RBE between 250 kVp X-rays and d(4)-Be neutrons (mean of 6 or more samples ± SEM) delivered as single doses alone (●) and with exposure to 33 μM cycloheximide (O). Cells were exposed to the drug 1.5 h prior to, and 6 h following irradiation.

3AB and not by β-ara-A, HU or Novobiocin. Treatment with cycloheximide, a protein synthesis inhibitor, employing the same treatment regime as used with the other repair inhibitors (Novobiocin, ara-A, 3AB, and HU), suppressed the rise in the RBE over the X-ray dose range of 0.2-0.6 Gy, suggesting that the protective mechanism requires the synthesis of new proteins, possibly repair enzymes or stress proteins (Fig. 7.10).

7.4.2 Stimulators of repair

7.4.2.1 Modification of survival by hydrogen peroxide

The cells were exposed to H_2O_2 for 20 minutes on ice 1.5 h before radiation treatment. This treatment protocol was chosen because a 20 minute exposure period was known to produce a large amount of DNA damage (Ward *et al.*, 1987), equivalent to the SSB damage that results from an 8 Gy dose of X-rays. A 1.5 h period was allowed following exposure to H_2O_2 before the cells were irradiated in order for the protective mechanism to be induced. The length of this induction period was selected primarily because it could be integrated into the recognition assay without the need to modify the plating procedure of the cells. Exposure to H_2O_2 took place on ice (0-4°C) to limit the amount of intracellular enzymatic breakdown of H_2O_2 by catalase and peroxidases (Hoffman *et al.*, 1984) and also to reduce the metabolic processing and repair of the hydrogen peroxide-induced damage during the incubation of the cells in the drug. This was desirable to maximise the amount of DNA damage that could be obtained from the lowest concentration of drug. No significant cell killing was observed when cells were exposed to only H_2O_2 at concentrations of 10^{-4} M and 10^{-6} M without radiation treatment (Fig. 7.11). Both the H_2O_2 concentrations used were non-cytotoxic. Exposing cells to a concentration of 10^{-4} M H_2O_2 induced a radioprotective mechanism which increased the radioresistance of cells to subsequent doses of X-rays over the dose range where an increased X-ray sensitivity is usually seen (Fig. 7.12). A H_2O_2 concentration of 10^{-6} M administered in the same way as the higher concentration of drug (10^{-4} M) did not induce the radioprotective mechanism, suggesting that a threshold of damage might have to be achieved for the induction process to be induced (Fig. 7.12).

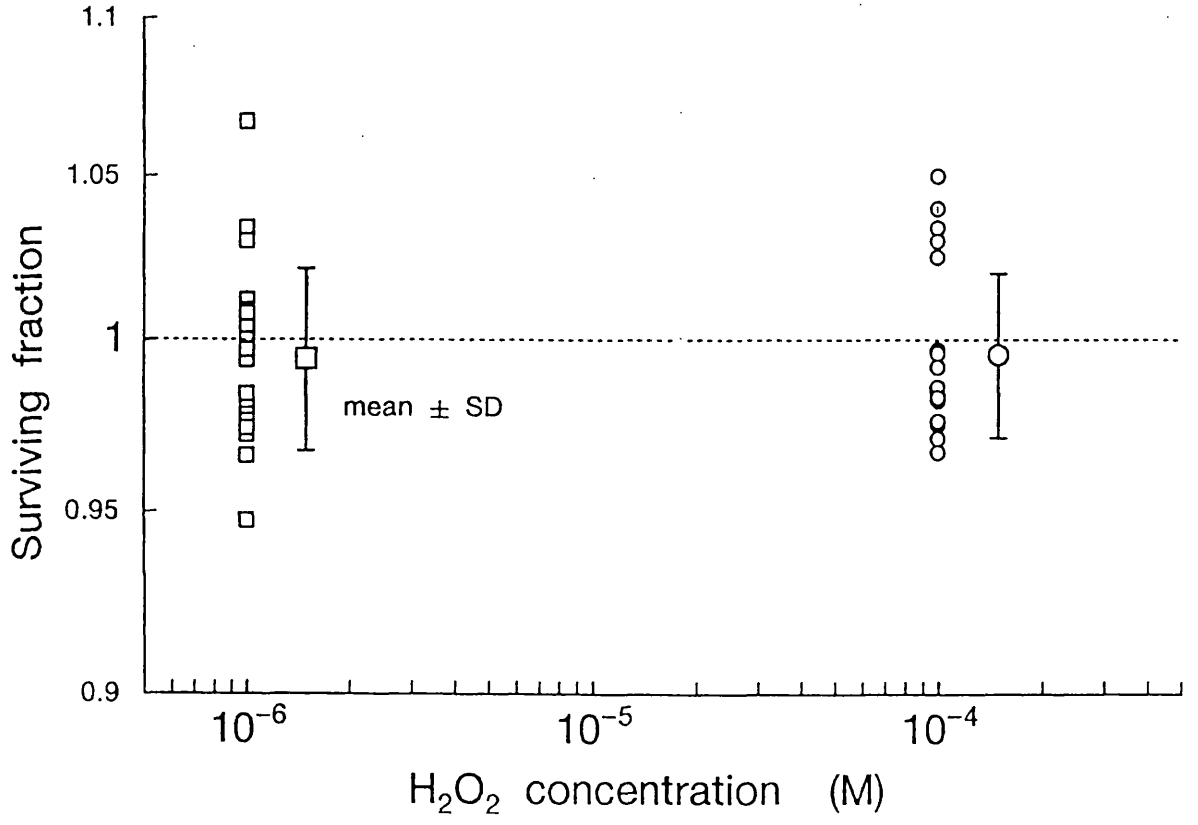

Fig. 7.11
The effect of incubating cells in 10^{-4} M and 10^{-6} M H_2O_2 on the survival of cells. Neither concentration of drug produced significant cell kill.

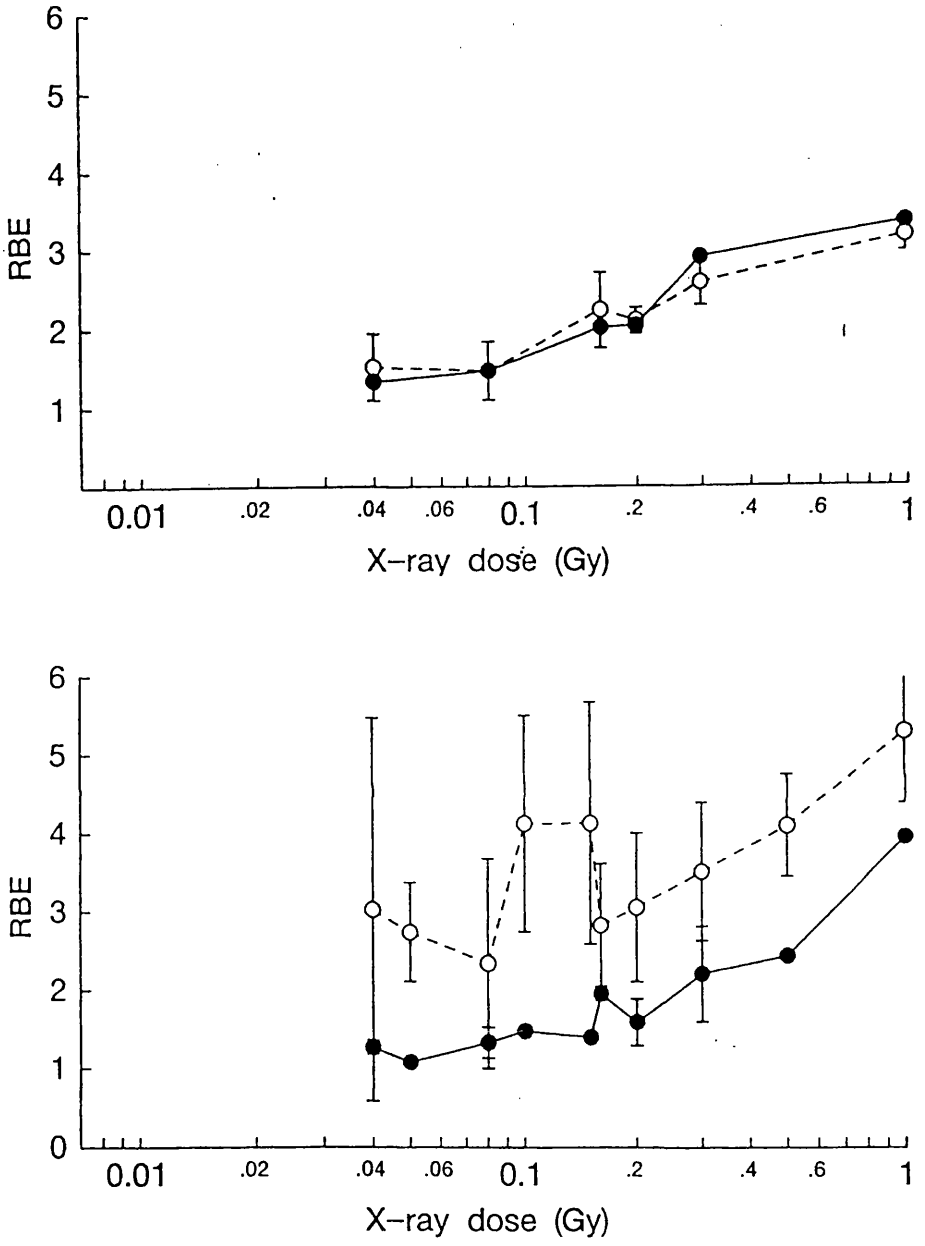

Fig. 7.12

RBE values between 250 kVp X-rays and d(4)-Be neutrons (lower panel 10^{-4} M, mean of 9 samples ± SEM; upper panel 10^{-6} M, mean of 3 samples ± SEM) delivered as single doses (●) and with prior treatment with 10^{-4} M H_2O_2 (O) or 10^{-6} M H_2O_2 (O). The same pattern of RBE against X-ray dose is seen for cells exposed to the lower concentration of drug but an increase in RBE (reflecting an increase in induced radioresistance) was only seen in cells exposed to 10^{-4} M H_2O_2.

7.4.2.2 Modification of the response using X-ray priming treatments

Cells were pretreated with 0.05, 0.20 or 1 Gy of X-rays given as a single dose at dose rates of 0.016 Gy min^{-1} (0.05, 0.20 Gy) or 0.44 Gy min^{-1} (1 Gy). The priming dose was given either at 4 (0.05, 0.20 Gy), 6 (1 Gy) or 24 (1 Gy) hours prior to a challenge dose of radiation (Table 7.4).

Pretreatment dose (Gy)	Dose rate Gy min^{-1}	Time interval (h)	Challenge dose (Gy)
0.05	0.016	4	0.04-1
0.20	0.016	4	0.04-1
1	0.44	6	0.04-0.3
1	0.44	24	0.04-0.5

Table 7.4 *A summary of the X-ray dose-rates and time intervals between the priming and challenge doses used in the X-irradiation pretreatment experiments.*

The priming treatments increased the radioresistance of cells to levels above that seen normally for cells only receiving the single low (<0.6 Gy) challenge dose of X-rays. Pretreating the cells with single doses of X-rays (0.05, 0.20 and 1 Gy) prior to the exposure to subsequent doses of X-rays, 4 or 6 hours later increased the radioresistance of cells at the lowest doses, producing higher values of RBE compared with cells receiving only the second dose of radiation after a 'sham' priming dose (Fig. 7.13). In terms of the induced repair theory this was interpreted as a stimulation of the radioprotective mechanism which increased the radioresistance of the cells to the challenge dose of X-rays. The 0.20 Gy priming dose produced the highest level of survival of all three priming treatments (0.05, 0.20 and 1 Gy) at the very lowest doses. When the interval between the priming dose and the challenge dose was extended to 24 h the increased level of survival produced by the priming treatment was no longer seen (Fig. 7.14), indicating that the previously induced radioprotective mechanism has diminished within 24 hours of the primary treatment which is equivalent to approximately 2 cell cycle times in this cell line. The presence of cycloheximide during the interval between the priming and subsequent X-ray challenge dose abolishes the protection induced by the first radiation treatment (Fig. 7.15) resulting in the same values of RBE being obtained for cells given the priming

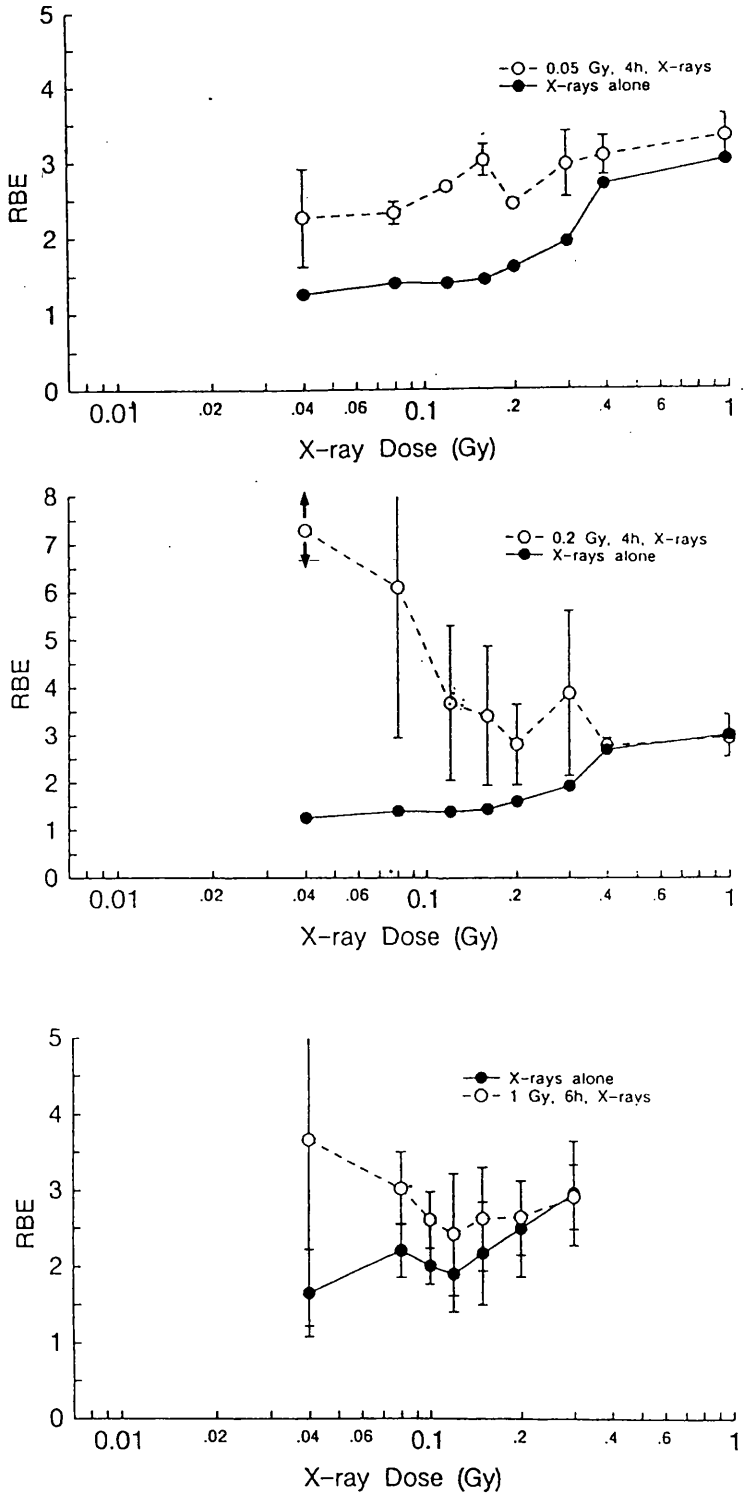

Fig. 7.13

RBE values between 250 kVp X-rays and d(4)-Be neutrons (mean of 3 or more samples ± SEM) delivered as single doses (●) or with an X-ray pretreatment (O) of 0.05 Gy (upper panel) or 0.20 Gy (middle panel) 4 h prior to the challenge doses or 1 Gy (lower panel) 6 hours prior to the challenge doses.

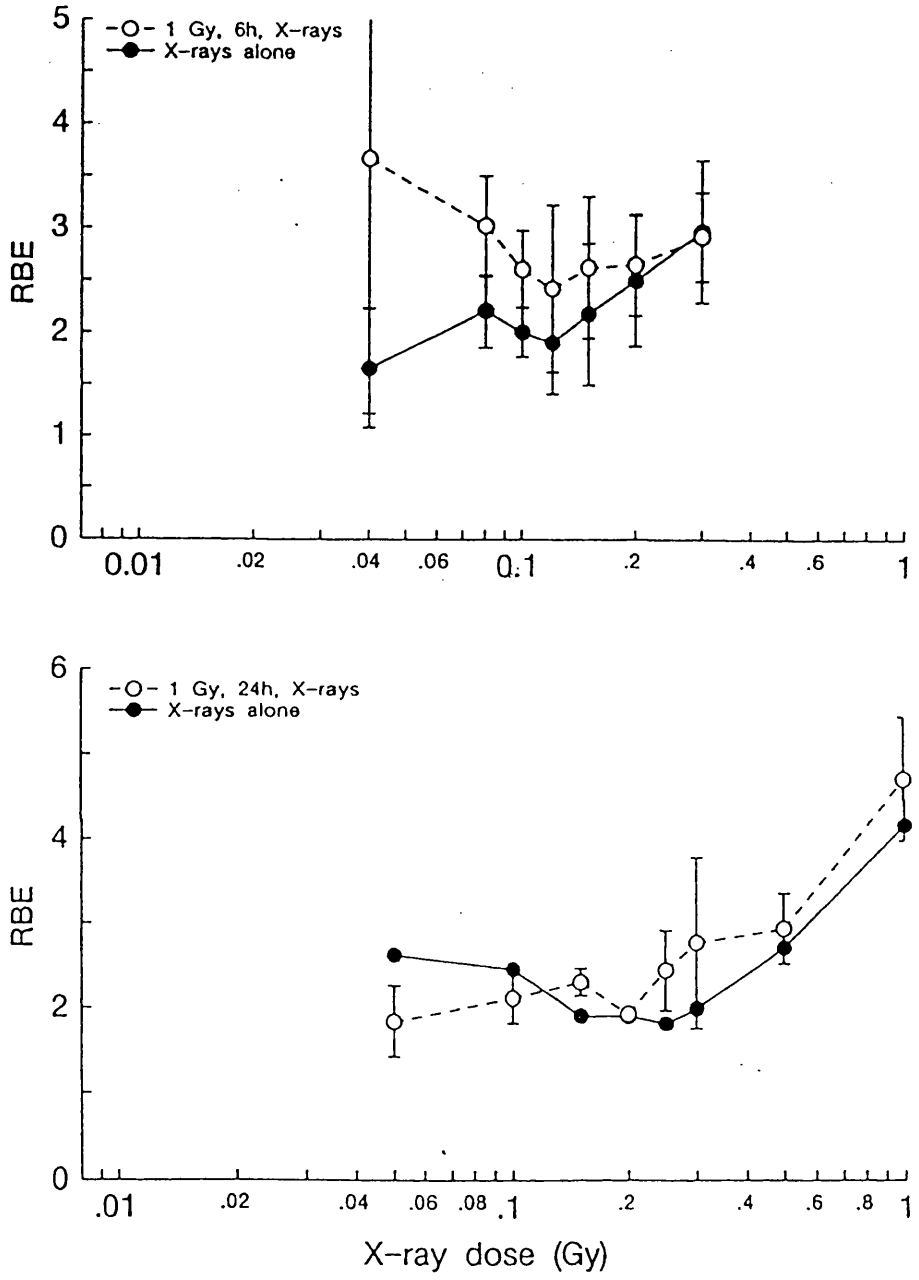

Fig. 7.14

RBE values between 250 kVp X-rays and d(4)-Be neutrons delivered as single doses (●) or with an X-ray pretreatment dose of 1 Gy (O, mean of at least 3 or more samples ± SEM). The induced X-ray radioresistance reflected by the high RBE values in the pretreated cells compared with the non-pretreated cells is present 6 h after an initial priming dose but had diminished 24 h after the priming dose.

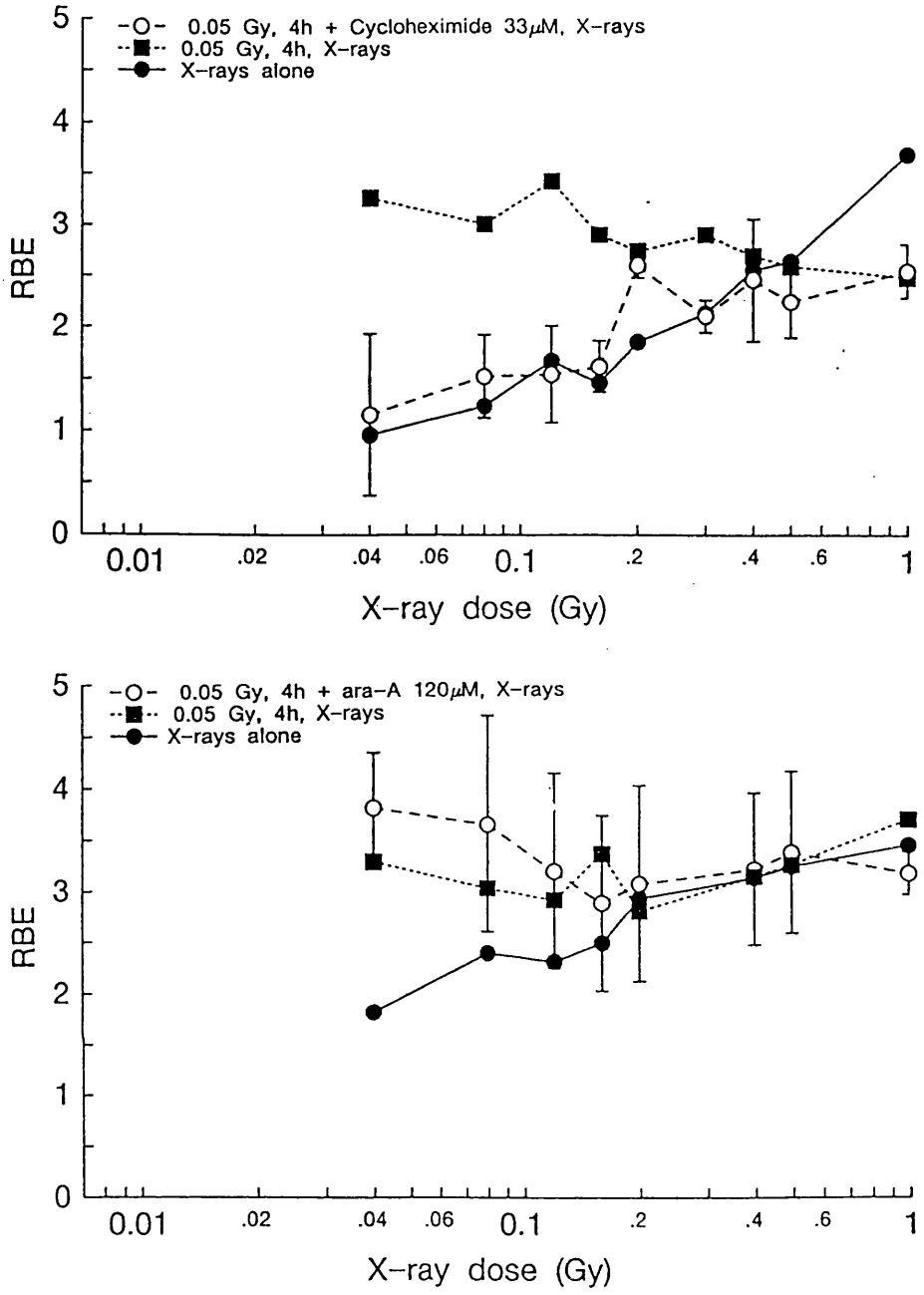

Fig. 7.15

RBE values between 250 kVp X-rays and d(4)-Be neutrons (mean of 3 or more values ± SEM) delivered as single doses (●) and with a 0.05 Gy X-ray pre-treatment (■). The small dose pretreatments produce an increase in the radioresistance of cells manifested by elevated levels of RBE compared with cells only given the challenge doses. Incubating the cells in 33 μM cycloheximide (O, upper panel) during the interval between the two doses prevented the increase in radioresistance. Treatment with β-ara-A (O, lower panel) however did not prevent the induction of radioresistance. The β-ara-A RBE data was calculated relative to cells exposed to neutrons and the drug; consequently the X-ray radiosensitization seen in Fig. 7.7 does not show here. The procedure of calculating RBE was changed in this case to emphasise the influence of β-ara-A on the repair induction by X-ray priming treatments.

treatment compared with cells not receiving the priming treatment. These data imply that *de novo* protein synthesis is required for the development of the protection mechanism brought about by the single-pretreatment X-ray doses. The presence of β-ara-A during the interval between the pretreatment and subsequent X-ray dose did not inhibit the protective response suggesting that the radioprotective mechanism induced by the priming treatment does not involve a DNA repair pathway inhibited by ara-A (Fig. 7.15).

7.5 Summary

1) The X-ray survival response that was obtained routinely of an increasing X-ray radioresistance over the dose range 0.04-1 Gy was altered in three ways by different biochemical repair modifiers.
2) 3-AB, an inhibitor of poly-(ADP-ribose) transferase, reduced the increase in RBE that occurred in non-drug treated cells as the X-ray dose was increased over the range 0.2-1 Gy, suggesting an inhibition of the radioprotective mechanism.
3) β-ara-A, an inhibitor of α and β polymerases sensitised cells to X-rays over the entire dose range investigated (0.04-1 Gy).
4) H_2O_2 induced a radioprotective mechanism(s) which increased the resistance of cells to subsequent doses of X-rays in the dose range characterised by the low-dose X-ray hypersensitive response.
5) Novobiocin, an inhibitor of DNA topoisomerase type II, and hydroxyurea, an inhibitor of ribonuclease reductase, had little effect on the radiation response over the dose range 0.2-0.6 Gy, although there was some evidence of induced radioresistance at the lowest X-ray doses following exposure to novobiocin.
6) Cycloheximide, an inhibitor of protein synthesis, suppressed the increase in radioresistance that was routinely seen over the X-ray dose range 0.4-1 Gy, suggesting that *de novo* protein synthesis was required for the induction of radioresistance.
7) Pretreatment of cells with small doses of X-rays (0.05, 0.20, 1 Gy) increased the radioresistance of the cells to subsequent X-ray doses over the range 0.04-0.6 Gy. This effect was not seen with a 24 h interval between the pretreatment

and subsequent X-ray doses.

8) Cycloheximide present during the interval between the pretreatment and subsequent X-ray doses prevented the increase in radioresistance that was induced by the pretreatment dose of X-rays, suggesting that protein synthesis was required for the increased radioresistance.

7.6 Discussion

There is considerable evidence to support the view that the lesions responsible for cell death following exposure to ionising radiation occur in the genomic DNA (Datta *et al.*, 1976; Warters *et al.*, 1977; Cole *et al.*, 1980). Ionizing radiation is known to produce a variety of discrete DNA lesions and in addition multiple lesions in small regions of DNA. However, a large body of evidence suggests that the DNA DSB is the critical lesion in cell killing (Frankenberg-Schwager, 1989). With such a variety of lesions there are inevitably many possible modes of repair. Understanding of the mechanisms involved in repairing-radiation induced damage in the DNA of mammalian cells has predominantly been derived from studies on the repair of DNA damage in prokaryotic systems where the biochemical processes of genetic repair are more clearly understood (Freidberg, 1985). Less is known about the repair pathways and the repair enzymes that are involved in the repair of DNA in mammalian cells. However, similar repair functions and processes are thought to occur in both prokaryotic and eukaryotic cells, such as excision of damage, insertion and polymerisation of new bases and ligation of the repaired DNA strand (Collins, 1977; Collins *et al.*, 1984). The purpose of the experiments in this part of the thesis was to determine whether the radiation response to low doses of X-rays could be modified by different drugs known to effect the major DNA repair pathways (Fig. 7.3). Integral elements of the repair response could therefore be inhibited individually in order to determine its role in the induction of radioresistance over the X-ray dose range 0.2 - 0.6 Gy. A possible criticism of this approach is the difficulty that can be encountered when attempting to interpret the effect of the different repair modifiers in the overall response of the cell to radiation treatment because of the lack of specificity of each

drug for a particular pathway associated with repair of radiation damage. While the predominant action of the drug on a DNA repair process may be understood, the effects of that drug on other cellular processes may also play a role in the overall cellular response to the radiation insult. Despite this problem of specificity, repair modifiers can represent a powerful tool for the biochemical dissection of DNA repair pathways.

To limit the possible cytotoxic effects of the different repair modifiers, preliminary experiments were performed to determine the maximum concentration of each drug that could be used without causing significant reductions in attachment and plating efficiency of cells, as this would detrimentally affect the assessment of cell survival by the cell analyser. It was important to achieve the maximum possible inhibition of the repair pathways by employing the highest concentration of drug that did not effect the assessment of cell survival. The repair modifiers that were investigated altered the radiation response of treated cells compared with cells not receiving the drug treatment in one of there ways. 3-AB increased the radiosensitivity of cells exposed to X-ray doses above approximately 0.2 Gy whereas β-ara-A sensitized the X-ray response over the entire dose range. HU and novobiocin had little effect on cell survival after X-rays although there was evidence that at the lowest X-ray doses novobiocin increased the radioresistance of cells.

If the increase in radioresistance seen over the X-ray dose range 0.2-0.6 Gy represents the triggering of a radioprotective mechanism which enhanced DNA repair, then the data can be used to suggest which elements of the major repair pathways might be stimulated in response to radiation insult. 3-AB is thought to exsert its action by inhibiting DNA ligase activity and preventing the synthesis of poly-(ADP-ribose) (Shall 1984). Therefore, the triggering of the radioprotective response may involve DNA ligase activity or the increased synthesis of poly-(ADP-ribose), because 3-AB prevented the increase in radioresistance once the radioprotective mechanism had been triggered presumably because DNA repair was not functioning correctly. Kelland and Steel (1988) have described differential radiosensitization by 3-AB in human tumour cell lines of varying radiosensitivity and 3-AB appears to be more effective in enhancing radiation-induced cell kill in radioresistant tumour cell lines compared with

radiosensitive cell lines. This observation is consistent with the idea that the increase in radioresistance is due to the induction of a repair process. Cells which are radiosensitive might have a reduced capacity for the induction of the radioprotective mechanism and therefore would be expected to have a lower enhancement to cell killing by 3-AB treatment than resistant cell lines which have a large capacity for induction of a radioprotective mechanism. 3-AB is also known to inhibit the repair of PLD (Little *et al.*, 1986). The 3-AB data from this study, when considered alone, could therefore be interpreted as representing an inhibition of PLD repair manifested by an inhibition of the induction of radioresistance leading to increased levels of cell killing over the X-ray dose range 0.2-0.6 Gy. If this were the correct explanation for the experimental data however, then an unknown phenomenon must occur as the X-ray dose increases over the range 0.2-0.6 Gy which allows the repair of PLD to take place.

β-ara-A sensitized the X-ray response over the entire dose range investigated but did not prevent the increase in radioresistance. This suggests that the triggering of the radioprotective mechanism is not prevented by inhibiting or blocking the action of α and β polymerases (Muller *et al.*, 1975). Therefore, these pathways are probably not relevant for the *induction* of the radioprotective mechanisms. The results of treatment with HU and novobiocin suggest that the triggering of repair is not prevented by inhibiting the synthesis of nucleotide precursors (Collins *et al.*, 1977) or by the inhibition of topoisomerase II (Mattern and Painter, 1979) respectively.

Ionising radiation produces a broad spectrum of DNA damage (Frankenberg-Schwager, 1989) and any of these lesions might be the stimulus responsible for inducing or triggering the radioprotective mechanism. However, H_2O_2 is only known to induce non-lethal SSBs which suggest that a component of SSB production and/or the repair of SSBs might be responsible for triggering the inducible-protective response. It is known that SSBs are repaired with a half life of about 10 minutes (see Frankenberg-Schwager, 1989) which suggests that the triggering of the inducible repair mechanism might be a rapid process. The radioresistance that is produced by H_2O_2 treatment was evident 1.5 hours after drug treatment indicating that the protective mechanism is fully induced in this time. The protective effect is known to diminish

within 24 hours of being triggered, as an increase in radioresistance was not apparent in cells irradiated with 1 Gy of X-rays 24 hours previously compared with cells treated with the same priming dose 6 h previously. The protective mechanism probably requires protein synthesis because cycloheximide, a known inhibitor of protein synthesis, prevented the induction response when present during the interval between the small priming doses of X-rays and subsequent X-ray challenge doses. There was some evidence that cycloheximide also prevented the increase in radioresistance when given 1.5 hours prior to, and removed 6 hours following, a single dose radiation treatment, indicating a possible role for protein synthesis in the induction of the radioprotective response after single doses of X-rays (Fig. 7.10).

Considering all the data involving DNA repair modifiers it is difficult to suggest a precise mechanism for induction of radioresistance over the X-ray dose range 0.2-0.6 Gy. The radioresistance is induced by damage resulting from H_2O_2 treatment, possibly SSBs and also damage caused by ionising radiation. The radioresistance is induced with 1.5 hours and diminishes within 24 hours, and possibly requiring protein synthesis. The effect involves a pathway that is inhibited by 3-AB but not HU, novobiocin or β-ara-A. It might therefore involve DNA ligase II or (ADP)-ribose synthesis.

Chapter 8: A preliminary two dimensional gel electrophoresis investigation

8.1 Introduction

The data described in the previous chapters in this thesis suggest that a radioprotective mechanism is triggered over the X-ray dose range 0.2-0.6 Gy that subsequently increases the radioresistance of cells to larger doses of X-rays. Biologically this may represent *de novo* synthesis of new proteins (e.g. stress proteins or repair enzymes) which act directly to repair X-ray-induced damage or indirectly (e.g. co-factors, enzyme precursors) and promote the action of DNA repair enzymes. Alternatively, the increased levels of damage that result from the increased X-ray dose may trigger a cascade mechanism which increases the efficiency of a component of the repair response, possibly in conjunction with an increase in the expression of one or several components or repair. Recently, Wolff *et al.* (1989) have found differences in the array of proteins between human lymphocytes 4 hours after receiving an X-ray dose of 1 cGy and unperturbed human lymphocytes. Boothman *et al.* (1989) have also demonstrated that X-irradiation of human melanoma cells (U1-Mel) induced the expression of a specific set of proteins. Both of these studies used two dimensional (2D) gel electrophoresis to demonstrate the appearance of the induced proteins.

Two dimensional gel electrophoresis is a powerful technique which is capable of separating a complex array of proteins. The two-stage separation process makes use of two independent characteristics of proteins. The first stage exploits the charge carried by the protein, which is reflected by its isoelectric point, and the second stage utilises the molecular weight of the protein.

The first dimension involves the method of isoelectric focusing (IEF) in an acrylamide gel to separate proteins as a function of their isoelectric point (pI) on a pH gradient established by ampholines. The charge carried by a protein depends on its molecular structure, primarily the number of amino acid residues. However, the *net* charge of the protein is a consequence of the pH of the surrounding environment. At each level of pH the side groups of the protein will be differentially charged and at

one specific pH value the protein will be neutral in respect of charge. This pH value is referred to as the isoelectric point (pI). Each protein migrates through the acrylamide gel until it reaches the point where it is electrically neutral and therefore cannot be drawn electrically any further through the gel by the current that crosses it.

The second dimension of the process, using slab polyacrylamide gel electrophoresis (PAGE) combined with sodium dodecyl sulphate (SDS) as a denaturing agent, is then used to separate the proteins of the same pI on a basis of molecular weight. Sodium dodecyl sulphate binds to the hydrophobic regions of the protein, increasing its mobility through the gel. The PAGE gel is composed of acrylamide copolymerised with N-N-1-methylene-bis acrylamide. Ammonium persulphate and tetramethylenediamine (TEMED) are used to polymerise the monomer subunits of acrylamide into long chains and the bis-acrylamide forms cross-links with the acrylamide resulting in the formation of a matrix containing pores. The size of the pores in the matrix depend on the concentrations of the acrylamide solutions and the concentration of the catalysts. The migration of proteins through the gel will depend on the pore size and the electric charge placed across the gel. A stacking gel, which has a larger pore size than the resolving gel (SDS-PAGE), is overlaid over the resolving gel. The proteins migrate rapidly through the large pores of the stacking gel and then accumulate at the boundary between the stacking gel and resolving gel owing to the sudden reduction in pore size between the two gels. This ensures the proteins enter the resolving gel in a uniform manner. The size of the pores in an IEF gel are much larger than those in a SDS-PAGE gel because the IEF gel separates proteins based on charge and any restriction on the movement of the proteins through the gel owing to size of the protein will affect the level of separation.

8.2 Aims

The experiments in this part of the thesis were designed to compare the protein array from a population of irradiated cells with that obtained from a population of unperturbed cells. This will determine whether the V79-379A cell line synthesises novel proteins in response to radiation treatment which are not normally present in the cell and therefore may account for the increase in radioresistance seen over the X-ray

dose range 0.2-0.6 Gy.

8.3 Materials and Methods

8.3.1 Electrophoresis buffer solutions

1. Lysis buffer

   9.5 M Urea (Sigma Cat. No. U5378)
   2% NP40 (Sigma Cat. No. N3516)
   1.6% Ampholine pH 5-7 (Sigma Cat. No. A5674)
   0.4% Ampholine pH 3-10 (Sigma Cat. No. A5174)
   5% β-mercaptoethanol (Sigma Cat. No. 3148)

2. Cathode buffer solution (IEF electrophoresis)

   0.02 M NaOH (Fisons Cat. No. 54920)
   Degassed prior to use

3. Anode buffer solution (IEF electrophoresis)

   0.01 M H_3PO_4 (BDH Cat. No. UN1805)

4. SDS-PAGE buffer solution

   0.025 M Tris base (Fisons Cat. No. T3712)
   0.25 M Glycerine
   0.01% SDS (Fisons Cat. No. F5202)

8.3.2 Electrophoresis gel solutions

1. 30% Acrylamide stock solution for IEF Gels

   28.4% acrylamide (Sigma Cat. No. A9099)
   1.6% bis acrylamide (BRL Cat. No. 5516UA)

2. 30% Acrylamide stock solution for SDS Gels

   29.2% acrylamide (Sigma Cat. No. A9099)
   0.8% bis-acrylamide (BRL Cat. No. 5516UA)

3. 1% Agarose for supporting IEF Gels

   0.01 g ml^{-1} of agarose (BRL Cat. No. 5510UB)
   10% Glycerol
   5% β-mercaptoethanol (Sigma Cat. No. 3148)
   2.3% SDS (Fisons Cat. No. F5202)
   0.0625 M Tris-HCl pH 6.8

8.3.3 Staining solutions

1. IEF staining solution

0.1% Coomassie blue (CB) in a solution of
1 part acetic acid: 5 parts methanol: 4 parts distilled H_2O

2. IEF Destaining solution

0.005% Coomassie blue (CB) in a solution of
7 parts acetic acid: 5 parts methanol: 88 parts distilled H_2O

8.3.4 Additional solutions

1. DNAase I

1 mg ml^{-1} DNAase I
0.01 M Tris-HCl pH 7.4
1 mM $MgCl_2$

Stored as frozen aliquots (0.5 ml)

2. 10% NP40

10 ml NP40
90 ml distilled H_2O

3. IEF equilibrating solution

0.0625 M Tris-HCl
2.3% SDS
5% β-mercaptoethanol (Sigma Cat. No. 3148)
10% Glycerol

4. Sample overlay solution

9 M Urea
0.8% Ampholines pH 5-7
0.2% Ampholines pH 3-10

stored as frozen aliquots (1 ml)

8.3.5 Preparation of the protein sample

Two populations of cells were grown in suspension culture and maintained at a cell density between 4-6 × 10^5 cells ml^{-1} until the total number of cells in each population had reached 2 × 10^8 cells ml^{-1} . One cell suspension was then irradiated with an X-ray dose of 1 Gy at a dose rate of 0.44 Gy min^{-1} and the second suspension was sham irradiated. The two samples of cells were then returned to a stirred water bath set at 37°C. After 6 hours of culture, each sample of cells was centrifuged and resuspended in 500 µl of lysis buffer and DNAase was added to make a concentration of 50 µg ml^{-1}. These solutions were left to stand on ice for 5 minutes after which they were centrifuged for 5 min at 1000 rpm. The supernatant containing the cellular proteins was removed and transferred into cyrostat tubes and frozen; the pellet

containing the cell membranes was discarded.

8.3.6 Iso-electric focusing (IEF) gels (based on the method of O'Farrell, 1975)

The electrophoresis gel tubes were washed with detergent followed by distilled water and then 70% ethanol and left to dry. The bases of the tubes were sealed with electrophoresis membrane held in place by two rubber sealing rings. The tubes were than placed in the electrophoresis running apparatus. 1 ml of IEF gel (Table 8.1) was added per tube.

IEF gel	
Constituent	Amount
Urea	2.75 g
30% acrylamide	0.67 ml
NP-40	1.0 ml
Distilled water	0.98 ml
Ampholine pH 5-7	0.2 ml
Ampholine pH 3-10	0.05 ml

Table 8.1 Constituents to make 5 ml of IEF gel

The IEF gel mixture (Table 8.1) was swirled until completely dissolved then 5 µl of 10% ammonium persulphate was added and the solution degassed using a vacuum pump. TEMED (National Diagnostics, Cat. No. EC508) (3.5 µl) was then added and the mixture gently swirled. The solution was then loaded in the electrophoresis gel tubes using a Pasteur pipette to a point 1 cm from the top of the tubes. Extreme care was taken to avoid air bubbles being introduced at the base of the gel tube as this would inhibit the polymerisation process. The IEF gel was covered with the sample overlay solution. The tubes were allowed 1-2 hours to set, following which the overlay solution was removed and the tube filled with 0.02 M NaOH. The upper reservoir of the apparatus was filled with 0.02 M NaOH and the lower reservoir with 0.01 M H_3PO_4. The gel was pre-run before the samples of protein were loaded (Table 8.2) .

Pre-run gel conditions		
Stage	Voltage (V)	Time (min)
1	200	15
2	300	30
3	400	30

Table 8.2 *The stages of the pre-run process of the IEF gel before the protein samples were loaded.*

Following the pre-run, the upper reservoir was drained and the NaOH solution overlaying the IEF gels was removed. A 20 µl sample of protein from the irradiated and control population of cells were loaded onto two separate gels and overlaid with 20 µl of the sample overlay solution, followed by 0.02 M NaOH. The upper reservoir was refilled with NaOH and the gel run at 400 V for 12 min followed at 800 V for 1 hour. When the electrophoresis run was complete, the gels were removed from the gel tubes using a fine needle by gently introducing water between the gel and side of the tube. The gels were placed in a solution of 0.1% Coomassie blue (CB) for 10 min and then destained in IEF destaining solution for 1 hour. The gels were then stored in 5 ml of a fresh sample of destaining solution. Before the second dimension of the electrophoresis procedure was performed the IEF gel was soaked in IEF equilibrating solution for 2 hours.

8.3.7 SDS-PAGE Electrophoresis (based on the method of O'Farrell, 1975)

The electrophoresis plates were thoroughly washed using detergent and rinsed with distilled water, then 70% ethanol, and left to dry. Spacers were placed at the vertical and bottom edges of the electrophoresis plates to keep them apart uniformly. These edges were then sealed securely with plastic sticking tape and large spring clips. A small quantity of 1% agarose gel was poured between the glass plates and manoeuvred to seal the bottom and vertical sides of the glass plates. Once this 1% agarose gel had polymerised it would provide an air-tight seal preventing the SDS-PAGE gel from leaking out once loaded. The SDS-PAGE gel solution was then mixed (Table 8.3), degassed and the TEMED was added. This solution was then swirled and poured between the glass plates to a point 1 cm from the top of the front plate.

SDS-PAGE Gel, acrylamide concentration 10%	
Constituent	Amount (ml)
Distilled H_2O	16.1
30% acrylamide	13.3
1.5 M Tris (pH 8.8)	10
20% SDS	0.2
10% Ammonium persulphate	0.4
TEMED	0.016

Table 8.3 *Constituents to make 40 ml of SDS-PAGE gel.*

The SDS-PAGE gel was covered with a water-saturated butanol solution until it polymerised, ensured a flat surface at the gel. The butanol solution also prevented air diffusing to the gel which inhibits the polymerisation process. When the gel had polymerised, the butanol was poured off and the surface dried carefully using a paper tissue. A stacking gel (Table 8.4) was then poured on top of the SDS-PAGE resolving gel to the level of the groove in the forward plate. Once this stacking gel had polymerised, the IEF gel could be placed on top. A 1% agarose gel was used to secure the IEF gel to the surface of the stacking gel. Extreme care was exercised to prevent air bubbles settling between the IEF gel and stacking gel as this would have disrupted the flow of current through the gel.

Stacking gel	
Constituent	Amount (ml)
H_2O	11.2
30% Acrylamide	3.4
0.5 M Tris (pH 6.8)	5.0
20% SDS	0.1
10% Ammonium persulphate	0.2
TEMED	0.02

Table 8.4 *Constituents to make 20 ml of stacking gel.*

Once the agarose had polymerised and cemented the IEF gel in place, the sticking tape from the bottom of the electrophoresis plates was removed carefully. The SDS-PAGE gel (still held between the two glass plates) was attached to the running apparatus using spring clips. The bottom reservoir was filled with Tris-glycine and all of the air buffers adjacent to the base of the running gel were removed. The upper reservoir was filled with the same solution and 0.04 ml of 0.1% bromophenol blue (BPB) added. Electrophoresis was performed at 20 mA until the band of BPB passed through the stacking gel and reached the resolving gel. Once the dye was above the surface of the resolving gel the voltage was turned up to 200 V. The power was turned off when the BPB ran into the lower reservoir. The gel was then removed from the glass plates and placed in a solution containing 40% methanol and 15% trichloroacetic acid (TCA). The gel was then silver stained.

8.3.8 Silver staining

Proteins in the polyacrylamide gel were silver stained by the method of Otsuka *et al.* (1988). The two SDS-PAGE gels (irradiated and sham-irradiated) were stained simultaneously. All solutions were prepared with distilled water and all steps were carried out with gentle agitation at room temperature under normal lighting.

Step 1: The gel was soaked three times for 20 min in fresh-40% methanol containing 15% TCA.

Step 2: The gel was stained with 0.25% CB in 50% methanol-12.5% TCA for 15 min.

Step 3: The gel was destained three times for 10 min with fresh-5% TCA, three times for 15 min with 40% methanol-10% acetic acid, and twice for 20 min with 10% ethanol-5% acetic acid.

Step 4: The gel was washed twice for 10 min with fresh water.

Step 5: The gel was soaked in 1% sodium thiosulphate for 15 min.

Step 6: The gel was washed twice for 5 min with fresh water.

Step 7: The gel was soaked in 0.0032 M potassium dichromate containing 0.0032 M nitric acid for 10 min.

Step 8: Potassium dichromate was removed from the gel by washing twice for 5 min with water.

Step 9: The gel was soaked in 0.2% silver nitrate for 20 min.

Step 10: The gel was washed with water for 1 min and then washed in developer (0.28 M sodium carbonate containing 0.0185%

formaldehyde) for 30 s.

Step 11: The gel was soaked in the developer until the desired image is obtained.

Step 12: The development was stopped by soaking the gel in 5% acetic acid for 5 min.

Step 13: The gels were photographed.

8.4 Results

The 'priming' experiments described in chapter 7 demonstrated that a radioprotective mechanism could be triggered by treatment with X-ray doses of 0.05 Gy, 0.20 Gy or 1 Gy (see section 7.4.2.2.). The induction of the protective mechanism in those studies (section 7.4.2.2.) was inhibited by cycloheximide, an inhibitor of *de novo* protein synthesis. This experiment was designed to induce the radioprotective mechanism and demonstrate the production of newly synthesised proteins in the irradiated cells which might account for the radioprotective mechanism. An X-ray dose of 1 Gy was chosen to trigger the response as it was known that this dose would produce the most DNA damage of the three doses. Therefore, it is probable that the damage from this dose would result in the largest production of the inducible proteins compared with the smaller priming doses and therefore make the detection of any proteins that are induced easier.

It can be seen from the two electrophoresis gels that the protein array of the radiated cells is very similar to that of the unirradiated cells (Fig. 8.1, enlarged in Figs. 8.2, 8.3). The protein spots on the gel from the unirradiated cells are clearer and sharper than those on the irradiated gel. The reason for this is unknown. Usually, blurring of the spots is caused by poor isoelectric focusing, but the two IEF gels were run simultaneously and the acrylamide gels and protein extraction procedures were made and performed using the same stock solutions. Despite the blurring of the protein spots on the gel from the irradiated cell sample, clearly some under expression of proteins can be seen on this gel compared with the corresponding spots on the gel from the unirradiated cells. Both IEF gels were loaded with the same volume of cell extract. Many of the spots on the 'control' gel are barely visible on the 'irradiated' gel which indicates that during the 6 hour period following the 1 Gy treatment the

production of several proteins was suppressed, presumably while repair of radiation induced damage continued and possibly because of the repair of damage. A few proteins in the irradiated sample of cells have been over expressed, resulting in larger spots on the gel produced from the irradiated cells compared with the control gel. Only one protein was found on the irradiated gel that was *not* present on the control gel. This protein was therefore produced in response to the radiation treatment and could therefore represent a protein involved in the repair of radiation-induced damage. It is not possible to ascribe a function to this protein or a precise measurement of size. The two large spots on the gel are almost certainly actin and tubulin and therefore the induced protein has a smaller molecular weight than these two proteins. Estimating the approximate size of the induced protein from the gel is difficult because the gel was not a size gradient SDS-PAGE gel. However, the size of the induced protein can be estimated by its position on the gel relative to actin and tubulin. It appears to be 20-25 kilodaltons in size.

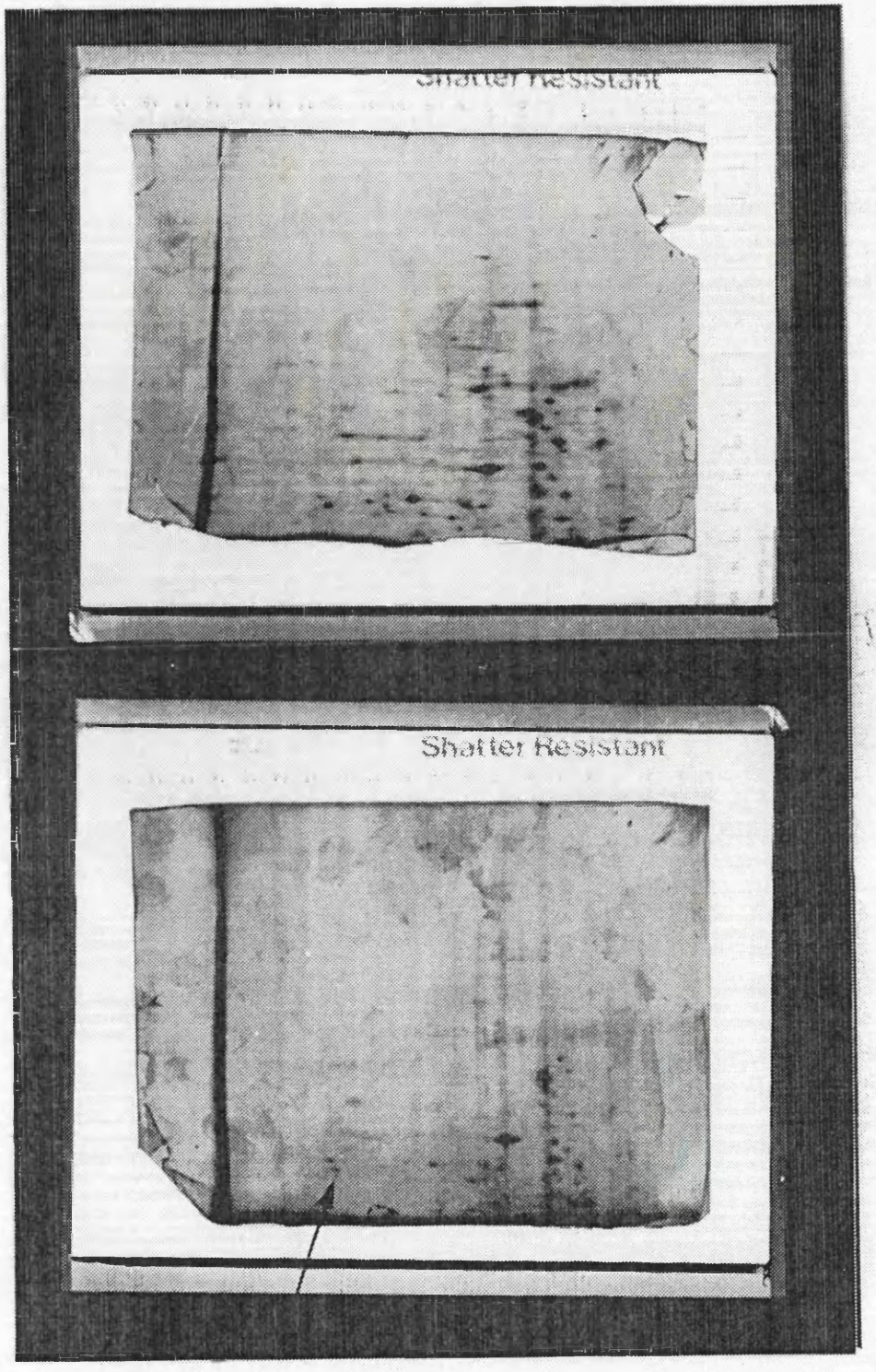

Fig. 8.1
A photographic comparison of the SDS-PAGE gels from an unperturbed and irradiated cell sample. The arrow (IP) indicates the position of the induced protein on the gel.

Fig. 8.2
Two dimensional gel electrophoresis of proteins found in a control cell sample. The two large spots (A and T) are probably actin and tubulin.

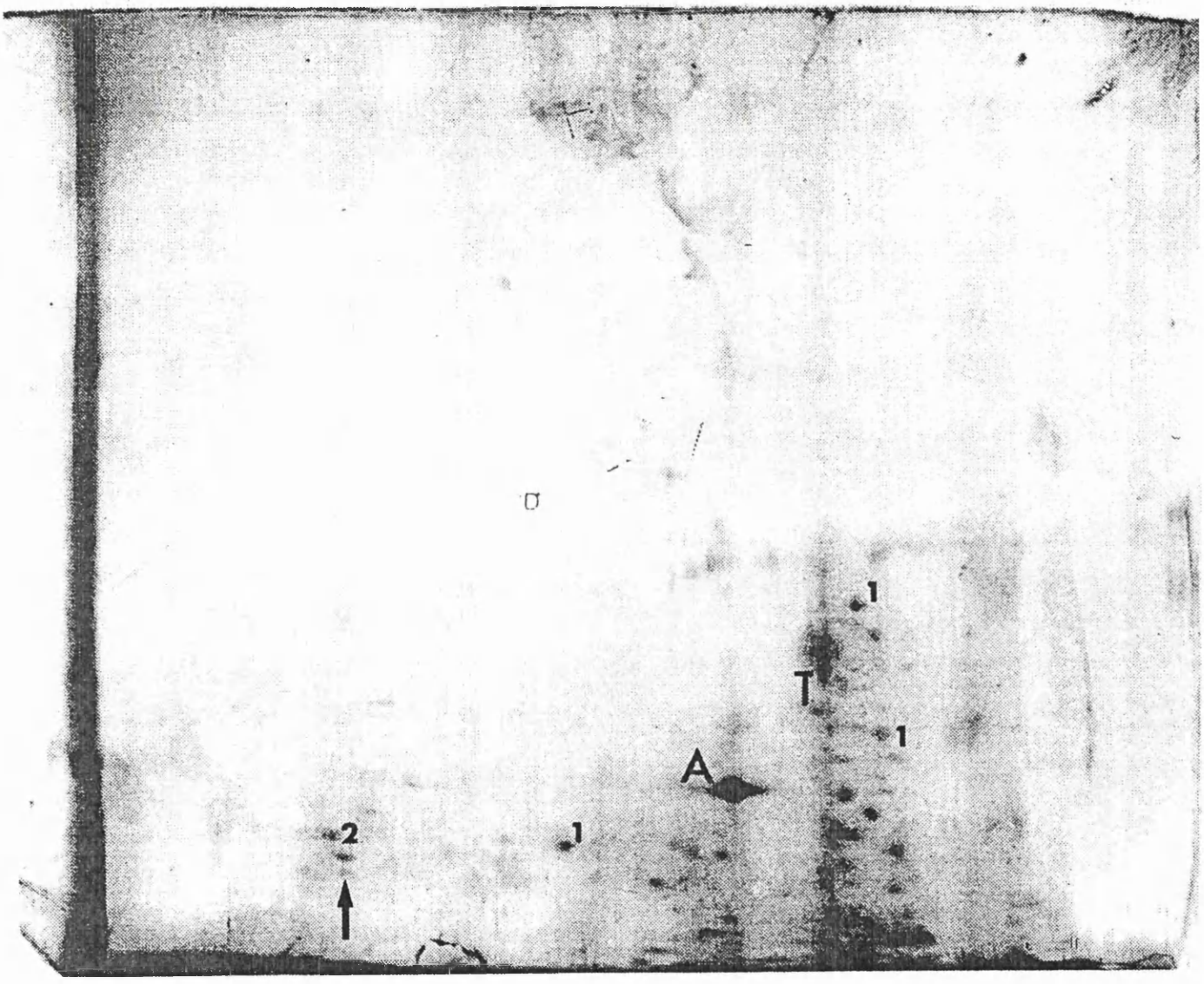

Fig. 8.3

A photographic magnification of the SDS-PAGE gel from a cell sample exposed to 1 Gy of 250 kVp X-rays, 6 hours prior to protein extraction. The two large spots (A and T) are probably actin and tubulin. The figure 1 marks proteins that are under expressed, 2 marks proteins over expressed compared with control (unirradiated) cells. The arrow indicates a protein which is present in the irradiated cells but not the unirradiated cells.

8.5 Summary

1. An X-ray dose of 1 Gy suppressed the production of many proteins to a level below that seen in a normal unirradiated cell sample.
2. The expression of a few proteins was seen to increase following radiation treatment.
3. Radiation treatment led to the production of one protein that is not normally present in unirradiated cells; this protein may possibly be involved in the repair of radiation damage.
4. The induced protein has a molecular weight in the range of 20-25 kilodaltons.

8.6 Discussion

It has been shown that a small pretreatment dose of X-rays (5, 20, 100 cGy) increased the radioresistance of cells to subsequent X-ray doses (in the range 0.04-0.6 Gy) administered 4-6 hours later compared with cells not given the priming X-ray doses. It has been postulated that the initial X-ray dose triggers an inducible repair system which is functional when the subsequent X-ray doses are given, resulting in the increased cellular radioresistance (chapter 7). Cycloheximide, a known inhibitor of protein synthesis (Kelland and Steel, 1989) prevented this increase in radioresistance when present during the interval between the two X-ray doses. These data therefore suggest that *de novo* protein synthesis might be required for the induction of the radioprotective mechanism.

This study was designed to detect proteins in irradiated cells that are not present in unperturbed cells to provide direct biochemical evidence for the existence of an X-ray induced response in this cell system. The protein array obtained from a cell sample irradiated with an X-ray dose of 1 Gy 6 hours prior to extraction of the cellular proteins was compared, using the technique of 2D dimensional electrophoresis, with the protein array from a 'sham' irradiated-cell population.

X-rays produce a wide spectrum of DNA lesions which may stimulate different

repair pathways. The expression of many proteins might therefore change following irradiation. This may reflect a change in the balance of protein synthesis between normally replicative DNA activity and the cellular processing of X-ray induced DNA damage. On examination of the 2D electrophoresis gels, differences in the protein array of the two cell samples (irradiated and unirradiated) was noted. The expression of several proteins was seen to change. However, one protein was detected in the irradiated cell population that was not present in the control cells and this could be considered as a candidate for the X-ray induced protein responsible for the increase in radioresistance seen in cells pretreated with small X-ray doses. The protein was only expressed after X-irradiation and therefore it is unlikely that it is involved in normal replicative or constitutive DNA repair.

The induced protein was estimated to be 25-35 kilodaltons in size. This is comparable to the size of some enzymes known to participate in the repair of radiation-induced damage. DNA glycosylases catalyse the cleavage of base-sugar bonds on altered or damaged nucleotide residues in DNA and have molecular weights of between 18-31 kilodaltons (Lindahl 1982). Apurinic and apyrimidinic endonucleases excise AP sites from damaged strands of DNA. An endonuclease enzyme purified from HeLa cells has been calculated to have a molecular weight of 32-41 kilodaltons (Lindahl 1982). It was not possible to assign a function to the X-ray induced protein seen in this V79 cell study but it has a comparable weight to enzymes known to be involved in repair. It is plausible therefore that this protein may be a repair enzyme. However, this protein is much smaller than the X-ray induced proteins (XIPs) reported by Boothman *et al.* (1989). Eight XIPs were detected in human melanoma cells which had molecular weights between 216-275 kilodaltons. These proteins were also specific for ionising radiation and were not induced by other DNA insults. The time course of the induction of the XIPs in the human melanoma study was similar to the induction response reported in thesis. The human XIPs were detected 3 hours after irradiation, required *de novo* protein synthesis and were maximally expressed 4-8 hours following irradiation.

The newly synthesised protein in this V79 study may be a repair enzyme which is required to repair specific lesions. Alternatively it may be another gene product

which facilitates the repair of radiation-induced damage, either directly or indirectly by increasing the efficiency of repair. The new protein might however function in the post translation modification of repair enzymes thereby increasing their efficiency or prevent the X-ray induced damage being fixed until it can be successfully repaired. This might explain why the protein detected in this study is smaller than those detected previously by Boothman *et al.* (1989) and the proteins of other inducible responses such as the heat shock proteins (for example HSP70, HSP110) (Lindquist 1986). The smaller molecular weight protein in this V79 study may increase the efficiency of repair or control the production of repair enzymes by repressing the production of other proteins in the cell not involved in DNA repair response. This type of repression of non-essential proteins following DNA insults is well characterized in the heat shock response (Lindquist, 1986).

This investigation was conducted to demonstrate the existence of X-ray induced proteins that might plausibly explain the increased radioresistance seen in this study. Clearly, it is not an exhaustive study and only demonstrates the presence of a single X-ray induced protein in this cell system while also noting the enhanced and suppressed expression of other proteins. Further work will have to be conducted and more 2D gels performed to characterise accurately this protein.

Chapter 9: The radiation response of other cell lines

9.1 Introduction

The increased X-ray sensitivity that is reported in this thesis following exposure to X-ray doses < 0.6 Gy compared with doses > 0.6 Gy might be a phenomenon common to a wide variety of cell lines. This effect may not have been noted previously because conventional assays which measure cell survival lack the necessary precision to assess cell survival accurately over the dose range where the increase in radioresistance has been observed in this study. It may have only been observed in insect cells (Koval, 1986) using a conventional assay owing to the high radiation resistance of insect cells e.g. $SF_{300} = 0.1$. Therefore, measuring the radiation response of a wide variety of cell lines using the DMIPS recognition assay might demonstrate whether the hypersensitivity to low doses of X-rays (< 0.6 Gy) seen in V79-379A cell line is a common phenomenon to all eukaryotic cell lines.

To measure the radiation response of a new cell line using the DMIPS cell analyser a recognition algorithm has to be constructed using the CELREC program so that the 'new' cells can be located and recorded. The efficiency of the cell recognition algorithm depends primarily on the methodology used to plate the cells as a monolayer culture. The number of cells recognised by the DMIPS cell analyser decreases with the length of time after plating because cells flatten out and lose their characteristic optical properties. The attachment time and flattening out time of cells are cell-line specific. In the V79-379A cell line for example, a 90 minute period is allowed for the cells to attach to the growth surface before the flask is scanned. Other parts of the cell plating methodology which effect the recognition efficiency are however, independent of the cell line. For example, standing the culture flasks vertically for 15 minutes prior to the initial CSCAN is known to reduce the amount of debris and the number of unattached cells that fall onto the scanned area once the scanning procedure has been completed (see section 3.7). The procedures in the recognition assay that are independent of the cell line are necessary to achieve consistency in measuring cell survival.

The optimum plating methodology for the V79-379A cell line used in this study took several months to develop and refine and is continually being reviewed. Clearly it is not possible in the time scale of this project to develop a precise and specific plating procedure for each new cell line, but the experience gained with the V79-379A cells can be used to design new plating procedures for pilot investigations with new cell lines. Fibroblasts, for example, are known to attach and flatten to a growth surface rapidly. Therefore, a short incubation period would be incorporated into the plating procedure for this to occur. In addition, more cells would be plated when a cell line is known to have a low plating efficiency so that a sufficient number of cells would be recorded to obtain an accurate assessment of survival. Combining the plating procedure for the V79-379A cell line with basic observations of the biology of the new cell line (i.e. attachment time of cells, flattening time of cells) then a simple plating methodology can be developed in a few weeks which permits the accurate assessment of cell survival below X-ray doses of 1 Gy.

9.2 Aims

The study described in this chapter was designed to measure the radiation response of a variety of cell lines over the X-ray dose range 0.04 - 1 Gy. These cell lines include another V79 cell subline (V79-B), a radiation sensitive cell line derived from this V79 subline (XR-V15B), a human epithelial lung cell line (L132), murine endothelial cell line (B_{10}/D_2) and a murine tumour cell line (WH-FIB).

9.3 Materials and Methods

9.3.1 Cell lines

9.3.1.1 V79-B fibroblasts

This cell line was originally isolated in 1958 from the lung tissue of a mature Chinese hamster (*Cricetulus griseus*) for use in genetic studies and was designated the V strain. These cells were later sub-cloned and redesignated the V79 strain. The V79-B strain of the V79 cell line used in this study was obtained from Dr. M. Zdzienicka at the Sylvius Laboratory, University of Leiden, The Netherlands, who obtained it from Dr. C.F. Arlett, MRC Cell Mutation Unit, University of Sussex, Brighton, U.K.

9.3.1.2 XR-V15B fibroblasts

The X-ray sensitive mutant XR-V15B was isolated from an ethyl nitrosourea mutagenised cell population of V79-B cells on the basis of its hypersensitivity to X-rays (Zdzienicka *et al.*, 1988). The parental V79-B Chinese hamster cell line originated from Dr C.F. Arlett at the MRC Cell Mutation Unit, University of Sussex, Brighton, U.K. The XR-V15B cell line demonstrates hypersensitivity to X-rays, exhibiting approximately an 8-fold increased X-ray sensitivity compared to the parental V79 cell line (Zdzienicka *et al.*, 1988). The XR-V15B mutant has a reduced rate of repair of double strand breaks induced by X-rays compared with the parental V79-B cell line. No difference exists between the wild type and XR-V15B cells in the initial number of single strand breaks induced, in the kinetics of their rejoining and in the final level of unrejoined single strand breaks (Zdzienicka *et al.*, 1988). XR-V15B mutants belong to the same complimentation group as the X-ray sensitive (*xrs*) mutants of Chinese hamster ovary cells described by Jeggo (1985).

9.3.1.3 B_{10}/D_2 lung endothelium

This cell line was obtained from Professor A. Curtis at the Department of Cell Biology, Glasgow University, and was isolated by collagenase perfusion of B_{10}/D_2 mouse lung. These cells express some endothelial cell characteristics in culture but no endothelial cell-specific antibodies confirm their identity. *In vitro* the cell line is grown and maintained as a monolayer culture in HAM's F-10 medium supplemented with 10% FCS.

9.3.1.4 L132 bronchial epithelium

This cell line was obtained from Dr. Janet Arrand at the Gray Laboratory. It is an epithelial human foetal lung fibroblast (Arrand and Murray, 1982) that grows in MEM culture medium supplemented with 10% FCS.

9.3.1.5 WH-FIB fibrosarcoma

WH-FIB is an undifferentiated fibrosarcoma. WH-FIB tumours are maintained by serial passage in male CBA mice, transplanted on the dorsal intramuscular surface. The WH-FIB cells used in this thesis were donated by Dr. Richard Hodgkiss at the Gray Laboratory.

9.3.2 Cell culture medium

Minimum essential medium (MEM)

A 10× MEM concentrate - Eagle modified (Flow Cat. No. 14-1002)
B Sterile water (residual ions << 1ppb)
C 1 N Sodium bicarbonate, 2 g l^{-1} (Flow Cat. No. 16-883)
D L Glutamine (Flow Cat. No. 16-801-49)
E 15% w/v Penicillin[1]
F 12% w/v Streptomycin[2]
G Foetal calf serum[3]

To make one litre:

Aseptically add 100 ml of A to 870 ml of B in a sterile litre bottle. Add 23.5 ml of C, 0.5 ml of E and F, previously filtered with a 0.22μm filter, and 10% v/v of G. Store at 4°C. Add 7 ml of D immediately prior to use.

HAM's nutrient mixture F-10 (HAM's F-10)

A Sodium bicarbonate
B 10 mg ml^{-1} Gentomycin
C F10 (HAM) nutrient mixture (Gibco Cat. No. N6635)
D Premix cell growth system (Collaborative Research Cat. No. 40351)
E 10% foetal calf serum[3]
G Sterile water (residual ions << 1ppb)

In 500 ml of G add 1.2 g of A, 5 ml of B, the contents of bottle C and 1 ml of D. Mix and make up to 1 dm^3 with G. Sterilise by filtration (0.22 μm pore size). Aseptically divide volumes into clean sterile bottles. Add E at desired concentration adjust pH 7.5 ± 0.2. Store at 4°C.

1. Glaxo, Benzylpenicillin sodium BP
2. Evans Medical Limited, Streptomycin sulphate BP
3. Gibco, Flow

9.4 Results

9.4.1 Generation of recognition algorithms

A CELREC procedure was performed on each of the cell lines to generate a parameter and feature file in order to carry out automatic cell location and recognition. A typical recognition image obtained from a minimum of 50 cells from each cell line

is shown in Fig. 9.1. The CELREC program was commenced when the majority of the cells had attached to the growth surface. This incubation time was dependent on the cell line (Table 9.1).

Cell line	Attachment time (min)	
	50% of cells	90% of cells
V79-B	90	310
XR-V15B	110	270
B_{10}/D_2	50	80
L132	80	140
WH-FIB	100	160

***Table 9.1** The attachment time, assessed by eye, for approximately 50% and 90% of the cells to attach firmly to the growth surface of the tissue culture flask. The cells were incubated at 37°C in a humidified atmosphere of 95% air + 5% CO_2. Approximately 3500 cells were plated in each flask.*

Once a parameter and feature file had been generated following the procedure used in section 2.1.6.7 the flask was rescanned to determine the recognition efficiency of the parameter file (Table 9.2). None of the parameter files had a recognition accuracy less than 88%. The higher false negative values for the B_{10}/D_2 and WH-FIB cells indicate the heterogeneity of cell size in these two populations: a large proportion of cells were incorrectly classified as debris in each of these samples because their optical images were not typical of the cell line. The most homogenous cell type was the V79-B line; only 5% of debris were scored as cells and less than 7% of cells were scored as debris: 95% of cells were correctly identified. The attachment efficiency (Table 9.3) indicates the number of cells that were located and remained attached 6 hours after location and recognition, and is dependent on the strength of attachment of cells to the growth surface.

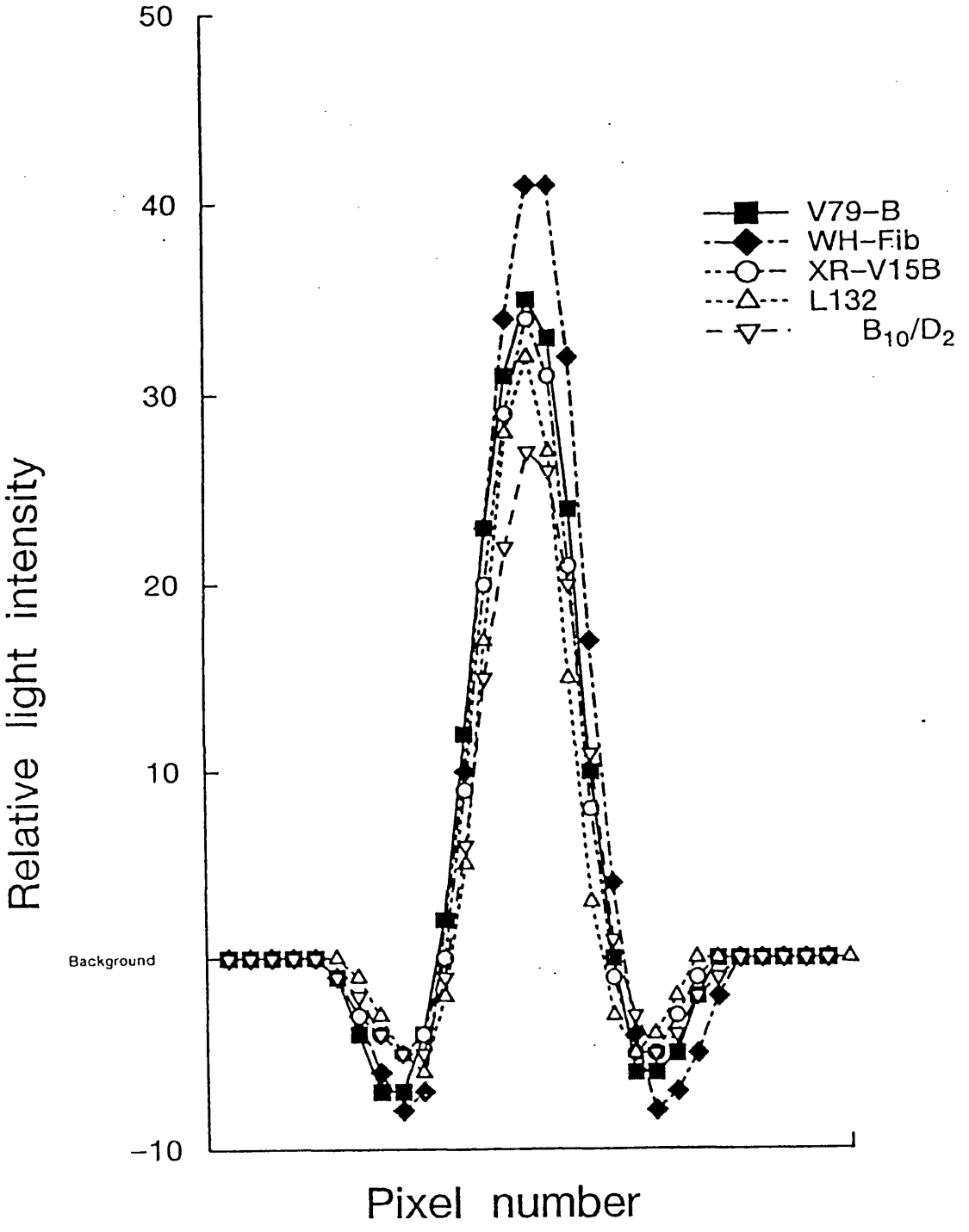

Fig. 9.1
Typical cell recognition signals for the five additional cell lines investigated. Each image was constructed by calculating the mean value of each feature from a single scan across at least 50 cells.

Cell line	Recognition efficiency		
	Fraction of objects located, correctly classified as cells (%)	False positive (%)	False negative (%)
V79-B	95	5	7
XR-V15B	87	13	16
B_{10}/D_2	88	12	14
L132	91	9	11
WH-FIB	92	8	23

Table 9.2 *The recognition efficiency of each cell-line specific recognition algorithm. The first column indicates the fraction of objects (%) that were correctly classified as cells by the cell analyser on an automatic scan. The second column indicates the fraction of objects (%) incorrectly scored as cells, typically these are pieces of debris. This is the critical parameter for the recognition algorithm; The lower the value the better the discrimination of the algorithm. The final column shows the number of cells that were scored as non-cells. This figure can be used to give an index of size heterogeneity, a large value suggests that many cells are atypical compared with the majority of cells in the population. The data were obtained by scanning 2 flasks soon after the parameter file had been generated and included typically 800 - 1000 cells of each cell type.*

Cell line	Attachment efficiency (%)	Plating Efficiency (%)
V79-B	94	95
XR-V15B	67	63
B_{10}/D_2	92	77
L132	89	92
WH-FIB	78	82

Table 9.3 *The attachment and plating efficiencies as calculated by the cell analyser. The attachment efficiency scores the number of cells which were located by the cell scan and remained attached 6 hours later when revisited. The plating efficiency is determined as the number of logged cells that grew into a colony.*

The plating efficiency was also determined from these experiments. The attachment efficiency and plating efficiency of the B_{10}/D_2 cell were difficult to assess because the cells were motile, exhibiting a tendency to migrate towards each other. Consequently, the cells were not located by the cell analyser at the positions logged initially by CSCAN when revisited to assess attachment and plating efficiencies.

The attachment and plating efficiencies of the additional cell lines were lower than for the V79-379A cell line. This may be because these cell lines were monolayer cell cultures and were plated using a procedure developed for V79-379A cells; a cell line grown routinely in suspension culture. These plating efficiency values are probably under estimated and if the plating procedures of the different cell lines had been developed and optimised further for the DMIPS cell analyser higher plating efficiencies might have been recorded.

9.4.2 V79-B and X-ray sensitive XR-V15B cell lines

It was hoped that by studying a normal V79 cell line and an X-ray sensitive mutant derived from that cell line that information would be obtained correlating the induction of radioresistance with overall radiosensitivity at 'high' doses >1 Gy. The V79-B and XR-V15B cell lines are grown routinely as monolayer cultures and maintained by conventional culture procedures whereby confluent monolayers of cells are trypsinised from the growth surface and the cells replated at lower densities. While this procedure is well established and is compatible with the conventional clonogenic assay devised by Puck and Marcus (1956) it can present problems for the DMIPS recognition assay, particularly at very low doses. The process of trypsinisation enzymatically detaches cells from the growth surface by digesting attachment proteins. This ultimately affects the re-attachment of the cells to new growth surfaces when the cells are eventually replated. If the procedure of trypsinisation i.e. the stripping of attachment proteins, is not a uniform process so that some cells in the population are exposed to a greater trypsinisation stress than other cells in the sample then a differential might exist between some cells which effects their subsequent attachment to a growth surface. This would effect the attachment *rate* of cells in the population producing a larger range of attachment times than would be seen normally for a cell

line grown in suspension culture. This inconsistency in the attachment of cells effects the plating procedure of the cells which can lead to errors in the assessment of cell survival. In a conventional clonogenic assay the cells that grow as monolayers are trypsinised, counted, diluted and then replated. The plated cells are then irradiated and incubated to allow for colony growth. The assessment of cell survival does not require the position of each cell to be logged. Therefore, the time at which a cell attaches to the growth surface of the culture flask is irrelevant in the assay procedure. In the recognition assay however, the cells are located precisely in the culture flask. If a cell which had been logged by the recognition assay was attached weakly to the growth surface and subsequently became detached, such a cell would be incorrectly classified as radiation killed. In a trypsinised cell population where a differential 'stripping' of surface proteins might have occurred, this effect will be amplified as some cells may require more time than the majority of the cells in the population to firmly attach to the growth surface. Despite strict trypsinisation procedures, the attachment time of cells varied considerably between individual culture flasks in the same experiment for the V79-B cell line and the mutant XR-V15B cell line. Some V79-B cells were seen to attach to the growth surface within 30 minutes of replating while others required 4-5 hours. This was not a problem in the V79-379A cell line as the cells were maintained in spinner culture and therefore did not require trypsinisation for cell plating. Trypsinisation also induces morphological changes in the shape of cells (Taylor, 1969) which might affect the efficiency of the recognition algorithm and consequently the accurate measurement of surviving fraction.

The survival curves obtained for the V79-B and XR-V15B cell lines are shown in Figs. 9.2 and 9.3. The error bars associated with the measurement of surviving fraction on the V79-B cells are larger that those seen on the survival curves obtained for V79-379A cells. This probably reflects the inconsistent attachment time of the cells which can lead to higher than expected measurements of surviving fraction. For example, two of the measurements of surviving fraction obtained for V79-B cells following exposure to 0.2 Gy of X-rays were inconsistent with the majority of the survival data. The high level of cell killing that occurred in this two flasks was probably due to some of the 'logged cells' detaching from the growth surface and subsequently being scored as radiation killed. In combination with the attachment error

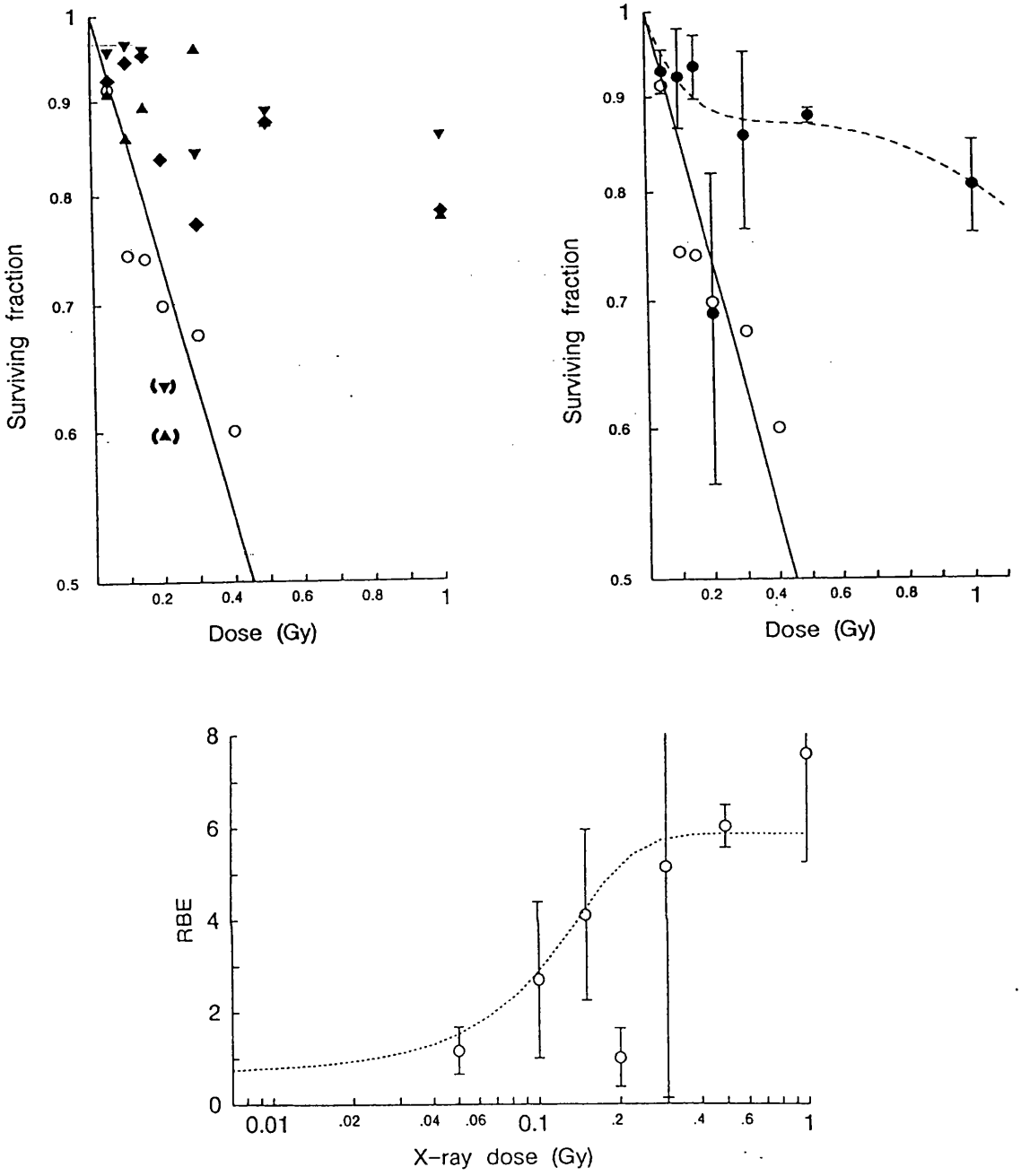

Fig. 9.2

Upper panel: Left, individual measurements of surviving fraction for V79-B cells irradiated with 250 kVp X-rays from three separate experiments (▼, ♦, ▲) and d(4)-Be neutrons (O). The variation in the measurement of surviving fraction that was obtained at each level of dose reflected the inconsistent attachment and plating efficiencies that were seen and the 'dispersed' colonies of this cell line. These two parameters are critical for the accurate measurement of survival using the cell analyser. Right, the X-ray data have been combined (●, mean ± SD) and are fitted with a modified LQ model (Eqn. 4.3). The neutron data are fitted with Eqn. 4.8
Lower panel: RBE values between 250 kVp X-rays and d(4)-Be neutrons for V79-B cells. The data are fitted with Eqn. 4.5

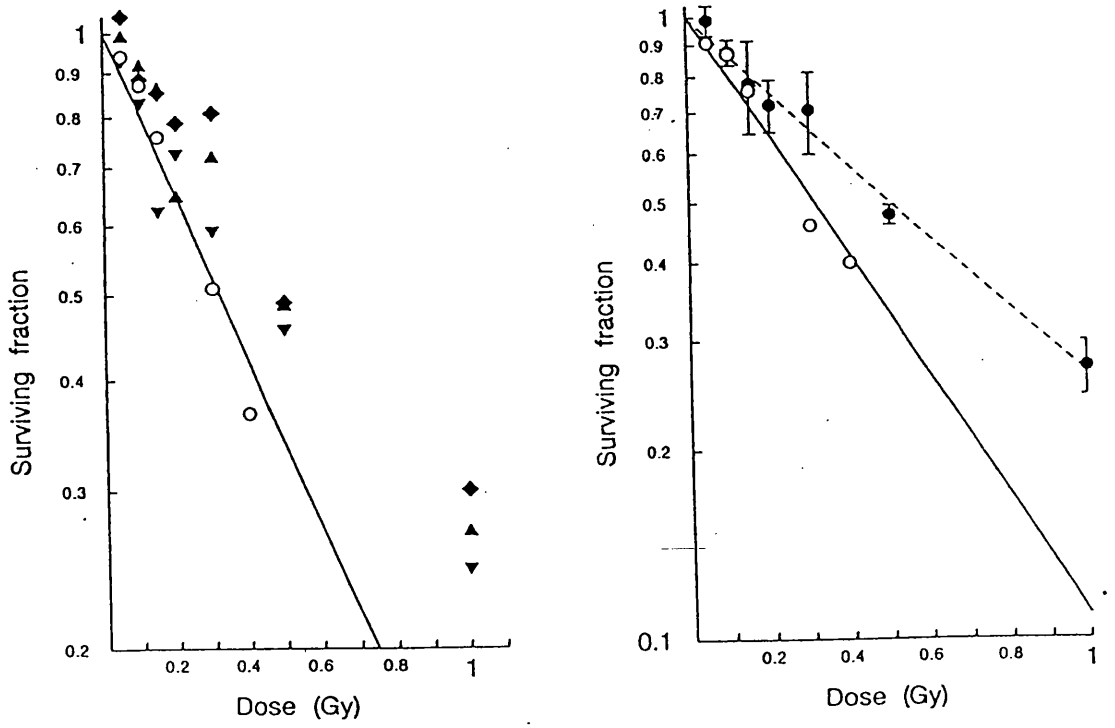

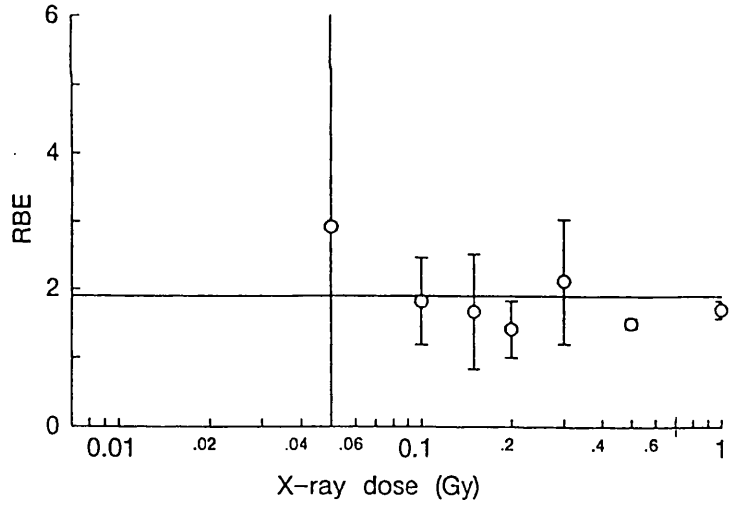

Fig. 9.3

Upper panel: Left, individual measurements of surviving fraction for XR-V15B cells irradiated with 250 kVp X-rays from 3 separate experiments (▾, ♦, ▴) and d(4)-Be neutrons (O). Right, the X-ray data have been combined (●, mean ± SD) and are fitted with a modified LQ model (Eqn. 4.3). The neutron data are fitted with Eqn. 4.8
Lower panel: RBE values between 250 kVp X-rays and d(4)-Be neutrons for XR-V15B cells. The data are fitted with Eqn. 4.5

an addition error caused by the colony morphology of the V79-B and XR-V15B cells might have contributed to the variation in surviving fraction that was seen. The cell colonies of these two cell lines were diffuse compared with the compact colonies of the V79-379A cells. Clonogenic survival is determined by measuring the area of the colony produced by each logged cell and comparing it with a previously determined value typical of a 50 cell colony of that cell line. The area of a colony is measured by the SSCAN program which calculates the number of pixels above and below background light level in a given region centred on the position of the logged cell, a diffuse colony will randomly extend beyond that area so that all the cell in the colony will not be measured. The area can be increased but this increases the possibility that adjacent cells or colonies not arising from the logged cell may be included in the size assessment. Despite these systematic errors, cell survival was measured for V79-B and XR-V15B cells down to X-rays doses of 0.04 Gy. The survival data from the XR-V15B cells did not show any evidence of a hypersensitivity to low doses of X-rays, cell survival decreased exponentially. The RBE data did not suggest an increase in RBE with an increase in X-ray dose over the dose range 0.2-0.6 Gy, which was characteristic of the hypersensitive response to low X-ray doses in the V79-379A cells. Fitting the induced repair model (Equation 4.5, section 4.5.2) to all the RBE data for the XR-V15B cell line produced a linear fit to the data (Fig. 9.3) supporting the postulate of a exponential survival response. Although the V79-B survival data is not as 'clean' as the XR-V15B data there is some evidence a hypersensitive response at very low doses (<0.2 Gy) may exist. If the two survival measurements at 0.2 Gy (indicated by brackets on the figure) are excluded from the data set then the data can be described with reasonable accuracy by the induced repair model (Equation 4.3, section 4.5.1). Fitting the V79-B RBE data with an induced repair model (Equation 4.5, section 4.5.2), using the same assumptions as in the surviving fraction data, then the fit to the data indicates an increase in RBE as the X-ray dose increases over the dose range 0.05-0.3 Gy. This suggests that the induced repair response seen in the V79-379A cell line may also exist in this cell line. Further development of the plating procedures for the V79-B and XR-V15B cell lines might reduce the size of the error bars on the measurement of surviving fraction which would help to confirm the results of this study.

9.4.3 B_{10}/D_2 cell line

This is a typical mammalian endothelial cell line which grows in monolayer culture. Once plated, the cells flattened out very rapidly which suggested that the process of trypsinisation which caused problems in the plating procedure of the V79-B and XR-V15B cells would not be so critical in this cell line. However, two additional problems arose. The first problem was potentially the more difficult to overcome and eventually led to work with this cell line being discontinued. Once flattened, the cells began to 'walk' over the growth surface, moving away from the position where they were located initially (Fig. 9.4). This migration of the cells effected the accurate measurement of cell survival because few cells could be reliably revisited. The second problem that was encountered was not as troublesome but still introduced error into the measurement of surviving fraction. Some of the cells in the population would flatten to such an extent that the detection threshold had to be lowered to a point where cell discrimination became difficult. The accurate recognition of a cell relies on the cell distorting the incidental light level above or below a set threshold level. This threshold light level is necessary to account for small variations in the light level that can be caused by imperfections in the tissue culture plastic. Very flat cells distort the incidental light minimally, compared with rounded cells, therefore their optical recognition image is not as distinct as that of a rounded cell, making cell recognition difficult.

9.4.4 WH-FIB cell line

The WH-FIB cell line was also grown in monolayer culture but a freshly trypsinised and replated cell population flattened rapidly on the growth surface. The problems encountered in the plating procedure of cells with the V79-B and XR-V15B cell lines were therefore not as important in this cell line. The cell colonies that were produced by the WH-FIB cells were compact and therefore more suitable than the colonies of the V79-B and XR-V15B cells for the assessment of survival by the SSCAN program (Fig. 9.5). The WH-FIB surviving fraction data did not show any evidence of the hypersensitivity to low doses of X-rays that was seen in the V79-379A cell survival data. However, the WH-FIB data only covered the X-ray dose range 0.05-0.5 Gy and no measurement of surviving fraction was obtained at an X-ray dose

of 1 Gy therefore the response can not be compared fully with the V79-379A survival data. The pattern of RBE against X-ray dose that was seen in the V79-379A cell line was not seen in the WH-FIB cell line and no consistent increase in RBE was seen over the X-ray dose range 0.05-0.5 Gy. The error bars on some data points make it difficult to ascribe a precise relationship to the RBE data but it is clear that the WH-FIB cell line does not exhibit the 'induced repair' response characteristic of the V79-379A cell line. Fitting all of the WH-FIB RBE data with the induced repair model (Equation 4.5, section 4.5.2) results in a linear fit to the data indicating an exponential survival response over the 0.05-0.5 Gy X-ray dose range supporting the hypothesis that this cell line does not exhibit a hypersensitive low dose X-ray response.

9.4.5 L132 cell line

This is another cell line that grows and is maintained in monolayer culture. It is an epithelial cell line and consequently attaches rapidly to the growth surface of the flask. Once attached, the cells remain attached firmly and are stationary unlike the B_{10}/D_2 epithelial cells which were motile. The cell colonies are compact and therefore suitable for accurate survival analysis by SSCAN. Survival curves over the X-ray dose range 0.04-1 Gy obtained for this cell line were consistent with an increased X-ray sensitivity at low doses (Fig. 9.6). The initial region of the survival curve over the dose range 0.04-0.20 Gy was steeper than that over the dose range 0.5-1.0 Gy, giving a concave survival curve indicated by the fit to the data that was obtained using the induced repair model (Equation 4.3, section 4.5.1). These cell survival data suggest that the induced repair response characterised in the V79-379A cell may also exist in the L132 human-bronchial epithelial cells.

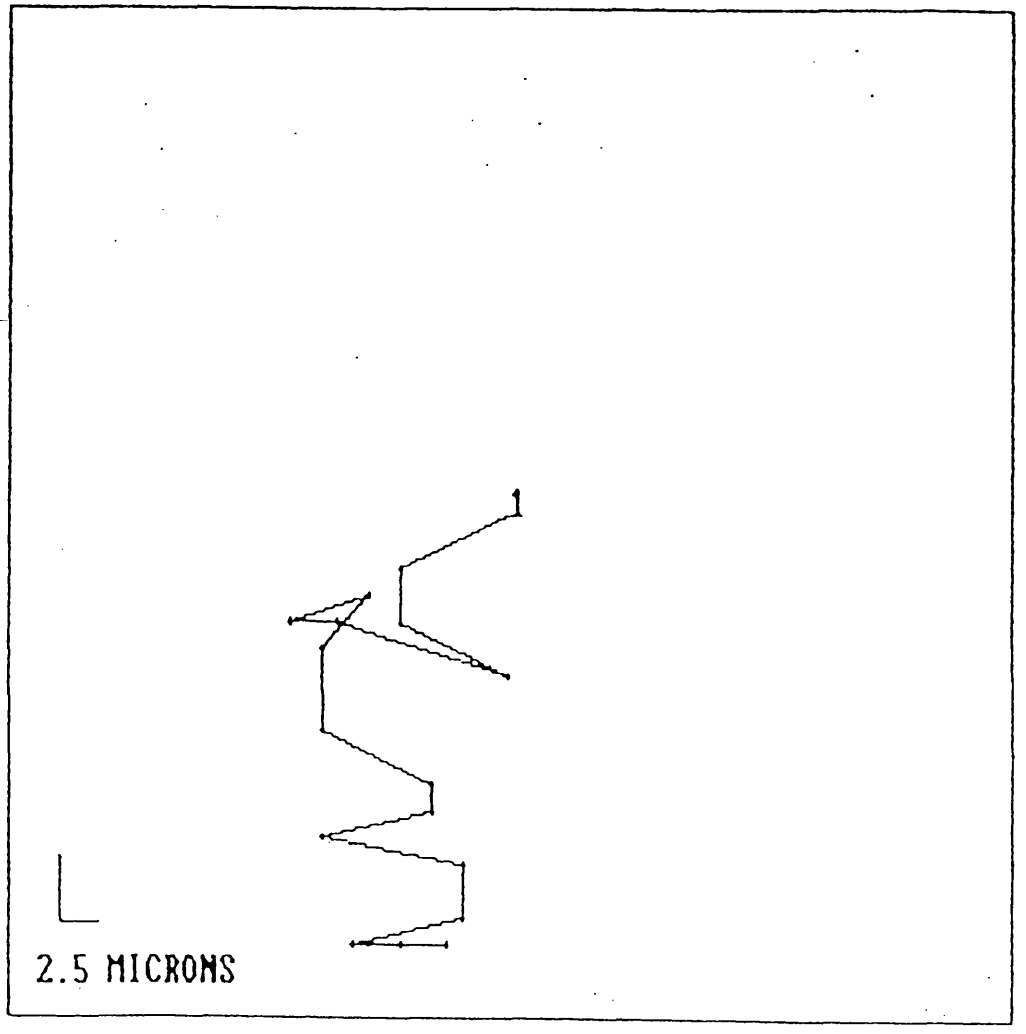

Fig. 9.4
A dynamic plot illustrating the migration of a single B_{10}/D_2 cell revisited every 10 minutes using the RSCAN program. The lines indicate the distance moved and the direction taken by the cell during the 10 minutes interval between revisits.

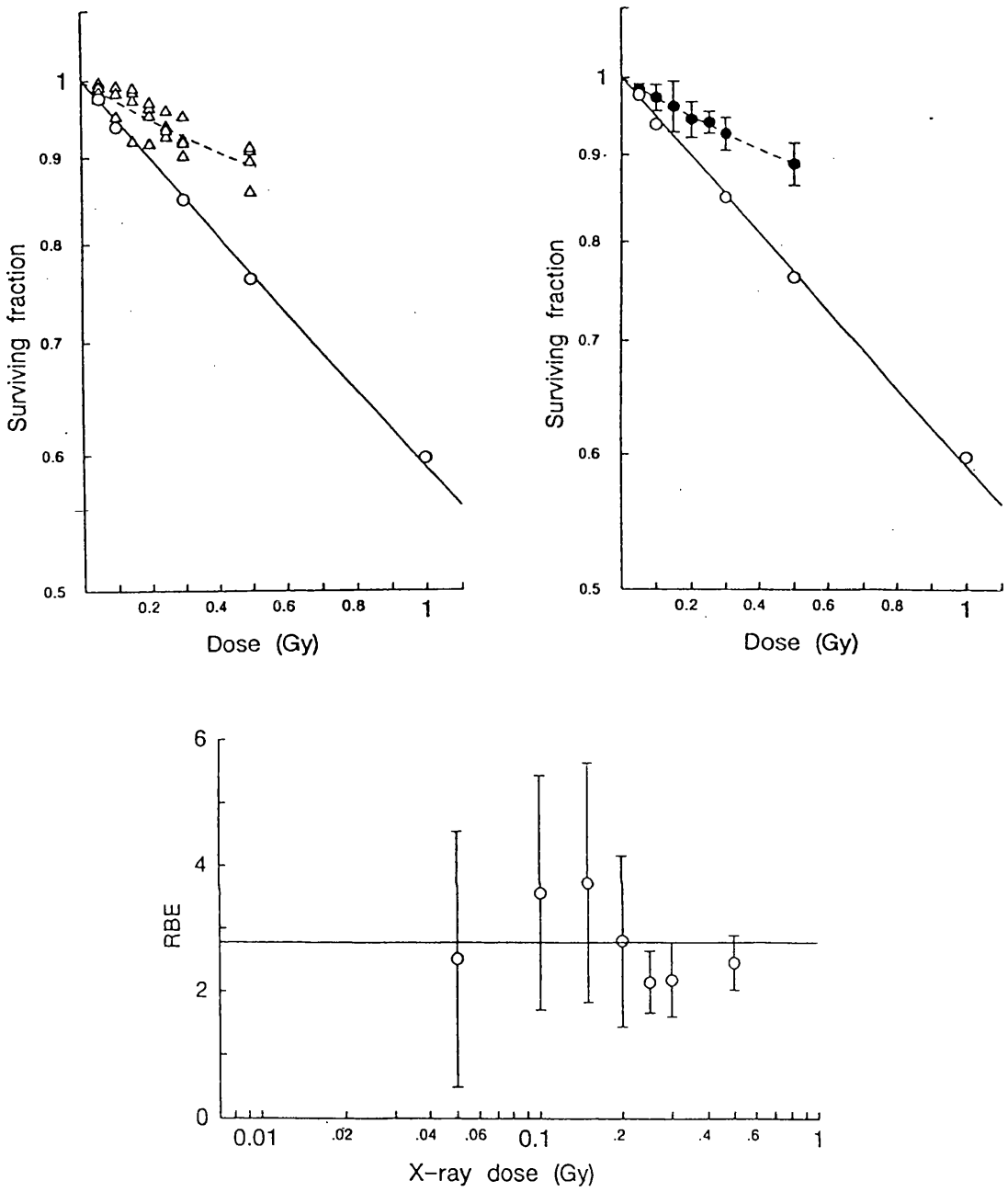

Fig. 9.5

Upper panel: Left, individual measurements of surviving fraction for WH-FIB cells irradiated with 250 kVp X-rays from 3 separate experiments (△) and d(4)-Be neutrons (O). Right, the X-ray data have been combined (●, mean ± SD) and are fitted with a modified LQ model (Eqn. 4.3). The neutron data are fitted with Eqn. 4.8

Lower panel: RBE values between 250 kVp X-rays and d(4)-Be neutrons for WH-FIB cells. The data are fitted with Eqn. 4.5

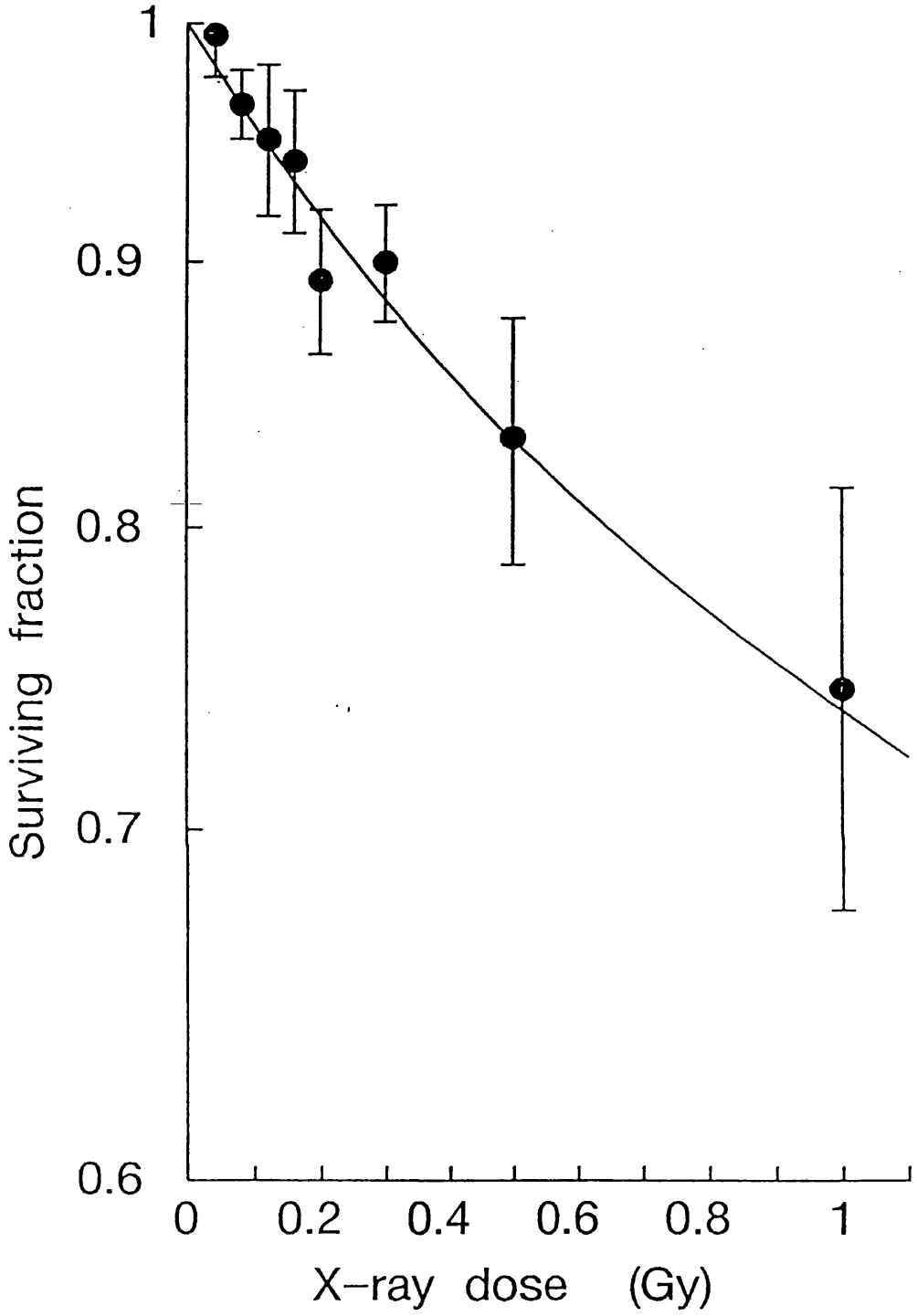

Fig. 9.6

Cell survival obtained following exposure to 250 kVp X-rays of L132 human foetal bronchial epithelial cells (●, mean of 3 experiments ± SD). These data suggest that this cell line exhibits the increased sensitivity to X-ray doses below 0.6 Gy that was observed in the V79-379A cells.

9.5 Summary

1. Recognition algorithms were generated for V79-B, XR-V15B, WH-FIB, L132 and B_{10}/D_2 cells which enabled the cell analyser to identify cells correctly with a recognition efficiency >88%.

2. Low-dose survival measurements were made for the V79-B, XR-V15B, WH-FIB and L132 cell lines with reasonable accuracy. Difficulty was encountered with the V79-B and XR-V15B cell lines because of variable and inconsistent attachment and plating efficiencies. The diffuse colonies that were produced by these two cell lines also made the accurate assessment of survival difficult. Despite these problems the survival data obtained for the V79-B cell line suggest that the induced repair response seen in the V79-379A cell line may also exist in this cell line. The repair deficient XR-V15B cell line and WH-FIB cell line did not show any evidence of an inducible repair component.

3. Accurate measurement of cell survival was obtained for the L132 cell line. This had a concave survival response over the X-ray dose range 0.04 - 1 Gy which demonstrates that the phenomenon of increased sensitivity to low dose X-rays that was first seen in the V79-379A cell line also occurs in this cell line.

4. The B_{10}/D_2 cell line was not suitable for the assessment of cell survival using the DMIPS recognition assay, as the cells are motile and migrate over the growth surface. Accurate measurements of cell survival rely on the growth of the colony being centred on the original position of the located cell.

9.6 Discussion

It has been shown in this thesis that V79-379A cells are hypersensitive to single X-ray doses below 0.6 Gy. In some experiments (e.g. see Fig. 3.3) at very low doses (<0.2 Gy) X-rays are nearly as effective at killing cells as neutrons, but as the

X-ray dose increased over the range 0.2-0.6 Gy an increase in radioresistance was observed. A similar effect has been characterised in insect cells at a similar level of surviving fraction (Koval, 1984). However, the phenomenon was characterised by much higher X-ray doses in the insect cell study as insect cells are extremely radioresistant compared with mammalian cells.

Hypersensitivity to low-dose X-rays might therefore be a common effect in all or most repair proficient mammalian cell lines and has remained undetected because until only recently has the technology been available to detect it. The experiments reported in this part of the thesis were designed to measure clonogenic cell survival in a further selection of cell lines over the X-ray dose range 0.04-1 Gy, to determine whether the low-dose hypersensitivity to X-rays noted for V79-379A cells is more widespread.

Of the 5 cell lines investigated L132 and V79-B exhibited a hypersensitivity to low-dose X-rays compared with higher doses. These cell lines are repair proficient. However, the XR-V15B repair deficient cell line did not have the hypersensitive response to low-dose X-rays compared with higher doses, characterised in the other cell lines by the subsequent increase in radioresistance over the dose range ≈0.2-1 Gy. A correlation therefore exists between the repair proficiency of a cell line and the increase in radioresistance over the dose range ≈0.2-1 Gy. If this increase in radioresistance is the manifestation of an inducible repair process then this might explain why repair proficient cell lines have an shallow slope to the initial region of the survival curve and repair deficient cell lines have steep survival curves (Denekamp *et al.*, 1989). The data reported in this thesis indicate that for X-ray doses < 0.2 Gy most repair proficient cell lines have an initial steep survival curve. However, as the X-ray-induced damage increases a radioprotective mechanism is induced in the repair proficient cells that repairs some of the damage resulting in a decrease in the slope of the survival curve over the dose range 0.2-0.6 Gy. This steep initial slope might be a measure of the intrinsic radiosensitivity of each cell line before the induction of the repair mechanism modifies the survival of cells. Whereas, the repair deficient cell lines does not have a change in the slope of the survival curve over the dose range 0.2-0.6 Gy because the inducible mechanism is either not triggered or the cell is

unable to respond to the triggering of the inducible system because of the deficiency in repair. The XR-V15B cell line is defective in DNA DSB repair (Zdzienicka *et al.*, 1988). This causal relationship suggests that the repair of DNA DSBs is essential for the correct functioning of the radioprotective mechanism.

The WH-FIB survival data are not conclusive (Fig. 9.5). If further studies show that this cell line does exhibit a hypersensitive low-dose X-ray response, followed by an increase in radioresistance at higher doses, then this cell line is consistent with the hypothesis that induced repair is an important factor in the radiosensitivity of repair proficient cells following X-irradiation. If, however, this cell line is subsequently found not to have a hypersensitive response to low doses of X-rays then this will provide further evidence that the phenomenon is not an experimental artefact of the recognition assay. It will also raise the question why some repair proficient cell lines exhibit the inducible response and others do not.

The biology and cell culture conditions of the V79-B, XR-V15B, WH-FIB and B_{10}/D_2 cell lines differed significantly from that of the V79-379A cells. This might have contributed to the larger error on some of the measurements of cell survival (Figs. 9.2, 9.3, 9.5) compared with that seen in the V79-379A study. This increased error would probably be reduced with further modifications to optimise the plating procedure of the cells. In the V79-379A cell line the error on the estimates of surviving fraction were reduced with the development of the standard plating procedure (SPP) (see chapter 3). When measuring cell survival with the recognition assay the most critical parameters in the SPP are the time required for the cells to attach to the growth surface, the attachment and plating efficiencies of the cells and the compactness of the resultant cell colony. V79-379A cells were grown in spinner culture, attached rapidly to the growth surface of the flask, were non-mobile, remained firmly fixed during the duration of the assay and produced discrete cell colonies. These are ideal characteristics for a cell line to be assayed by the DMIPS recognition assay. However, the data for these other cell lines indicate that the DMIPS recognition assay is versatile and can be modified for a selection of cell lines by changing the cell plating procedure.

Other cell lines are routinely studied at other laboratories using the other DMIPS cell analysers. A different V79 cell sub-line to the one used in this study (Korbelik and Skov, 1989; Spadinger *et al.*, 1989) and fibroblast 3T3 cells (Thurston *et al.*, 1986) have been examined following exposure to low doses of radiation, but the lowest X-ray dose studied in either of these investigations was 0.4 Gy. The hypersensitivity to low dose X-rays reported in this study would not therefore have been detected in these other DMIPS recognition assay studies.

Chapter 10: Summary and discussion of results

The survival of V79-379A cells exposed to single doses of X-rays (0.01-10 Gy) and neutrons (0.02-3 Gy) was measured using a clonogenic recognition assay with a computer aided microscope. This method employed a cell-line specific algorithm to locate and identify individual freshly-plated cells, allowing precise estimates of cell survival to be made in the low dose, high survival region of the survival curve.

A linear quadratic (LQ) equation was used to describe mathematically the cell survival data following X-irradiation. It is a simple equation that has been found to simulate experimental data for many different mammalian cell lines over the dose range used in this study (e.g. Watts *et al.*, 1986; Steel and Peacock, 1989). Survival estimates over the X-ray dose range 1 to 10 Gy showed a good fit to a LQ model. However, for X-ray doses <<1 Gy an increased X-ray sensitivity was observed compared with survival estimates predicted from a LQ extrapolation of the higher-dose data (Fig. 3.3). Therefore, the data in this thesis indicate that a LQ model does not describe accurately the survival response of V79-379A cells following exposure to extremely small X-ray doses. This observation supports the work of Joiner and Johns (1987) and Joiner (1990) which also concluded that a LQ model did not describe accurately low-dose X-ray sensitivity.

The results of the mathematical modelling performed on the survival data (see section 4.5) suggested that if the low-dose X-ray hypersensitivity was due to the presence of a static subpopulation of intrinsically radiosensitive cells (e.g. in a specific phase of the cell cycle) then this population would have to be ≈6% of the total population with a sensitivity (defined by the α in a modified LQ model) of ≈50× that of the balance of the population. This seems unlikely. Experimental evidence which confirmed that the low-dose X-ray hypersensitivity was unlikely to be due to an heterogeneous intrinsically radiosensitive subpopulation of cells was described in section 4.4.1: a population of cells cloned from a single cell taken from the stock cell culture exhibited a biphasic survival curve over the same dose range as the parental cell population. The experiments reported in chapter 5 demonstrated that the low-dose X-ray hypersensitivity was probably independent of cell-cycle phase, indicating the

response was unlikely to be due to a cell cycle phenomenon, as populations of cells enriched in G_1 or S phase cells had comparable RBE responses to an asynchronous cell population (see section 5.9.2). The biphasic nature of the survival curve was also shown to be independent of X-ray dose-rate and the irradiation exposure time (see section 6.4).

The phenomenon of low-dose X-ray hypersensitivity and the subsequent increase in radioresistance over the dose range 0.01-1 Gy may, instead, reflect the induction of a radioprotective mechanism as the radiation response of the V79-379A cells was described accurately by a modified LQ equation (Eqn. 4.3) in which α was allowed to decrease with an increase in X-ray dose (Fig. 4.3). In the lethal, potentially lethal model (Curtis, 1986), α depends on the number of the initial induced lesions allowed to repair, and so a biological explanation of a dose dependent α may be induced repair (Joiner, 1990).

Documented inducible-repair responses

Mammalian cells (Samson and Schwartz, 1980) and prokaryote cells (Samson and Cairns, 1977) exposed to small quantities of alkylating agents are reported to be resistant to the induction of cellular damage following the subsequent exposure of the cell to the same agent. This adaption response apparently results from the induction and synthesis of adaptation proteins such as DNA methyl-transferases (Bridges and Lehmann, 1982). DNA repair genes are also known to be directly expressed as a result of exposure to a wide range of cytotoxic stresses. The exposure of *Escherichia coli* to DNA-damaging agents can induce the expression of several gene responses e.g. the SOS response which includes genes that are involved in excision (*uvr* gene), recombinational repair (*rec A* gene) and mutagenesis (*umuCD* gene) (Little and Mount, 1982; Freidberg, 1985), the heat shock response (Lindquist, 1986) and an adaptive repair response (Walker, 1985). Probably the inducible response most extensively characterised in cells is the heat shock response. When eukaryotic or prokaryotic cells grown in culture are exposed to mild heat treatment they respond by synthesising a small number of well-defined proteins known as heat shock proteins (HSP) (reviewed by Lindquist, 1986). The response is induced within minutes and is associated with newly synthesised RNA, while both the transcription of previously active genes and

the translation of pre-existing mRNA messages not associated with the production of HSPs are repressed (Lindquist, 1981). It is conceivable therefore, that a similar system exists in prokaryotic and eukaryotic cells in response to the DNA damage that results from ionising radiation. However, despite the widespread acceptance of inducible biochemical pathways in general, the existence of inducible repair systems in mammalian cells that respond to ionising radiation has remained controversial.

Recently however, several studies have established that human lymphocytes exposed to low doses of ionising radiation from incorporated tritiated thymidine, or X-rays, become less susceptible to the induction of chromatid breaks by higher doses of X-rays given 4-6 h after the initial small radiation doses (Olivieri *et al.*, 1984; Wiencke *et al.*, 1986; Shadley and Wolff, 1987; Wolff *et al.*, 1989). This adaptive response to ionising radiation was postulated to be due to an inducible repair process. This process is stimulated by the initial low dose of radiation, and if still in place at the time of the higher dose exposure it causes the repair of some of the primary breaks in the DNA that result from the second exposure. A similar adaptive response, measured by a reduction of sister chromatid exchanges, has also been reported in V79-B310H cells (Ikushima, 1987). Clearly, several investigations have produced experimental data that have demonstrated the existence of an inducible repair response in mammalian cells following exposure to ionising radiation. The data in this thesis appear to provide further evidence that mammalian cells contain an inducible repair mechanism that is triggered in response to ionising radiation.

Triggering of the protective mechanism

If the data in this thesis do represent the manifestation of 'induced repair', how would such a system be triggered? It was postulated (see chapter 3) that at the very lowest X-ray doses (<0.2 Gy) the inducible repair mechanism would not be fully functional but as the dose increased (e.g. over the range 0.2-0.6 Gy) sufficient damage would be received to trigger the repair system. At doses above 1 Gy the system would be fully induced. The precise stimulus that triggers the inducible repair system is unknown. However, as it is a dose dependent process, it is probable that the increasing amounts of specific types of DNA lesion(s) or the spatial distribution of those DNA lesion(s) in the genome (either all lesions or a particular type of lesion) are involved.

Alternatively, the mechanism that triggers the inducible repair system might be the temporal distribution of initial ionisation events throughout the genome or the entire cell. The distinction between the initial ionisation event (a physical process) and the eventual DNA lesions that are produced (a biological process) is unimportant in terms of cell lethality, but for the purposes of demonstrating a possible trigger for the inducible repair response the two processes will be considered separately.

Type of Lesion

As was described earlier (chapter 7), ionising radiation produces a range of lesions in DNA (Ward, 1988). These include breaks to the DNA strands (either single-strand breaks (SSB), or double-strand breaks (DSB)) and damage to the individual base or sugar molecules within the DNA (Frankenberg-Schwager, 1989). Crosslinks within the DNA itself, or between DNA and closely associated proteins, also occur (see Fig. 7.2). Although SSBs and the various types of base damage induced in mammalian cells by ionising radiation might not appear to be important in determining cell lethality (for a review see Frankenberg-Schwager, 1989) any of these classes of DNA lesions might be responsible for the triggering of the inducible protective mechanism. Each type of lesion stimulates different cellular responses which require a variety of DNA repair pathways (Collins, 1987) any of which could be involved in, or precipitate the triggering of, the inducible mechanism. DNA base damage is known to trigger an inducible response in prokaryote and eukaryote cells (Samson and Cairns, 1977; Samson and Schwartz, 1980). However, it is more probable that the DNA lesions that are 'potentially' lethal to the cell (if not correctly repaired) would be the most likely to trigger the inducible repair system as a failure to do so would result ultimately in cell death.

However, pre-treatment of cells with a non-cytotoxic concentration of H_2O_2 (10^{-4} M) prior to the radiation exposure (section 7.4.1.2) was seen to induce the protective mechanism. It has been calculated that exposing a cell to a concentration of 10^{-4} M H_2O_2 induces SSB damage to the DNA, by the action of oxidative free radicals, with an equivalent yield to that produced by 8 Gy of low LET X-rays (Ward *et al.*, 1985). This is equivalent to approximately 8000 SSBs in the DNA (Ward, 1985) and although this appears not to be lethal to the cell this level of damage, or possibly

the distribution of this damage in the genome, appeared to be sufficient to trigger the protective mechanism. These data indicated that the protective mechanism can be induced by DNA damage which does not appear directly to be important in determining cell lethality, indicating that the triggering of the response might be a more complex process than has just been postulated. The inducible response might also function to repair larger numbers of potentially mutagenic lesions as well as potentially lethal lesions. Other studies have reported previously that non-toxic levels of H_2O_2 induce a repair mechanism in *Escherichia coli* that makes the bacteria less susceptible to killing from subsequent exposures to ionising radiation (Demple and Halbrook, 1983) supporting this hypothesis.

The protective mechanism was also induced by small, single doses of ionising radiation (see section 7.4.2.2). For the smaller of these doses (0.05 Gy), this corresponds to average DNA damage of about 50 SSBs, 2 DSBs and 8 DNA protein crosslinks per cell (Ward, 1988). Clearly, these values represent an extremely small amount of damage per cell, however they may prove lethal if they are not repaired correctly. Substantial evidence, particularly obtained with mutant yeast strains which are defective in their ability to repair DNA DSBs, have shown that there is an approximately one-to-one correlation between unrepaired DSBs and cell killing (Frankenberg *et al.*, 1981; Blöcher & Pohlit, 1982). Similar studies have suggested that this may also true in mammalian cells and several extremely radiosensitive mutants have been isolated which are defective in DSB rejoining (Jeggo and Kemp, 1983). Possibly not just one, but two or more unrepaired double strand breaks, in a vital section of DNA, are sufficient to prevent successful replication of the cell (Ward, 1988; Goodhead, 1989). Good correlations have been found between unrepaired double strand breaks and chromosome aberrations in mammalian cells (Cornforth, 1989) and chromosome aberrations are known to be critical lesions responsible for cell death (Bryant, 1984; Natarjan and Obe, 1980; Frankenberg *et al.*, 1981). Correlations do not prove a causal relationship; however as a DSB is known to be a cause of cell lethality, it is plausible that a DSB in an essential region of the genome could trigger the radioprotective mechanism because failure to repair the DSB might lead to cell death. The spatial distribution of DSBs in the genome might also contribute to the induction response. The failure of the XR-V15B cell line, known to be deficient in the

repair of DSBs, not to show a biphasic survival curve (see section 9.4) provides circumstantial evidence which supports the concept that DSBs might be important in the triggering of the induction process.

Temporal distribution of the energy depositions

Shadley and Wiencke (1987) reported that the induction of the adaptive response in human lymphocytes was dependent on the radiation dose rate. A 0.5 Gy pretreatment dose of X-rays given at a low dose rate (0.005 or 0.01 Gy min^{-1}) was capable of inducing the adaptive response. When the same pretreatment dose was given at a dose rate of either 0.1, 0.2 or 0.5 Gy min^{-1} the adaption response was not seen. The temporal distribution of the initial energy depositions in a cell during the exposure to radiation might therefore provide an alternative explanation for the triggering of the protective mechanism in this V79 study. The initial track structure of ionising radiation is recognised to be important in the efficiency of a given dose of radiation in cell killing (Goodhead, 1989). It is plausible therefore that the distribution of ionisations in a cell after high-LET and low-LET radiation is not only critical in cell killing but also in the induction of the radioprotective mechanism.

Goodhead (1989) has proposed that a continuous spectrum of initial physical damage from ionising radiation exists as the LET of the radiation increases through a range from low-LET γ-rays to high-LET radiations such as α particles. For low-LET radiation, ionisations are produced predominantly by a localised cluster of ionisations within a single electron track end. Whereas, high-LET radiations are characterised by a greater density of energy depositions per unit volume than low-LET radiations. This distinction might explain why the inducible response was seen only after X-ray, and not after neutron irradiation. However, high-LET radiations also produce large numbers of smaller energy depositions inducing the types of lesions produced by low-LET radiations, and if these are responsible for the triggering of the radioprotective mechanism following exposure to low-LET radiation why is the effect absent after high-LET radiation? After high-LET irradiation a large number of potentially irreparable lesions (e.g. LMDS) might be produced which might be less easily repaired and therefore prove lethal to the cell despite the triggering of the radioprotective process.

Kinetics of the induction process

The kinetics of the induction process may provide evidence to elucidate the stimulus that triggers the radioprotective mechanism. The pretreatment studies, in which cells were given two doses of radiation separated by 4 or 6 hours (section 7.4.2.2) is comparable with the irradiation regime that was used in the adaptive response reported by several authors (Wolff *et al.*, 1989; Shadley and Wiencke, 1989; Shadley *et al.*, 1987; Wiencke *et al.*, 1986). These authors showed that the adaptive response in human lymphocytes was not fully induced until 4 hours following the pretreatment dose and was subsequently fully expressed 4-6 hours after the pretreatment dose. The stimulatory effect of the pretreatment was also reported to diminish after 3 cell cycle times (Wolff *et al.*, 1989). In this V79 study the stimulation of repair was noted 4-6 hours after pretreatment and diminished 24 hours (≈2 cell cycle times) after the initial pretreatment dose. The requirement of a minimum period of time for the radioprotective mechanism to be fully induced, and loss of the protective effect after 2 or 3 cell cycles in both of human and V79 pretreatment studies, imply that the synthesis of new compounds might be necessary for the correct functioning of the response (possibly the production of DNA repair enzymes). The disappearance of the inducible protective effect after a few cell cycle times would be due to the normal biological degradation of the synthesised products.

This RBE-X-ray dose relationship over the dose range 0.04-1 Gy was modified when the cells were exposed to an inhibitor of protein synthesis in the interval between the pretreatment and subsequent X-ray dose (Fig. 7.15). These data demonstrate that *de novo* protein synthesis is required for the radioprotective mechanism to be fully induced, once it has been triggered by the pretreatment dose of irradiation. Incubating cells in cycloheximide after radiation treatment was also reported to prevent the manifestation of the inducible repair process in insect cells (Koval, 1986) and human lymphocytes (Wolff *et al.*, 1989). It is plausible that the inhibition of protein synthesis prevented the inducible repair response from increasing radioresistance because essential proteins required for the induction could not be synthesised. These proteins might be repair enzymes which are involved in a repair pathway inhibited by 3-aminobenzamide (3-AB) since the presence of 3-AB 1.5 hours prior to, and 6 hours following a single dose of radiation was also found to prevent

the correct functioning of the inducible repair mechanism once it had been triggered (see section 7.4.1.2). Interestingly, the effect of cycloheximide, preventing the induction of the protective mechanism by the inhibition of protein synthesis, was also evident when cycloheximide was present 1.5 hours prior to, and 6 hours following a single dose of radiation over the dose range 0.6-1 Gy (see section 7.4.1.2). These data suggest that *de novo* protein synthesis is also required for the induction of the radioprotective mechanism in this V79-379A cell system.

X-ray induced proteins

The results of the preliminary 2D gel electrophoresis experiments (chapter 8) demonstrated the existence of an X-ray induced protein in this V79 cell system which might be responsible for the increase in radioresistance following the induction of the repair process. The X-ray induced protein was not present in unperturbed cells (sham irradiated) but was visible in the protein array of a population of cells which had received an X-ray dose of 1 Gy (see Fig. 8.2 c.f. Fig. 8.3). The suppression and increased expression of other proteins was also noted in the irradiated cell sample (Fig. 8.3).

Others studies that have postulated the induction of DNA repair processes following ionising radiation treatment have also demonstrated the existence of X-ray induced proteins that were not present in unperturbed cells (Wolff *et al.*, 1989). Boothman *et al.* (1989) have demonstrated the expression of several proteins in human melanoma cells (U1-Mel) synthesised as a result of exposure to ionising radiation. The XIPs were not induced by heat shock, hypoxia or alkylating agents but were specific for ionising radiation damage and had molecular weights which ranged from 135-269 kilodaltons. They were detected within 3 hours of radiation treatment and were expressed maximally 4-6 hours after induction. The kinetics of XIP induction correlate with the development of the adaptive response reported in human lymphocytes (Wolff, 1989; Shadley and Wiencke, 1989; Wiencke *et al.*, 1986) and the development of the protective mechanism observed in the pretreatment experiments reported in this V79 study (chapter 7).

The X-ray induced protein reported in this thesis (chapter 8) was not fully

characterised but appears to be much smaller than those observed by Boothman *et al.* (1989). Cycloheximide inhibited the induction of the radioprotective mechanism in this study (see section 7.4.1) and also prevented the synthesis of the XIPs reported by Boothman *et al.* (1989) indicating the necessity for *de novo* protein synthesis in both studies. Interestingly the dose-response characteristics of some of the XIPs (see Fig. 10.1) are dose dependent. The expression of all the classes of XIPs noted by Boothman *et al.* (1989) increased over the X-ray dose range 0-1 Gy and the expression of XIP 147 and XIP 126 plateaux at this level of dose. XIPs 275/135, 141 and 136 all increase in expression up to a dose of 2 Gy and then plateaux. These dose-response characteristics of the XIPs correlate approximately to the induction of the radioprotective mechanism in this V79 study: the induction of radioprotection was demonstrated to occur over the dose range 0.2-0.6 Gy (chapter 3) and was fully induced at an X-ray dose of 1 Gy.

Also of interest is the difference in induction of XIPs between normal, repair proficient cells and cells from cancer-prone patients with suspected deficiencies in DNA repair (Boothman *et al.*, 1989). Irradiation of cancer-prone cells predominantly induces small molecular weight XIPs which may reflect defective transcriptional or translational processing in these cells. The induction of the protective mechanism in this study (chapter 9) is postulated not to occur in radiosensitive cells (see below) and the lack of induction of high molecular weight XIPs in these types of cells in the Boothman *et al.* study, implicates XIPs in the protective mechanism noted in this study and possibly in the intrinsic radiosensitivity of cells.

A mechanism to explain the inducible protective mechanism reported in this thesis

The radioprotective mechanism reported in this thesis was evident after single doses of X-rays (chapter 3) and in the priming experiments (chapter 7). It is postulated that X-ray induced damage over the dose range 0.01-0.2 Gy would be repaired by limited capacity repair systems already present in the cell which do not require *de novo* protein synthesis to operate. Cell killing would occur over this dose region because the cells with potentially lethal lesions would pass through fixation points in the cell cycle before they could be repaired by these primary systems. These primary repair systems might be limited in their repair capacities because, for example, the

repair molecules might not be recycled or might remain bound to the substrate for a long time producing an effect akin to repair saturation. The repair of DNA double strand breaks in cerebellar cells has been shown to saturate (Wheeler and Wierowski, 1983; Wierowski *et al.*, 1984). However, as the X-ray dose increased (e.g. > ≈0.2 Gy) a second system would be induced to repair the increasing levels of damage. The secondary repair system would represent the radioprotective mechanism reported in this thesis. It would require the production of the new proteins and would be triggered by any one of the mechanisms discussed earlier (either specific types of lesions or the temporal distribution of those lesions in the genome). The two component response would function in tandem to repair radiation-induced damage.

A two-branched system would explain why a 0.05 Gy X-ray dose appeared to *trigger* the radioprotective mechanism when given 4 hours prior to subsequent X-ray doses (section 7.4.2.2) but not when given as a single dose. In both irradiation regimes the resultant damage from the 0.05 Gy X-ray dose would be repaired by the primary repair system(s). However, in the pretreatment experiments the primary repair system(s) that repaired the damage from the 0.05 Gy X-ray dose given 4 hours earlier would remain in place and facilitate the repair of radiation-induced lesions from the subsequent X-ray doses, therefore increasing cell survival (see Fig. 7.13). Such a process might explain why an over stimulation of repair occurred with a priming dose of 0.2 Gy of X-rays (see Fig. 7.13). This dose overlaps the region between the primary and secondary repair systems and causes sufficient damage to trigger partially the secondary system while not fully overwhelming the capacity of the primary system. Therefore, in the pretreatment experiments the damage that results from the priming 0.2 Gy X-ray dose is repaired by the primary system but the level of damage received is also sufficient to trigger the secondary system. When the subsequent doses are given 4 hours later both systems are active and a large increase in survival is seen. With a 1 Gy priming dose the primary system is overwhelmed rapidly (possibly by the mechanisms stated above) and the secondary system is triggered. The subsequent damage that is received from the X-ray doses given 4 hours later is only repaired by the secondary system, the primary system having been overwhelmed, and consequently the increase in cell survival is not as great as that seen with a smaller 0.2 Gy priming dose. Whereas, in the single dose experiments the damage received from the 1 Gy X-

ray dose is sufficient to induce *fully* the secondary repair system and therefore an increase in radioresistance (decrease in effect per gray (EPG)) is observed in these cells compared with cells irradiated with doses << 1 Gy (e.g. 0.05 and 0.2 Gy). This hypothesis could also explain why non-cytotoxic doses of H_2O_2 triggered the protective mechanism. The SSB damage that resulted from the H_2O_2 treatment would either be sufficient to trigger the inducible-secondary system or otherwise be repaired by the primary repair system(s) which would remain available to facilitate the repair of the subsequent radiation-induced damage leading to increased levels of cell survival in cells receiving the H_2O_2 treatment compared with cells not receiving the H_2O_2 treatment.

This hypothesis assumes that the cell contains a rapidly-acting primary repair process whereby cells can be correctly or transiently repaired before the radiation damage is fixed. The transiently repaired damage might then be correctly repaired at a later time, possibly by the secondary system if induced. Such an error-prone repair system has been postulated to occur in hamster embryo fibroblasts (CHEF/18 cells) in which the cell initiates an error-prone DNA repair process immediately the damage is detected, regardless of the carcinogenic consequences (Boothman and Pardee, 1989).

The stimulus that induced the secondary repair system in the V79 cell might also trigger a process whereby the essential gene products that are required for the inducible repair system are transcribed in preference to the genome as a whole, thereby ensuring a rapid repair response. Such a process, characterised by the preferential transcription of essential genes during the repair of UV radiation damage, has been previously reported (Bohr *et al.*, 1987). The repression of previously active genes and the inhibition of the translation of pre-existing mRNA messages not essential for the response of a cell to a DNA insult has also been reported to occur in the 'heat-shock response' of cells to elevated temperatures (Findly and Pederson, 1981; Lindquist, 1981). SSBs are thought to be repaired by two components, the first component repairs 70-90% of all SSBs independent of radiation dose received with a $t_{1/2}$ value of between 2 and 10 minutes, whereas the slower component has a $t_{1/2}$ of 10 minutes (Frankenberg-Schwager, 1989). These SSB data indicate that the cell has the capacity to respond rapidly to DNA damage and the kinetics of SSB repair and

PLD repair (see below) provide evidence that the cell might contain a two component repair function and therefore the two stage repair process postulated above.

A Role for X-ray induced responses

The two DNA repair processes which have been most extensively investigated are potentially lethal damage repair (PLDR) and sublethal damage repair (SLDR). As was discussed earlier (section 1.6) these operational definitions may be the same manifestation of a series of common repair pathways. PLD repair as noted by Iliakis (1988) has two distinct phases, the first phase occurs rapidly ($t_{1/2}$: 2-20 minutes) and the second phase more slowly ($t_{1/2}$ > 1-2 hours). This first phase of repair is probably associated with a rapid resealing of single and double strand breaks necessary for the survival of the cell, whereas the second phase of PLDR is characterised by the complete repair of DSBs and possibly the correction of misrepaired lesions. Boothman *et al.* (1989) proposed that the initial fast phase of PLDR involved constitutively synthesised enzymes (e.g. ligases, polymerases) which acted immediately to repair X-ray induced DNA damage and thereby enhanced the survival of cells, whereas the second-slower phase of PLDR required the induction of specific genes and production of unique gene products needed for the repair of more complex chromosomal damage. The second phase would correct lesions that were missed or incorrectly repaired by the error-prone first phase of PLDR. Failure to repair these lesions would result in cell death, or misrepair may have mutagenic consequences. Boothman and Pardee (1989) have shown that the first phase of PLDR is error prone, evidence which supports the hypothesis that the immediate response of X-irradiated cells is to initiate DNA repair processes required for their survival regardless of the mutagenic consequences. During this initial rapid response, genes for repair enzymes may be actively transcribed in preference to non-essential genes in the genome as found for UV-irradiation (Bohr *et al.*, 1987) and the HSP response (Lindquist, 1986). The number of transformed cells following irradiation has been shown to decrease over the same time frame as the second phase of PLDR (Boothman and Pardee, 1989). This is seen as evidence that lesions incorrectly repaired by the first phase of PLDR are subsequently correctly repaired by the second phase of PLDR, possibly by an induced DNA repair pathway thereby reducing the biological effect of radiation treatment. The secondary repair system reported in this thesis and proposed to exist in V79-379A cells might be

similar in nature to the second phase of induced PLDR proposed by Boothman and Pardee (1989) that requires *de novo* protein synthesis. The primary repair system postulated in this thesis might be similar to the first phase of PLDR, as proposed by Boothman and Pardee (1989), as it is rapid ($t_{1/2}$: 2-20 minutes) and does not require protein synthesis.

Significance of the X-ray induced response

If the increase in X-ray radioresistance observed in this study over the X-ray dose range 0.2-1 Gy (see Fig. 3.3) is a manifestation of induced repair then the results from chapter 9 might indicate the biological significance of the induction process. The two repair proficient V79 cell lines (V79-379A and V79-B) investigated in this thesis both had biphasic X-ray survival curves, over the dose range 0.04-1 Gy, and were described with reasonable accuracy by an induced repair model (Eqn. 4.3). The X-ray survival curve obtained for the repair proficient L132 human epithelial cell line suggested that this cell line was also hypersensitive to low doses of X-rays (see section 9.4). The repair proficient WH-FIB cell line did not appear to exhibit the extreme low-dose X-ray hypersensitivity; however, as cell survival was only measured over the dose range 0.05-0.5 Gy it is not possible to exclude the existence of hypersensitivity to low-dose X-rays from the available data. The repair deficient subline (XR-V15B) of the repair proficient V79-B cell line however, did *not* have a bi-phasic survival curve or exhibit low-dose X-ray hypersensitivity. The X-ray survival response of the repair deficient XR-V15B cell line was exponential. In this study all of the repair proficient cell lines investigated (excluding WH-FIB where the data are insufficient to be conclusive) were characterised by a hypersensitive response to low doses of X-rays subsequently followed by an increase in radioresistance (decrease in EPG) with an increase in X-ray dose, whereas, the repair deficient XR-V15B cell line did not exhibit this survival response and was described accurately by an exponential survival curve. A correlation therefore exists (albeit with limited data) between the repair proficiency of a cell and an increase in radioresistance over an X-ray dose range ≈0.2-1 Gy. Although a correlation is not evidence of a causal relationship, the survival data in this thesis would be consistent with a hypothesis that differences in intrinsic radiosensitivity seen between repair-proficient and repair-deficient cell lines might, in part, be due to the induced repair function reported in this thesis. Mechanistically, the

initial survival response (< 0.2 Gy), before the inducible repair mechanism (secondary system) had been triggered, would reflect the initial number of *unrepaired* lesions. These lesions would become lethal as the cell passed through fixation points in the cell cycle (e.g. mitosis) unless repaired by the limited-capacity primary repair system(s). Once the inducible repair mechanism had been triggered more of the radiation-induced lesions would be repaired, before they could become fixed, leading to the increase in radioresistance manifested as the biphasic survival response. The XR-V15B cell line has an exponential survival response after exposure to ionising radiation because either the inducible mechanism is not triggered, or the cell is unable to repair the radiation-induced lesions once the inducible mechanism has been triggered.

If this hypothesis is valid then it might explain why several genetic conditions which are characterised by a defect in an aspect of DNA repair are associated with an increased radiation sensitivity e.g. Ataxia telangiectasia, Fanconi's anaemia, Cockayne's syndrome (Freidberg, 1985) and Xeroderma Pigmentosum (Cleaver, 1968). An inducible repair mechanism might also explain why some tumours are more less radioresponsive than others. The radioresistant tumours would be intrinsically radioresistant to radiation treatment because they have a large inducible repair response whereas radiosensitive tumours which respond well to radiation treatment are intrinsically radiosensitive because they have a diminished inducible response. The radiosensitive tumours would therefore have initial steeper survival curves over the dose range 0.01-1 Gy than the radioresistant tumours. Fertil and Malaise (1981) and Deacon *et al.* (1984) have established a positive correlation between the steepness of the initial slope of the survival curve for human tumour cells and their clinical response. The survival data (Fertil and Malaise, 1981; Deacon *et al.*, 1984) were fitted with an LQ model and therefore the correlation between the steepness of the initial slope of the survival curve and clinical response was related to the value of the α parameter in the model: the larger the α value the more radioresponsive the tumour. This correlation between the α value in the LQ model and the clinical radioresponsiveness of some tumours might be explained by the inducible repair response reported in this thesis which is characterised by a dose dependent α at very low doses.

Other factors reported to be involved in intrinsic radiosensitivity: heterogenous DNA damage and repair?

Some evidence exists that both DNA damage and repair are heterogenous in the genome. Bohr *et al.* (1987) reported a heterogenous distribution of DNA damage and repair in mammalian cells. The extremely tight packing of the DNA in the nucleus (for a review see Pienta and Coffey, 1984) might be expected to render some regions of the genome inaccessible to DNA repair enzymes and therefore more radiosensitive than more accessible regions of the genome. Evidence that pyrimidine dimers in mammalian chromatin are not equally accessible to repair enzymes was reported by Wilkins and Hart (1974) and van Zeeland (1981). It has also been reported that actively transcribed regions of the genome are packaged in altered nucleosome structures and found in genomic regions that are less condensed and therefore more accessible than are those regions containing inactive genes or noncoding sequences (Weintraub and Groudine, 1976). Transcriptionally active regions of the genome would presumably have the least degree of coiling to remain accessible to enzymes and consequently be more accessible to repair enzymes for the repair of radiation induced lesions than more tightly packed regions of the genome. Such a system has been reported for heat shock proteins (Lindquist, 1981). The HSP genes are essentially quiescent at normal temperatures and are reported to be in an open chromatin configuration and therefore they could be rapidly transcribed when induced. Sinclair (1966) suggests that DNA conformation might explain the differences in radiosensitivity between the different phases of the cell cycle. This distinction between different regions of the genome provides some circumstantial evidence to support the non-uniformity of the genome to DNA damage.

While the vulnerability of different parts of the genome might contribute to the variation in radiosensitivity between different cell lines it is likely that the repair of radiation damage may also be important in determining the initial slope of the survival curve. Evidence for this is the correlation between the increased radiosensitivity (see above) associated with patients with hereditary genetic diseases and the deficiencies in DNA damage processing that characterise these disorders (Freidberg, 1985). Cells are also known to contain many repair genes; studies in yeast have implicated at least

30 genes in the processing of DNA damage (Friedberg, 1985). The importance of repair genes is reflected by their highly conserved nature and level of homology in prokaryote and eukaryote cells e.g. SOS gene response (Radman, 1980). Therefore, while the initial level of damage induced in the DNA might be an important factor in determining intrinsic sensitivity (because the initial damage received by a cell will be affected by the level of chemical modifiers of repair present at the time of radiation e.g. endogenous levels of glutathione and oxygen) the data in this thesis suggest that the induction of a repair mechanism that repairs radiation-induced damage is the most critical factor in determining the intrinsic radiosensitivity of cells.

Chapter 11: References

AHNSTRÖM, G. AND BRYANT, P.E., DNA double-strand breaks generated by the repair of X-ray damage in Chinese hamster cells. *Int. J. Radiat. Biol.* **4**, 671-676 (1982).

ALPER, T., Elkind recovery and 'sub-lethal damage': a misleading association? *Brit. J. Radiol.*, **50**, 459-467 (1977).

ALPER, T., Cellular Radiobiology. Cambridge University Press pp 33-50 (1979).

ALPER. T., Cell survival after low doses of radiation. *6th L. H. Gray Conference* (1975).

ANDERSON, E.C., Cell growth and division. IV. Determination of volume growth rate and division probability. *Biophys. J.* **9**, 246 (1969).

ARRAND, J.E. AND MURRAY A.M., Benzpyrene groups bind preferentially to the DNA of active chromatin in human lung cells. *Nuclei acids research.* **10**, 1547-1555 (1982)

BARENDSEN, G.W., Responses of cultured cells, tumours and normal tissues to radiation of different linear energy transfer. In: *Current Topics in Radiation Research*, ed. M. Ebert and A. Howard vol 4, Amsterdam: North-Holland Publishing Co. pp 295-356 (1968).

BAUER, K.D., KENG, P.C. AND SUTHERLAND, R.M., Isolation of quiescent cells from multicellular tumor spheroids using centrifugal elutriation. *Can. Res.* **42**, 72-78 (1982).

BEAM. C.A., MORTIMER, R.K., WOLFF R.G. AND TOBIAS C.A., The relationship of radioresistance to budding in *Saccharomyces cerevisiae*. Arch. Biochem. Biophys. **49**, 110-112 (1954).

BEDFORD, J.S. AND GRIGGS, H.G., The estimation of survival at low doses and the limits of resolution of the single-cell-plating technique In: Cell survival after low doses of radiation. *6th L. H. Gray Conference* pp. 34-39 (1975).

BEDFORD, J.S. AND MITCHELL, J.B., Dose-rate effects in synchronous mammalian cells in culture. *Radiat. Res.* **54**, 316-327 (1973).

BEETHAM, K.L. AND TOLMACH, L.J., The action of caffeine on X-irradaited HeLa cells. VIII. Recovery from potentially lethal damage. *Radiat. Res.* **107**, 272-85 (1986).

BELLI, S.A. AND SHELTON, M., Potentially lethal radiation damage: repair of mammalian cells in culture. *Science* **165**, 490-492 (1969).

BENDER, M.A., GRIGGS, H.G. AND BEDFORD, J.S., Mechanisms of chromosomal aberration production. III. Chemicals and ionizing radiation. *Mutat. Res.* **23**, 197-212 (1974).

BENDER, M.A. AND GOOCH, P.C., The kinetics of X-ray survival of mammalian cells *in vitro*. *Int. J. Radiat. Biol.* **5**, 133-45 (1962).

BENJAMIN, R.C. AND GILL, D.M., ADP-ribosylation in mammalian cell ghosts. Dependence of poly(ADP-ribose) synthesis on strand breakage in DNA. *J. Biol. Chem.* **255**, 10493-501 (1980).

BIENZ, M. AND PELHAM, R.B., Heat shock regulatory elements function as an inducible enhancer in the Xenopus hsp70 gene and when linked to a heterologous promoter. *Cell* **45**, 753-760 (1986).

BLÖCHER, D. AND POHLIT, W., DNA double strand breaks in Ehrlich ascites tumour cells at low doses of X-rays. II. Can cell death be attributed to double strand breaks? *Int. J. Radiat. Biol.* **42**, 329-338 (1982).

BOAG, J.W., The statistical treatment of cell survival data In: Cell survival after low doses of radiation. *6th L. H. Gray Conference* pp. 40-53 (1975).

BOHR, V.A., PHILLIPS, D.H. AND HANAWALT, P.C., Heterogenous DNA damage and repair in the mammalian genome. *Cancer Res.* 47, 6426-6436 (1987).

BOHR, V. A., AND HANAWALT, P.C., Factors that affect the initiation of repair in chromatin. In: DNA repair and its inhibition edited by A. Collins, C.S. Downes and R.T. Johnson (Oxford: IRL press) pp. 109-125 (1984).

BOOTHMAN, D.A. AND PARDEE, A.B. Inhibition of radiation-induced neoplastic transformation by β-lapachone. Proc. Natl. Acad. Sci **86**, in press

BOOTHMAN, D.A., BOUVARD, I. AND HUGHES, E.N., Identification and characterization of X-ray-induced proteins in human cells. *Cancer Res.* **49**, 2871-2878 (1989).

BREIMER, L.H., Ionising radiation-induced mutagenesis. *Br. J. Cancer.* **57**, 6-18 (1988)

BRIDGES, B. AND LEHMANN, A., Inducible responses to DNA damage. *Nature* **298**, 118-119 (1982).

BRYANT, P.E., Enzymatic restriction of mammalian cell DNA using Pvu II and Bam H1: evidence for the double-strand break origin of chromosomal aberrations. *Int. J. Radiat. Biol.* **46**, 57-65 (1984).

Bryant, P.E., Use of restriction endocunleases to study relationships between DNA double-strand breaks, chromosomal aberrations and other end-points in mammalian cells. *Int. J. Radiat. Biol.* **54**, 869-890 (1988).

BURGMAN, P. AND KONINGS, A.W.T., Effect of inhibitors of poly (ADP-ribose) polymerase on the radiation response of HeLa S3 cells. *Radiat. Res.* **119**, 380-386 (1989).

CALKINS, J., EINSPENNER, M., BLOCHER, D. AND GREER, W., Responses of two

mammalian cell lines to low gamma-ray doses. *Rapid communication* Radiat. Res. **119**, 869-875 (1989).

CALKINS, J. AND TODD, W., Evidence for a triggered or activated repair system in *Saccharomyces cerevisiae. Int. J. Radiat. Biol.* **14**, 487-491 (1968).

CALKINS. J., An unusual response in X-irradiated protozoa and a hypothesis as to it's origin. *Int. J. Radiat. Biol.* **12**, 297-301 (1967).

CARRANO, A.V., Chromosomal aberrations and radiation-induced cell death, II. Predicted and observed cell survival. *Mutat. Res.* **17**, 355-357 (1973).

CHADWICK, K.H. and LEENHOUTS, H.P., A molecular theory of cell survival. *Phys. Med. Biol.* **18**, 78-87 (1973).

CHAPMAN. J.D., GILLISPIE, C.J., REUVERS, A.P. AND DUGLE, D.L., Radioprotectors, radiosensitisers, and the shape of the mammalian cell survival curve. In: Cell survival after low doses of radiation. *6th L. H. Gray Conference* pp. 135-140 (1975).

CLEAVER, J. E., Defective repair replication of DNA in Xeroderma Pigmentosum. *Nature* **218**, 652-656 (1968).

COLE, A., MEYN, R.E., CHEN, R., CORRY, P.M. AND HITTELMAN, W., Mechanisms of cell injury. Radiation Biology in Cancer Research eds. R.E. Meyn and H.R. Withers Raven Press pp. 33-58 (1980).

COLE, A., GRANT COOPER, W., SHONKA, F., CORRY, P.M., HUMPHREY, R.M. AND ANSEVIN, A.T., DNA scission in hamster cells and isolated nuclei studied by low-voltage electron beam irradiation. *Radiat. Res.* **60**, 1-33 (1974).

COLLINS, A. AND JOHNSON, R.T., The inhibition of DNA repair. *Adv. Radiat. Biol.* **11**, 72-131 (1984).

COLLINS, A.R.S., DOWNES, C.S. AND JOHNSON, R.T., An integrated view of inhibited repair. In: DNA repair and its inhibition eds A. Collins, C.S. Downes and R.T. Johnson. IRL Press Ltd. pp 1-11 (1984).

COLLINS, A., Cellular responses to ionizing radiation: effects of interrupting DNA repair with chemical agents. *Int. J. Radiat. Biol.* **51**, 971-983 (1987).

CONKIE, D., Separation of viable cells by centrifugal elutriation. *Animal cell culture - a practical approach.* eds. D. Rickwood and Hames, B.D. IRL Press pp. 113-125. (1986).

CORNFORTH, M.N., Chromosome break rejoining and cellular recovery from X-rays. In *'Radiation Research: Proc. 8th ICRR at Edinburgh, July 1987'* ed. by E.M. Fielden *et al.* (Taylor & Francis, London, New York, Philadelphia) pp. 468-473 (1989).

CORNFORTH, M.N., On the nature of interactions leading to radiation-induced chromosomal exchange. *Int. J. Radiat. Biol.* **56**, 635-643 (1989).

COULONIDRE, C. AND MILLER, J.H., Genetic studies on the *lac* repressor. IV. Mutagenic specificity in the *lacI* gene of *Escherichia coli*. *J. Molec. Biol.*, **117**, 577-606 (1977).

COURTENAY. V.D., The response to continuous irradiation of the mouse lymphoma L1578Y grown *in vitro*. *Int. J. Radiat. Biol.* **9**, 581-592 (1965).

CURTIS, S.B., Lethal and potentially lethal lesions induced by radiation - a unified repair model. *Radiat. Res.* **106**, 252-270 (1986).

DATTA R., COLE A. AND ROBINSON S., Use of track-end alpha particles from ^{241}Am to study radiosensitive sites in CHO cells. *Radiat. Res.* **65**, 139-151 (1976).

DEACON, J., PECKHAM, M.J. AND STEEL, G.G., The radioresponsiveness of human tumours and the initial slope of the cell survival curve. *Radiotherapy and Oncology* 2 317-323 (1984).

DEMPLE, B. AND HALBROOK, J., Inducible repair of oxidative DNA damage in *Escherichia coli*. *Nature*, **304**, 466-468 (1983).

DENEKAMP. J., G.F. WHITMORE, AND P. JEGGO., Bi-phasic survival curves for XRS radiosensitive cells: subpopulation or transient expression of repair competence? *Int. J. Radiat. Biol.* **55**, 605-617 (1989).

DEWEY, W.C., NOEL, J.S. AND DETTOR, C.M., Changes in radiosensitivity and dispersion of chromatin during the cell cycle of synchronous Chinese hamster cells. *Radiat. Res.* **52**, 373-394 (1972).

DOIDA, Y. AND OKADA, S., Radiation-induced mitotic delay in cultured mammalian cells (L5T78TY). *Radiat. Res.* **38**, 513-529 (1969).

DOWNES, C.S. AND JOHNSON, R.T., DNA topoisomerases and DNA repair. *Bioessays*, **8**, 179-184, (1988).

ELKIND, M.M., Repair processes in radiation biology. *Radiat. Res.* **100**, 425-499 (1984).

ELKIND, M.M., UTSUMI, H., BEN-HUR, E., Are single or multiple mechanisms involved in radiation-induced mammalian cell killing? *Br. J. Cancer* **55**, Suppl. VIII. 24-31 (1987).

ELKIND, M.M., SUTTON-GILBERT, H., MOSES, W.B. AND KAMPER, C., Sub-lethal and lethal radiation damage. *Nature* **214**, 1088-1092 (1967).

ELKIND, M.M. AND SINCLAIR, W.K., Recovery in X-irradiated mammalian cells. *Curr. Topics Radiat. Res.* **1**, 165-220 (1965).

ELKIND, M.M. AND SUTTON, H., Radiation response of mammalian cells grown in culture. I. Repair of X-ray damage in surviving Chinese hamster cells. *Radiat. Res.* **13**, 556-93 (1960).

Elkind, M.M. and Sutton, H., Sites of action of lethal irradiation: overlap in sites for X-ray, ultraviolet, photoreactivation, and ultraviolet protection and reactivation in dividing yeast cells. *Radiat. Res.* **10**, 296-312 (1959).

Elkind. M. M. and H. Sutton., The relationship between division and X-ray sensitivity, ultraviolet sensitivity and photoreactivation in yeast *Radiat. Res.* **10**, 283-295 (1959).

EPP., E. R., WEISS. H. AND SANTOMASSO. A., The oxygen effect in bacterial cells irradiated with high intensity pulsed electrons. *Radiat. Res.* **34**, 320-325 (1968).

EVANS, R.G., BAGSHAW, M.A., GORDON, L.F., KURKJIAN, S.D. AND HAHN, G.M., Modification of recovery from potentially lethal x-ray damage in plateau-phase Chinese hamster cells. *Radiat. Res.* **59**, 596-605, (1974).

FERTIL, B. AND MALAISE, E.P., Intrinsic radiosensitivity of human cell lines if correlated with radioresponsiveness of human tumors: analysis of 101 published survival curves. *Int. J. Radiat. Oncol. Biol. Phys.* **11**, 1699-1707 (1985).

FERTIL, B. AND MALAISE, E.P., Inherent cellular radiosensitivity as a basic concept for human tumor radiotherapy. *Int. J. Radiat. Oncol. Biol. Phys.* **7**, 621-629 (1981).

FINDLY, R. C. AND PEDERSON T., Regulated transcription of the genes for actin and heat shock proteins in cultured Drosophilia cells. *J. Cell Biol.* 88, 223-228 (1981).

FRANKENBERG, D. AND FRANKENBERG-SCHWAGER M., BLÖCHER. D., HARBICH, R., Evidence for DNA double-strand breaks as the critical lesions in yeast cells irradiated with sparsely or densely ionizing radiation under oxic or anoxic conditions. *Radiat. Res.* **88**, 524-532 (1981).

FRANKENBERG-SCHWAGER M. AND FRANKENBERG, D., DNA double-strand breaks: their repair and relationship to cell killing in yeast. *Int. J. Radiat. Biol.* **4**, 569-575 (1990).

FRANKENBERG-SCHWAGER, M., Review of repair kinetics for DNA damage induced in eukaryotic cells *in vitro* by ionizing radiation. *Radiother. and Oncol.* **14**, 307-320 (1989).

FREIDBERG, E.C. DNA repair. New York: W.H. Freeman. 1985

FREYER, J.P., WILDER, M.E. AND RAJU, M.R., Coulter volume cell sorting to improve the precision of radiation survival assays. *Radiat. Res.* 97, 608-614 (1984).

FRIED, A.Y.J., KITAHARA, T., STRIFE, A. AND CLARKSON, B.D., The kinetic significance of cell size. 1. Variation of Cell Cycle Parameters with size measured at mitosis. *Exp. Cell Res.* **95**, 295-302 (1975).

GARCIA-GIRALT, M., BERUMAN, L. AND MACIEIRA-COELHO, A., Growth inhibitory activity in the supernatent of non-dividing WI-38 cells. *J. Natl. Cancer Inst.* **45** 649-655 (1970).

GLICK, D., VON REDLICH, D., JUHOS, E.TH. AND MCEWEN, C.R., Separation of mast cells by centrifugal elutriation. *Exp. Cell Res.* **65**, 23-26 (1971).

GOODHEAD, D.T., Models of radiation inactivation and mutagenesis. Radiation Biology in Cancer Research. eds. R.E. Meyn and H.R. Withers Raven Press pp. 231-246 (1980).

GOODHEAD, D.T. The initial physical damage produced by ionizing radiations. *Int. J. Radiat. Biol.* **56**, 623-634 (1989).

GOODHEAD, D.T. An assessment of the role of microdosimetry in radiobiology. *Radiat. Res.* **91**, 45-76 (1982).

GOODHEAD, D.T., Saturable repair models of radiation action in mammalian cells. *Radiat. Res.* **104**, S58-S67 (1985).

GOODHEAD, D.T., Biophysical models of radaition action; Introductory review. In *'Radiation Research: Proc. 8th ICRR at Edinburgh, July 1987'* ed. by E.M. Fielden et al (Taylor & Francis, London, New York, Philadelphia) pp. 306-311 (1989).

GRAGG, R.L., HUMPHREY, R.M., THAMES, H.D., MEYN, R.E., The response of Chinese hamster ovary cells to fast neutron radiotherapy beams III. Variation in relative biological effectiveness with position in the cell cycle. *Radiat. Res.* **76**, 283-291 (1978).

GRDINA, D.J., MEISTRICH, M.L., MEYN, R.E., JOHNSON, T.S. AND WHITE, R.A., Cell synchrony techniques I. A comparison of methods. *Cell Tissue Kinet.* **17**, 223-236 (1984).

GRIFFITHS, J.B., Role of serum, insulin and amino acid concentration in contact inhibition of growth of human cells in culture. *Exp. Cell Res.* **75**, 47-56 (1972).

GUPTA, S.S. AND BHATTACHARJEE, S.B., Induction of repair functions by hydrogen peroxide in Chinese hamster cells. *Int. J. Radiat. Biol.* **53**, 6, 935-942 (1988).

HAHN, G.M., BAGSHAW, M.A., EVANS, R.G. AND GORDON, L.F., Repair of potentially lethal lesions in X-irradiated, density-inhibited Chinese hamster cells: metabolic effects and hypoxia. *Radiat. Res.* **55**, 280-290 (1973).

Hall, E.J., Radiation dose-rate: a factor of importance in radiobiology and radiotherapy. *Brit. J. of Radiol.* **45**, 81-97 (1972).

HALL, E.J., Radiobiology for the radiologist. Second edition, Harper and Row pp 29-63, (1978).

HALL, E.J., Biological problems in the measurement of survival at low doses. In: Cell

survival after low doses of radiation. *6th L. H. Gray Conference* pp. 13-53 (1975).

HALL, E.J. AND MILLAR, R.C., The how and why of *in vitro* oncogenic transformation. *Radiat. Res.* **87**, 208-223 (1981)

HAYNES, R.H., The interpretation of microbial inactivation and recovery phenomena. *Radiat. Res. Suppl.* **6**, 1-29 (1966).

HILL, B.T., The cell cycle and its significance for cancer treatment. *Cancer Treatment Reviews* **2**, 159-175 (1975).

HOFER, K.G., HARRIS, C.R. AND SMITH, J.M., Radiotoxicity of intracellular ^{67}Ga, ^{125}I and ^{3}H. Nuclear versus cytoplasmic radiation effects in murine L1210 leukaemia *Int. J. Radiat. Biol.* **28**, 225-241 (1975).

HOFFMAN, M.E., MELLO-FILHO, A.C. AND MENEGHINI, R., Correlation between the Cytotoxic effects of hydrogen peroxide and the yield of DNA strand breaks in cells of different species. *Biochimica et Biophysica Acta*, **781**, 234-238 (1984).

HORSLEY, R.J. AND PUJARA C.M., Study of the inflexion in X radiation survival curves for synchronised cell populations of green algae *(Oedogonium cardiacum) Radiat. Res.* **40**, 440-449 (1969).

HOWARD., A. AND PELC., S. R., Synthesis of DNA in normal and irradiated cells and its relation to chromosome breakage. *Heredity (suppl.)* **6**, 261-273 (1953).

IKUSHIMA, T., Chromosomal responses to ionising radiation reminiscent of an adaptive response in cultured Chinese hamster cells. *Mut. Res.* **180**, 215-221 (1987).

ILIAKIS, G., Effects of beta-arabinofuranosyladenine on the growth and repair of potentially lethal damage in Ehrlich ascites tumour cells. *Radiat. Res.* **83**, 537-552 (1980).

ILIAKIS, G., Radiation-induced potentially lethal damage: DNA lesions susceptible to fixation. *Int. J. Radiat. Biol.* **53**, 541-584 (1988).

ILIAKIS, G. AND NUESSE, M., The importance of G_1/S-border and mitosis in the fixation of potentially lethal damage. *Radiation and Environmental Biophysics.* **22**, 210-207 (1983).

ILIAKIS, G. AND NUESSE, M., Arrest of irradiated G_1, S or G_2-cells at mitosis using nocodazole promotes repair of potentially lethal damage. *Radiat. Res.* **99**, 3462-351 (1984).

JEGGO, P.A. AND KEMP, L.M., X-ray sensitive mutants of the Chinese hamster ovary cell line. Isolation and cross sensitivity to other DNA-damaging agents. *Mut. Res.* **112**, 313-327 (1983).

JEGGO., P.A., Genetic analysis of X-ray sensitive hamster cells. *Mut. Res.* **146**, 265-

270 (1985).

JOINER, M.C. AND JOHNS, H., Renal damage in the mouse: the response to very small doses per fraction. *Radiat. Res.* **114**, 1-14 (1988).

JOINER, M.C., The dependence of radiation response on the dose per fraction. *BIR report 19*, (1990).

JOINER, M.C. AND DENEKAMP, J., The effect of small radiation doses on mouse skin. *Br. J. Cancer* **53** supl. VII, 63-66 (1986).

KAPPOS, A. AND POHLIT, W., A cybernetic model for radiation reactions in living cells. I. Sparsely-ionizing radiations; stationary cells. *Int. J. Radiat. Biol. Relat. Stud. Phys. Chem. Med.* **22**, 51-65 (1972).

KELLAND, L.R. AND STEEL, G.G., Inhibition of recovery from damage induced by ionizing radiation in mammalian cells. *Radioth. and Oncol.* **13**, 285-299 (1988).

KELLAND, L.R., BURGESS, L. AND STEEL, G.G., Differential radiosensitization by the poly (ADP-ribose) transferase inhibitor 3-aminobenzamide in human tumor cells of varying radiosensitivity. *Int. J. Radiat. Oncol. Biol. Phys.* **14**, 1239-1246 (1988).

KELLERER, A.M. AND ROSSI, H.H., The theory of dual radiation action. *Current Topics in Radiat. Res. Quarterly* **8**, 85-158 (1972).

KEMP, L.M., SEDGWICK, S.G. AND JEGGO, P.A., X-ray sensitive mutants of Chinese hamster overy cells defective in double-strand break rejoining. *Mutat. Res.* **132**, 189-196 (1984).

KENG, P.C., WHEELER, K.T., SIEMANN, LORD, E.M., Direct synchronization of cells from solid tumors by centrifugal elutriation. *Exp. Cell Res.* **134**, 15-22 (1981).

KENG, P.C., LI, C.K.N. AND WHEELER, K.T., Synchronization of 9L rat brain tumor cells by centrifugal elutriation. *Cell Biophys.* **2**, 191-206 (1980).

KENG, P.C., LI, C.K.N. AND WHEELER, K.T., Characterization of the separation properties of the Beckman elutriator system. *Cell Biophysics* **3**, 41-56 (1981).

KORBELIK, M. AND SKOV, K.A., Inactivation of hypoxic cells by cisplatin and radiation at clinically relevant doses. *Radiat. Res.* **119**, 145-156 (1989).

KOVAL, T.M., Inducible repair of ionising radiation damage in higher eukaryotic cells. *Mut. Res.* **173**, 291-293 (1986).

KOVAL, T.M., Multiphasic survival response of a radioresistant lepidopteran insect cell line. *Radiat. Res.* **98**, 642-648 (1984).

KOVAL, T.M., Enhanced recovery from ionizing radiation damage in a lepidopteran insect cell line. *Radiat. Res.* **115**, 413-420 (1988).

LEA, D.E., Actions of Radiations on Living Cells. Cambridge University Press (1946).

LEEPER, D.B., SCHNEIDERMANN, M.H. AND DEWEY, W.C., Radiation-induced cycle delay in synchronous Chinese hamster cells: Comparison between DNA synthesis and division. *Radiat. Res.* **53**, 326-337 (1973).

LINDAHL, T., DNA repair enzymes. *Ann. Rev. Biochem.* **51**, 61-87 (1982).

LINDAHL P.E. AND SÖRENBY, L., A new method for the continuous selection of cells in mitosis. *Exp. Cell Res.* **43**, 424-434 (1966).

LINDQUIST, S., The heat shock response. *Ann. Rev. Biochem.* 55, 1151-91 (1986).

LINDQUIST, S., Regulation of protein synthesis during heat shock. *Nature.* 293, 311-314 (1981).

LITTLE, J.B., Factors influencing the repair of potentially lethal damage in growth-inhibited human cells. *Rad. Res.* **56**, 320-333 (1973).

LITTLE, J.W. AND MOUNT, D.W., The SOS regulatory system of *Escherichia coli. Cell.* 29, 11-22 (1982).

LUNEC, J., Introductory review: involvement of ADP-ribosylation in cellular recovery from some forms of DNA damage. *Br. J. Cancer* **49**, Suppl. VI, 13-18 (1984).

MACIERA-COELHO, A., GARCIA-GIRALT, E. AND ADRIAN, M., Changes in lysosomal associated structures in human firoblasts kept in resting phase. *Proc. Soc. Exp. Biol. Med.* **138**, 712-8 (1971).

MALAISE, E.P., FERTIL, B., DESCHAVANNE, P.J., CHAVAUDRA, N., AND BROCK, W.A., Initial slope of radiation survival curves is characteristic of the origin of primary and established cultures of human tumor cells and fibroblasts. *Radiat. Res.* **111**, 319-333 (1987).

MALCOLM, A.W. AND LITTLE, J.B., Rapid recovery in plateau-phase mammalian cells. *Radiat. Res.* **80**, 38-48 (1979).

MARPLES, B., The measurement of low dose cell survival. Msc thesis. University of London. (1987)

MATTERN, M.R. AND PAINTER, R.B., Dependence of mammalian DNA replication on DNA supercoiling. II. Effects of novobiocin on DNA synthesis in Chinese hamster ovary cells. *Biophys. Acta* **563**, 306-312 (1979).

MEISTRICH, M.L., GRDINA, D.J., MEYN, R.E. AND BARLOGIE, B., Separation of cells from mouse solid tumors by centrifugal elutriation. *Cancer Res.* **37**, 4291-4293 (1977).

MEISTRICH, M.L., MEYN, R.E. AND BARLOGIE, B., Synchronization of mouse L-P59 cells by centrifugal elutriation separation. *Exp. Cell Res.* **105**, 169-177 (1977).

MEISTRICH, M.L., Application of cell separation methods to the study of cell kinetics and proliferation. In: Growth Kinetics and Biochemical Regulation of Normal and Malignant Cells ed: B. Drewinko & R.M. Humphrey pp. 131-142 Williams & Wilkins, Baltimore Maryland. (1977).

MEISTRICH, M.L., Experimental factors involved in separation by centrifugal elutriation. *Cell Separation: Methods and selected applications Vol.2* Academic Press Inc. pp. 33-60 (1978).

MEYN, R.E., MEISTRICH, M.L. AND WHITE, R.A., Cycle-dependent anticancer drug cytotoxicity in mammalian cells synchronized by centrifugal elutriation *J. National Cancer Inst.* **64**, 1215-1219 (1980).

MITCHELL, J.B., BEDFORD, J.S. AND BAILEY, S.M., Dose-rate effects on the cell cycle and survival of S3 HeLa and V79 cells. *Radiat. Res.* **79**, 520-536 (1979).

MITCHELL, J.B., BEDFORD, J.S. AND BAILEY, S.M., Dose-rate effect between 1 and 10 Gy/min in mammalian cell culture. *Radiat. Res.* **83**, 537-552 (1980).

MOLE, R.H., Carcinogenesis following medical uses of ionising radiation. In: Low dose radiation: Biological bases of risk assessment eds K. F. Baverstock and J.W. Stather Taylor and Francis pp 100-113 (1989).

MONTESANO, R., BRÉSIL AND MARGISON, G.P., Increased excision of O^6-Methylguanine from rat liver DNA after chronic administeration of dimethylnitrosamine. *Cancer Res.* **39**, 1798-1802. (1979).

MOTHERSILL, C. AND SEYMOUR, C.B., Lethal mutations in mammalian cells. *Int. J. of Radiat. Biol.* **55**, 155-156 (1989).

MOTHERSILL, C., SEYMOUR, C.B. AND MORIARTY, M., Development of radiation transformation systems for epithelial cells - problems and perspectives. In: Low dose radiation: Biological bases of risk assessment eds K.F. Baverstock and J. W. Stather Taylor and Francis pp 414-422 (1989).

MULLER, W.E.G., ROHDE, H.J., BEYER, R., MAIDHOF, A., LACHMANN, M., TASCHNER, H. AND ZAHN, R.K., Mode of action of 9-β-D-arabinofuranosyladenine on the synthesis of DNA, RNA and protein *in vivo* and *in vitro*. *Cancer Res.* **35**, 2160-2168 (1975).

NATARAJAN, A.T. AND OBE, G., Molecular mechanisms involved in the production of chromosomal aberrations; II,. Utilization of *Neurospora* endonuclease for the study of aberration production by X-rays in G_1 and G_2 stages of the cell cycle. *Mutat. Res.* **69**, 293-305 (1980).

NIAS, A.H.W. AND FOX, M., Synchronization of mammalian cells with respect to the mitotic cycle. *Cell Tissue Kinet.* **4**, 375-398 (1971).

NIAS., A.H.W. AND LAJTHA., L.G., Continuous irradation with tritiated water of mammalian cells in a monolayer. *Nature*, **202**, 613-614 (1964).

O'FARRELL, P.H. High resolution two-dimensional electrophoresis of proteins. *J. Biol. Chem.* **250**, 4007-4021 (1975).

OFTEBRO, R. AND NORDBYE, K., Establishment of four new cell strains from human uterine cervix. II. *Exp. Cell Res.* **58**, 459-460 (1969).

OLIVIERI, G., BODYCOTE, J. AND WOLFF, S., Adaptive response of human lymphocytes to low concentrations of radioactive thymidine. *Science* **223**, 594-597 (1984).

OLSSON, M. AND LINDAHL, T., Repair of alkylated DNA in escherichia coli. Methyl group transfer from 06-methylguanine to a protein cysteine residue. *J. Biol. Chem.* **255**, 10569-71 (1980).

ORMEROD, M.G., PAYNE, A.W.R. AND WATSON, J.V. Improved program for the analysis of DNA histograms. *Cytometry* **8**, 637-641 (1987).

ORR, J.S., WAKERLEY, S.E. AND STARK, J.M., A metabolic theory of cell survival curves. *Physics Med. Biol.* **27**, 103-8 (1966).

ORR, J.S., Concepts, problems and the role of modifying agents in the relationship between recovery of cells' survival ability and mechanisms of repair of radiation lesions. *Br. J. Cancer Supplement VI* **49**, 1-6 (1984).

OTSUKA, F., KOIZUMI, S., KIMURA, M. AND OHSAWA, M., Silver staining for carboxymethylated metallothioneins in polyacrylamide gels. *Anal. Biochem.* **168** 184-192 (1988).

PAINTER, R.B., The role of DNA damage and repair in cell killing induced by ionizing radiation. Radiation Biology in Cancer Research eds. R.E. Meyn and H.R. Withers Raven Press pp. 59-68 (1980).

PAINTER, R.B. The role of DNA damage and repair in cell killing induced by ionizing radiation. In: *'Radiation Biology in Cancer Research'*, ed. by R.E. Meyn and H.R. Withers (Raven Press, New York) pp. 59-68 (1980).

PALCIC, B. AND JAGGI, B., The use of solid state sensor technology to detect and characterise live mammalian cells growing in tissue culture. *Int. J. Radiat. Biol.* **50**, 345-352 (1986).

PALCIC, B., KORBELIK, M., TROTTER, M. AND REVESZ, L., Oxygen enhancement ratio of fractionated regimens *in vitro*. *Radiat. Res.* **117**, 409-418 (1989).

PALCIC, B., BROSING, J.W. AND SKARSGARD, L.D., Survival measurements at low doses: oxygen enhancement ratio. *Br. J. Cancer* **46**, 980 (1982).

PALCIC, B., FADDEGON, B., JAGGI, B. AND SKARSGARD, L.D., Automated low dose

assay system for survival measurements of mammalian cells *in vitro*. *J. of Tissue Culture Methods* **8**, 103-107 (1983).

Palcic, B. and Skarsgard, L.D., Reduced oxygen enhancement ratio at low doses of ionizing radiation. *Radiat. Res.* **100**, 328-339 (1984).

PAYNE, M.G. AND GARRETT, W.R., Models for cell survival with low LET radiation. *Radiat. Res.* **62**, 169-179 (1975).

PETERS, J. AND JAGGER, J., Inducible repair of near-UV radiation lethal damage in *E. coli*. *Nature* **289**, 194-195 (1981).

PETERSON., D.F., TOBEY,. R. A. AND ANDERSON, E.C., Synchronously dividing mammalian cells *Fed. Proc.* **28**, 1771 (1969).

PHILLIPS, R.A. AND TOLMACH, L.J., Repair of potentially lethal damage in X-irradiated HeLa cells. *Radiat. Res.* **29**, 413-32 (1966).

PIENTA, K.J. AND COFFEY, D.S. A structural analysis of the role of the nuclear matrix and DNA loops in the organisation of the nucleus and chromosome. *J. Cell Sci. Suppl.* 1, 123-135 (1984)

PIERCE, D.A. AND VAETH, M., Cancer risk estimation from the A-bomb survivors: extrapolation to low doses, use the relative risk models and other uncertainties. In: Low dose radiation: Biological bases of risk assessments eds K.F. Baverstock and J.W. Stather. Taylor and Francis pp 54-76 (1989).

POHL-RÜLING, J., The dose-effect relationship of chromosome aberrations to α and γ irradiation in a population subjected to an increased burden of natural radioactivity. *Radiat. Res.* **80**, 61-81 (1979).

POON, S.S.S., JAGGI, B. AND PALCIC, B., Cell recognition algorithms for the cell analyzer. *Ninth Annual Conference of the Engineering in Medicine and Biolocy Society* pp. 1454-1456 (1987).

POWELL, S. AND MCMILLAN, T.J., DNA damage and repair following treatment with ionizing radiation. *Radiother. and Oncol.* **19**, 95-108 (1990).

POWERS, E.L., Consideration of survival curves and target theory. *Physics Med. Biol.* **7**, 3-28 (1962).

PRISE, K.M., DAVIES, S. AND MICHAEL, B.D., The relationship between radiation-induced DNA double-strand breaks and cell killing in hamster V79 fiboblasts irradiated with 250 kVp X-rays, 2.3 MeV neutrons or ^{238}Pu α-particles. *Int. J. Radiat. Biol.* 52 893-902 (1987).

PRISE, K.M., DAVIES, S. AND MICHAEL, B.D., Cell killing and DNA damage in Chinese hamster V79 cells treated with hydrogen peroxide. *Int. J. Radiat. Biol.* **55**, 583-592 (1989).

PUCK, T.T. AND MARCUS, P.I., Action of X-rays on mammalian cells. *J. Exp. Med.* **103**, 653-66 (1956).

RADMAN , M., Is there SOS induction in mammalian cells. *Photochem. Photobiol.* 32, 823-830 (1980)

RASEY, J.S. AND NELSON, N.J., Repair of potentially lethal damage following irradaition with X-rays and cyclotron neutrons: responses of the EMT-6/UW tumour system treated under various growth conditions *in vitro* and *in vivo*. *Radiat. Res.* **85**, 69-84 (1981).

RASMUSSEN, R.E. AND PAINTER, R.B., Evidence for repair of ultra-violet damaged deoxyribonucleic acid in cultured mammalian cells. *Nature* **203**, 1360-1361 (1964).

RESNICK, M. A., The repair of double strand breaks in DNA: a model involving recombination. *J. Theor. Biol.* **59**, 97 (1978).

ROBBINS. E. AND MARCUS. P. I., Mitotically synchronised mammalian cells: A simple method for obtaining large populations. *Science* **114**, 1152 (1964).

ROOTS, R. AND OKADA, S., Estimation of life times and diffusion distances of radicals involved in X-ray-induced DNA strand breaks or killing of mammalian cells. *Radiat. Res.* **64**, 306-320 (1975).

ROOTS, R. AND OKADA, S., Protection of DNA molecules of cultured mammalian cells from radiation-induced single-strand scissions by various alcohols and SH compounds. *Int. J. Radiat. Biol.* **21**, 329-342 (1972).

ROSS, D.W. AND SINCLAIR, W.K., Cell cycle compartment analysis of Chinese hamster cells in stationary phase cultures. *Cell Tissue Kinet.* **5**, 1-14 (1972).

RUBY, S.W. AND SZOSTAK, J.W., Specific *Saccharomyces cerevisiae* genes are expressed in response to DNA-damaging agents. *Mol. and Cell. Biol.* **5**, 75-84 (1985).

RYDBERG, B., Repair of DNA double strand-breaks in colemid-arrested mitotic Chinese hamster cells. *Int. J. Radiat. Biol.* **46**, 299 (1984).

SAMSON, L. AND SCHWARTZ, J.L., Evidence for an adaptive DNA repair pathway in CHO and human skin fibroblast cell lines. *Nature* **287**, 861-3 (1980).

SAMSON., L. AND CAIRNS., J., A new pathway of repair in *Escherichia coli*. *Nature*, **267**, 281-283 (1977).

SANDERSON, R.J., SHEPPERDSON, R.T., VATTER, A.E. AND TALMAGE, D.W., Isolation and Enumeration of peripherial blood monocytes. *J. Immunol.* **118**, 1409-1414 (1977).

SANTIER, S., GILET, R. AND MALAISE, E.P., Induced radiation resistance during low-dose rate γ irradiation in plateau-phase *chlorella* cells. *Radiat. Res.* **104**, 224-233 (1985).

SETLOW, R.B. AND CARRIER, W.L., The disappearance of thymine dimers from DNA: an error-correcting mechanism. *Proc. Nat. Acad. Science* **51**, 226-231 (1964).

SHADLEY, J.D. AND WOLFF, S., Very low doses of X-rays can cause human lymphocytes to become less susceptible to ionizing radiation. *Mutagenesis* **2**, 95-96 (1987).

SHADLEY, J.D. AND WIENCKE, J.K., Induction of the adaptive response by X-rays is dependent on radiation intensity. *Int. J. Radiat. Biol.* **56**, 107-118 (1989).

SHADLEY, J.D., AFZAL, V. AND WOLFF, S., Characterization of the adaptive response to ionizing radiation induced by low doses of X-rays to human lymphocytes. *Radiat. Res.* **111**, 511-517 (1987).

Shall, S., ADP-ribose in DNA repair: a new component of DNA excision repair. *Advances in Radiat. Biol.* **11**, 1-69 (1984).

SIEMANN, D.W., LORD, E.M., KENG, P.C. AND WHEELER, K.T., Cell subpopulation dispersed from solid tumours and separated by centrifugal elutriation. *Br. J. Cancer* **44**, 100-108 (1981).

SINCLAIR, W.K., Cyclic X-ray responses in mammalian cells *in vitro*. *Radiat. Res.* **33**, 620-643 (1968).

SINCLAIR, W. K. AND ROSS, D.W., Modes of growth in mammalian cells. *Biophys J.* **9**, 1056 (1969).

SINCLAIR, W.K. AND MORTON, R.A., X-ray sensitivity during the cell generation cycle of cultured Chinese hamster cells. *Radiat. Res.* **29**, 450-474 (1966).

SINCLAIR, W.K. AND MORTON, R.A., X-ray and ultraviolet sensitivity of synchronized Chinese hamster cells at various stages of the cell cycle. *Biophysics* **5**, 1-25 (1965).

SINCLAIR, W.K. AND MORTON, R.A., Variations in X-ray response during the division cycle of partially synchronized Chinese hamster cells in culture. *Nature* **199**, 1158-1160 (1963).

SINCLAIR, W.K., N-ethylmaleimide and the cyclic response to X-rays of synchronous Chinese hamster cells. *Radiat. Res.* **55**, 41-57 (1973).

SINCLAIR., W. K., Hydroxyurea: Differential lethal effects on cultured mammalian cells during the cell cycle. *Science* **150**, 1729-31 (1965).

SINCLAIR., W. K., Hydroxyurea: Effects of Chinese hamster cells grown in culture., *Cancer Research* **27**, 297-308 (1967).

SMITH, C.A. AND HANAWALT, P.C., *Molecular Photobiology* (New York: Academic Press), pp. 145-154 (1969)

SONTAG, W., A cell survival model with saturable repair after irradiation. *Radiat. Environ. Biophys.* **26**, 63-79 (1987).

SPADINGER, I., POON, S.S.S. AND PALCIC, B., Automated detection and recognition of live cells in tissue culture using image cytometry. *Cytometry* **10**, 375-381 (1989).

STEEL, G.G., DEACON, J.M., DUCHESNE, G.M., HORWICH, A., KELLAND, L.R. AND PEACOCK, J.H., The dose-rate effect in human tumour cells. *Radiother. and Oncol.* **9**, 299-310 (1987).

STEEL, G.G., DOWN, J.D., PEACOCK, J.H. AND T.C. STEPHENS,. Dose-rate effects and the repair of radiation damage. *Radiother. and Oncol.* **5**, 321-331 (1986).

STEEL, G.G. AND PEACOCK, J.H., Why are some human tumours more radiosensitive than others? *Radiother. Oncol.* 15, 63-72 (1989).

Steel, G.G., Cellular sensitivity to low dose-rate irradiation focuses the problem of tumour radioresistance. *Radiother. and Oncol.* 20, 71-83 (1991).

STEEN. H.B. AND LINDMO, T., Cellular and nuclear volumes during the cell cycle of NHIK 3025 cells. *Cell. Tissue. Kinet.* **11**, 69-81 (1978).

SYNDER, R.D., VAN HOUTEN, B. AND REGAN, J.D., The accumulation of DNA breaks due to incision; comparative studies with various inhibitors. In: DNA repair and its inhibition edited by A. Collins, C.S. Downes and R.T. Johnson (Oxford: IRL press) pp. 13-33 (1984).

TAYLOR, A.C., Attachment and spreading of cells in culture. *Exp. Cell Res.* Suppl. **8**, 154-173 (1969).

TEOULE, R., Review: radiation-induced DNA damage and its repair. *Int. J. Radiat. Biol.* **51**, 573-589 (1987).

TERASIMA T. AND TOLMACH L. J., Changes in X-ray sensitivity of HeLa cell during the division cycle., *Nature* **190**, 1210 (1961).

TERASIMA, T. AND TOLMACH, L.J., Variations in several responses of HeLa cells to X-irradiation during the division cycle. *Biophys. Journal* **3**, 11-33 (1963).

THACKER, J. AND STRETCH, A., Responses of 4 X-ray-sensitive CHO cell mutants to different radiations and to irradiation conditions promoting cellular recovery. *Mutat. Res.* **146**, 99-108 (1985).

THURSTON, G., JAGGI, B. AND PALCIC, B., Cell motility measurements with an automated microscope system. *Exp. Cell Res.* **165**, 380-390 (1986).

TOBEY, R.A., CRISSMAN, H.A., WILDER, M.E., TRAGANOS AND DARZYNKIEWICZ, Z., Sensitivity to X-irradiation in relation to cell size of CHO cells synchronized in early G_1. *Cell Tissue Kinet.* **20**, 363-366 (1987).

TOBEY, R.A., ANDERSON, C. AND PETERSEN, D.F., Properties of mitotic cells prepared by mechanically shaking monolayer cultures of Chinese hamster cells. *J. Cell Physiol.* **70**, 63-68 (1967).

TOBIAS, C.A., BLAKELY, E.A., NGO, F.Q.H. AND YANG, T.C.H., The Repair-Misrepair model of cell survival. In: Radiation Biology in Cancer Research eds. R.E. Meyn and H.R. Withers Raven Press pp. 195-230 (1980).

TUSCHL, H., KOVAC, R. AND WOTTAWA, A. T-lymphocyte subsets in occupationally exposed persons. *Int. J. Radiat. Biol.* **58**, 651-659 (1990).

TUSCHL, H., ALTMANN, H., KOVAC, R., TOPALOGLOU, A., EGG, D., AND GÜNTHER, R., Effects of low-dose radiation on repair processes in human lymphocytes. *Radiat. Res.* **81**, 1-9 (1980).

ULLRICH, R.L., Carcinogenesis in mice after low doses and dose rates In: Radiation Biology in Cancer Research eds. R.E. Meyn and H.R. Withers Raven Press pp. 309-319 (1980).

UTSUMI, H. AND ELKIND, M.M. Potentially lethal damage versus sublethal damage: independent repair processes in actively growing chinese hamster cells. *Radiat. Res.* **77**, 346-360 (1979).

VAN OOSTRUM, I.E.A. AND RUTGERS, D.H., Cell cycle traverse in NHIK-3025 carcinoma of the uterine cervix after low-dose-rate irradiation. *Radiat. Res.* **118**, 101-111 (1989).

VAN ZEELAND, A.A., SMITH, C.A. AND HANAWALT, P.C., Introduction of T4 endonuclease V into frozen and thawed cells. *Mutat. Res.*, 82, 173-189 (1981).

VAN ES. W.L. AND BONT, W.S., An improved method for the fractionation of human blood cells by centrifugal elutriation. *Anal Biochem* **103**, 295-301 (1980).

WALKER, G.C., Inducible DNA repair systems. *Ann. Rev. Biochem.* 54, 425-457 (1985).

WALTERS, R.A. AND PETERSEN, D.F., Radiosensitivity of mammalian cells. I. Timing and dose-dependence of radiation-induced division delay. *Biophys. J.* **8**, 1475-1486 (1968).

WARD, J.F., DNA damage produced by ionising radiation in mammalian cells: identies, mechanisms of formatiom and reparability. *Progress in Nuclei Acid Research and Molecular Biology*. **35**, 95-125 (1988).

WARD, J.F., BLAKELY, W.F. AND JONER, E.I., Mammalian cells are not killed by DNA single-strand breaks caused by hydroxyl radicals from hydrogen peroxide. *Radiat. Res.* **103**, 383-392 (1985).

WARD, J.F. The yield of DNA double-strand breaks produced intracellularly by

ionizing radiation review. *Int. J. Radiat. Biol.* **57**, 1141-1150 (1990).

WARD, J.F., EVANS, J.W., LIMOLI, C.L. AND CALABRO-JONES, P.M., Radiation and hydrogen peroxide induced free radical damage to DNA. *Br. J. Cancer* **55**, 105-112 (1987).

WARD, J.F., Mechanisms of DNA repair and their potential modification for radiotherapy. *Int. J. Radiat. Oncol. Biol. Phys.* **12**, 1027-1032 (1986).

WARD, J.F., Biochemistry of DNA lesions. *Radiat. Res.* **104**, S103-111 (1985).

WARTERS, R. L., HOFER, K. G., HARRIS, C. R., AND SMITH, J. M., Radio nucleotide toxicity in mammalian cells: Elucidation of the primary site of radiation damage, *Curr. Tops. Radiat. Res.* **12**, 389-407 (1977).

WATTS, M.E., HODGKISS, R.J., JONES, N.R. AND FOWLER, J.F. Radiosensitization of Chinese hamster cells by oxygen and misonidazole at low X-ray doses. *Int. J. Radiat. Biol.* **50**, 1009-1021 (1986).

WEINTRAUB, H. AND GROUDINE, M., Chromosomal subunits in active genes have altered confirmation. *Science.* 194, 848-856 (1976)

WHEELER, K.T. AND WIEROWSKI, J.V., DNA repair kinetics in irradiated undifferentiated and terminally differentiated cells. *Radiat. Environ. Biophys.* **22**, 3-19 (1983).

WHITE, R.A., GRDINA, D.J., MEISTRICH, M.L., MEYN, R.E. AND JOHNSON, T.S., Cell synchrony techniques. II. Analysis of cell progression data. *Cell Tissue Kinet.* **17**, 237-245 (1984).

WHITFIELD, J.F. AND YOUDALE, T., Synchronisation of cell division in suspension cultures of L strain mouse cells. *Exp. Cell Res.* **38**, 208-210 (1964).

WHITFIELD, J.F. AND RIXON, R.H., Radiation resistant derivatives of L strain mouse cells. *Exp. Cell Res.* **19**, 531-538 (1960).

WHITMORE, G.F. AND GULYUS, S., Studies on recovery processes in mouse cells. *Nat. Cancer Inst. Monograph.* **24**, 14 (1967).

WHITMORE, G.F. AND VARGHESE, A.J. AND GULYAS, S., Cell cycle responses of two X-ray sensitive mutants defective in DNA repair. *Int. J. Radiat. Biol.* **56**, 657-665 (1989).

WIENCKE, J.K., AFZAL, V., OLIVIERI, G. AND WOLFF, S., Evidence that the [^{3}H] thymidine-induced adaptive response of human lymphocytes to subsequent doses of X-rays involves the induction of chromosomal repair mechanism. *Mutagenesis.* **1**, 375-380 (1986).

WIEROWSKI, J.V., THOMAS, R.R. AND WHEELER, K.T., DNA repair kinetics in

mammalian cells following split-dose irradiation. *Radiat. Res.* **98**, 242-253 (1984).

WILKINS, R. J. AND HART, R., Preferential DNA repair in human cells. *Nature.* **247**, 35-36 (1974).

WOLFF, S., WIENCKE, J.K., AFZAL, V., YOUNGBLOM, J. AND CORTES, F., The adaptive response of human lymphocytes to very low doses of ionising radiation: a case of induced chromosomal repair with the induction of specific proteins. In: Low Dose radiation: Biological Bases of Risk Assessment eds. K.F. Baverstock and S.W. Statler (London: Taylor and Francis), pp. 446-454 (1989).

YOUNG, C.W. AND HODAS, S., Hydroxyurea: Inhibitory effect on DNA metabolism. *Science.* **146**, 1172 (1964).

ZDZIENICKA, M.Z., TRAN, Q., VAN DE SCHANS, G.P. AND SIMONS, J.W.I.M., Characterisation of an X-ray-hypersensitive mutant of V79 Chinese hamster cells. *Mut. Res.* **194**, 239-249 (1988).